Final Report on:

Magnetotelluric and AudioMagnetotelluric Surveys on

Department of Hawaiian Home Lands

Mauna Kea East Flank

Submitted By:
Donald Thomas
Hawaii Institute of Geophysics and Planetology
Center for the Study of Active Volcanoes
December 9, 2016

Executive Summary

This project has collected electromagnetic and electrical potential data from 70 locations collected in multiple linear transect intervals along a 28 km section of Mauna Kea's mid-elevation eastern flank. The measurements were all made on Department of Hawaiian Home Lands (DHHL) property that flanks the Mana/Keanakolu Road that runs from the intersection with the Mauna Kea Observatory Access Road north toward Waimea where it eventually intersects with Hawaii State 19. The electrical potential and electromagnetic measurements were made with Magnetotelluric (10 stations) and AudioMagnetotelluric (60 stations) instruments that allow us to process and model the recovered data to produce a map of the subsurface electrical resistivity distributions down to depths of more than 10 kilometers below the ground surface. These electrical resistivity distributions are widely used in the energy and minerals industries to identify and narrow the search for oil and gas or mineral prospects as well as for identification of both geothermal and groundwater resource potential. The collected data have been reviewed and refined to minimize the effects of interfering electromagnetic noise; inverted using 1D modeling to yield apparent resistivity with depth curves; and modeled using 2D inversion programs. Electrical resistivity versus depth profiles have been constructed along the survey transects using both the 1D and 2D modeling results to yield a resistivity cross section through the east flank of Mauna Kea. These cross sections reveal three moderate to low resistivity intervals at depths of 3 km or less. All three low resistivity intervals are interpreted to reflect current or prior thermal activity at shallow depths. The northern and southern low resistivity intervals are believed to be associated with subsidiary dike complexes of Mauna Kea and therefore may have limited geothermal potential, whereas the central resistivity low is, based on both the results of the current surveys as well as geological analysis, to correspond to a Mauna Kea East Rift Zone that would represent the highest geothermal resource potential. Analysis of the shallower resistivity distributions along the composite transect lines suggests that there is also potential for high elevation groundwater resources in the region that could, if carefully developed, provide a viable water supply for DHHL lessees.

Additional exploration work that could be pursued to better characterize the prospective geothermal resource would be additional Magnetotelluric and AudioMagnetotelluric surveys, as well as gravity surveys, across the postulated rift zone at higher and lower elevations on Mauna Kea's east flank. The former work would further confirm the width and extent of the identified resistivity anomaly whereas the latter would provide an estimate of the volume of magmatic intrusions within this inferred rift zone and some estimate of the heat content.

Introduction

Electrical geophysical survey methods are frequently used in exploration for natural geological features (faults, fractures, mineral veins) or resources (oil, gas, water) because the electrical properties of different types of rocks, as well as accessory fluids, are highly variable. Because of this variability, electrical resistivity measurements can be used to distinguish between dry rocks, which are highly resistive, and rocks saturated with freshwater, which are much less resistive, or rocks saturated with seawater that have much lower resistivities. Likewise, rocks that are cold (ambient ground temperatures), will have a moderate to high resistivity, whereas rocks that are saturated with hot water or hot saline water, will have much lower resistivities. As a result, electrical geophysical survey methods can be extremely valuable in identifying regions where underlying thermal activity presents no surface evidence of hydrothermal activity; equally important, these methods can allow us to exclude areas where very high resistivities indicate no thermal source is present.

During the last half century, new and increasingly advanced methods of sensing the subsurface electrical characteristics of geologic formations have been under continuous development. Collectively, these applications use a variety of approaches to determine how easily electrical current (or electromagnetic radiation) passes through subsurface rock formations. These methods vary from: passing electrical current through the ground and measuring the electrical resistance directly; to generating electromagnetic signals (radio-waves) at the surface (e.g. controlled-source electromagnetic methods) and measuring how electrical currents in the earth respond to those signals; or the measurement of induced electrical voltages and currents in the ground generated by naturally-occurring electromagnetic signals produced in the atmosphere (e.g. lightening), the ionosphere, or magnetosphere. Depending on the depth of the features of interest, the methods have the ability to characterize the electrical resistivity of rocks at a few meters depth to as deep as fifty kilometers; with today's sophisticated computer models of the data collected from an array of surface instruments, we can develop a two- or three-dimensional map of the electrical resistivity over a broad region of interest.

Even though these electrical geophysical methods have proven to be extremely valuable, they are characterized by a number of serious limitations as well. It should always be understood that the measurements, and the inferred resistivity models, are assessing electrical resistivity distributions, and only resistivity distributions, beneath the ground surface. The interpretation of the resistivity distribution of a given subsurface feature (e.g. thermal activity, freshwater saturation, salt water saturation) is inferential and not unique. This is because the resistivity of geologic formations can depend on multiple characteristics and conditions: whether the rocks are wet or dry; whether they are made up of primary minerals (the original minerals formed when magma cools) or clay minerals formed as a result of weathering, or minerals resulting

from hydrothermal activity (the latter being less resistive than the former); and whether the rocks are cold or hot (or molten – magma has a very low resistivity). In order to reduce the uncertainties in interpretation of resistivity results, we frequently conduct resistivity measurements over a known resource or feature to determine its electrical characteristics (resistivity) in the geologic environment of interest. Those data serve as reference points when conducting surveys over nearby regions for which a resource or feature of interest has not been proven to exist by direct measurement. Even with the baseline or reference measurements, there is always a degree of uncertainty regarding a resource even when we find matching resistivity values.

In the present study, we are investigating the subsurface electrical resistivity of the eastern, mid-elevation (~2000 m amsl) flank of Mauna Kea volcano in an effort to determine whether there is evidence of geothermal potential as indicated by: subsurface geological structures, or anomalously conductive regions that may be associated with thermal or saline water, or hydro-thermally altered subsurface rocks. The surface measurements consist of ten Magnetotelluric (MT) stations and sixty AudioMagnetotelluric (AMT) stations (see Appendix A for more detail on the method and discussion of the field protocols). Under favorable conditions, the former are able to sense the effects of resistivity variations to more than 20 km depths, whereas the latter are supplemental to the deep measurements, but are most sensitive to resistivity variations in the first 1 to 2 km depths below the ground surface. In the current study, all measurements were performed along the Mana/Keanakolu Road on Mauna Kea's east flank.

Background

The first electrical geophysical surveys conducted in the Humu'ula Saddle, for the purpose of investigating ground water potential, were conducted as early as the 1960's (Zohdy and Jackson, 1969). The results of those surveys suggested that the minimum depth to ground-water was in the range of 2700' (823 m) to 3000' (914 m) below ground surface (BGS). More recently, at the request of the Army Garrison Hawaii, the United States Geological Survey (USGS), in cooperation with University of Hawaii, conducted AudioMagnetotelluric surveys in 2004 and Magnetotelluric surveys in 2008 that crossed Hawaii Island from an elevation of about 650 m amsl on the east flank of Mauna Kea to an elevation of ~1000 m on the west flank of Mauna Kea. The surveys were conducted generally along the transect of the Saddle Road across public and private lands, but were located on Department of Defense leased lands in the vicinity of Pohakuloa Training Area (Figure 1; Pierce and Thomas, 2008).

Overall, those survey results showed (Figure 2) shallow rocks as being highly resistive within the center of the Saddle region, but deeper rocks having resistivities in the range of 1000 ohm-meters to as low as 5 to 10 ohm-meters near sea level. We postulated groundwater saturation

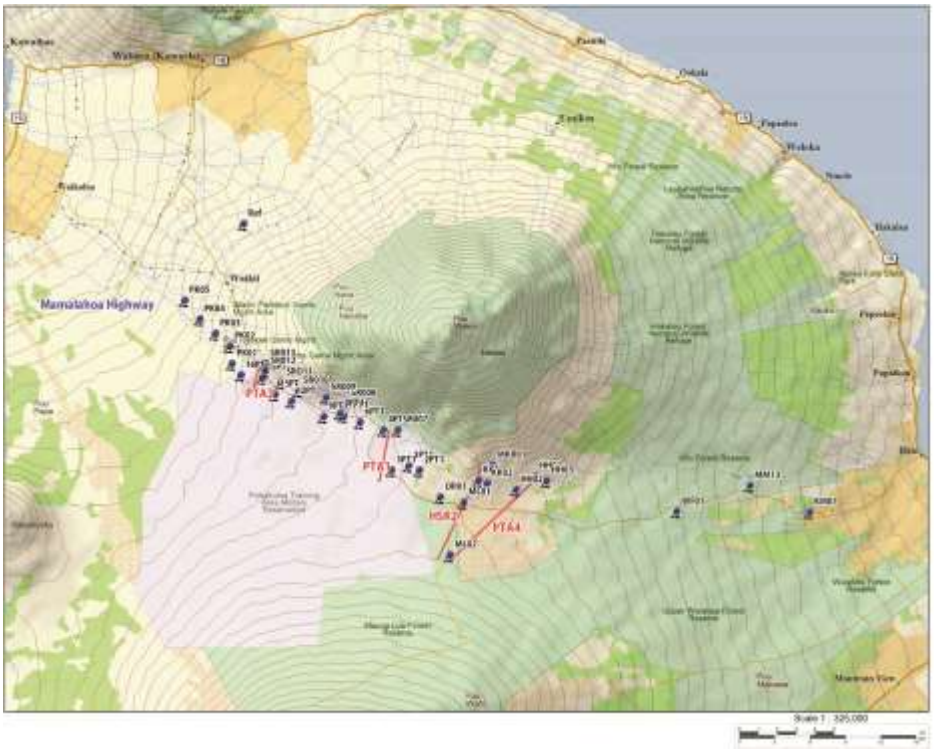

Figure 1. Map of Mauna Kea and Humu'ula Saddle showing data collection points for Magnetotelluric and AudioMagnetotelluric surveys assessing potential for high elevation groundwater in the Saddle region. The gray region in the left center of the map is DOD land, the focus of the surveys, whereas the other survey locations for that study are on State of Hawaii and private lands

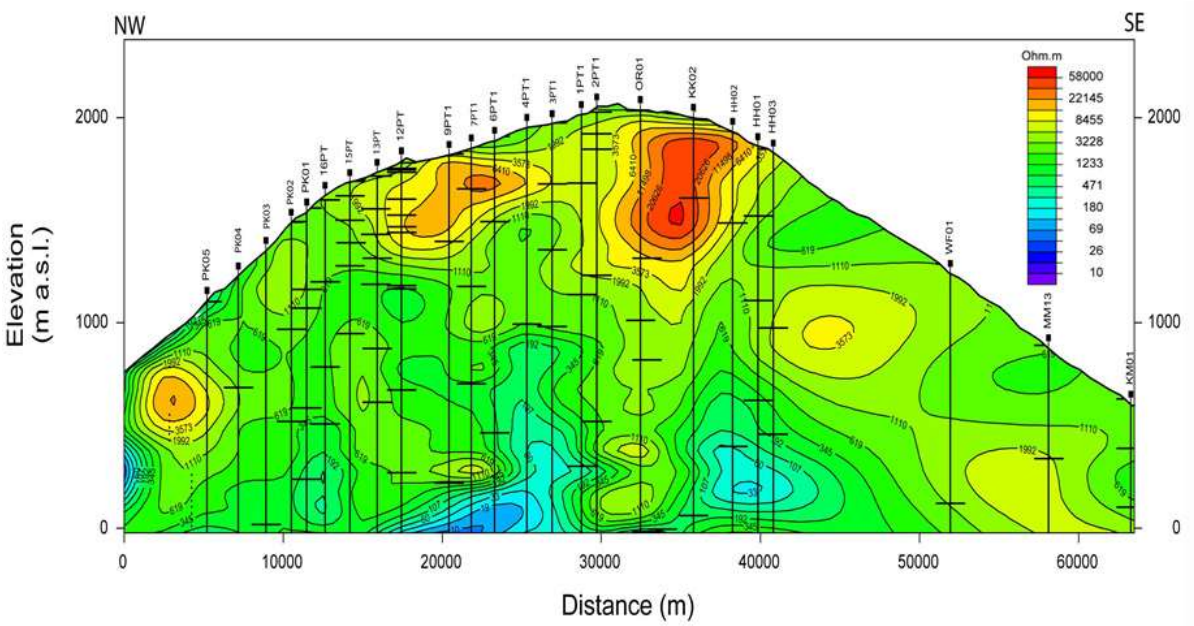

Figure 2. A resistivity cross section of the Humu'ula Saddle region, based on MT surveys conducted in 2008 for Department of Defense, showing resistivity distributions from ground surface to sea level. The warmer colors in this image represent higher resistivity and the cooler colors represent lower resistivity. An approximate scale is shown at the right.

in the rock formations having resistivities of 600 to 1100 ohm-meters, based on a known water table elevation near the easternmost survey sites. The lower resistivities, at 500 m amsl and below, beneath the central Saddle region, were more problematic: resistivities in the 5 to 10 ohm-meters are usually associated with basalts saturated with sea water but, because these rocks were well above sea level, seawater saturation appeared unlikely. Hence, it was thought that the lower resistivities were associated with either clay-rich formations or hydrothermally altered formations, or with deep thermal activity. In order to confirm the presence of a shallow aquifer that was suggested by these resistivity surveys, a water test hole, PTA-1, was drilled immediately north of the survey site 4PT1 (in Figure 2). The presence of high elevation water was confirmed at that location and continued drilling into the underlying rocks encountered formation temperatures of ~140°C and a temperature gradient of approximately 165°C/km.

Of relevance to the present investigation, Figure 2 also shows low resistivity values east of the central Saddle region, centered on stations HH002 and HH003 that were located on Department of Hawaiian Home Lands. Based on our findings in the test drilling conducted near the 4PT1 location, the lower resistivities beneath the DHHL lands are also inferred to be associated with increased potential for a geothermal resource in this region.

Field Surveys

In an effort to determine how extensive that thermal activity may be below the DHHL properties in this area, the present survey temporarily installed 10 Magnetotelluric stations and 60 Audio Magnetotelluric stations along four transects across the Mana/Keanakolu Road that extends from the Mauna Kea Observatory Access Road around the mid-level elevations of Mauna Kea toward Kohala Volcano to the north (Figures 3 and 4). A total of four transects were run: the initial MT transect (stations MR001 to MR011 in Table 1) spanned the entire survey area; the AMT transects spanned sites ZMR003 – ZMR027, ZMR028 – ZMR044, and ZMR045 – ZMR057, respectively. Sites designated ZMR213, ZMR214, ZMR219, ZMR236, ZMR245, and ZMR254 were repeat measurements of individual sites to collect additional data where initial data collections were affected by interference or adverse field conditions.

The MT measurements collect electromagnetic data at very low frequencies, a few cycles per second down to 1000 seconds per cycle, and hence data collection periods extend over two to three days at each location. (A more detailed discussion of the field procedures are presented in Appendix A.) The AMT signals of interest are of much higher frequency and we are able to collect adequate data for our survey needs at each location over a period of several hours. The data recovered from the instruments include measurements of the electrical potential (voltage) variations measured along N-S and E-W measurement legs, as well as the electric and magnetic field variations along the N-S, E-W, and vertical orientations. An example of the raw data is presented in Figure 5, below.

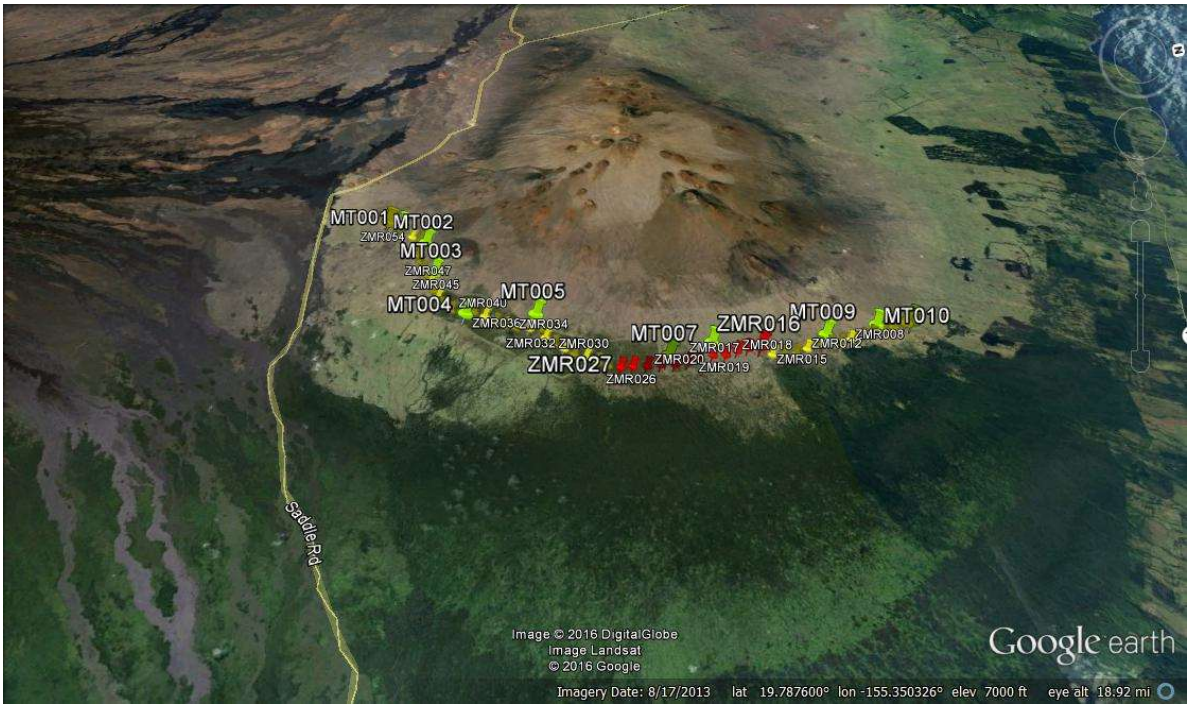

Figure 3. Satellite image, looking west, of the east flank of Mauna Kea showing the locations of the MT (designated MT 001 through MT 010) and AMT survey stations (designated ZMR001 through ZMR054). The MT stations are shown in green and the AMT stations shown in yellow and red. The stations shown in red correspond to a section of the survey that shows low resistivity values that may reflect evidence of current or past thermal activity within this region. A full page image is provided in Appendix A.

Data Analysis

The antenna coils that collect the electromagnetic signals are extraordinarily sensitive and can receive interfering noise generated by lightening discharges occurring at distances of several thousand kilometers, by variations in high tension power line currents at distances of several tens of kilometers away, and even by electrical signals generated by large amplitude ocean waves. Likewise, the electrical potential measurements can be affected by variations in the ambient ground temperatures as well as environmental conditions like rainfall. Hence, the raw data need to be intensively processed in order to filter out extraneous signals that are irrelevant to our measurement objectives. After the data processing, we are able to compute an apparent resistivity of the subsurface below that station as a function of frequency (Figure 6, below). Error bars are shown on the apparent resistivity points where the error exceeds the size of the data point; where no error bars are shown, the error of the value is less than the size of the data point. Because the frequency of the electromagnetic signals affects the distance of rock through which the signals can pass, the apparent resistivity as a function of frequency can be converted to an apparent resistivity as a function of depth below the ground surface to yield an apparent resistivity profile below each station (Figure 7, below). These apparent resistivity curves show a modeled resistivity versus depth based on the data collected at each station. The determination of the modeled resistivity with depth is done by an iterative process where

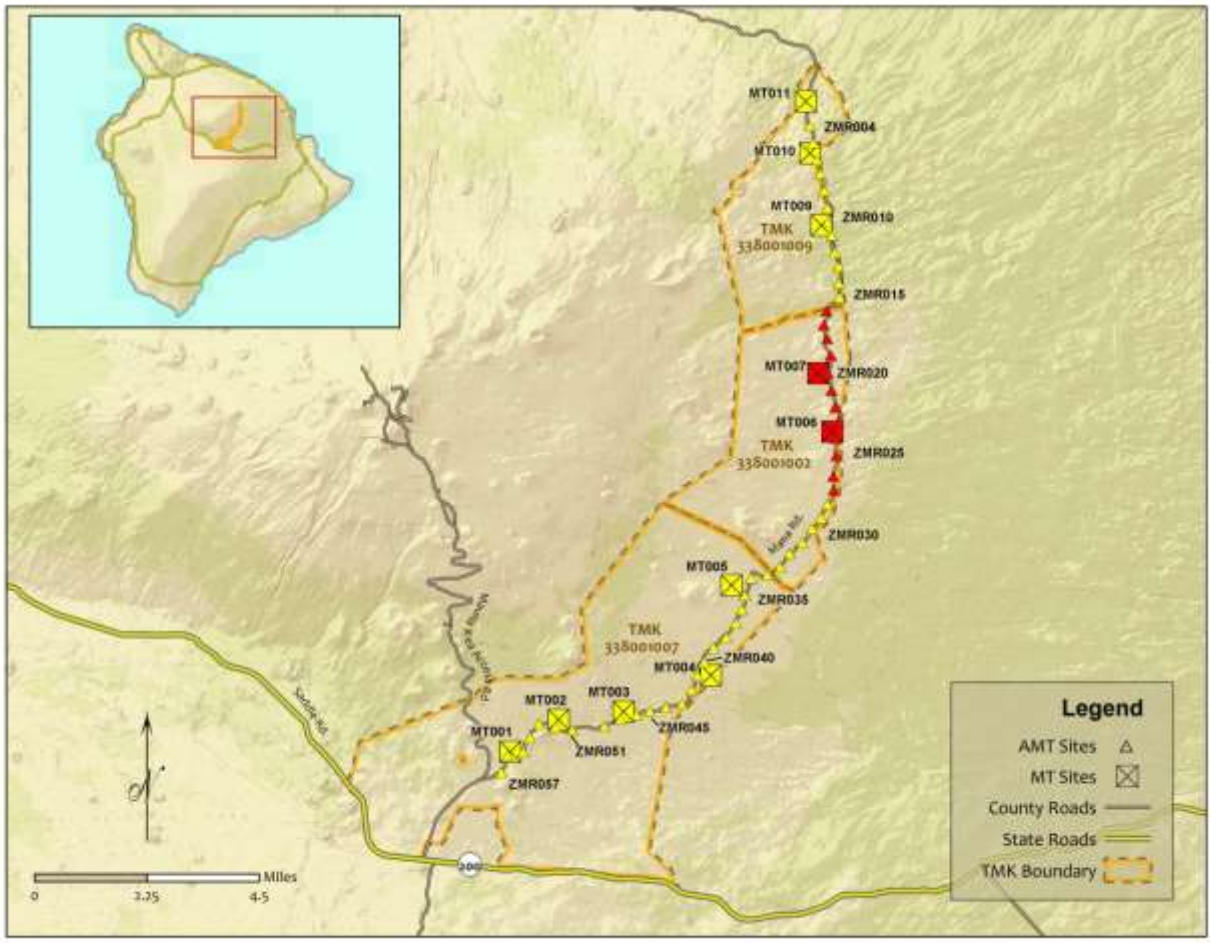

Figure 4. Map showing the locations of the AMT and MT stations for the DHHL survey transects. Also shown are State Highway 200, Saddle Road, the Mauna Kea Access Rd., and Mana Rd. as well as the Tax Map Key boundaries for the DHHL properties surveyed.

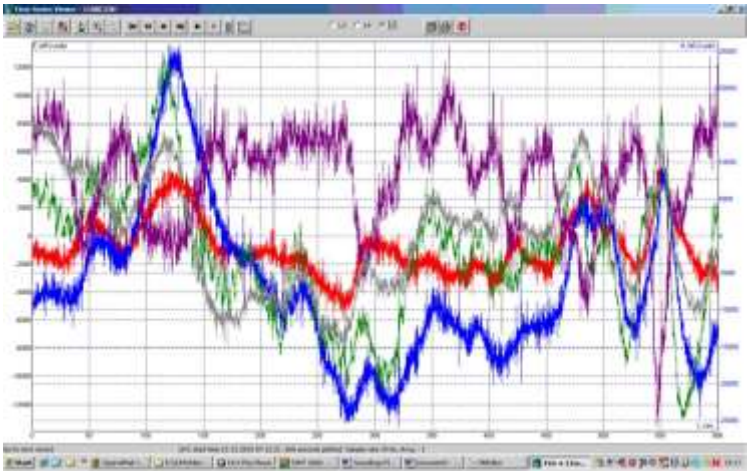

Figure 5. Raw electrical potential and electromagnetic (radio wave) amplitude measured over a 600 second interval at one of the Mana Rd. stations.

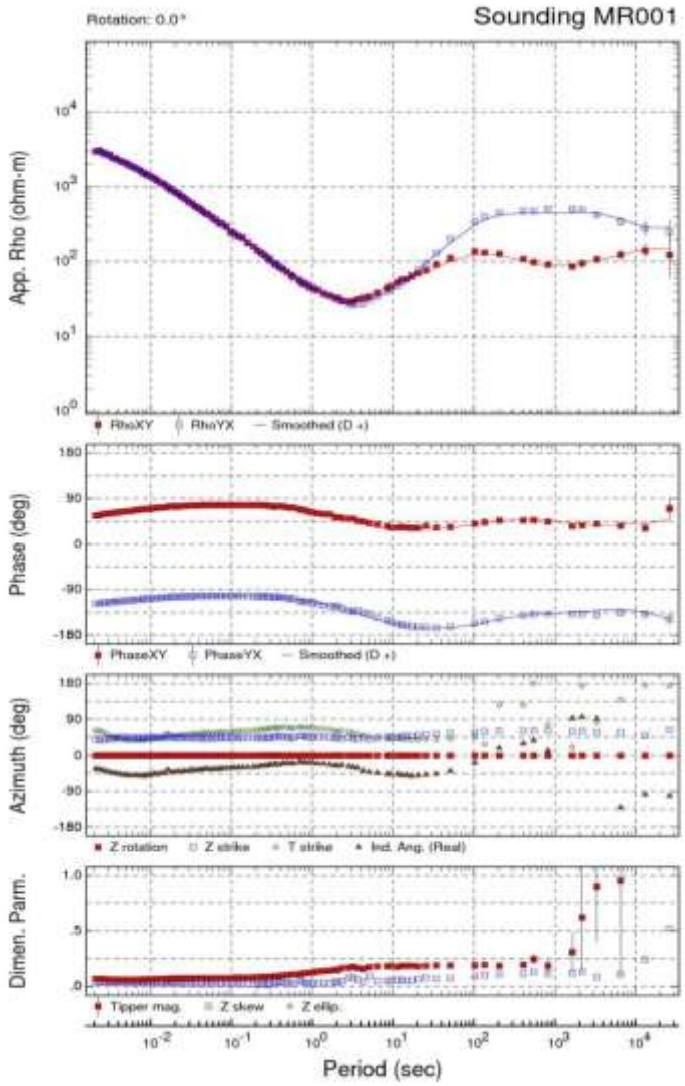

Figure 6. Showing the result of the processed electrical potential and electromagnetic signals collected at Station MR001 along the Mana Rd. The upper curve shows the apparent resistivity as a function of the frequency of the signals collected. The second plot shows the relative phase of the electrical and magnetic fields as a function of frequency; the third curve shows the primary orientation (azimuth) of the electrical and magnetic signals as a function of frequency; and the lowest plot is of dimensionless parameters computed from the relationships of the electrical and electromagnetic signals. In all four plots, the error of the individual parameter is plotted as a vertical line if the error is greater than the size of the plot symbol; otherwise, the error is smaller than the unit size of the plot symbol. The apparent resistivity and phase data are used in the AMT computations whereas all of these parameters are used in the MT modeling computation of the electrical resistivity with depth shown in the following figures.

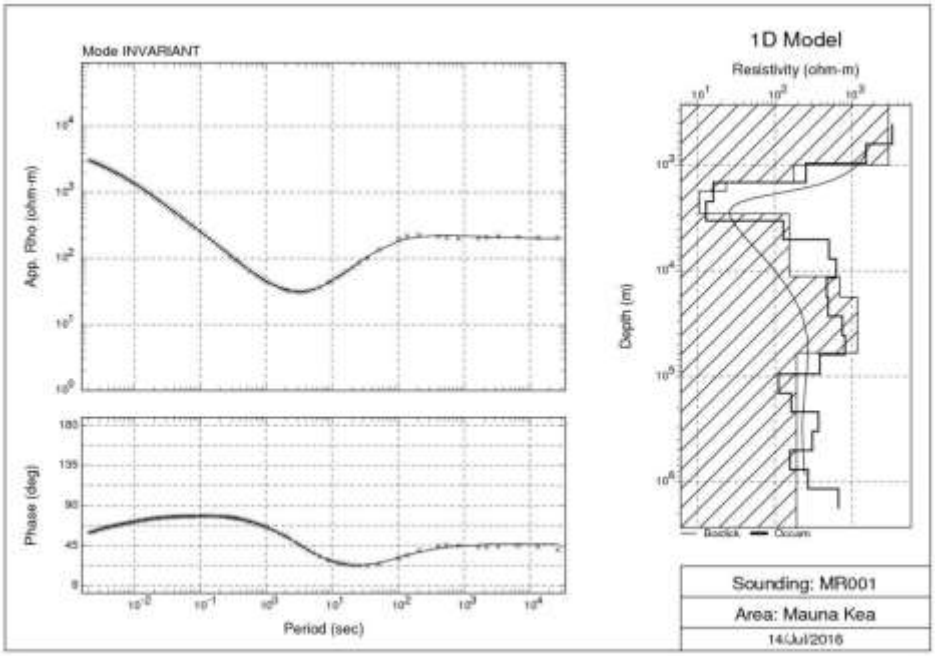

Figure 7. Presenting a 1-D model of the computed resistivity versus depth profile below MR001 measurement station. The graphics on the left show apparent resistivity verses the period of the signals processed (period is the inverse of frequency). The graphic on the right shows the computed resistivity versus depth, in meters, presented on a log scale (the uppermost division is 1000 m depth, the second division is 10,000 m depth).

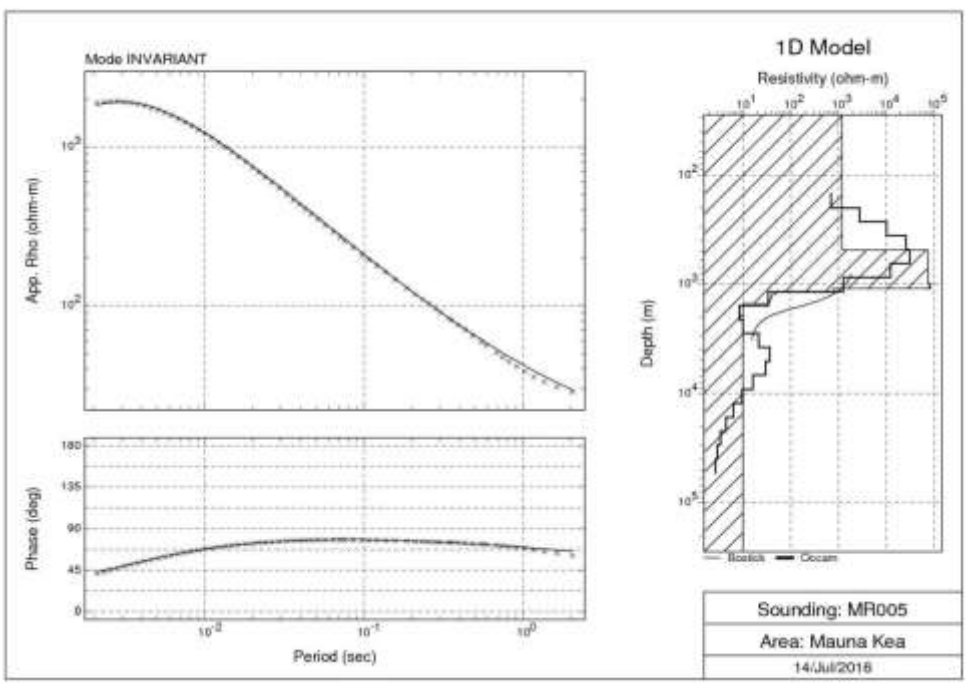

Figure 8. Presenting a 1-D model of the computed resistivity versus depth profile below MR005 measurement station. Comparing the modeled resistivity with depth between Station MR001 and MR005, it is apparent that the computed resistivity curves are quite different with the former showing a reduced resistivity at a shallower depth that remains low to depths much greater than those computed for Station MR001.

the resistivity and thickness of each layer is varied systematically to a point of model convergence. Convergence is assumed when the difference between model run output varies by less than 5%, or after 100 iterations of the model computation; where data are affected by extraneous noise signals or other site conditions and 100 runs is unable to arrive at a 5% error, model results with up to 10% error can be used, but larger modeled error outputs are discarded from the survey sequence.

In the model output for station MR001, the resistivity is computed to be ~3000 ohm-meters that declines to less than 2000 ohm-meters at a depth of approximately 700 m, and then to about 300 ohm-meters at a depth of ~1000 m and then drops to about 20 ohm meters at a depth of 1500 m, but then rises again at depths of 3000 m. Comparing the MR001 model with that for Station MR005 (Figure 8), we see distinct differences in the computed resistivity profile: the shallow resistivity is significantly lower, about 1000 ohm-meters, and remains low until a depth of several hundred meters. It then rises over a narrow depth interval but falls off again at 1000 m bgs and remains very low, ~10 ohm meters, from that depth to the total depth of penetration of the signals collected. These results indicate that the computed resistivities deep beneath Station MR005 are significantly lower than those below Station MR001 and hence have a higher likelihood to be associated with a potential geothermal resource.

The 1-D models, when plotted together can give us a sense of how the resistivity with depth varies along the Mana Road on the east flank of the island, but the computed resistivity for each station relies on the data from that station alone. However, more sophisticated modeling programs are able to, in effect, integrate the data collected at multiple stations in the sequence of transects to yield a more accurate picture of the resistivity along the survey track. For this type of analysis, we are using the WinGlink software package licensed from Schlumberger, one of the large exploration and oil-service companies serving the energy and exploration industries. That software allows us to integrate the MT and AMT measurements from multiple stations to compute the resistivity distribution below (and adjacent to) the transects over the entire interval surveyed. That distribution is depicted in Figure 9, below (We note here that the resistivity color scale produced with this software is reversed from that used in the Humu'ula Saddle cross section: here warm colors are used to show conductive formations and cold colors reflect higher resistivities). In that resistivity model we see that surface resistivities are moderate to high (2500 to >4000 ohm-meters) down to depths of ~1000m but then begin to fall off rapidly below that depth down to and somewhat below sea level, but then rise again at increasing depth. The obvious exception to that broad trend is in the central region of the survey: between stations ZMR027 and XMR016, there is a broad region of conductive material that begins at somewhat higher elevations above sea level and extends to depths of about 5 km

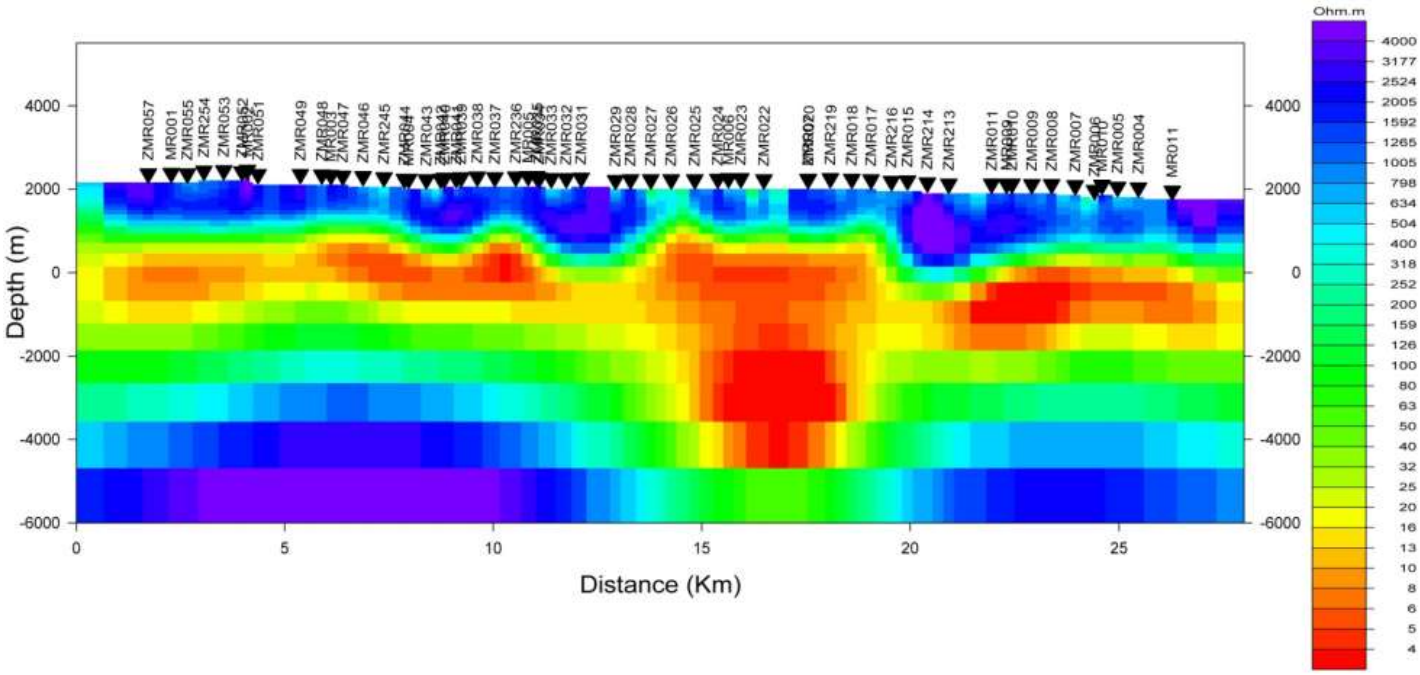

Figure 9. A resistivity cross section through the eastern flank of Mauna Kea along the path of the Mana Road. The station locations are shown along the top of the modeled surface with the AMT station locations designated as ZMR0XX and the MT stations designated as MR0XX. On the left hand axis, the elevations are shown, in meters, relative to sea level. The color scale (in ohm-meters) is shown to the right; it should be noted that the scales here are the reverse of those used in the Humu'ula transect: warm colors are conductive, cold colors are resistive. Full page images of the model outputs are provided in Appendix A.

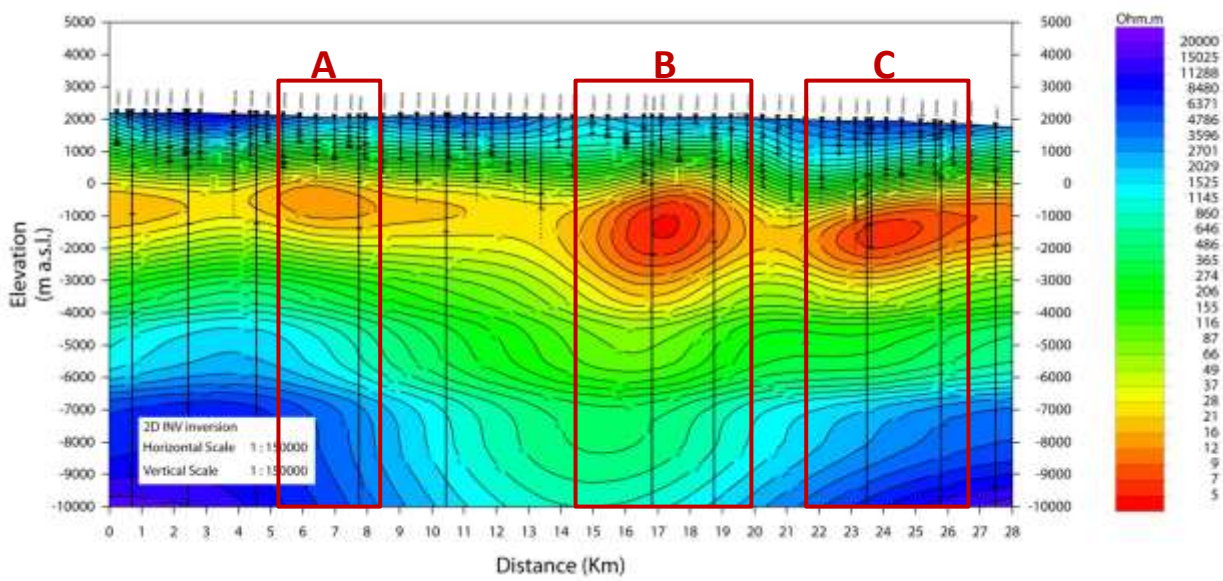

Figure 10. Showing a 2D modeling inversion of the resistivity distribution along the eastern flank of Mauna Kea using the more highly refined data set. The vertical black lines show the inferred depth of penetration of the MT and AMT soundings below each station. The vertical and horizontal scales are in meters and km, respectively, as in Figure 9, but the depth of modeling is somewhat deeper in Figure 10.

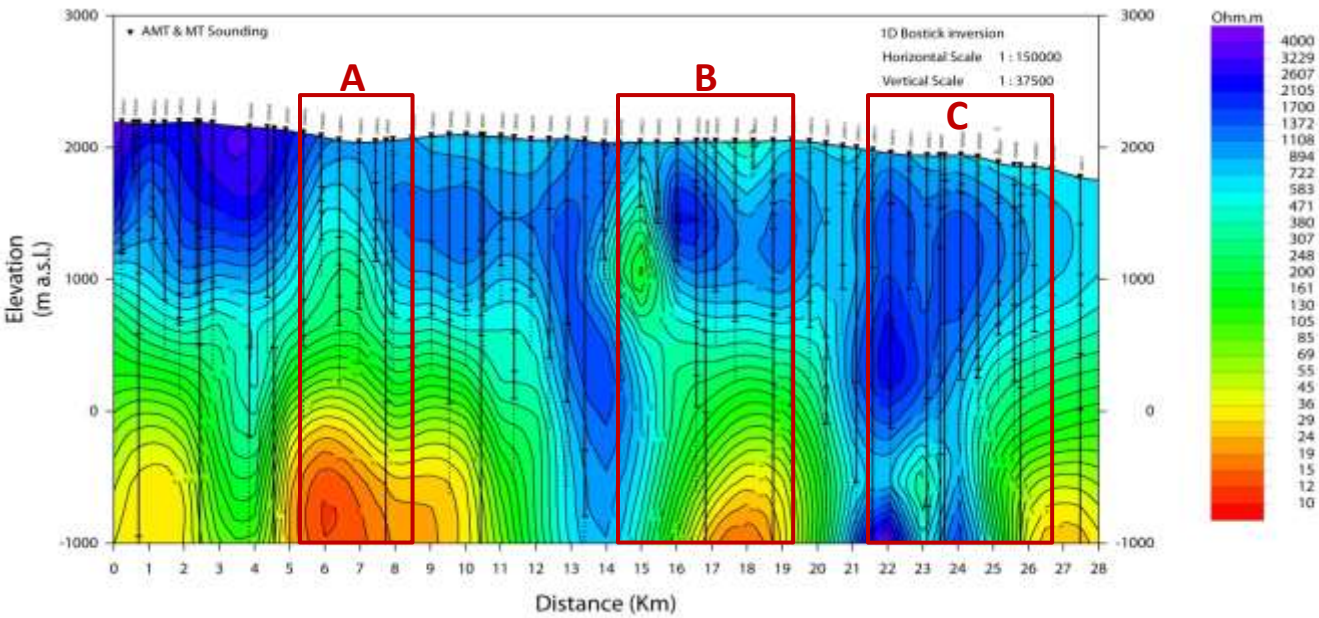

Figure 11. Showing a contoured 1D model of the survey data. In this image we show the model output only to a depth of 1000 m below sea level in order to gain more detail on the resistivity distributions at depths that can be economically drilled.

below sea level. To provide a sense of the location of this region along the Mana Rd. transects, Figures 3 and 4 show the sequence of stations spanning the low resistivity interval in red.

As noted previously, the analysis of the data is an iterative process where we perform initial modelling runs and then return to the data and further process it to yield more detailed and/or a finer grained image of the resistivity distribution over the area surveyed. Figure 10 presents an image of the 2D model for the transects using the more refined data sets. The overall resistivity distribution in Figure 10 is similar to that in Figure 9 but shows more detail and smoother resistivity variations than the earlier modeling results. We note here that, even though the 2D model is considered to be more reliable overall than the contoured 1D models, there is significant detail lost in the resistivity distributions due to the averaging effects incorporated into the 2D modeling. Hence, we also present a contoured 1D model in Figure 11 that can provide more detail on the resistivity distributions at a finer scale and to a shallower depth than the 2D model. Although the overall resistivity distributions in the 1D image are similar to the 2D model, it is clearly possible to distinguish smaller scale resistivity distributions in the shallow subsurface.

Interpretation

Our interpretation of the resistivity distribution along the survey line follows the pattern applied to the Humu'ula Saddle transect: the higher resistivities (cooler colors, resistivity >2000 ohm-meters) are assumed to correspond to unsaturated Mauna Kea basalts; the moderately conductive formations (300 to 1000 ohm-meters) are likely to correspond to freshwater saturated basalts; and the lowest resistivities may reflect rocks saturated with thermal or saline waters. There is, however, also a clear possibility that the lower resistivities may be associated with clay-rich rocks that have been hydrothermally altered at some point in the past.

One caution on the interpretation of the computed resistivities is that, in the present survey, we were unable to include a station with a known water table that we could use as a point of reference for interpretation of the resistivity distributions modeled. However, the modeled resistivities are not considered unreasonable for the ground being surveyed: this area of Mauna Kea is draped with thicker soils and ash; it currently receives significantly more rainfall than the central Humu'ula Saddle region; and, during its geologic evolution, it has been exposed to higher rates of rainfall, and more intense weathering. Hence, subsurface structures can be expected to have overall lower resistivities than were found beneath the central Humu'ula Saddle survey stations.

There are three regions within the survey area where conductive formations, having resistivities less than 100 ohm-meters, are present well above sea level: these regions are delineated in Figures 10 and 11 in boxes labelled A, B, and C. As noted above, lower resistivities can be associated with rocks saturated with seawater (or brackish water); however, the presence of these low resistivity layers above sea level and more than 20 km from the shoreline, strongly suggests that this source for the lower resistivities is unlikely. Hence, we believe that the observed resistivity within each of the labelled boxes is the result of current thermal activity that has lowered resistivity directly, or is the result of previous thermal activity in the past that has produced secondary alteration and clay deposition that has reduced the formation resistivity. The low resistivity zone within Box B is of particular interest for several reasons: at increasing depths the resistivity continues to drop to values that would be consistent with substantially elevated temperatures; the overall shape of the anomaly, as delineated in Figures 9 and 10 is suggestive of a deeply rooted structure; the surface topography of Mauna Kea, as well as the off-shore bathymetry to the east of this section of our survey line is consistent with a possible rift zone of Mauna Kea. We note that the presence of an East Rift Zone of Mauna Kea, similar to those of Mauna Loa and Kilauea, has long been debated. Even though the general topography of the east flank of Mauna Kea suggests that a rift zone may have been present during the shield-building stage of Mauna Kea's formation, the later stages of alkalic volcanism on Mauna Kea has largely obscured any other surface expression of a rift zone

(e.g. vents, linear fracture systems, etc.) in this area. Further, research conducted on a submarine ridge extending offshore of Mauna Kea's east flank recovered data on lava chemistry that suggested that the ridge was composed of lavas from Kohala volcano that further challenged inferences of an east rift zone. These geophysical soundings provide the first modern data that a rift zone developed in this region during Mauna Kea's growth. We believe that the shape of the conductive feature, in particular the much greater depth of the conductive zone to >5 km, as compared to the shallower extent of the other conductive zones along the survey line, further supports the hypothesis that this is a buried rift zone. The presence of a rift zone in this region would indicate that, similar to the Kilauea East Rift Zone, magma was injected into this region and that a geothermal resource may have been present, or may still be present here.

The interpretation of the broader conductive features, outlined in boxes designated A and C in Figure 10, that extend north and south of the central conductive formation is less certain. In their current state, the modeling results of the data show most of the conductive layer at and below sea level. At these elevations, there is an increased likelihood that the conductive formations are simply ambient temperature basalts that are saturated with seawater since the computed resistivities are consistent with those of seawater saturated basalts. However, given our recent observations regarding the hydrology of the interior of the island, with fresh groundwater being present at high elevations, we might reasonably expect seawater to be displaced to substantial depths beneath the high elevation fresh groundwater found within Mauna Kea. If this is in fact the case, then the conductive features observed near sea level along the survey line could potentially be associated with thermal water being discharged from the still cooling central dike complex of the mountain. We note too that there are sequences of cinder cones at higher elevations on Mauna Kea above both of these features that could mark an intrusive sequence that extends down the flank toward these conductive features.

Analysis of conductive features as they are depicted in the 1D model of Figure 11 also provides additional insights into the heat distribution. As noted above, the 2D analysis tends to average the electromagnetic effects of resistivity distributions over a broader area whereas the 1D model more clearly differentiates local effects from those more distant from each station. In the 1D model, there is a suggestion that the low resistivity formations may be shallower in the conductive feature outlined in box A whereas the low resistivity formations may be deeper in B and C conductive formations. The upward extensions of moderate resistivities, in the range of a few hundred ohm meters, to depths of less than 1000 m may also be indicating more modest temperatures at these depths. This inference is supported by our observations of subsurface temperatures of a few 10's of degrees Celsius above ambient at shallow depths in the KMA-1 test hole drilled on the western flank of the Saddle at Keamuku (Thomas, unpublished data).

Ancillary Note on Shallow Resistivity and Groundwater Potential

Although the primary purpose of the data collected during the current survey was to evaluate the geothermal resource potential for this region, the data also provides insight into the prospect of identifying high level groundwater resources along the survey line. Based on the resistivity surveys conducted across the Humu'ula Saddle described above, we expect that water saturated formations in this region to have resistivities in the range of a several hundred to about 1000 ohm meters. Figure 11 identifies several areas along the survey line where shallow resistivities fell within this range: in the interval of the survey designated by box A, there is a "ridge" of conductive formation that extends quite close to the surface with resistivities in the 300 to 700 ohm meter range; further north, between boxes A and B, there is a pocket of resistivity that falls within the range of 700 to 900 ohm meters, and within box B are formations ranging as low as 400 ohm meters. These shallow, low resistivity, formations would have the highest potential for encountering a groundwater resource at shallow depths.

The nature of the aquifers here is, however, somewhat uncertain: the results of our exploratory drilling work in the Saddle region demonstrated that both perched aquifers, of significant thickness, as well as dike impounded aquifers were present within the central and western Saddle region. With the higher rates of rainfall on the eastern flank of Mauna Kea, there is a significant likelihood that both of these aquifer types would be present along the track surveyed in the current study. Development of a water supply either by drilling, or by tunneling along the top of perching formations (similar to water tunnels at Pahala in the Kau District), could prove beneficial to the lessees of the Hawaiian Homes land surveyed.

Assessment of Resource Potential

The current modeling results of the MT and AMT data collected along the Mana Road transects on the upper slope of Mauna Kea has provided us with inferred resistivity distributions that are suggestive of as many as three geothermal prospects on the east flank of the mountain. The lowest overall resistivity observed in the transect is within the central low-resistivity region designed B; this lower resistivity can be interpreted to reflect the greatest likelihood of encountering higher temperatures but the non-uniqueness of the resistivity-temperature relationship, and the possibility of seawater intrusion into this deeper formation, would nonetheless have to be considered. The association of this low-resistivity feature with an inferred Mauna Kea East Rift Zone would suggest that a borehole into this section of the survey transect would have the greatest potential for encountering a viable geothermal resource.
Our results are interpreted to indicate that the southern low-resistivity feature, designated A in the above figures, would be the next most likely thermal source and the northern low-resistivity feature would, based on the available data, be ranked the least likely to host a significant resource.

A quantitative estimate of the probability for a thermal resource can be approximated, using the methods of Ito, et al., (2016), but, because it would be based on the geophysical results alone, that estimate would have a high degree of uncertainty. When comparing the observed resistivities encountered in the Humu'ula Saddle survey (Pierce and Thomas, 2008) with those observed in the current surveys, there is a likelihood of about 40% to 50% of encountering a thermal resource in the lowest resistivity formations. The presence of an inferred rift zone through this region would raise that probability to a somewhat higher value, but the absence of data on shallow groundwater temperatures or chemistry in the area, as well as uncertainties about the volume of the formation involved, would reduce our confidence in that value to 50% or less.

It is not possible, using geophysics alone, to prove a viable geothermal resource; and the level of confidence one can place in the results of a single geophysical survey line is lower still. However, additional geophysical surveys could be performed that would increase the level of confidence (or the converse) in making a decision to invest the necessary resources into a deep exploration hole into any of these low-resistivity features. Our inference, based on the resistivity distributions and topographic evidence, of a Mauna Kea East Rift Zone is less than certain but additional resistivity surveys across the inferred strike of the postulated rift at lower and higher elevations on the east flank of Mauna Kea could provide strong supporting evidence of a substantial dike complex. Similarly, two or more gravity transects across the postulated rift would allow us to make a somewhat more informed estimate of the intrusive mass associated with the inferred rift zone and, from that, an approximate magnitude of the heat source available. Both surveys, if they provide encouraging results with respect to resistivity distributions and substantial intrusive volumes in that structure, would offer a higher level of confidence that a significant and potentially viable thermal resource is associated with the identified resistivity anomaly and that more expensive exploration options were justified.

Acknowledgements

A number of individuals have contributed to the work performed under this project. They include:

Dr. Erin Wallin, a Post Doctoral trainee, who managed the field program and performed the initial data validation;

Dr. Barry Lienert, who developed software for the processing and smoothing of the raw data signals;

Dr. Graham Hill, who performed the initial data processing and modeling under this project;

Mr. Herb Pierce, who conducted the final data refinement and modeling of the data;

Ms. Georgianna Zelenak, who assisted with the field program and data validation; and

Mr. Ikaika Villanueva and Mr. Damian Aguier who conducted the field installations of the survey stations and recorded field data.

References

Ito, G., N. Frazer, N. Lautze, D. Thomas, N. Hinz, D. Waller, R. Whittier, E. Wallin, 2016, Play fairway analysis of geothermal resources across the state of Hawaii: 2. Resource probability mapping, Geothermics, in press.

Pierce, H.A. and D.M. Thomas, 2009, Magnetotelluric and Audiomagnetotelluric Groundwater Survey Along the Humu'ula Portion of Saddle Road Near and Around the Pohakuloa Training Area, Hawaii, USGS Open File Report 2009–1135, 160 p.

Zohdy, A.A.R, and D. B. Jackson, 1969, Application of Deep Electrical Soundings for Groundwater Exploration in Hawaii. Geophysics, Vol. 34, No. 4, pp. 584-600.

Table 1. List of the MT and AMT stations for which measurements were made during the current survey. Stations designated MRXXX are Magnetotelluric stations whereas those designated ZMRXXX are AudioMagnetotelluric stations.

Station ID	Longitude	Latitude	Elevation (m)	TMK Parcel Designation
Transect 1				
MR001	-155.439	19.720	2180	380010070000
MR002	-155.424	19.729	2260	380010070000
MR003	-155.404	19.731	2138	380010070000
MR004	-155.377	19.741	2050	380010070000
MR005	-155.370	19.767	2106	380010070000
MR006	-155.338	19.811	2056	380010020000
MR007	-155.342	19.828	2049	380010020000
MR009	-155.340	19.871	1923	380010090000
MR010	-155.343	19.892	1905	380010090000
MR011	-155.344	19.907	1767	380010090000
Transect 2				
AMR003	-155.343	19.903	1770	
ZMR004	-155.343	19.900	1838	380010090000
ZMR005	-155.342	19.895	1851	380010090000
ZMR006	-155.341	19.890	1773	380010090000
ZMR007	-155.340	19.886	1887	380010090000
ZMR008	-155.339	19.881	1913	380010090000
ZMR009	-155.338	19.876	1913	380010090000
ZMR010	-155.338	19.872	1922	380010090000
ZMR011	-155.337	19.868	1924	380010090000
ZMR012	-155.336	19.863	1939	380010090000
ZMR013	-155.335	19.859	1927	380010090000
ZMR213	-155.335	19.859	1927	380010090000
ZMR014	-155.335	19.854	1952	380010090000
ZMR214	-155.335	19.854	1952	380010090000
ZMR015	-155.335	19.850	2000	380010020000
ZMR016	-155.339	19.846	1998	380010020000
ZMR216	-155.339	19.846	1998	380010020000
ZMR017	-155.340	19.842	2033	380010020000
ZMR018	-155.339	19.838	2042	380010020000
ZMR019	-155.338	19.833	2052	380010020000
ZMR219	-155.338	19.833	2052	380010020000
ZMR020	-155.339	19.828	2049	380010020000
ZMR021	-155.338	19.823	2040	380010020000
ZMR022	-155.337	19.818	2036	380010020000

ZMR023	-155.336	19.814	2055	380010020000
ZMR024	-155.337	19.809	2048	380010020000
ZMR025	-155.337	19.804	2033	380010020000
ZMR026	-155.338	19.798	2036	380010020000
Transect 3				
ZMR027	-155.338	19.794	2033	380010020000
ZMR028	-155.340	19.790	2033	380010020000
ZMR029	-155.342	19.786	2023	380010020000
ZMR030	-155.345	19.783	2045	380010020000
ZMR031	-155.348	19.779	2074	380010020000
ZMR032	-155.352	19.776	2057	380010020000
ZMR033	-155.355	19.772	2053	380010020000
ZMR034	-155.359	19.770	2072	380010070000
ZMR035	-155.364	19.769	2110	380010070000
ZMR236	-155.366	19.764	2101	380010070000
ZMR036	-155.366	19.764	2101	380010070000
ZMR037	-155.367	19.760	2082	380010070000
ZMR038	-155.369	19.756	2094	380010070000
ZMR039	-155.372	19.752	2077	380010070000
ZMR040	-155.376	19.749	2070	380010070000
ZMR041	-155.379	19.745	2058	380010070000
ZMR042	-155.381	19.741	2042	380010070000
ZMR043	-155.383	19.737	2035	380010070000
ZMR044	-155.386	19.733	2044	380010070000
Transect 4				
ZMR045	-155.391	19.732	2086	380010070000
ZMR245	-155.391	19.732	2086	380010070000
ZMR046	-155.396	19.731	2108	380010070000
ZMR047	-155.400	19.730	2124	380010070000
ZMR048	-155.405	19.729	2151	380010070000
ZMR049	-155.410	19.727	2155	380010070000
ZMR051	-155.420	19.726	2156	380010070000
ZMR052	-155.425	19.727	2220	380010070000
ZMR053	-155.430	19.728	2244	380010070000
ZMR054	-155.433	19.724	2230	380010070000
ZMR254	-155.433	19.724	2230	380010070000
ZMR055	-155.435	19.720	2177	380010070000
ZMR056	-155.440	19.719	2185	380010070000
ZMR057	-155.442	19.714	2172	380010070000

Appendix A

The purpose of a Magnetotelluric and AudioMagnetotelluric Survey Program

These geophysical survey techniques will allow us to better map underground geologic structures, water resources, and magmatic and hydrothermal systems. Current technology, called magnetotelluric surveys (usually referred to as MT and AMT), allow us to map the electrical conductivity of rocks at depths ranging from several hundred feet below the surface to as much as 20,000 feet below the surface. Because the electrical conductivity of geologic formations is the result of the type of rocks present, the presence (and salt content) of water in the rocks, and the temperature of the rock, the method can identify groundwater aquifers, distinguish between salt water and freshwater aquifers, and distinguish between different types of rocks and can even be used to map underground pockets of magma. With appropriately designed surveys, we can develop an image of the electrical conductivity similar to that shown in Figure 1 below; the warmer colors represent highly conductive rocks whereas the cooler colors represent more resistive rock formations. These surveys allow us to map the electrical resistivity of the subsurface to depths of four to six kilometers below the ground surface. Areas of highly resistive rocks (having resistivities more than several thousand ohm-meters) are likely to be dense and dry rocks with neither water nor useable significant heat present; regions with intermediate resistivity (several hundred to a few thousand ohm-meters) are likely to be less dense rocks saturated with freshwater; and rocks with low resistivities (a few to a few tens of ohm-meters) are likely to be rocks, at elevated temperatures, saturated with freshwater, or rocks at ambient temperatures saturated with highly saline (sea) water.

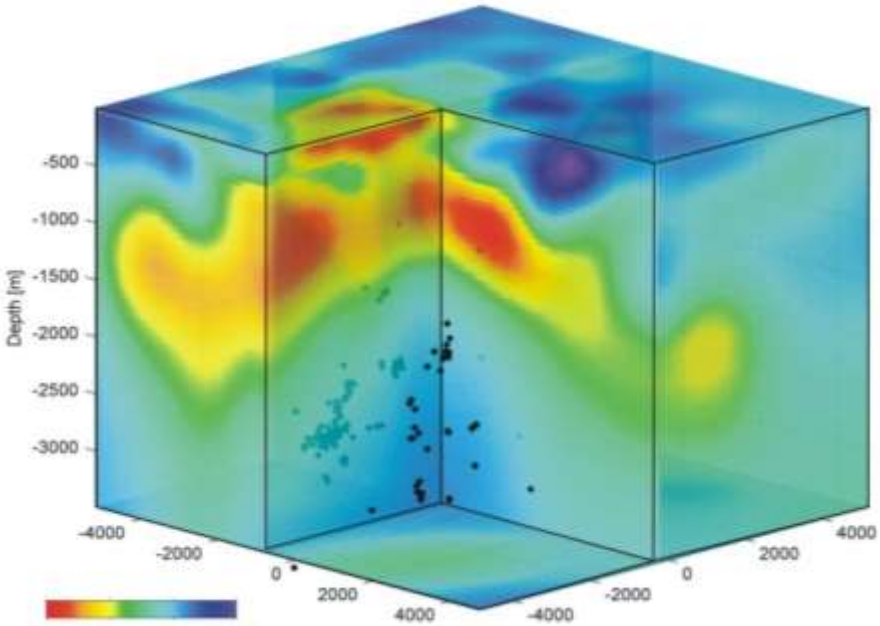

Figure 1. A computer-generated image of the electrical conductivity of subsurface rocks down to a depth of more than 10,000' below the ground surface. The blue and green colors represent more resistive formations where the rocks are not saturated with water while the warmer colors represent rocks where the pores are filled with liquid water and, as a result, are more electrically conductive.

Description of the field methods using
Magnetotelluric Surveys

Magnetotelluric surveys are considered a passive, non-invasive geophysical investigation. The measurements are called passive because the instruments measure naturally occurring, very low frequency, electromagnetic (EM) waves that penetrate into the earth. The instruments don't generate any EM signals or transmit any energy into the earth, they simply detect and record variations in the electrical voltage and EM signals that continuously pass into and out of the earth. The naturally occurring EM signals are similar to radio waves, but much lower power and frequency. They induce the telluric currents that flow within the earth that this technique measures. Analysis of the variations in the electric and magnetic signals enables us to determine the electrical resistivity of the rocks and to identify groundwater flow occurring at varying depths in the subsurface. Those measurements will also allow us to infer something about the types of rocks that are present in the subsurface, the water present in those rocks (whether salt or fresh), and their temperatures.

In order to perform a magnetotelluric survey, we use two (in some cases, three) antennas and four specialized ground-contact electrodes with each connected to a data recording system. The data system continuously records the voltage difference between the pairs of electrodes and records the magnetic wave signals received by the antennas. The antennas consist of an iron rod that is wrapped with many thousands of turns of fine copper wire, all encased in a fiberglass tube. They are designed to collect incoming natural signals that, depending on their frequency, penetrate to varying depths in the ground. The electrodes consist of a metal wire suspended in a sodium chloride (table salt) solution contained in a plastic cup with a porous ceramic disk at the bottom for electrical contact to the ground.

A photo of the antennas and electrodes, along with the recording box and the cables used is shown in Figure 1. When placed at a field station, the equipment is laid out similar to that shown in Figure 2. The electrodes and the antennas are laid out in a north-south and east-west configuration with the electrodes being separated by a distance of 100 m to 200 m (330' to 660') and the antennas separated by about 20 m (66'). A photo of a typical data collection station is shown in Figure 3. The data acquisition unit is housed in a weatherproof box and is powered with a conventional car battery. Once configured and data collection initiated, we would cover

the equipment with a tarp to further protect it from the weather and to reduce its visibility. Figure 4 shows the shallow trench in which the antenna coil is buried; Figure 5 shows the antenna after burial and ready to begin collecting data.

Figure 6 shows a typical electrode as it is placed in a shallow hole in the ground and prepared to collect data; for our surveys, we will place the electrode in a fabric bag that has been partially filled with hydrated bentonite clay to ensure good electrical contact with the ground. By using the fabric bag, we will be able to recover all the clay from the hole leaving nothing behind at the survey sites. Each of the electrodes and antenna coils are connected to the data collection box using the wire cables shown in Figure 1. The need to bury the electrodes and antenna coils is because of their extreme sensitivity; any type of vibration from wind or rain would produce electrical "noise" that would interfere with the signals we are trying to record. In areas where shallow trenching isn't feasible or is not acceptable, we can weigh down the antennas with sand bags to hold them in a stable configuration. Likewise, we will need to have the cables connecting the electrodes and antennas to the data acquisition box held in a stable configuration, and, in areas that are heavily vegetated, we may need to clear some vegetation to allow us to weight the entire length of the cables to the ground with sand bags or soil.

We have four sets of instruments allowing us to install up to four stations at one time. We expect to have each station in place for about three days to allow us to collect the data we need to perform our analysis. As an example, the measurement stations will be spaced at distances of 1600' to 3200' apart over the geologic structure we are surveying. Depending on the size of the area we are surveying, we may need to conduct measurements at as many as twenty to thirty locations; this means that we would need to relocate all four stations, five to seven times, at three-day intervals, in order to complete the survey. The field crew will restore each station site to its original condition, by filling in the electrode holes and the antenna trenches, as they remove the equipment.

The AudioMagnetotelluric stations are considerably less elaborate and require only a set of steel stakes, driven into the ground by about 20 cm, and a data collection box and 12 volt battery. A photo of a typical AMT station is shown in Figure 7.

Figure 1. This shows the individual instruments that are used in the survey. The orange box is the data recording unit; the black tubes to the left of the recording unit are the antennas or coils; the gray cylinders to the lower right of the recording unit are the electrodes; the small diameter tubes to the right of the electrodes will not be used in these surveys. The blue and the black cables will connect the coils and the electrodes to the data recording unit, and the laptop computer at the upper left is used to download the data from the recording box but is not left at the field station.

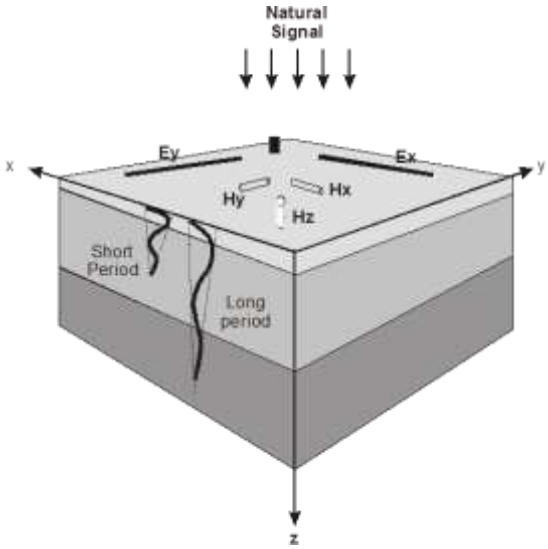

Figure 2. This shows how the instruments are laid out in the field. The electrodes, labeled as Ex and Ey, are set along a north-south and east-west alignment and are connected to the data acquisition unit; likewise, two of the coils (Hx and Hy) are laid out along a N-S and E-W alignment and a third coil (Hz), oriented in a vertical configuration, is sometimes used (the quality of the data from the vertical coil is often poor; we will have to conduct tests to determine whether we will use the vertical coil for our studies or not).

Figure 3. The data collection station consists of the data recorder, housed in a weatherproof box, along with a standard car battery to provide power for the recording system. We typically cover the station with a tarp to provide further protection from the weather and to make the station less visible.

Figure 4. Showing the shallow trench used to bury the antenna coil.

Figure 5. The antenna coil buried at the field site: once the coil is aligned and leveled in the trench, it is then covered with soil from the trench to stabilize it for the duration of the data recording interval; after the coil is recovered, we refill the trench with its original soil.

Figure 6. This is an image of a typical installation of an electrode for this type of survey. The mud at the bottom of the hole is a slurry of soil and bentonite clay that has been hydrated with fresh water to allow for good contact with the ground. For our surveys, we will place the electrode into a fabric bag with hydrated bentonite clay; the bag will be placed in the hole with some water and, at the end of the data collection interval, we will remove the bagged electrode and all the bentonite clay and refill the shallow hole with its original soil.

Figure 7. Photo of a typical deployment of an AMT station. The orange box is the data collection system with the standard 12 volt car battery providing power. The metal arches above the orange box are used in some environments where there is significant anthropogenic noise; for our surveys along Mana Road, these were not used.

Appendix B
Full Page Images of Transect Station Locations and Model Outputs

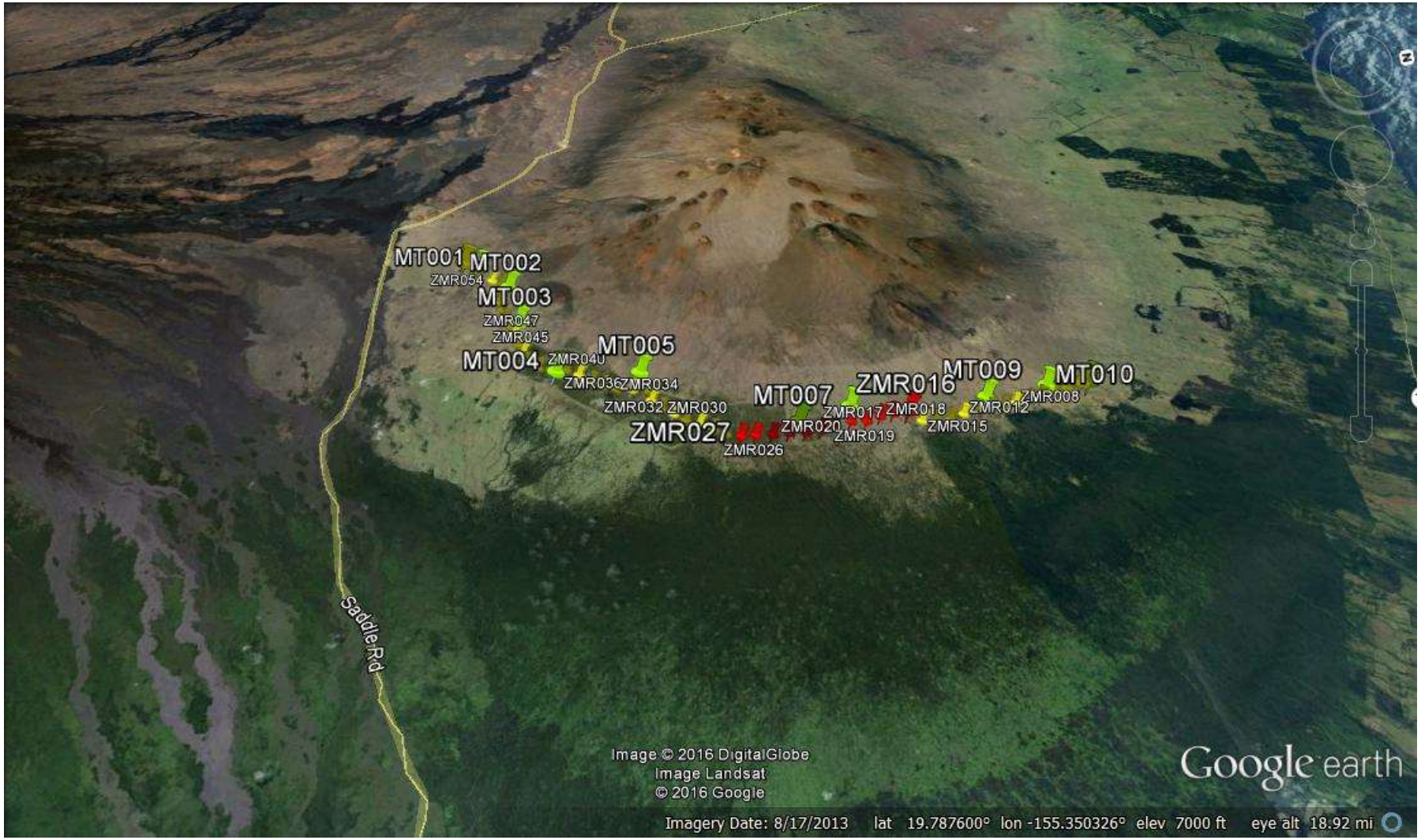

Figure 3. Satellite image, looking west, of the east flank of Mauna Kea showing the locations of the MT (designated MT 001 through MT 010) and AMT survey stations (designated ZMR001 through ZMR054). The MT stations are shown in green and the AMT stations shown in yellow and red. The stations shown in red correspond to a section of the survey that shows low resistivity values that may reflect evidence of current or past thermal activity within this region.

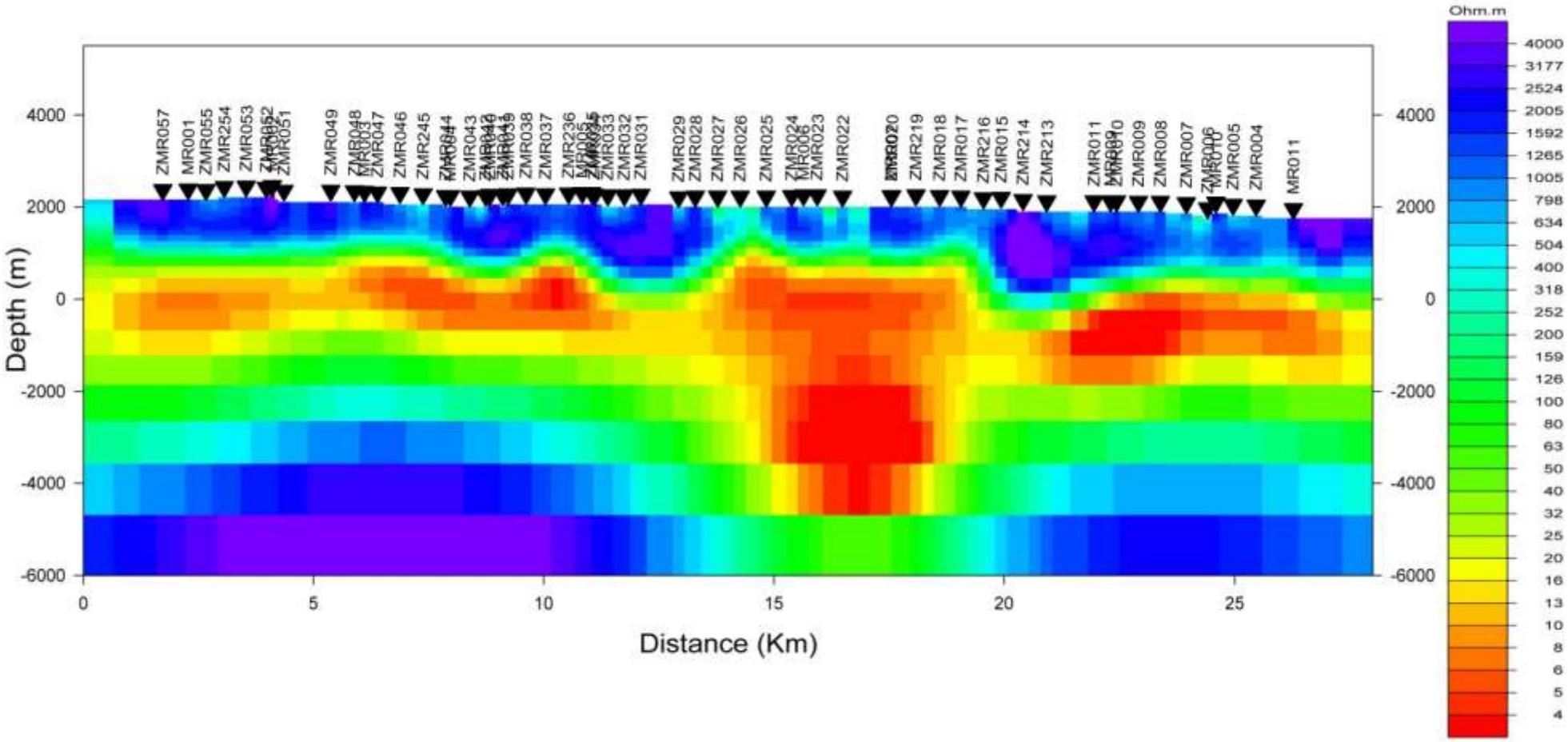

Figure 9. A resistivity cross section through the eastern flank of Mauna Kea along the path of the Mana Road. The station locations are shown along the top of the modeled surface with the AMT station locations designated as ZMR0XX and the MT stations designated as MR0XX. On the left hand axis, the elevations are shown, in meters, relative to sea level. The color scale (in ohm-meters) is shown to the right; it should be noted that the scales here are the reverse of those used in the Humu'ula transect: warm colors are conductive, cold colors are resistive. Full page images of the model outputs are provided in Appendix A.

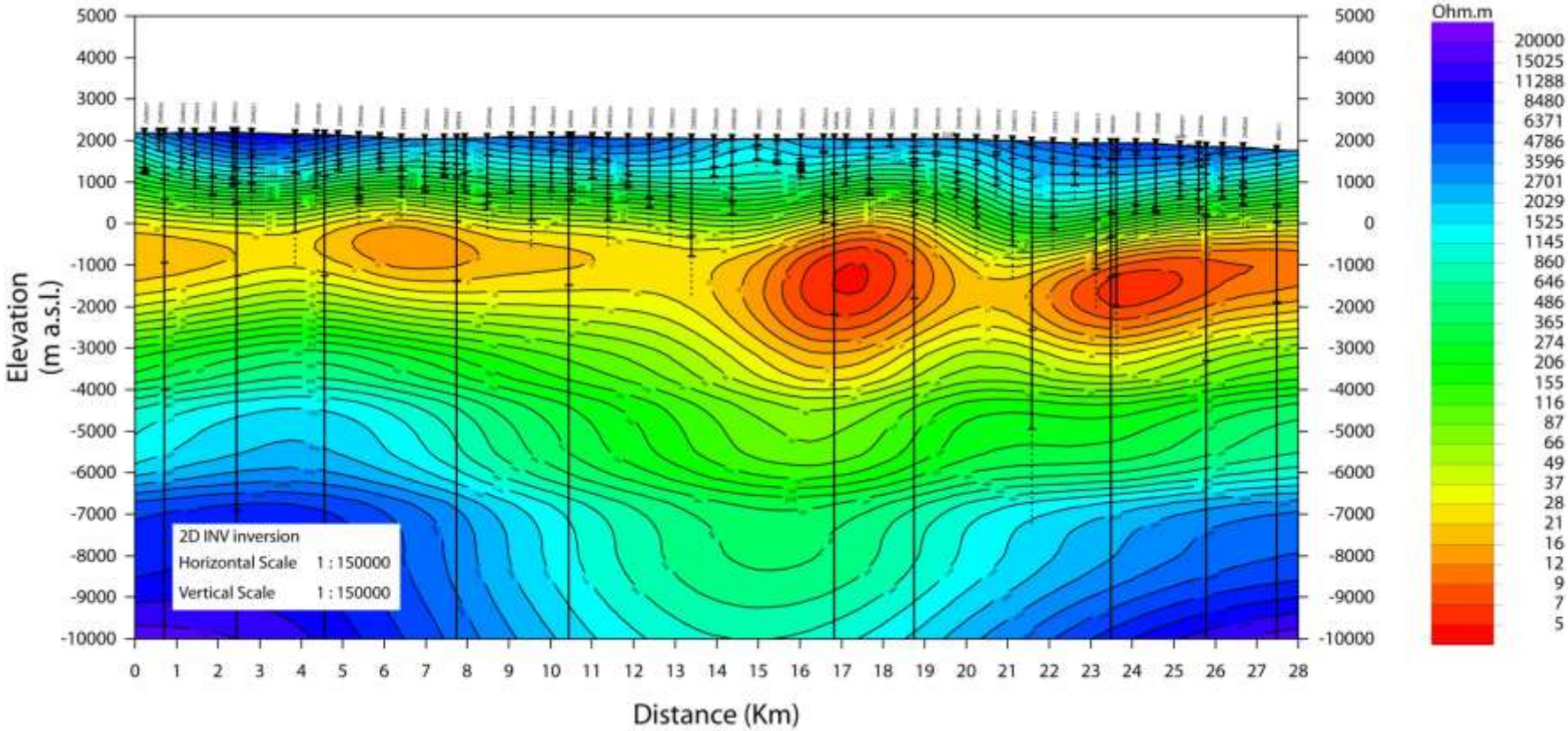

Figure 10. Showing a 2D modeling inversion of the resistivity distribution along the eastern flank of Mauna Kea using the more highly refined data set. The vertical black lines show the inferred depth of penetration of the MT and AMT soundings below each station. The vertical and horizontal scales are in meters and km, respectively, as in Figure 9, but the depth of modeling is somewhat deeper in Figure 10.

Appendix C

Plots of the Processed MT Data and 1D Apparent Resistivity Curves

Rotation: 0.0°

Sounding MR001

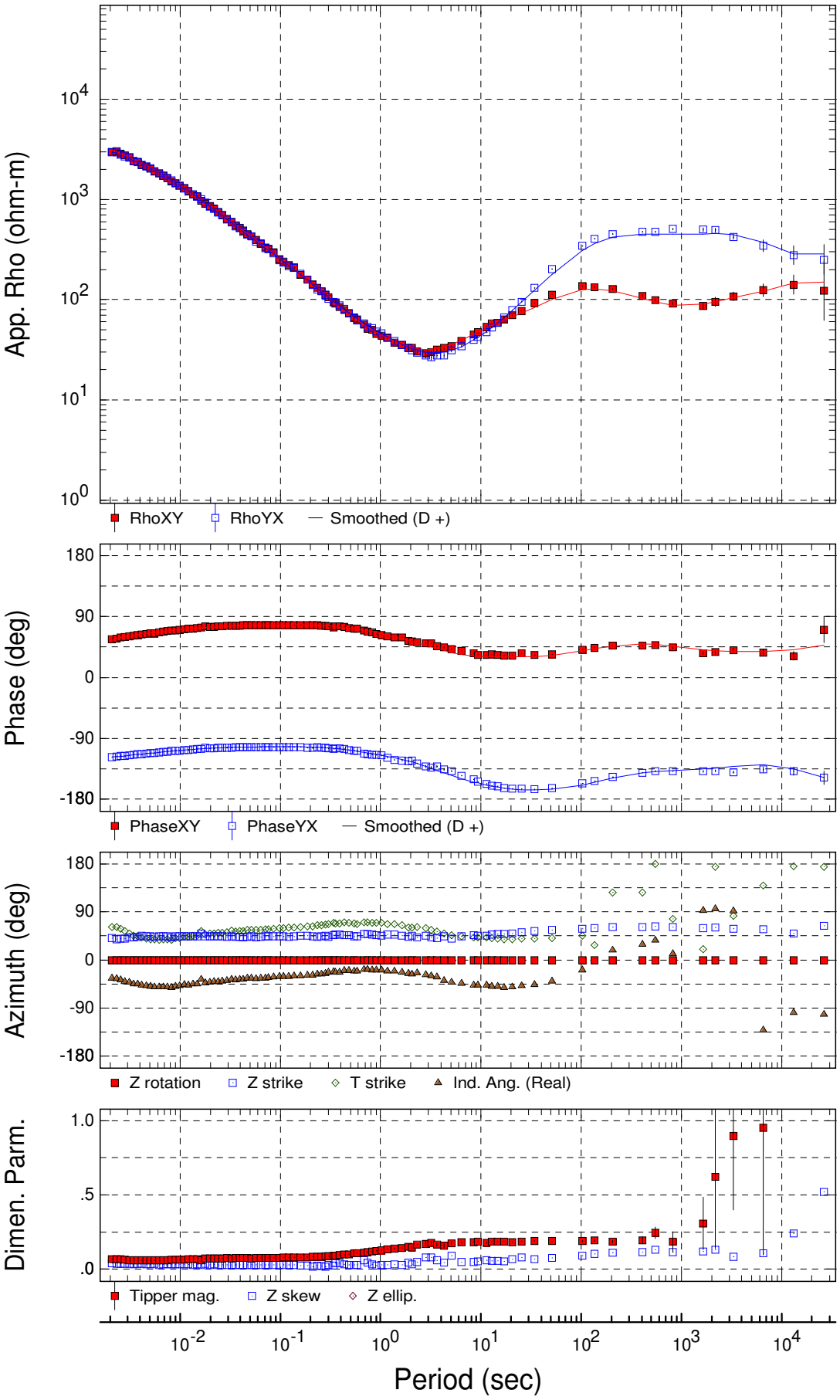

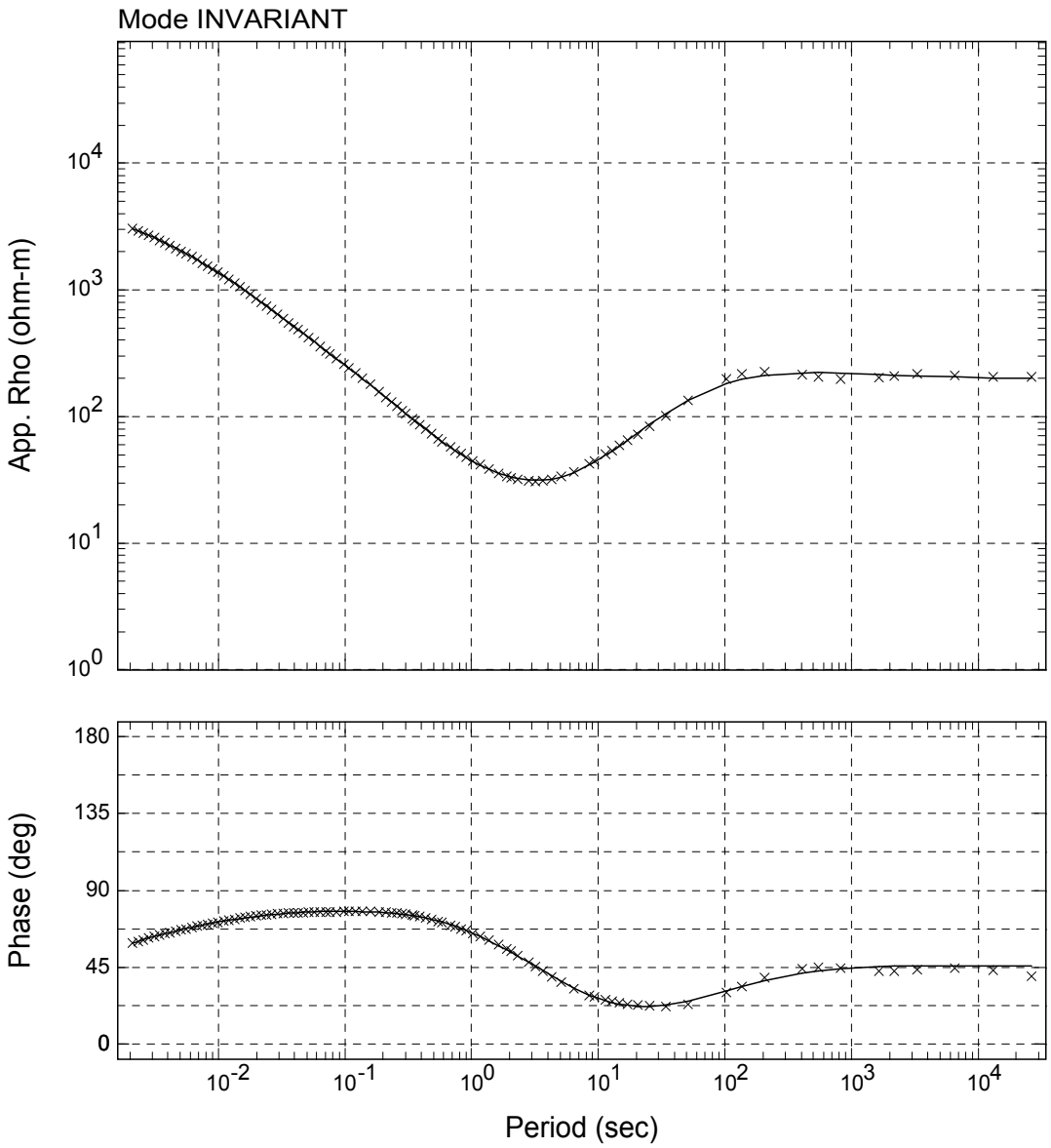

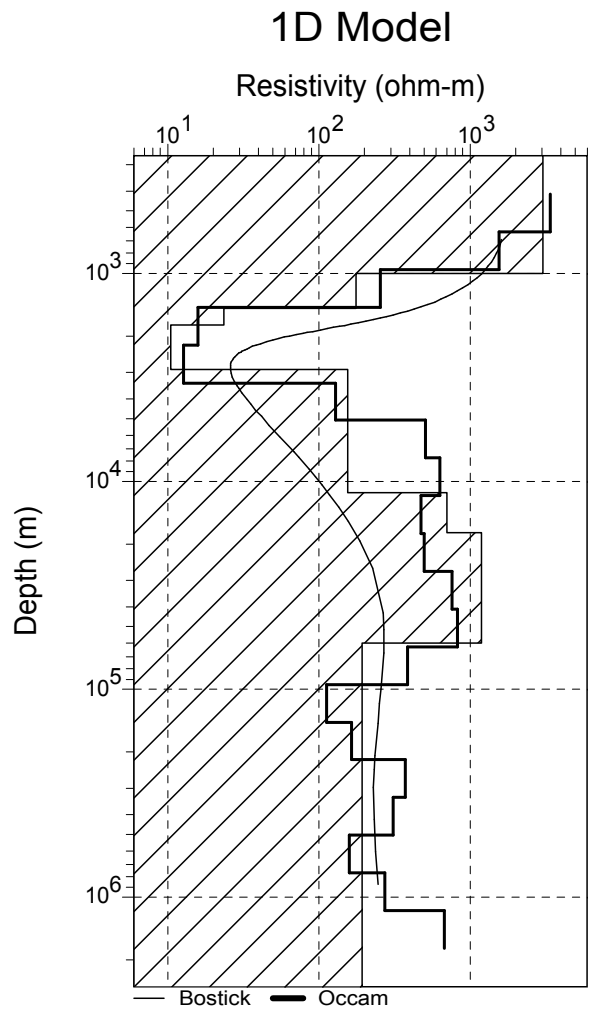

Sounding: MR001

Area: Mauna Kea

14/Jul/2016

Rotation: 0.0°

Sounding MR002

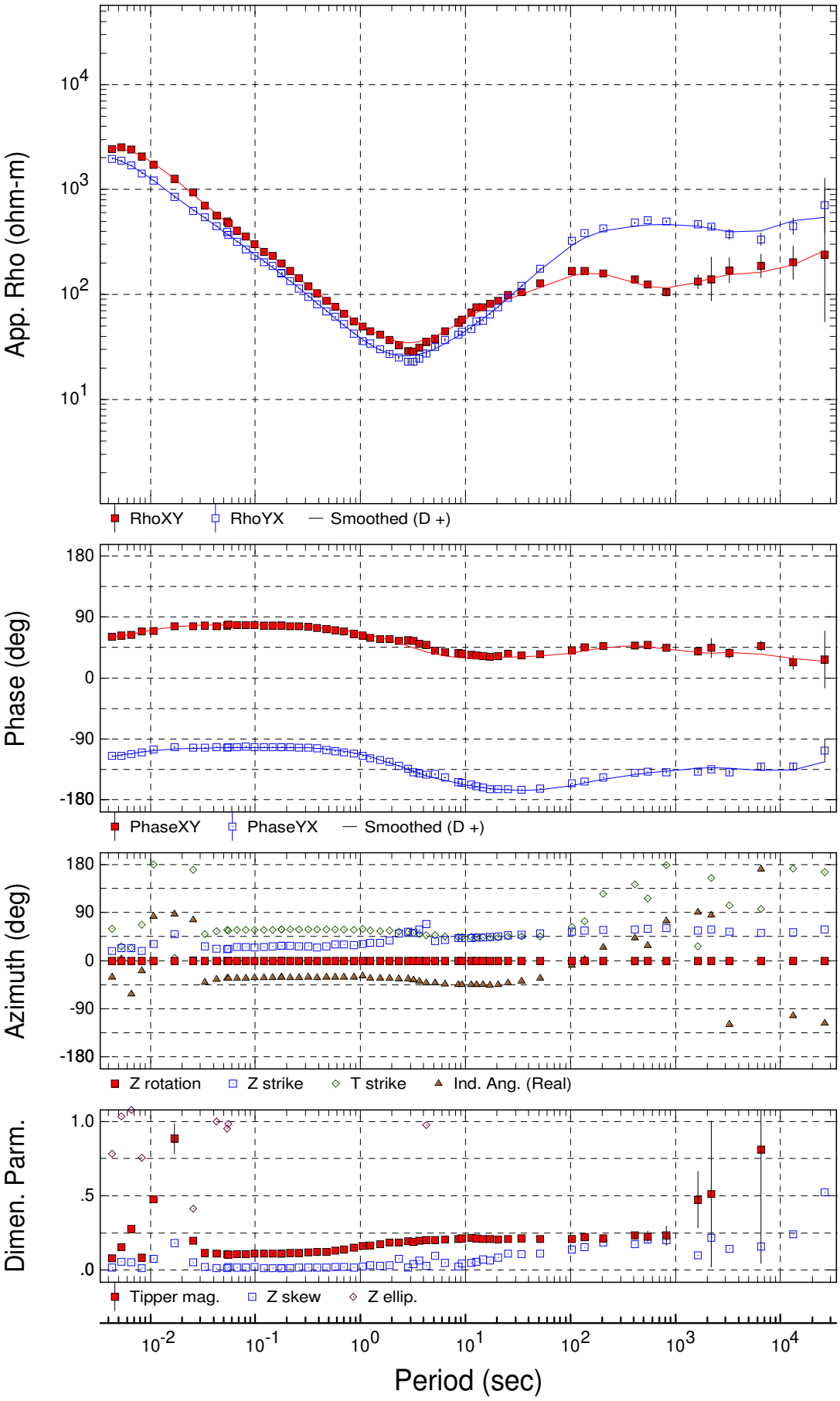

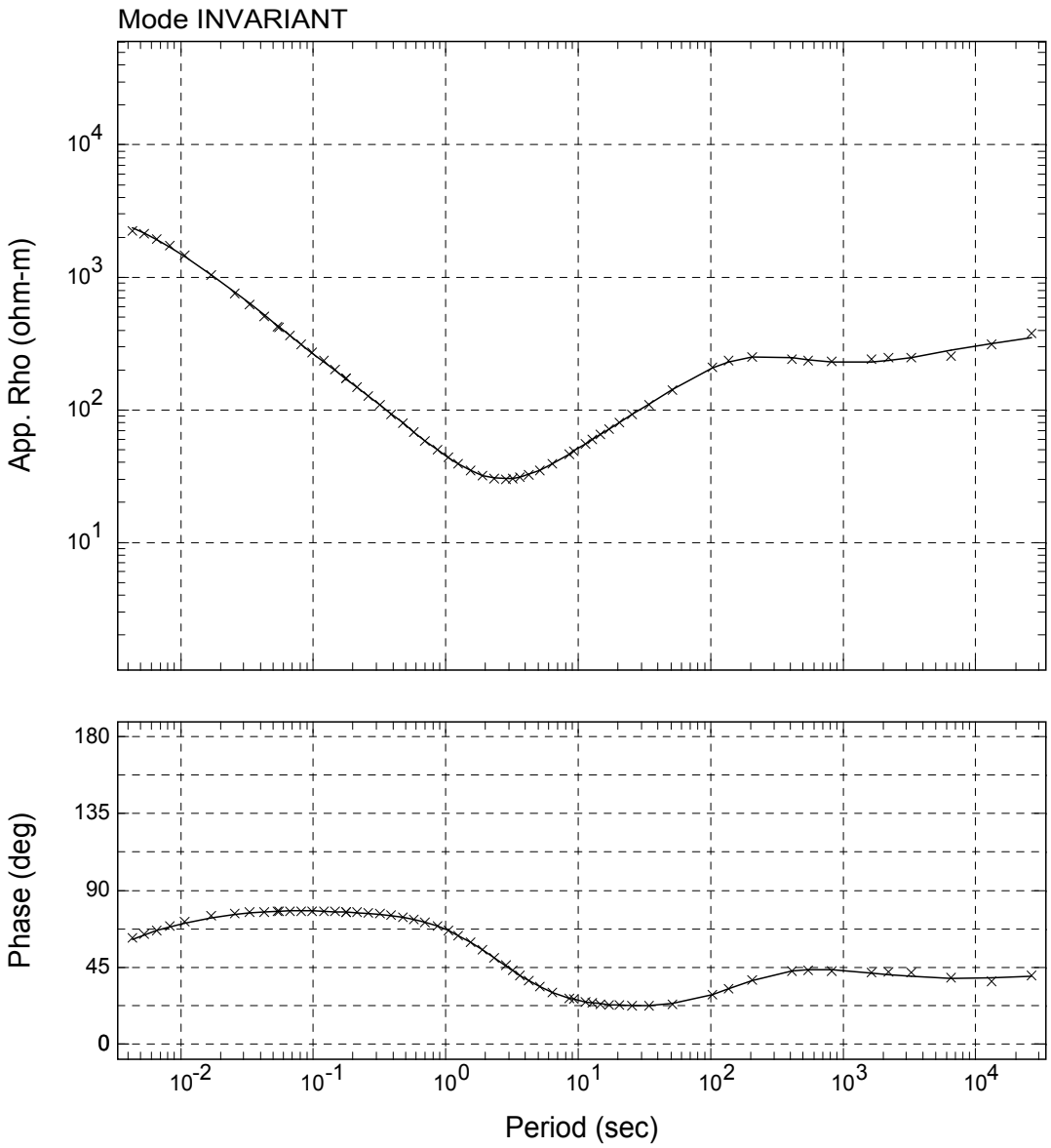

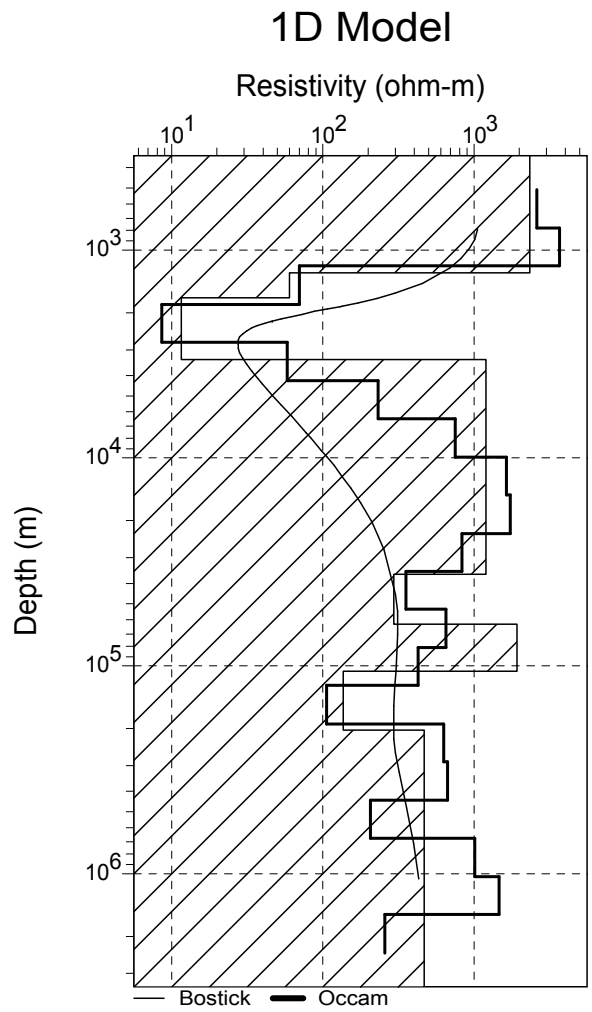

Sounding: MR002
Area: Mauna Kea
14/Jul/2016

Rotation: 0.0°

Sounding MR003

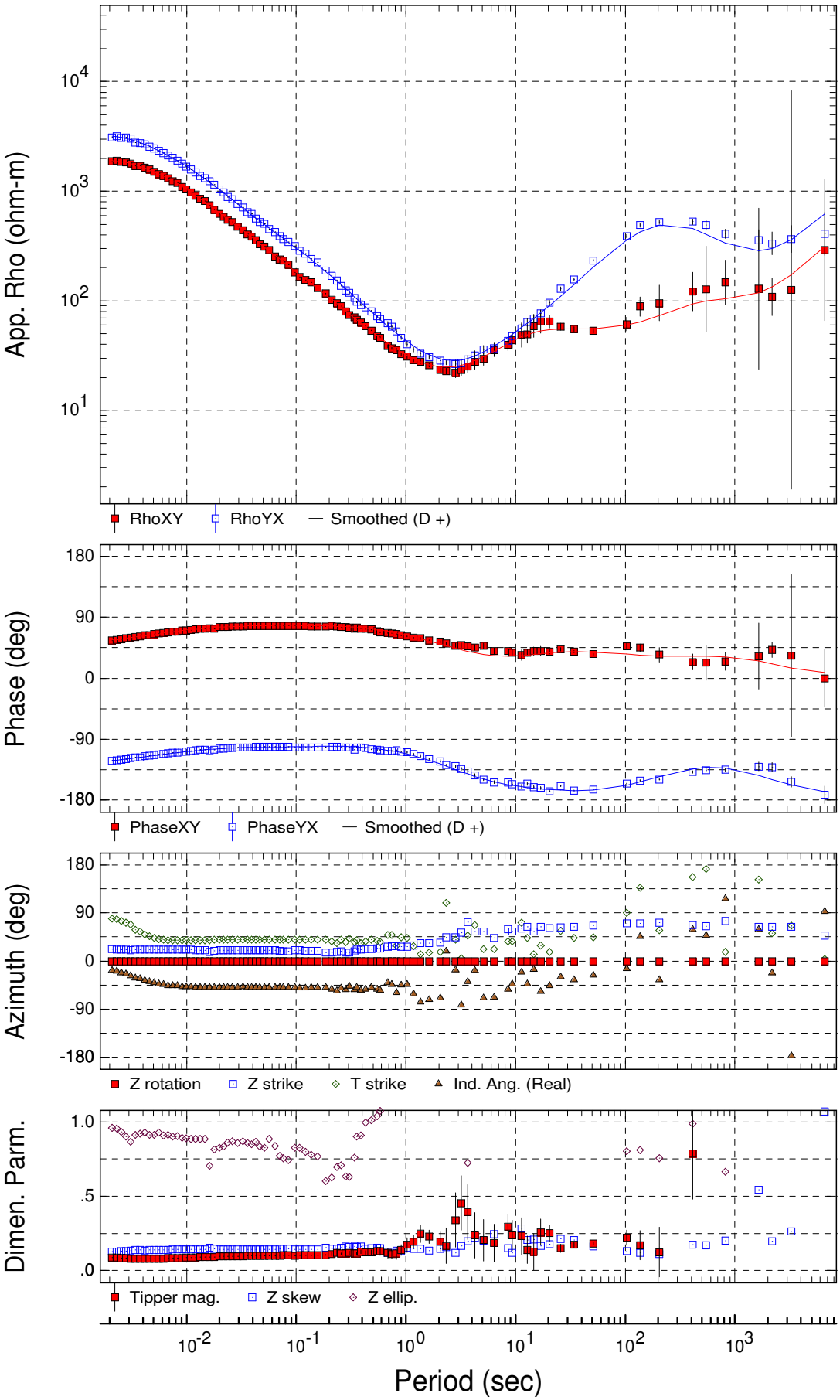

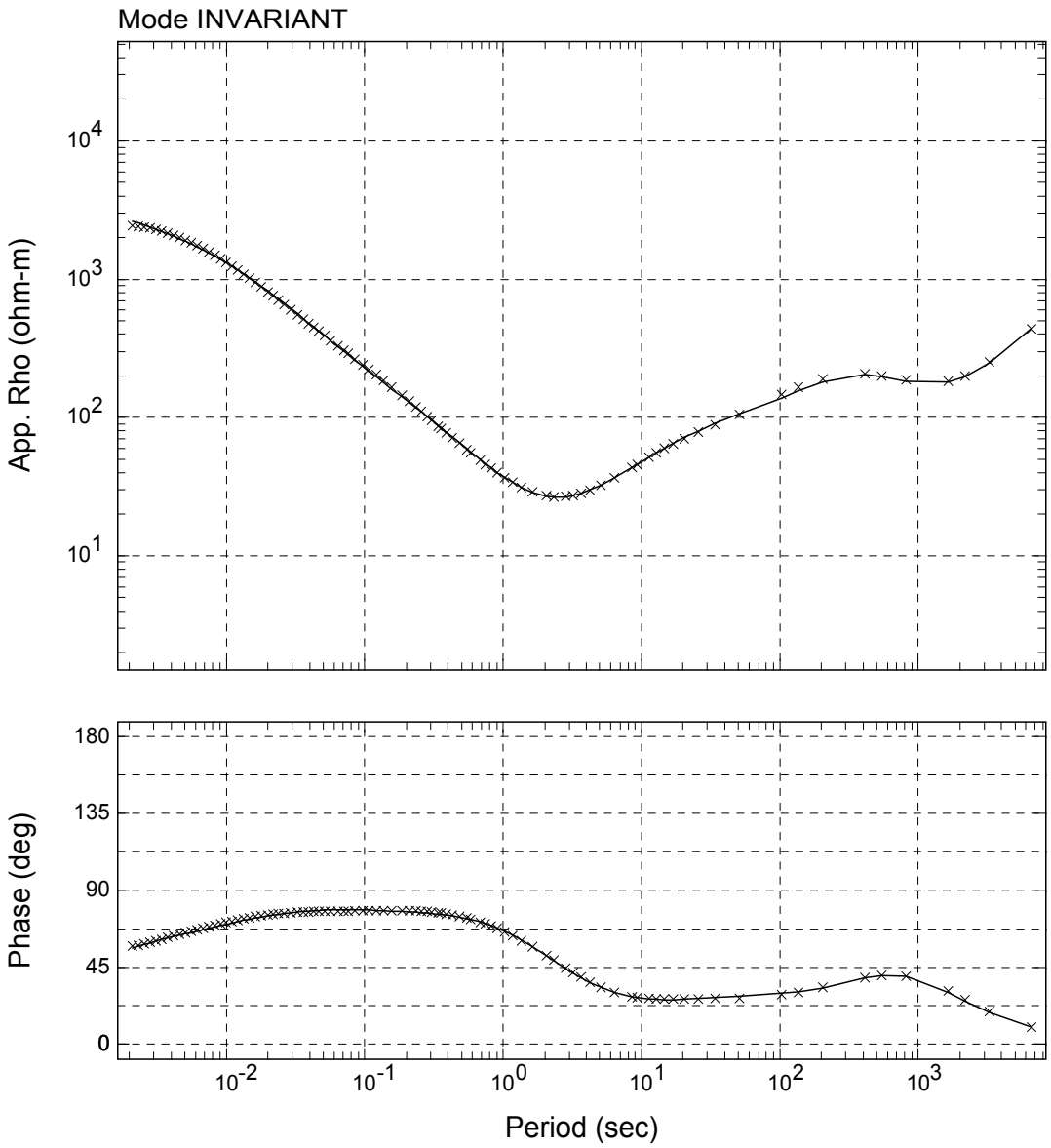

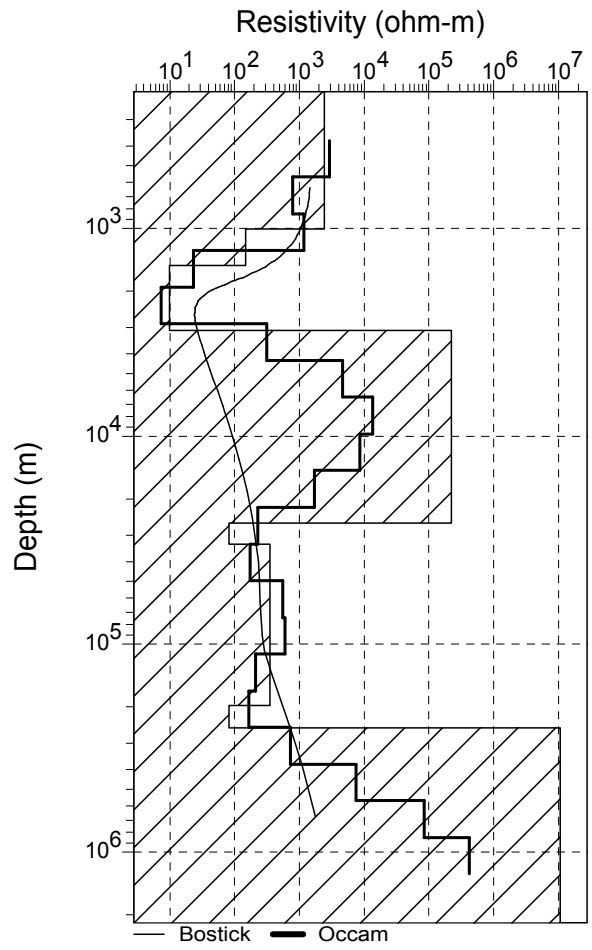

Sounding: MR003
Area: Mauna Kea
14/Jul/2016

Rotation: 0.0°

Sounding MR004

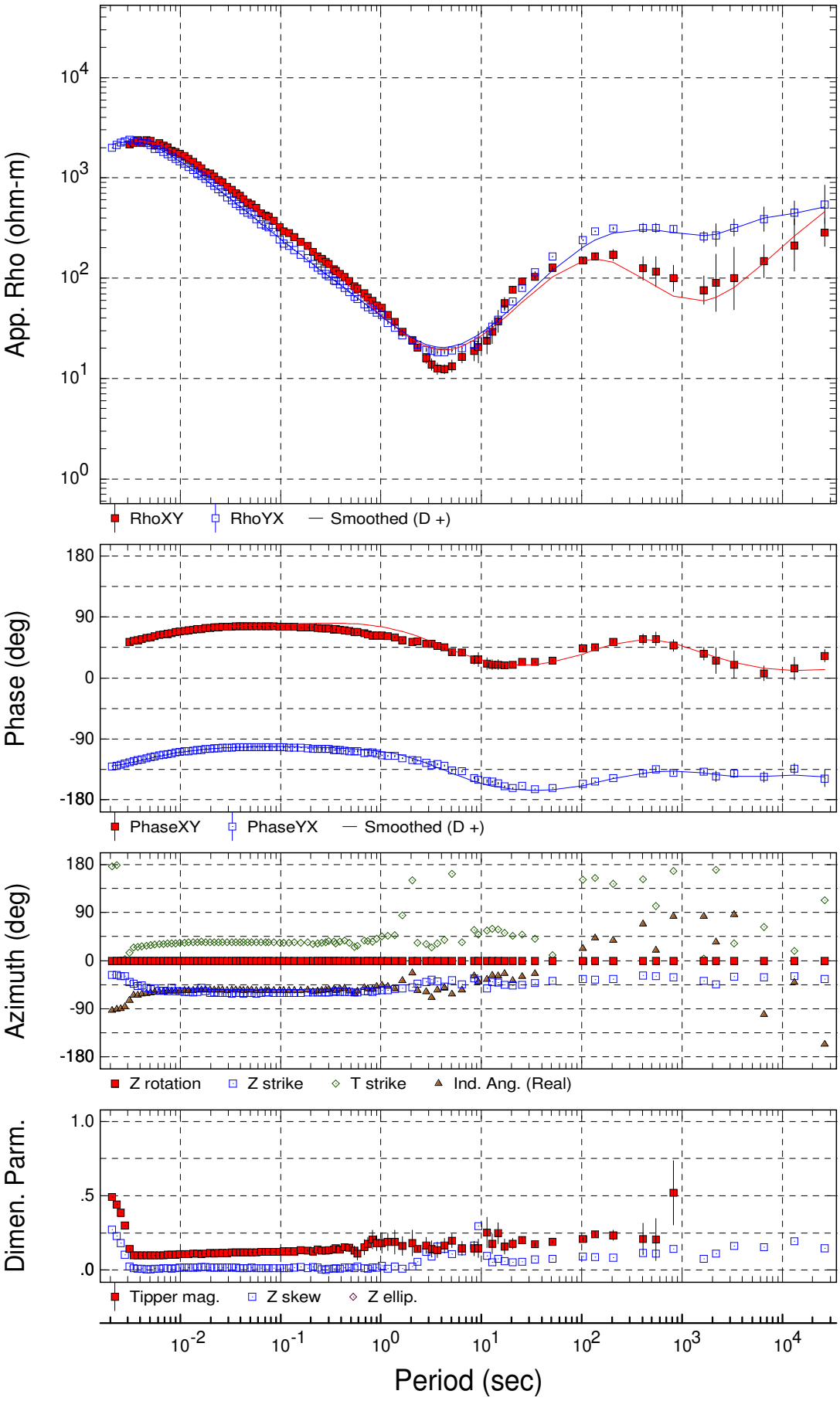

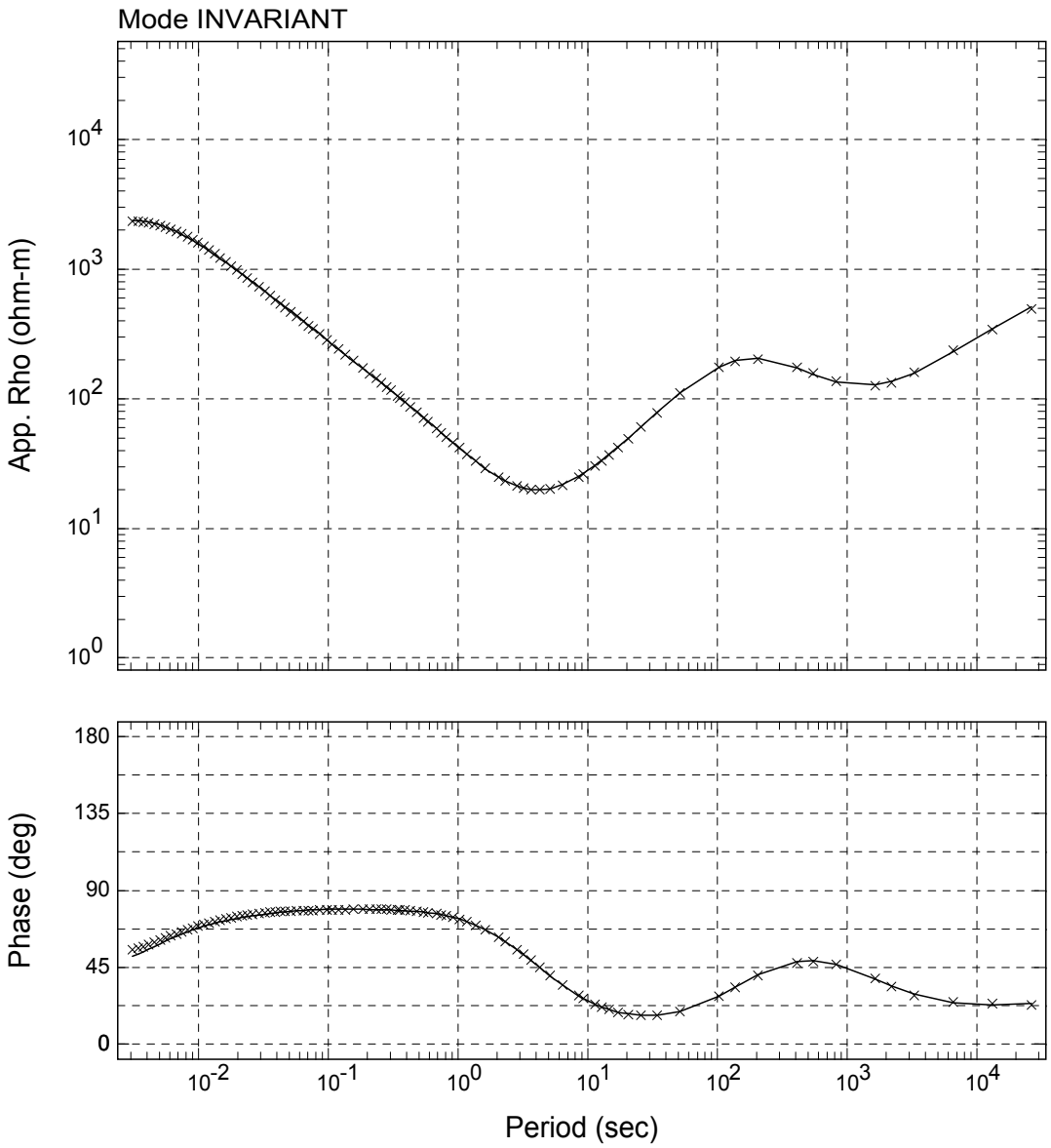

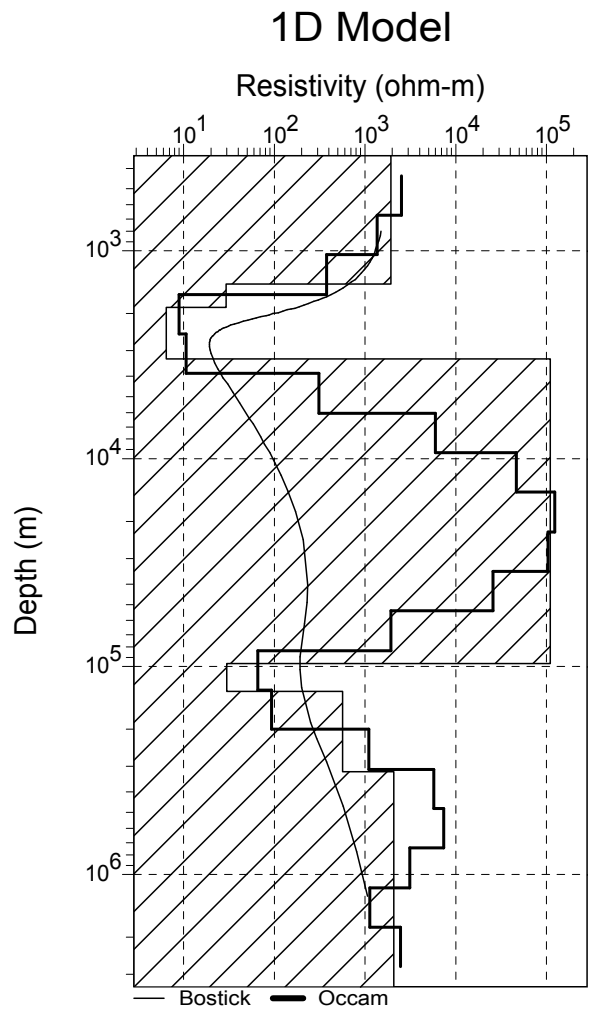

Sounding: MR004

Area: Mauna Kea

14/Jul/2016

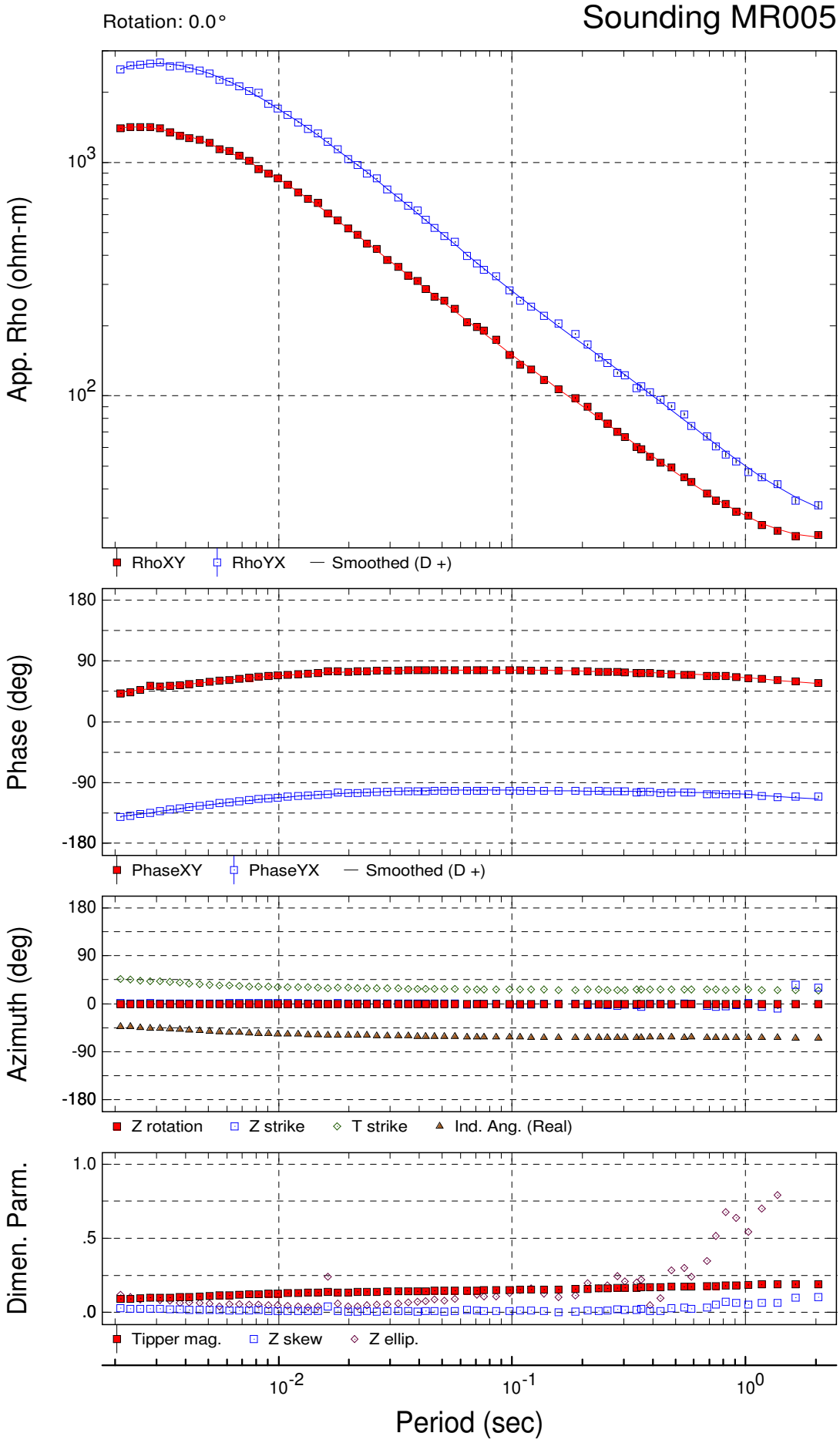
Rotation: 0.0°
Sounding MR005
App. Rho (ohm-m)
10^3
10^2
RhoXY
RhoYX
Smoothed (D +)
Phase (deg)
180
90
0
-90
-180
PhaseXY
PhaseYX
Smoothed (D +)
Azimuth (deg)
180
90
0
-90
-180
Z rotation
Z strike
T strike
Ind. Ang. (Real)
Dimen. Parm.
1.0
.5
.0
Tipper mag.
Z skew
Z ellip.
10^{-2}
10^{-1}
10^{0}
Period (sec)

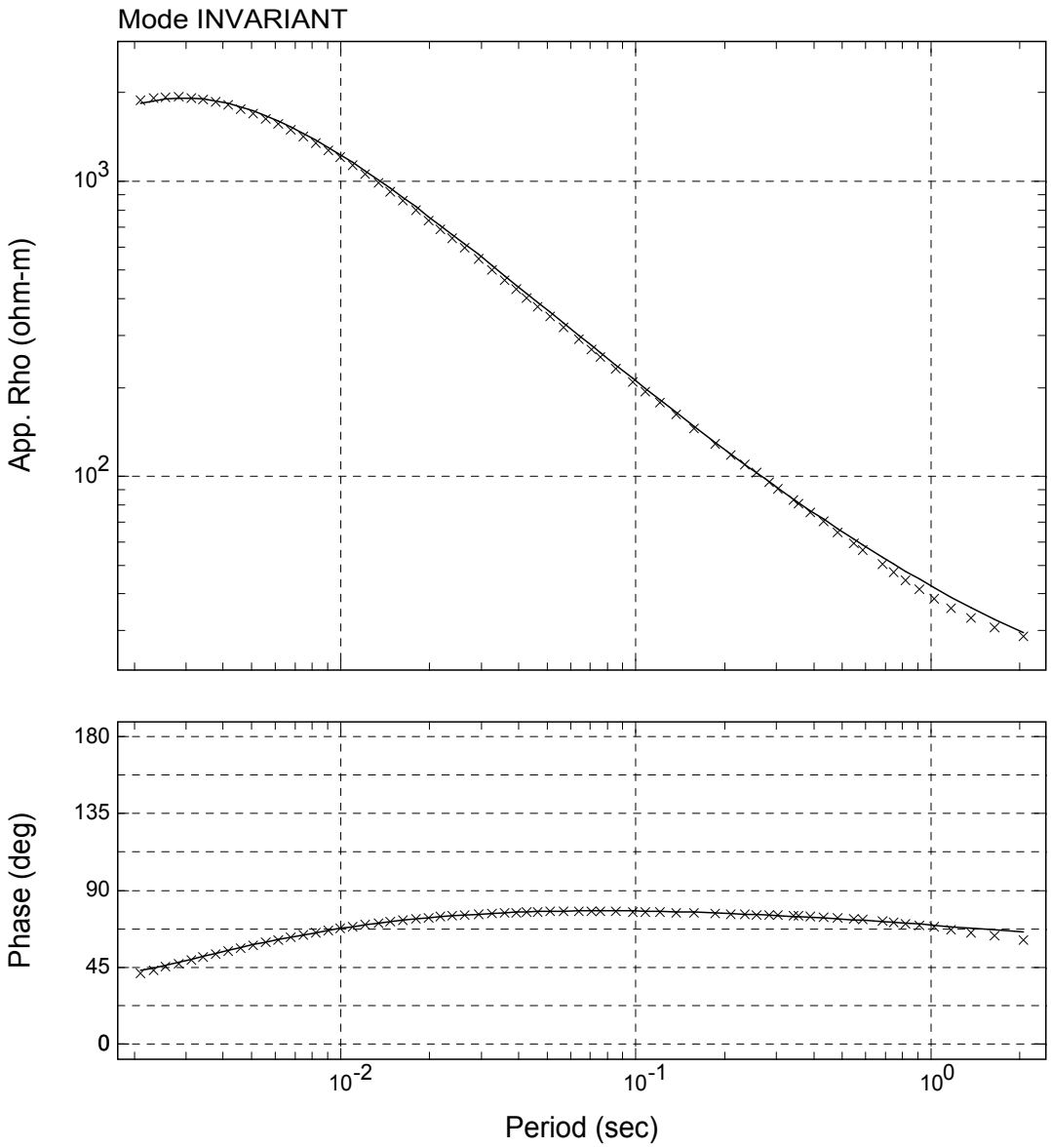

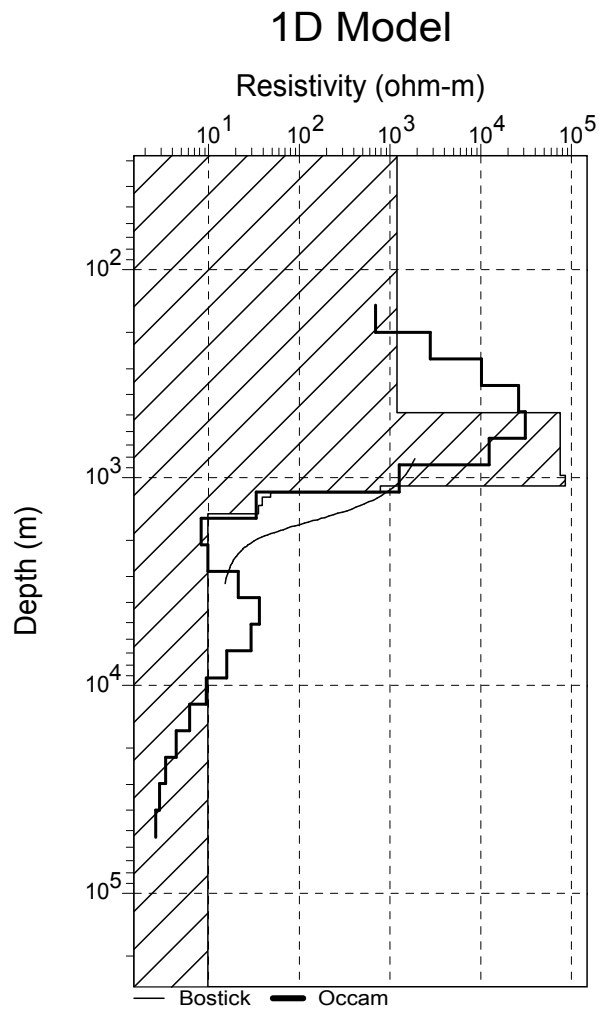

Sounding: MR005
Area: Mauna Kea
14/Jul/2016

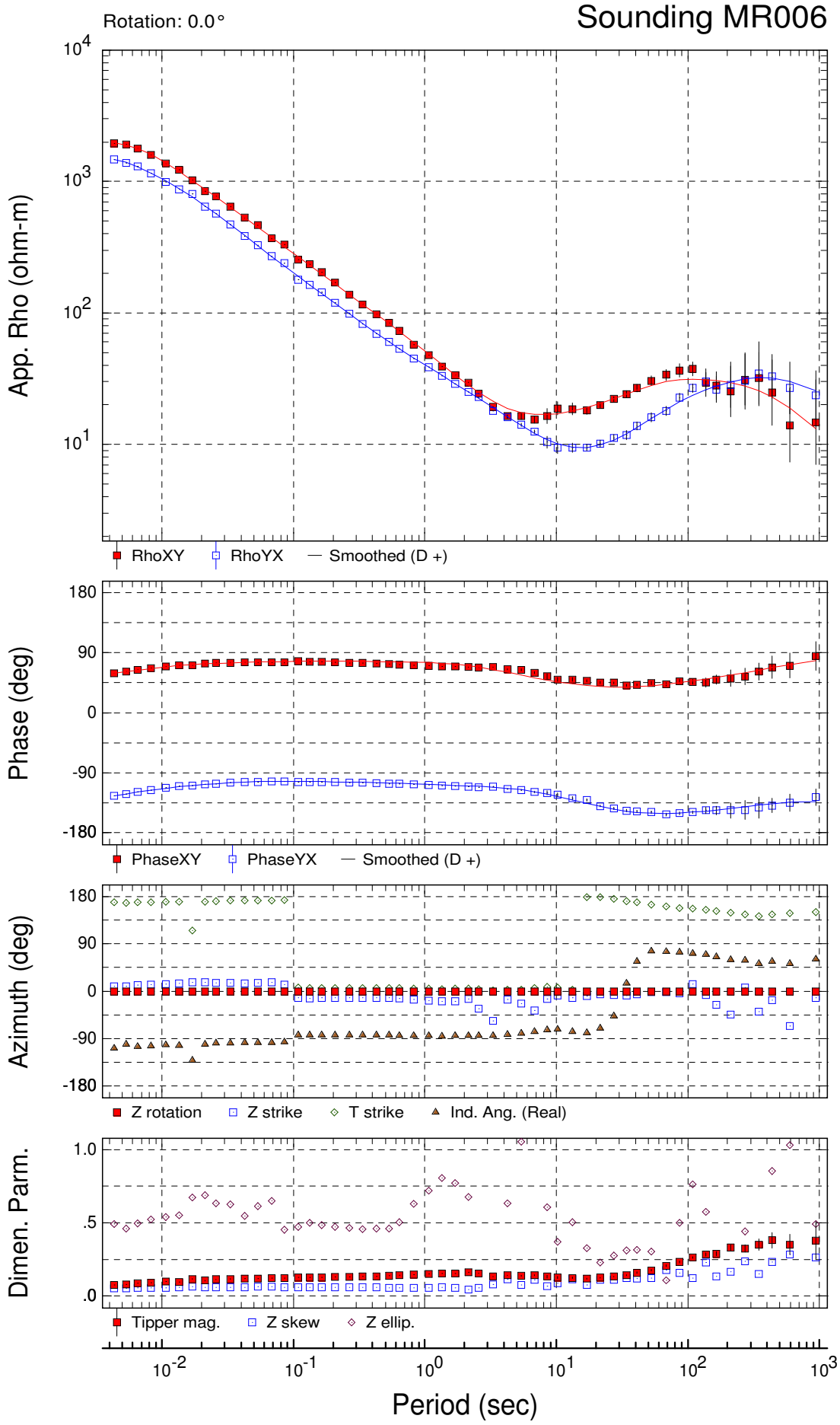
Rotation: 0.0°
Sounding MR006
App. Rho (ohm-m)
RhoXY
RhoYX
Smoothed (D +)
Phase (deg)
PhaseXY
PhaseYX
Smoothed (D +)
Azimuth (deg)
Z rotation
Z strike
T strike
Ind. Ang. (Real)
Dimen. Parm.
Tipper mag.
Z skew
Z ellip.
Period (sec)

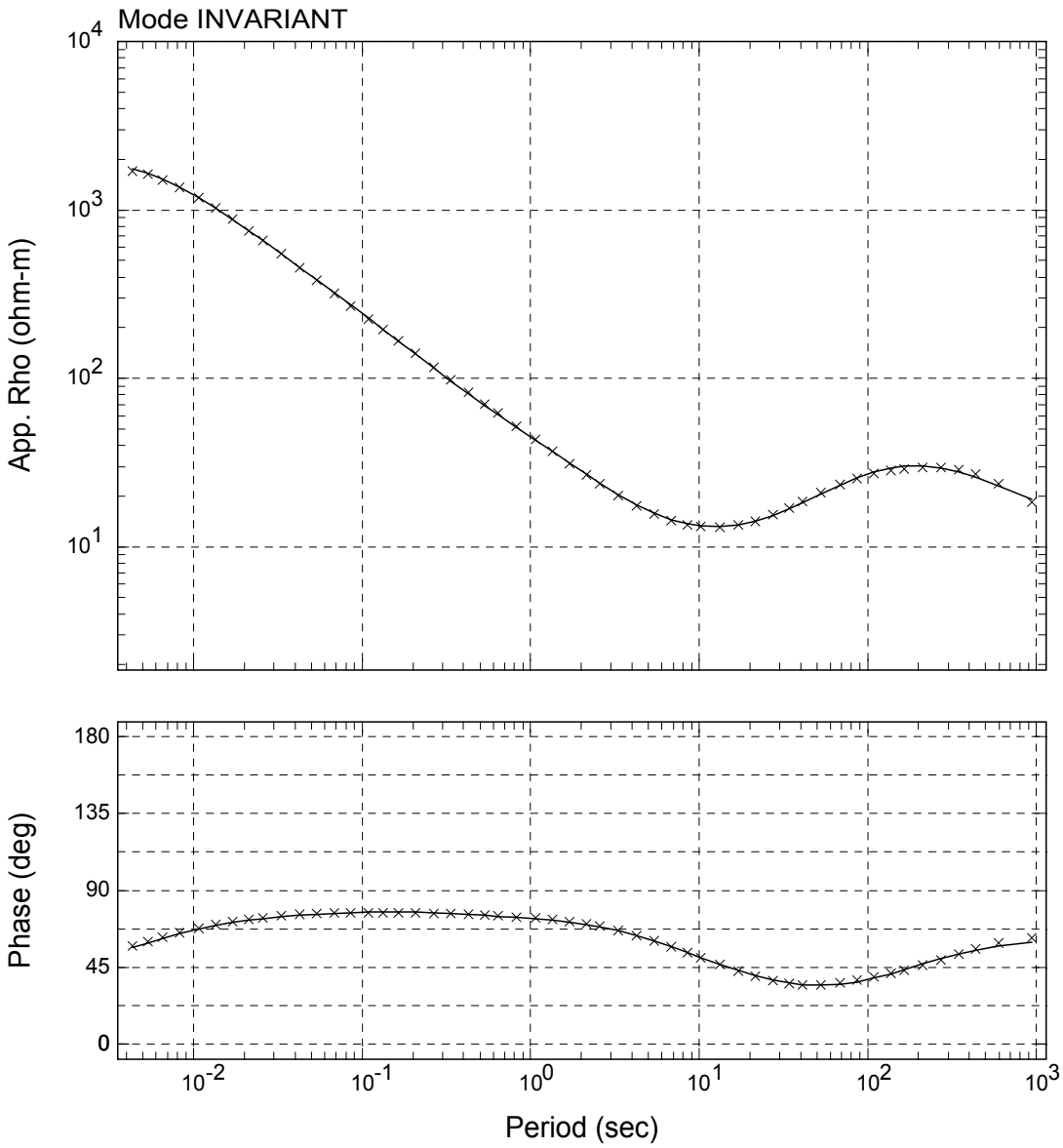

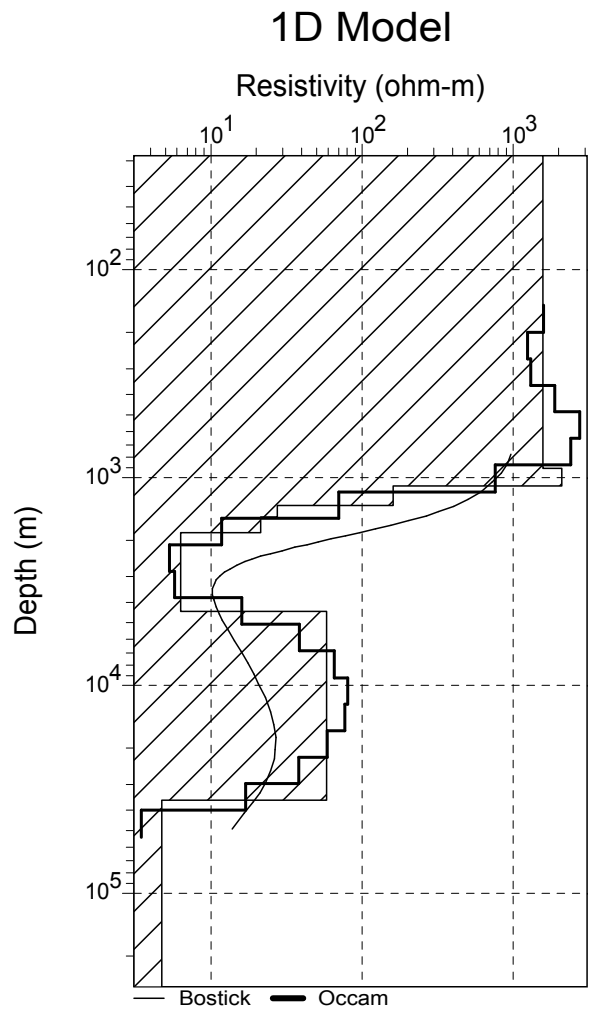

Sounding: MR006

Area: Mauna Kea

14/Jul/2016

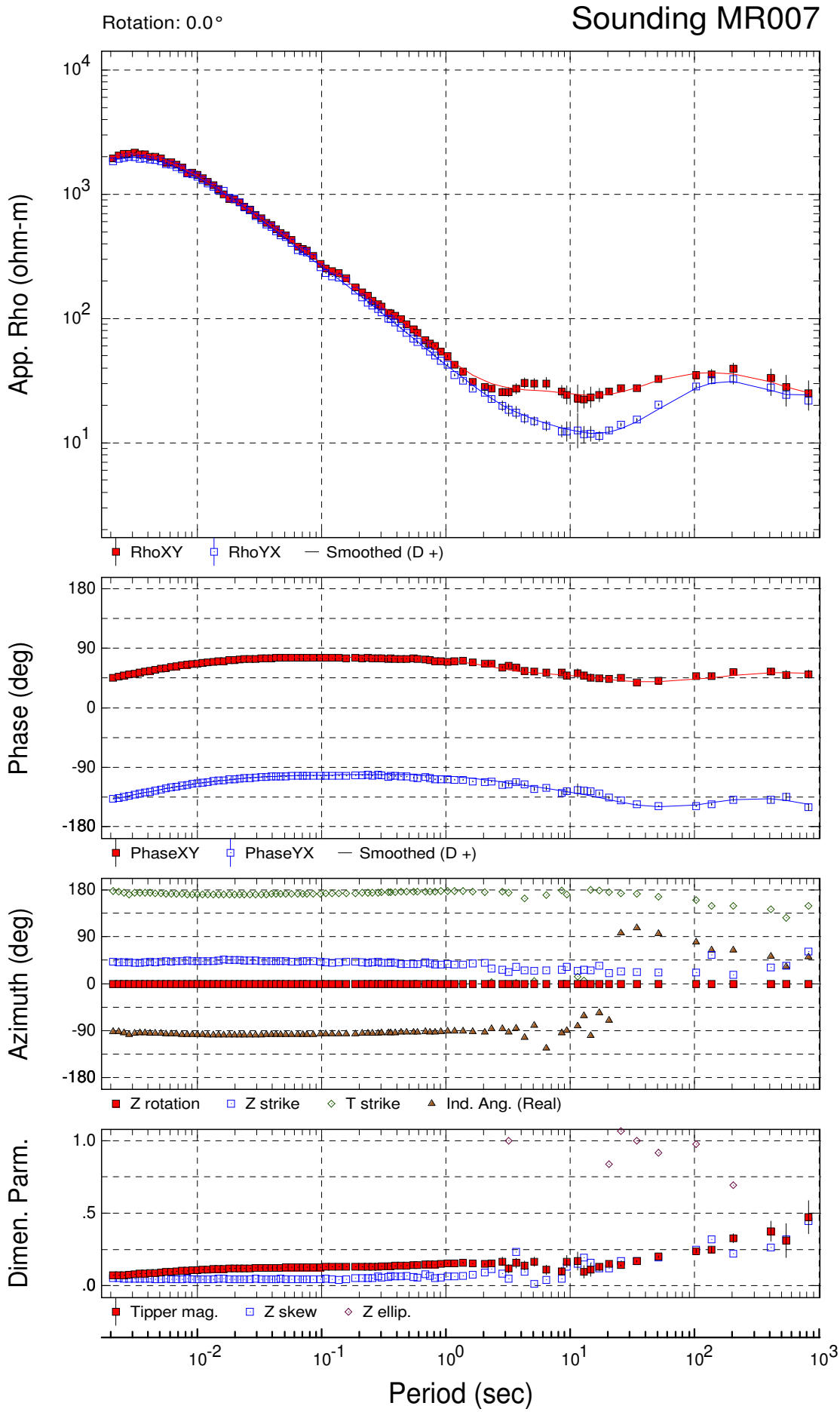
Rotation: 0.0°
Sounding MR007
App. Rho (ohm-m)
RhoXY
RhoYX
Smoothed (D +)
Phase (deg)
PhaseXY
PhaseYX
Smoothed (D +)
Azimuth (deg)
Z rotation
Z strike
T strike
Ind. Ang. (Real)
Dimen. Parm.
Tipper mag.
Z skew
Z ellip.
Period (sec)

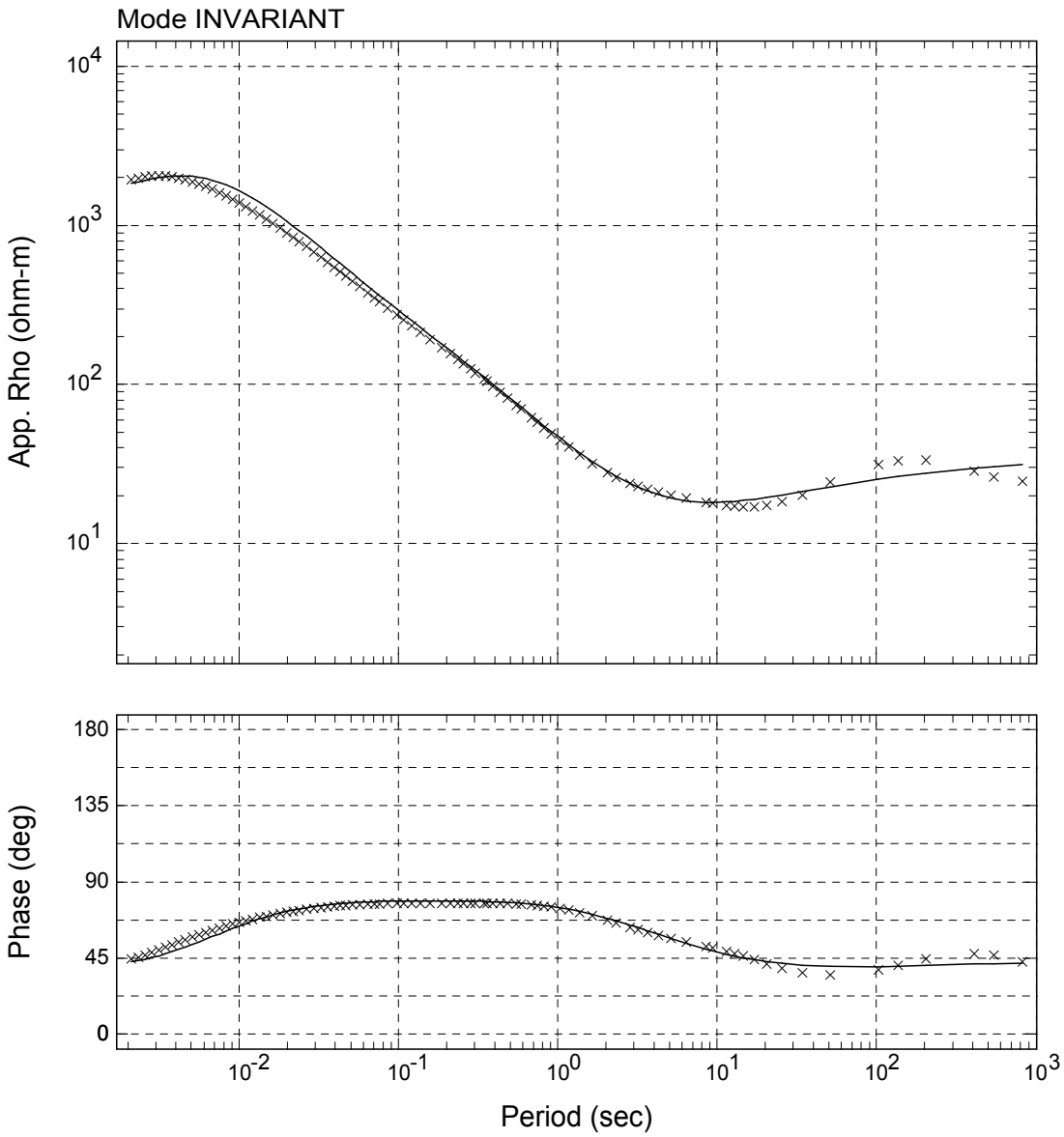

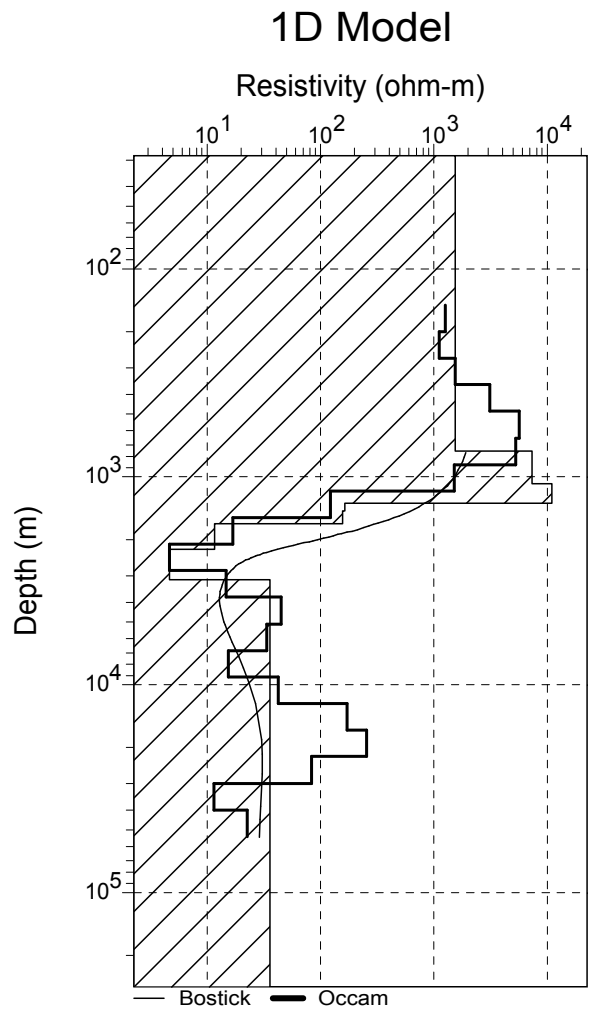

Sounding: MR007

Area: Mauna Kea

14/Jul/2016

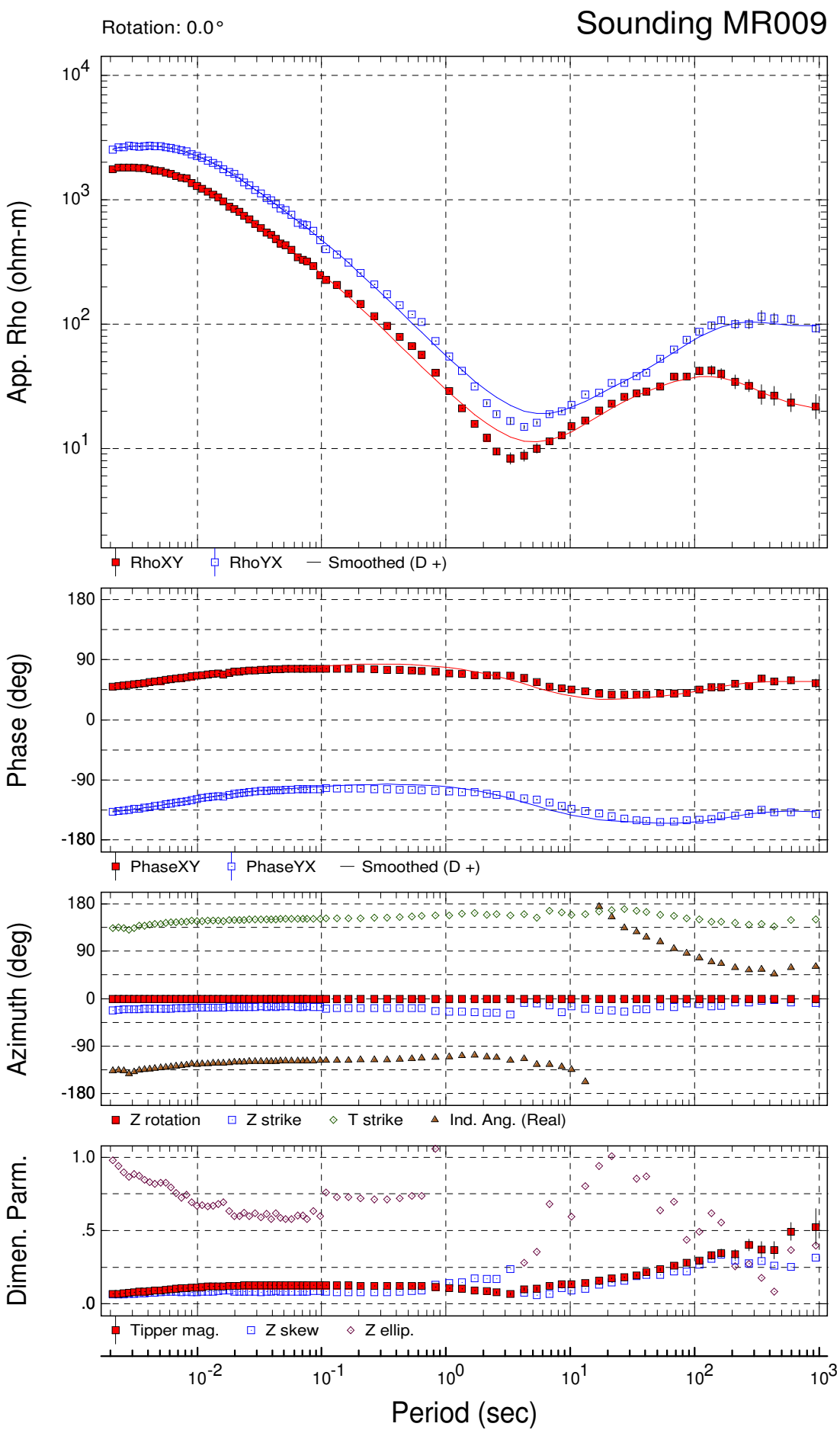
Rotation: 0.0°
Sounding MR009
App. Rho (ohm-m)
RhoXY
RhoYX
Smoothed (D +)
Phase (deg)
PhaseXY
PhaseYX
Smoothed (D +)
Azimuth (deg)
Z rotation
Z strike
T strike
Ind. Ang. (Real)
Dimen. Parm.
Tipper mag.
Z skew
Z ellip.
Period (sec)

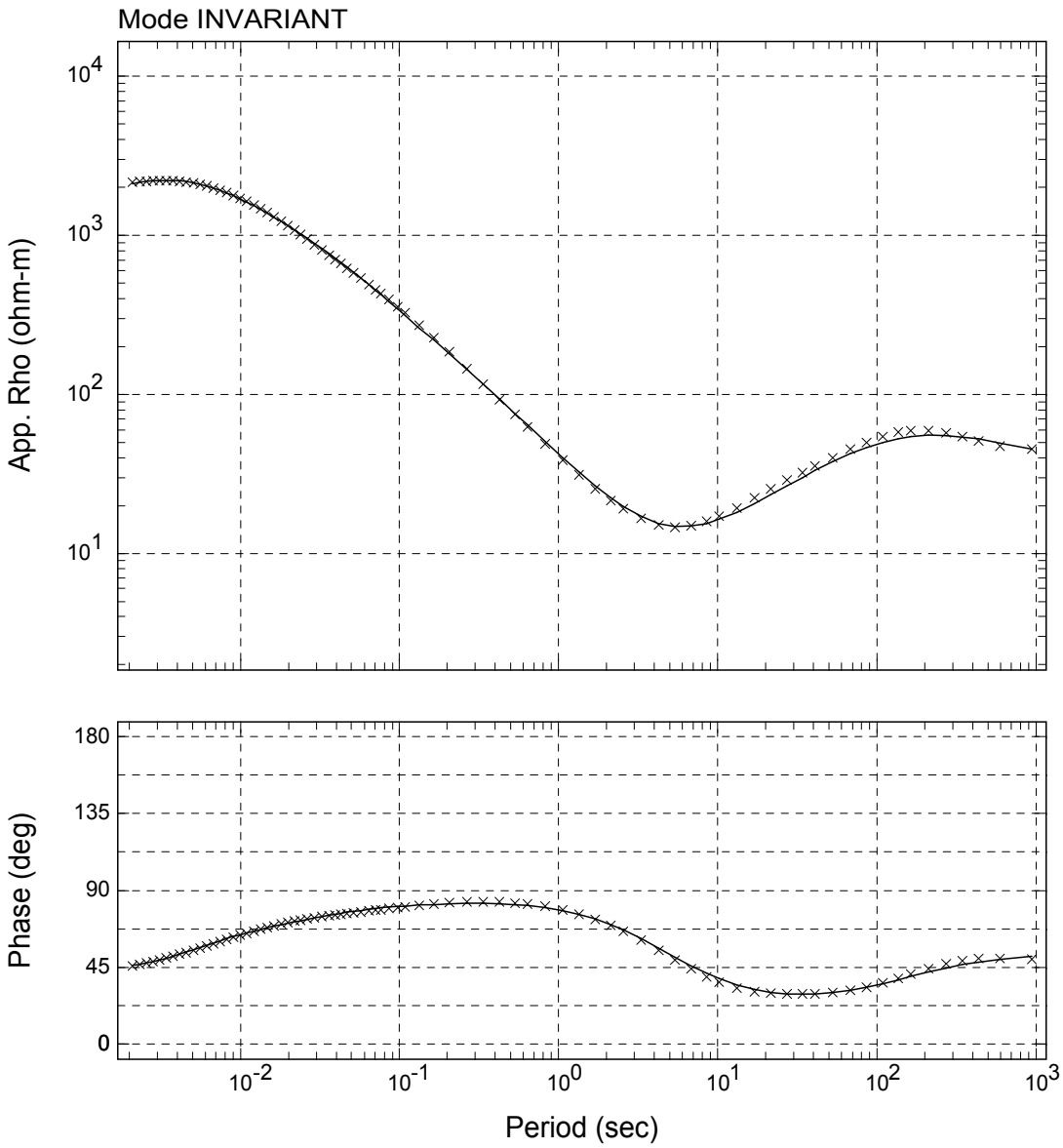

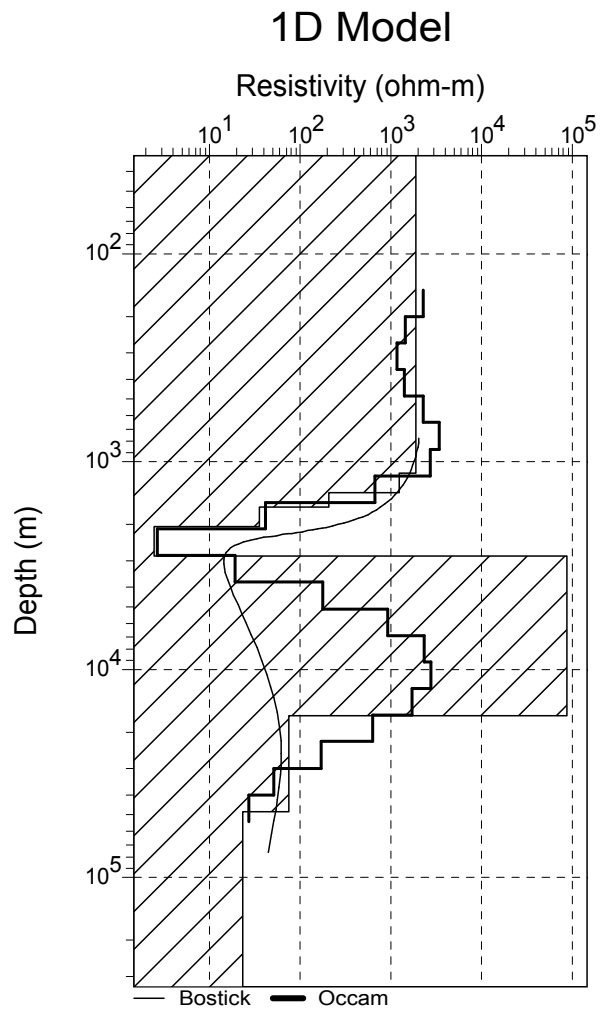

Sounding: MR009

Area: Mauna Kea

14/Jul/2016

Rotation: 0.0°

Sounding MR010

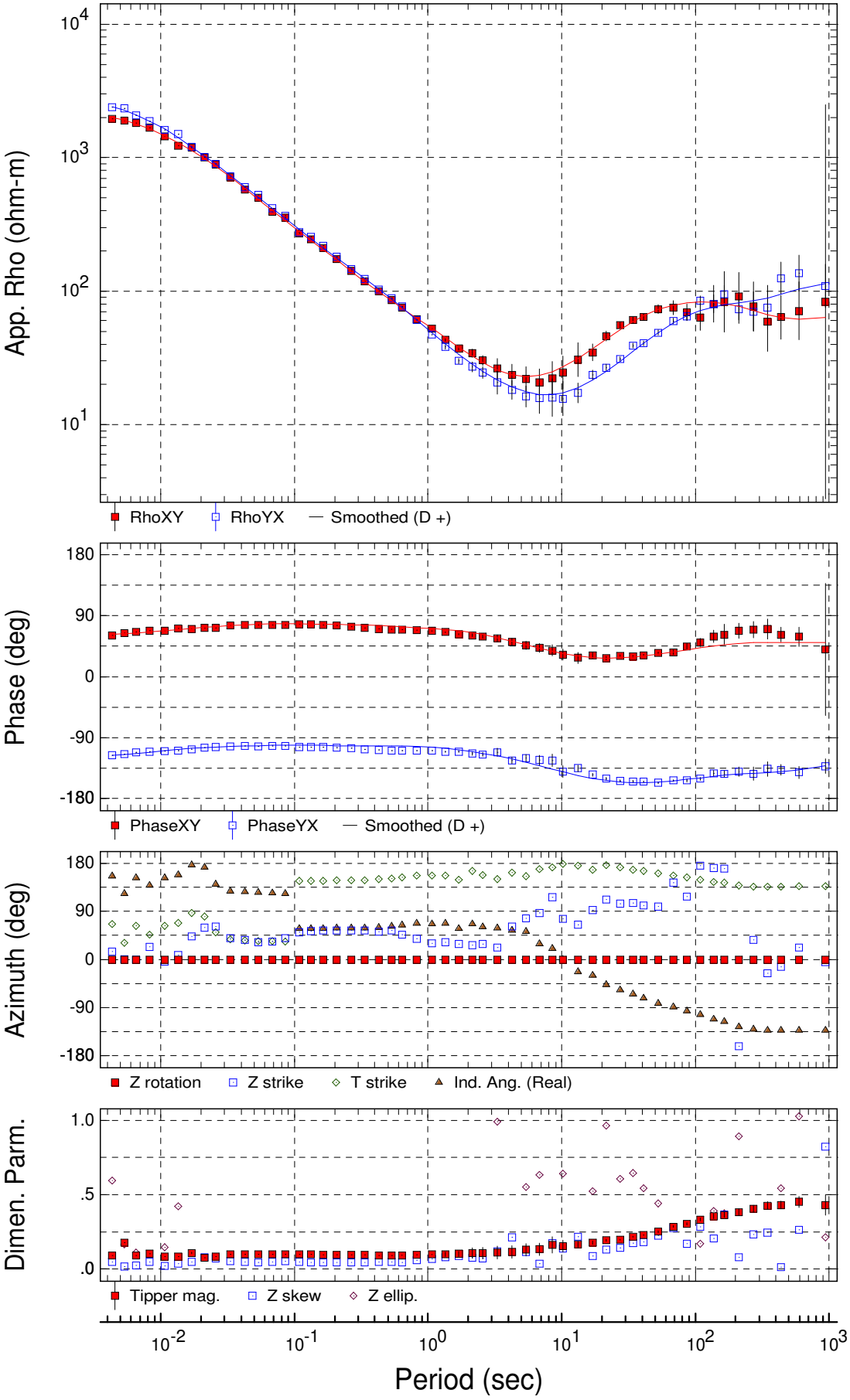

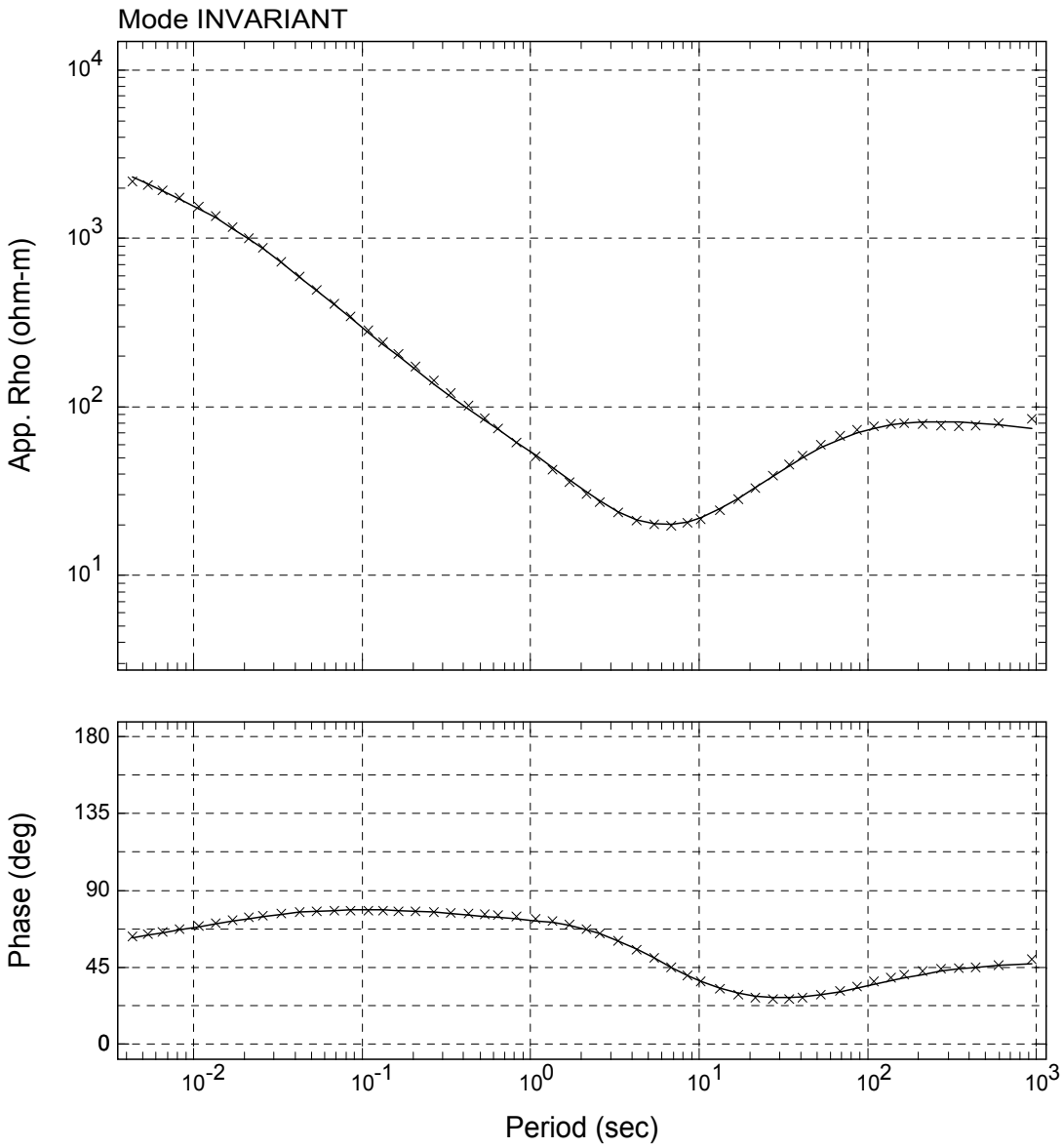

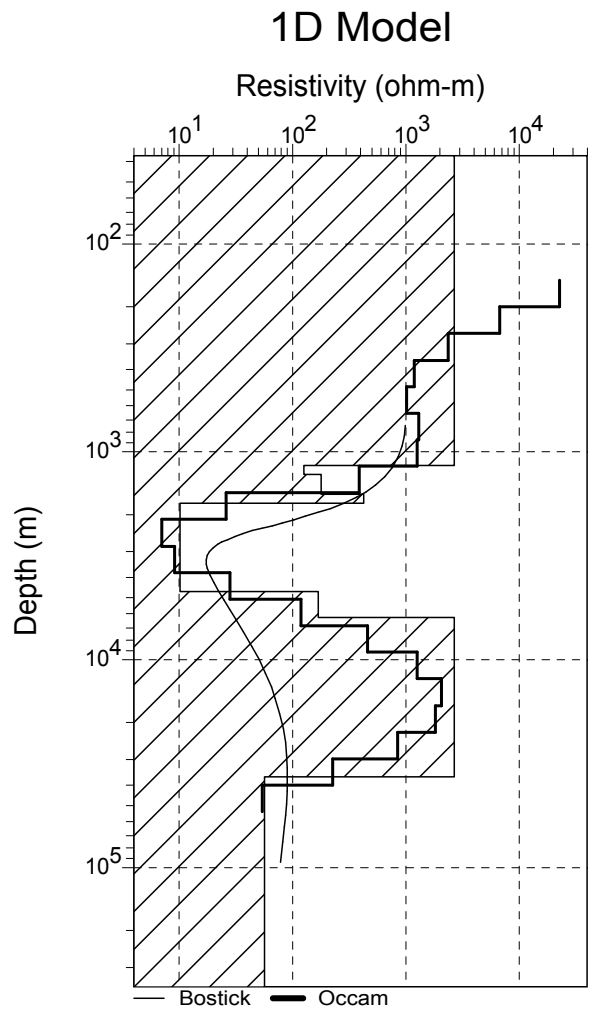

Sounding: MR010

Area: Mauna Kea

14/Jul/2016

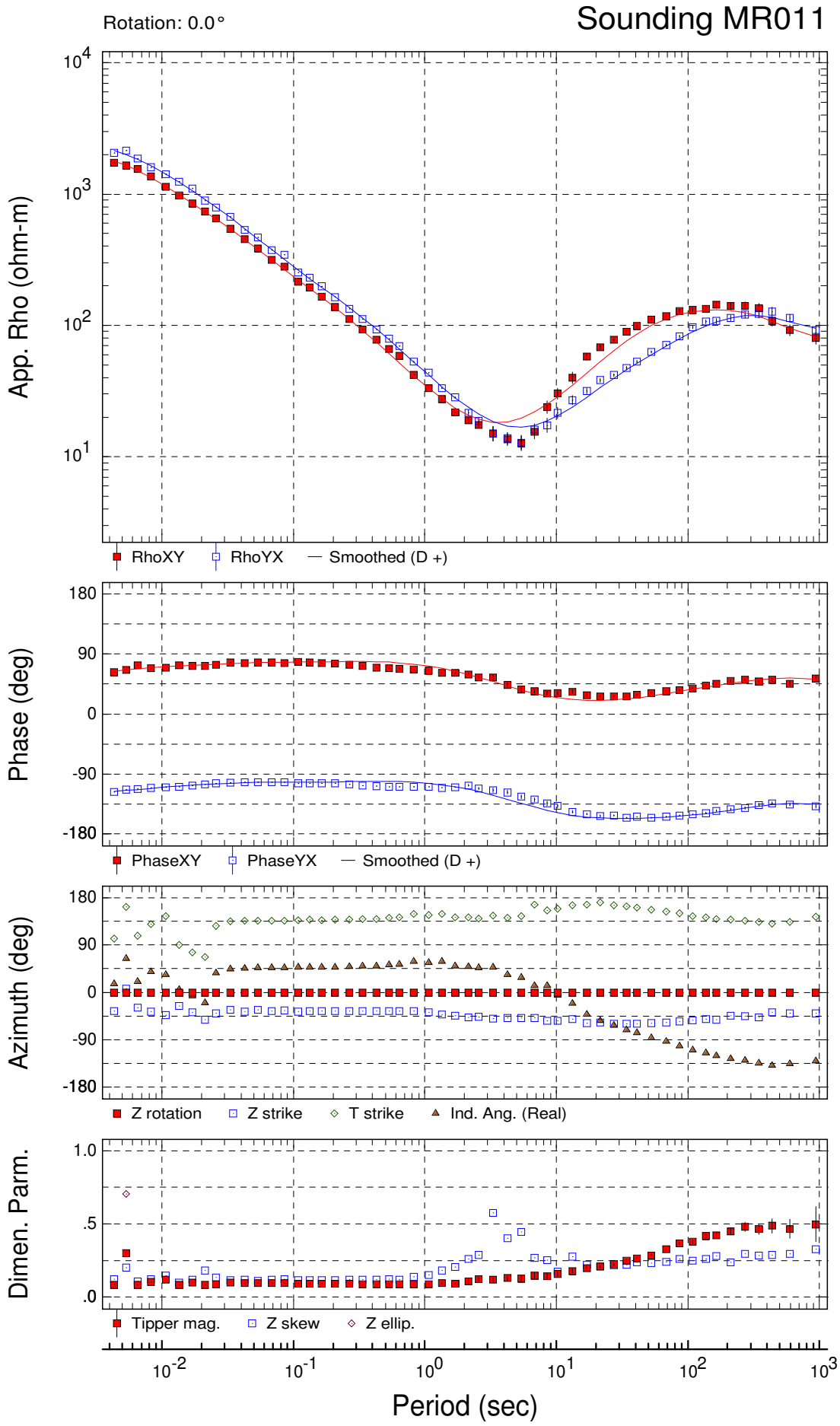
Rotation: 0.0°
Sounding MR011
App. Rho (ohm-m)
RhoXY
RhoYX
Smoothed (D +)
Phase (deg)
PhaseXY
PhaseYX
Smoothed (D +)
Azimuth (deg)
Z rotation
Z strike
T strike
Ind. Ang. (Real)
Dimen. Parm.
Tipper mag.
Z skew
Z ellip.
Period (sec)

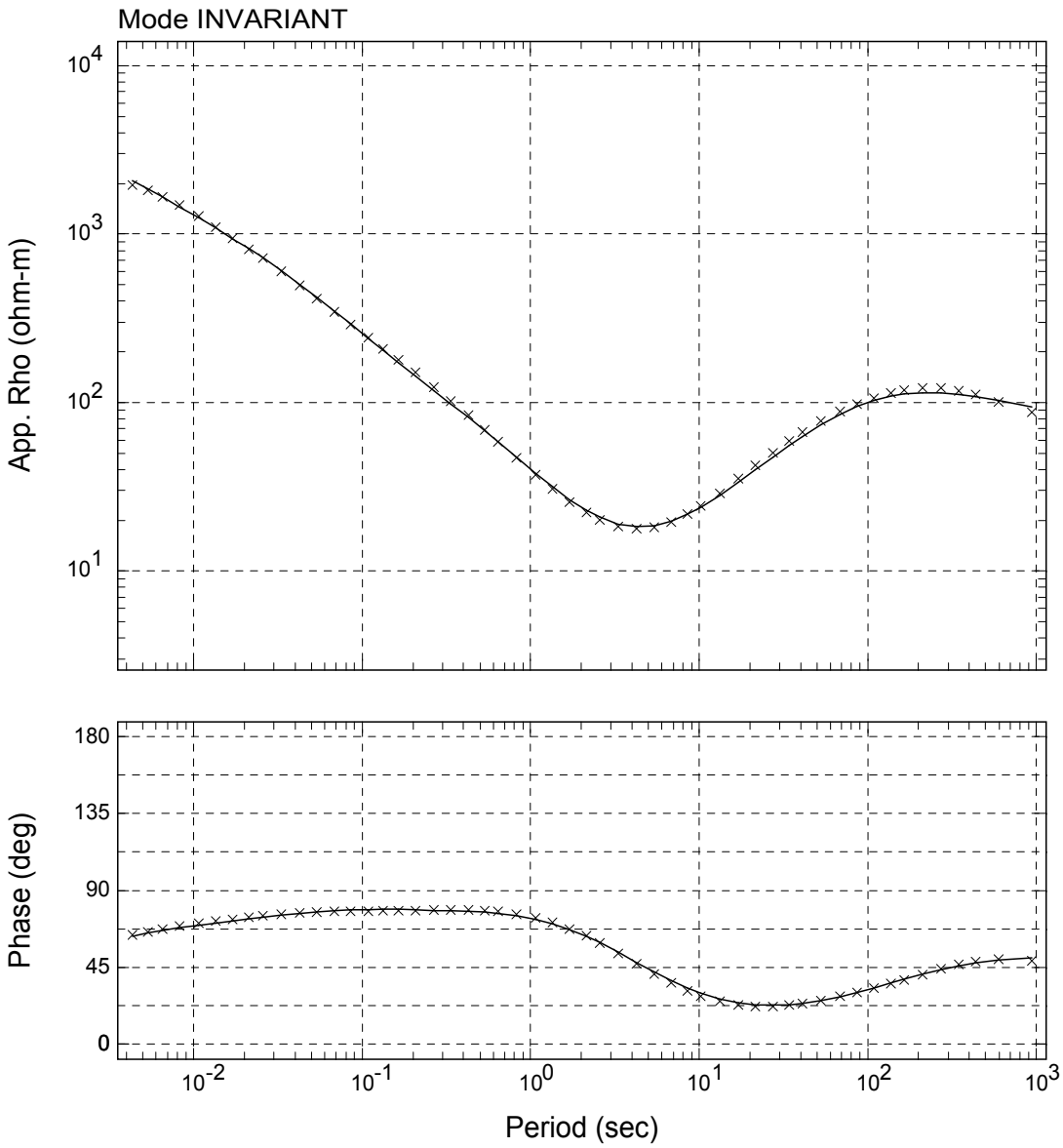

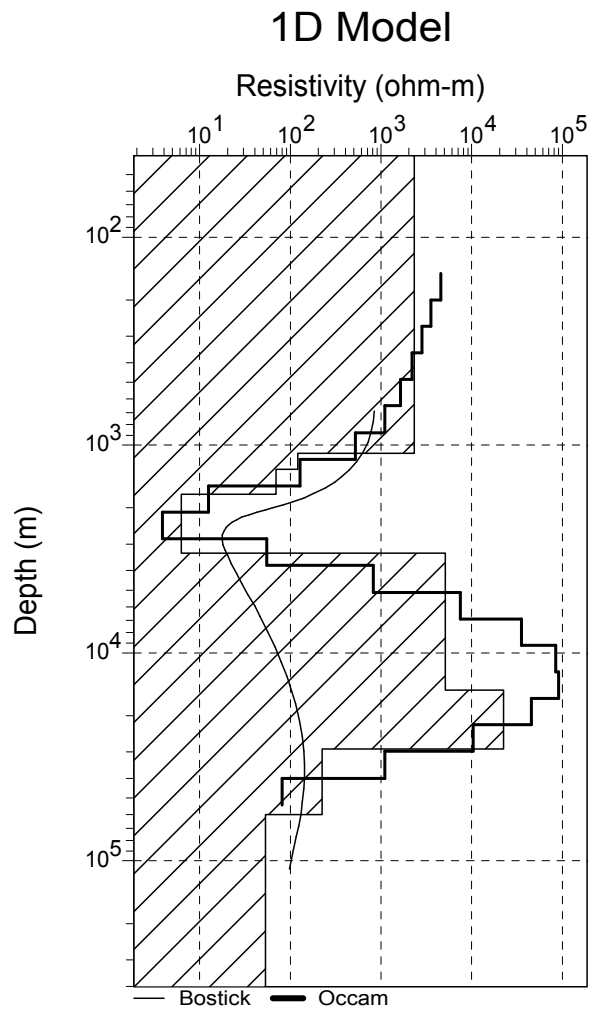

Sounding: MR011

Area: Mauna Kea

14/Jul/2016

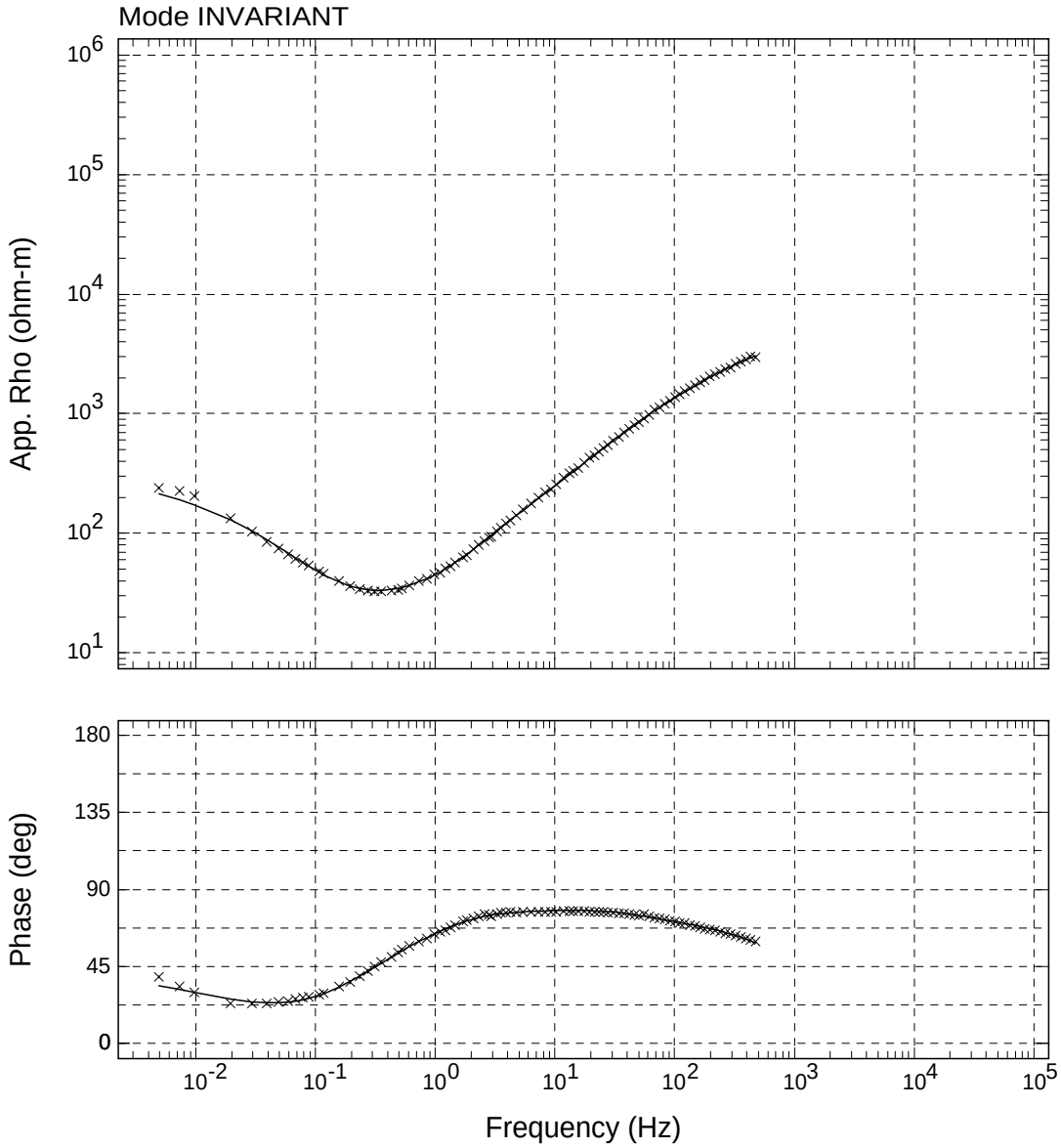

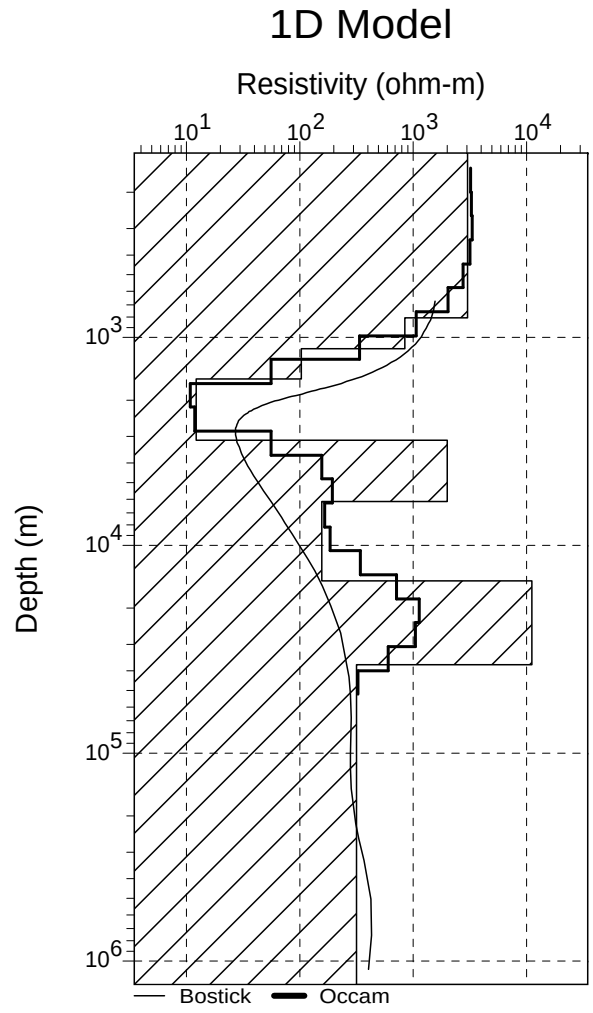

Sounding: MR001
Area: Mauna Kea
22/Dec/2016

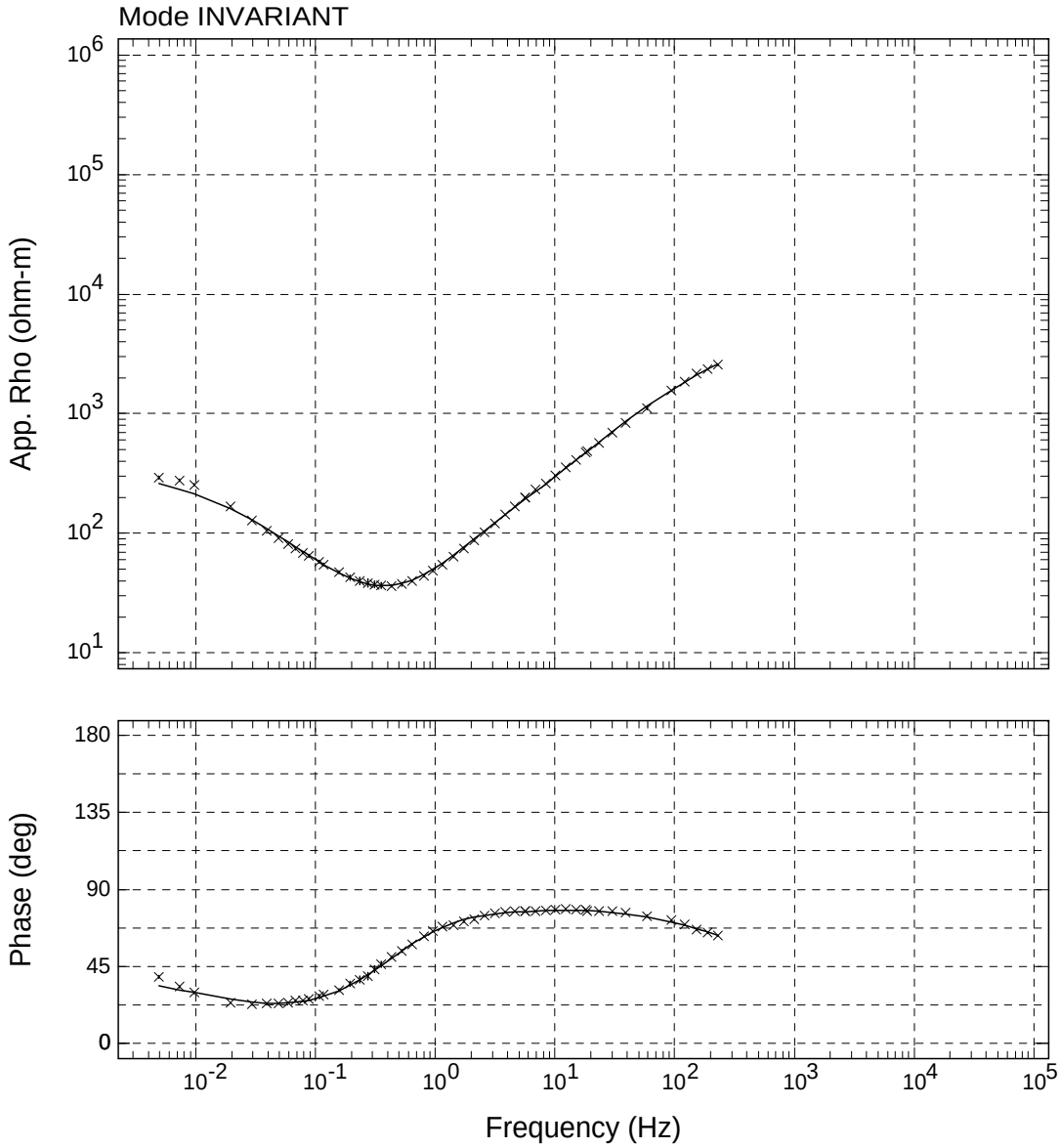

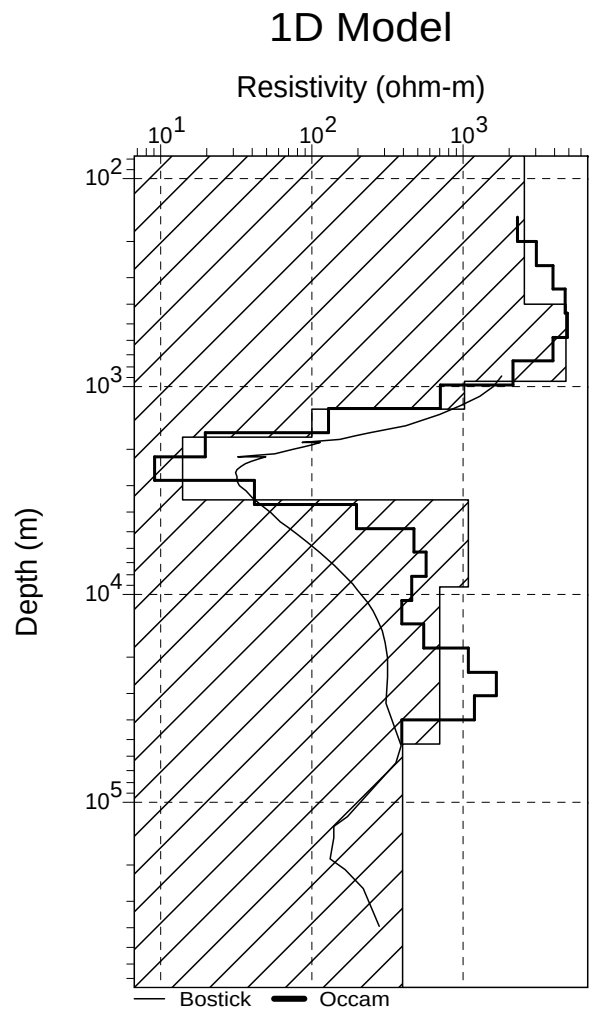

Sounding: MR002
Area: Mauna Kea
26/Dec/2016

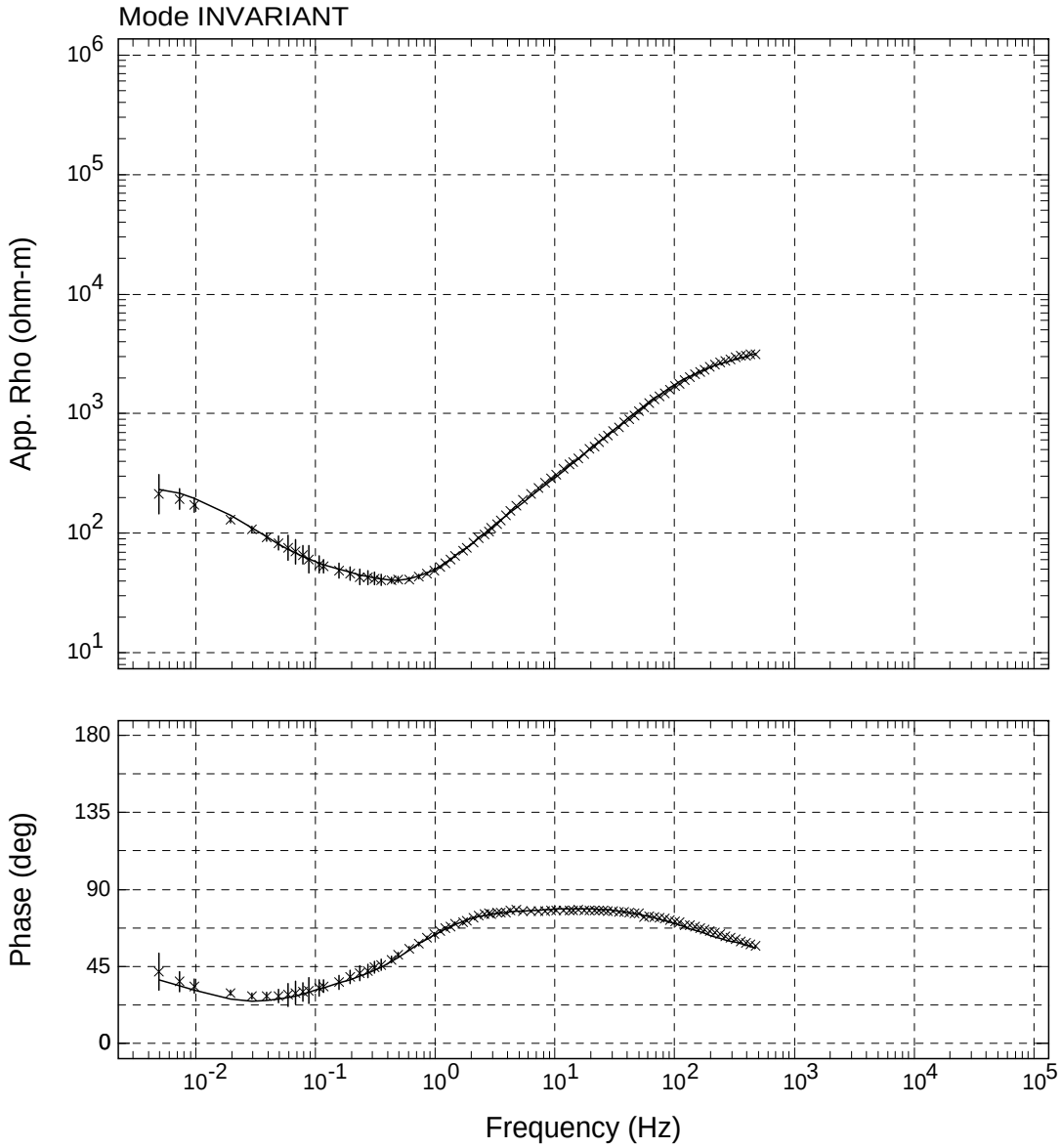

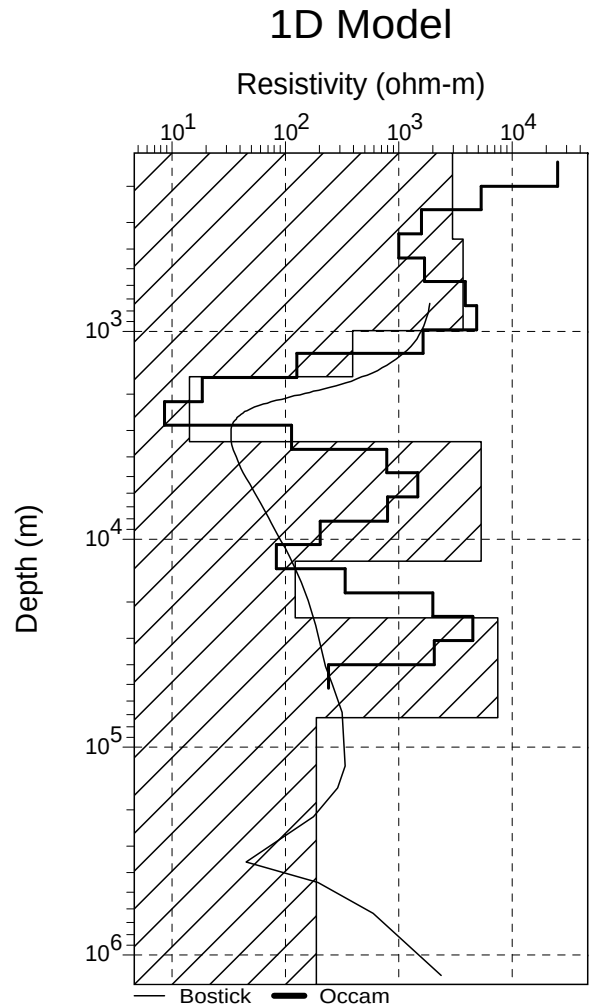

Sounding: MR003
Area: Mauna Kea
26/Dec/2016

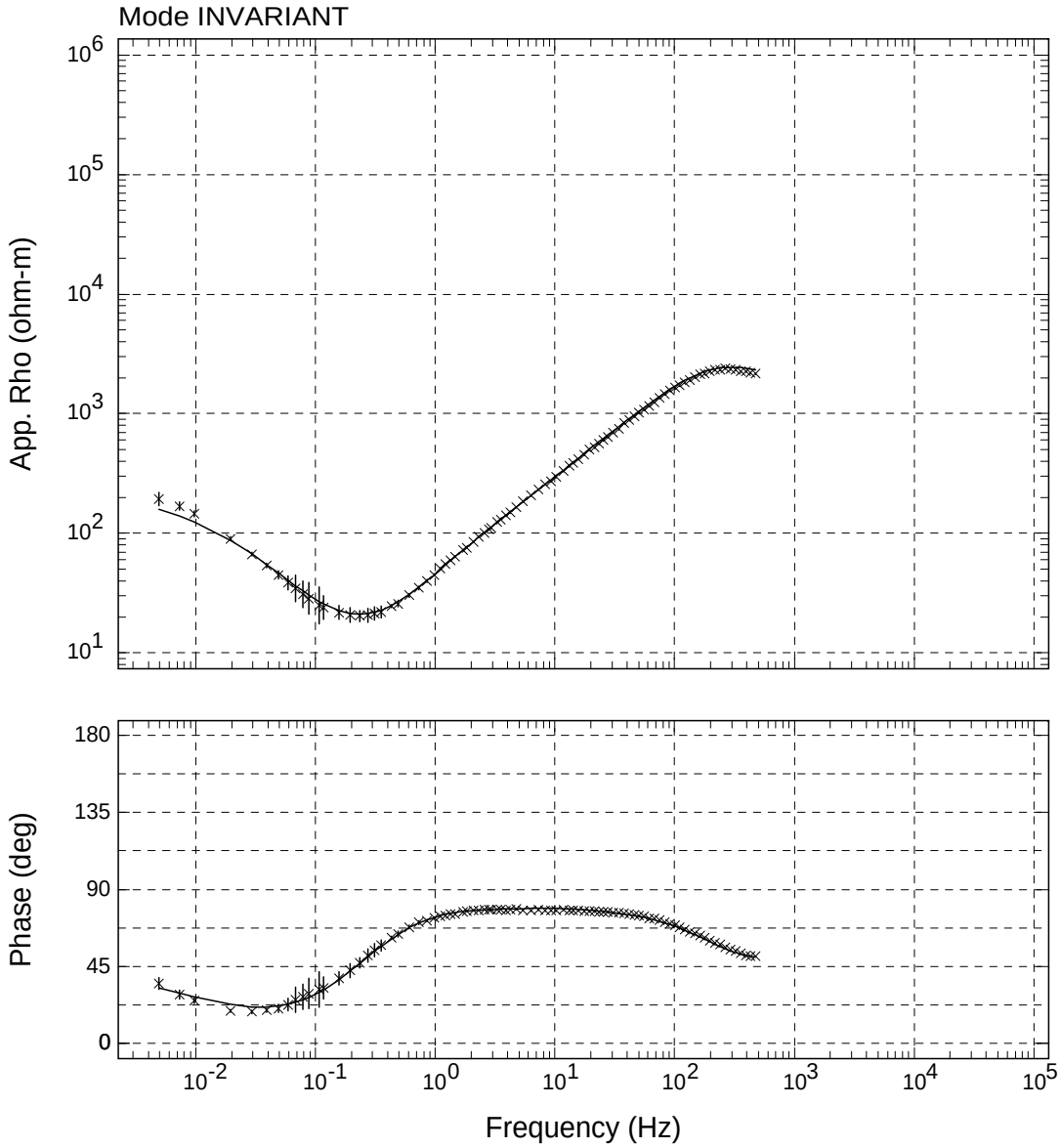

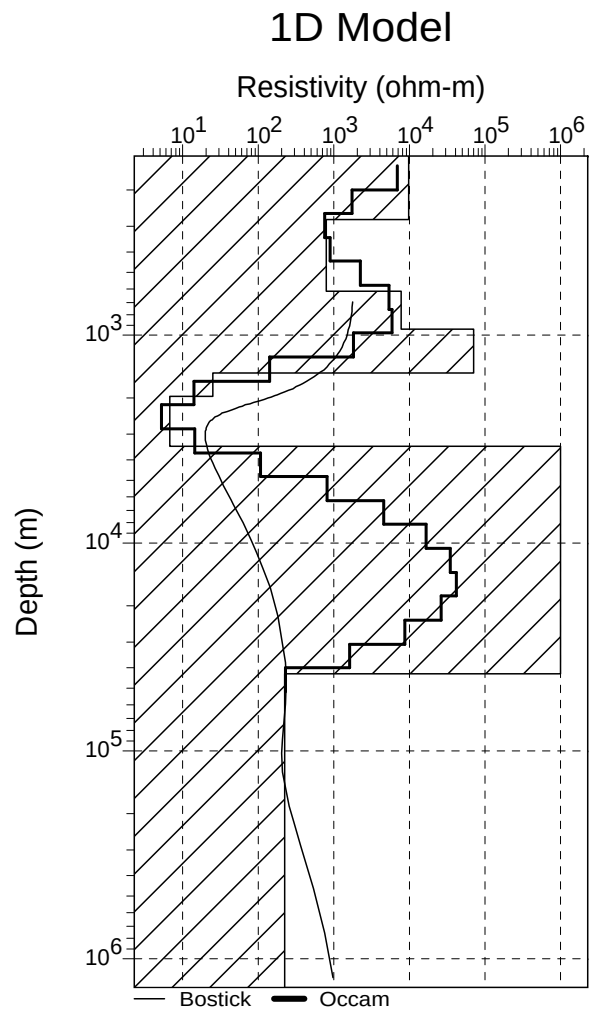

Sounding: MR004
Area: Mauna Kea
26/Dec/2016

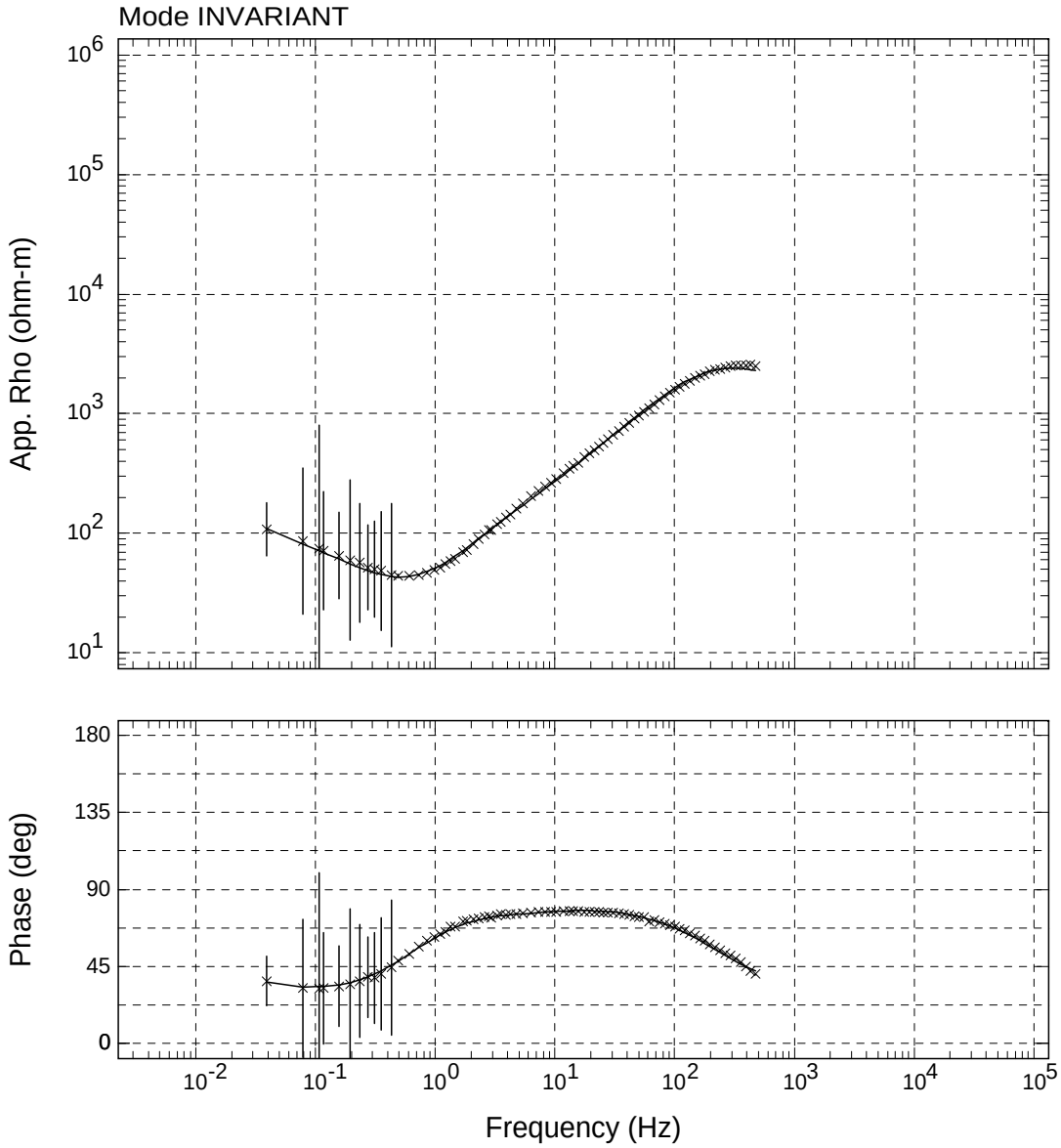

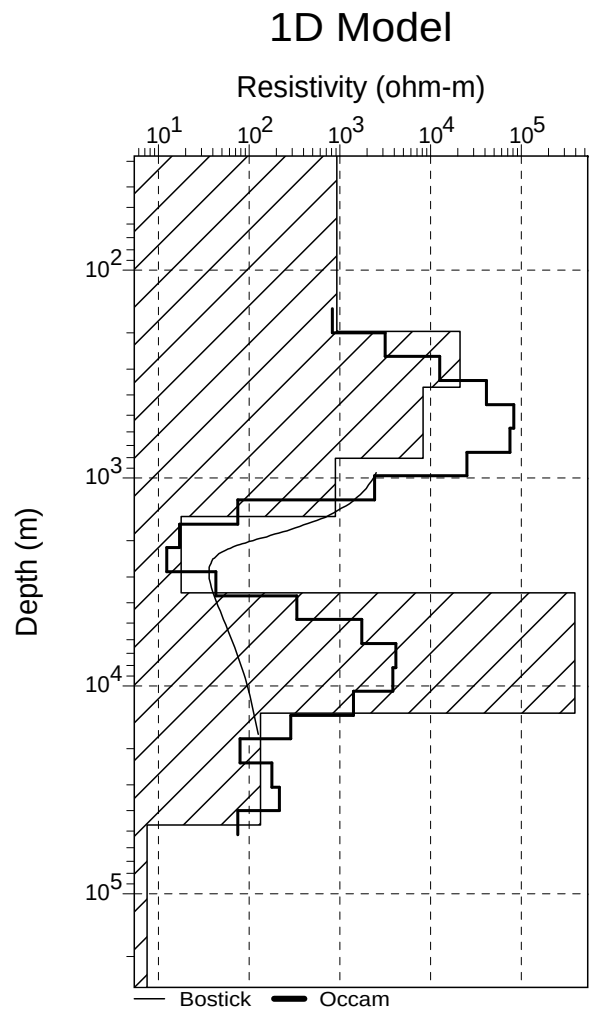

Sounding: MR005
Area: Mauna Kea
22/Dec/2016

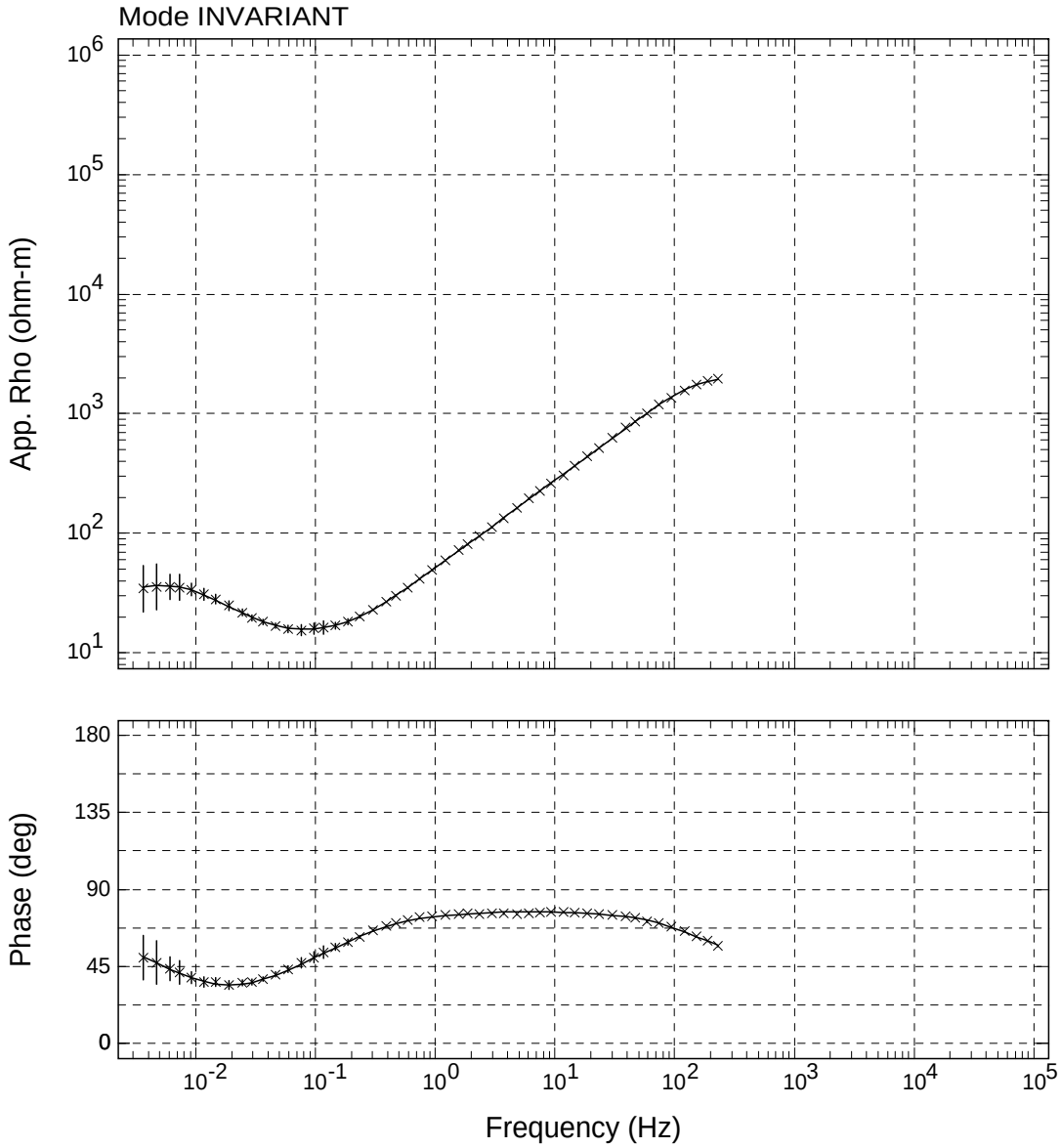

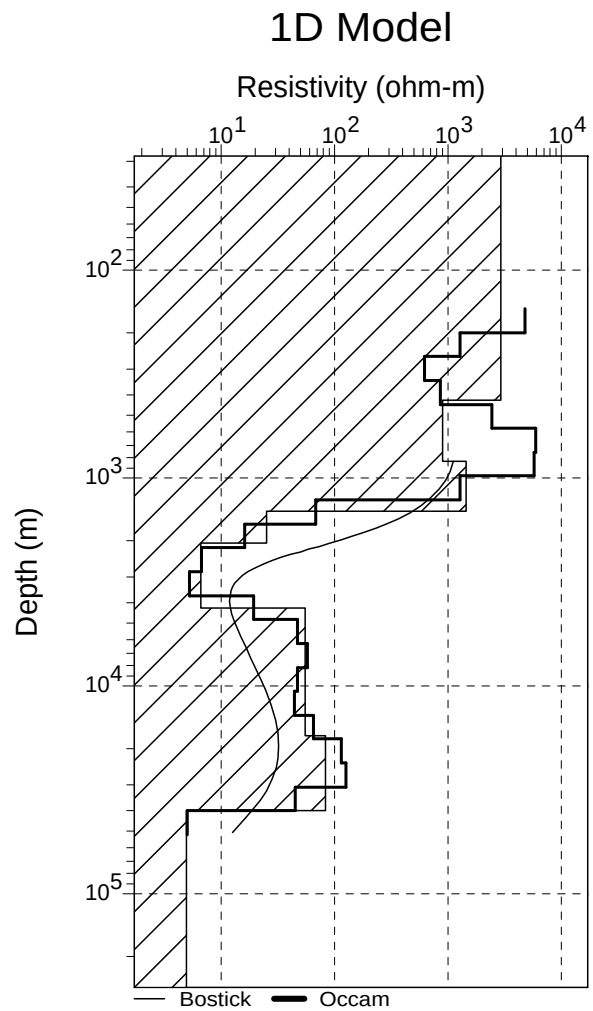

Sounding: MR006
Area: Mauna Kea
26/Dec/2016

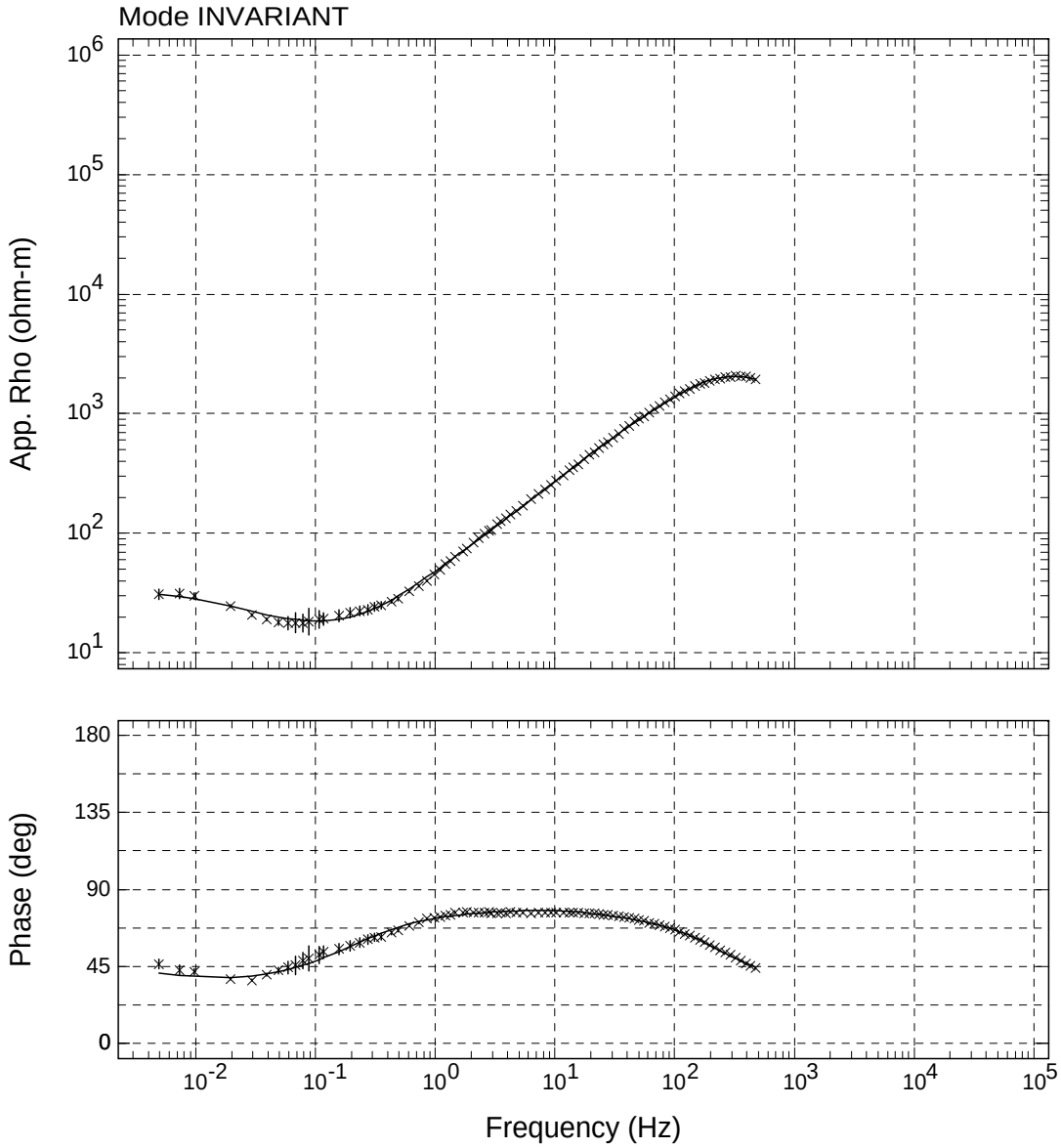

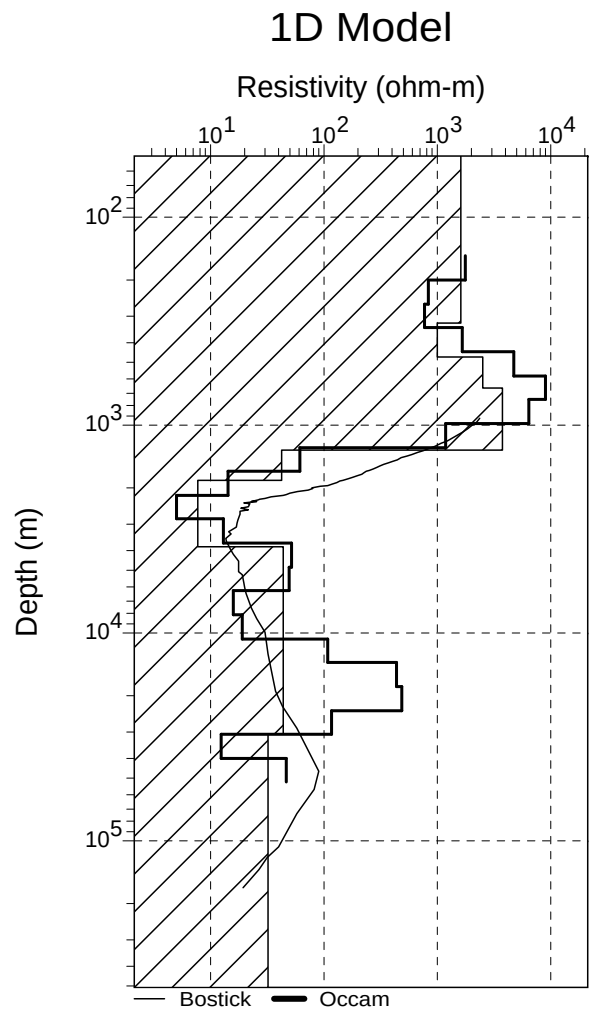

Sounding: MR007

Area: Mauna Kea

26/Dec/2016

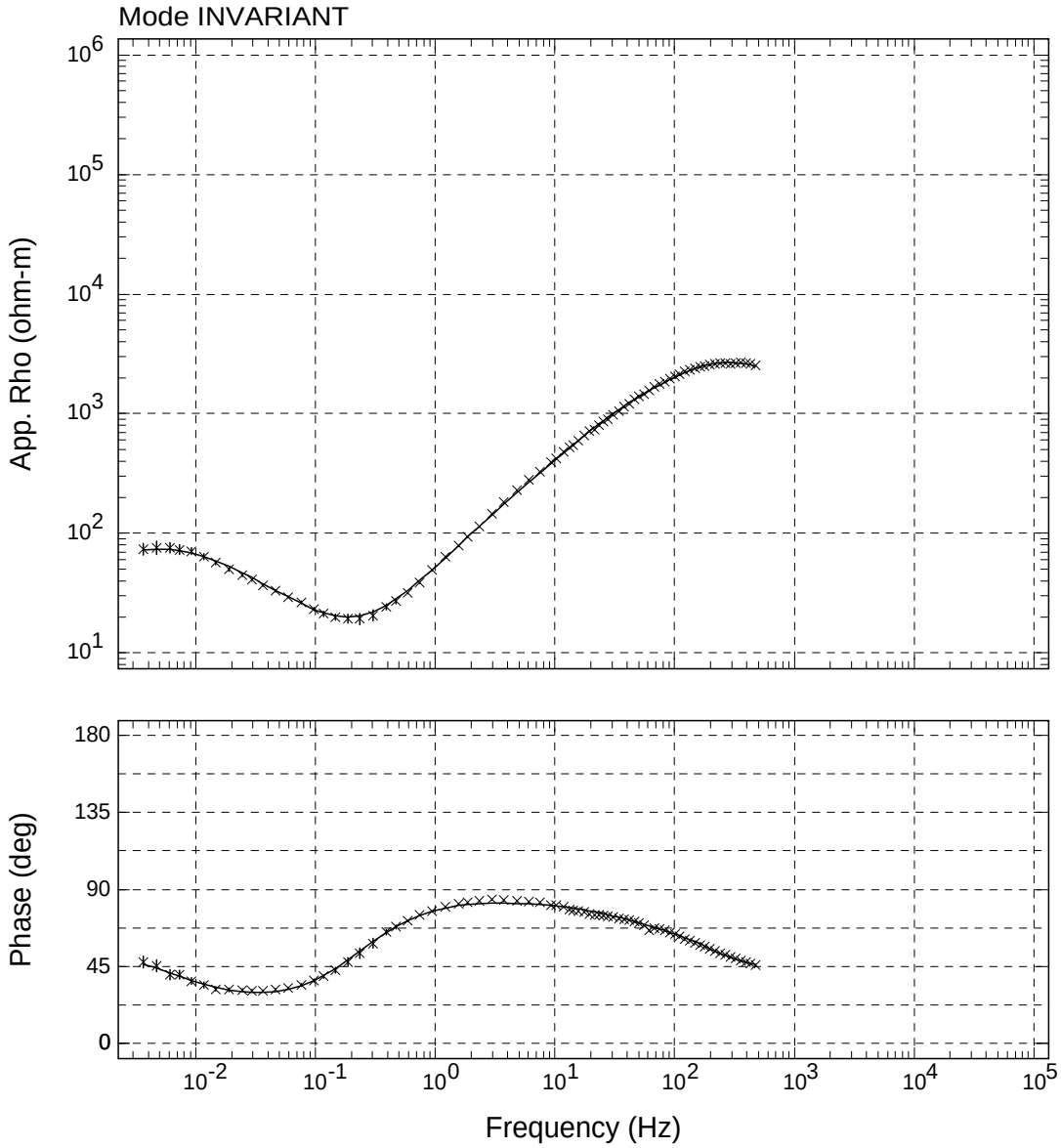

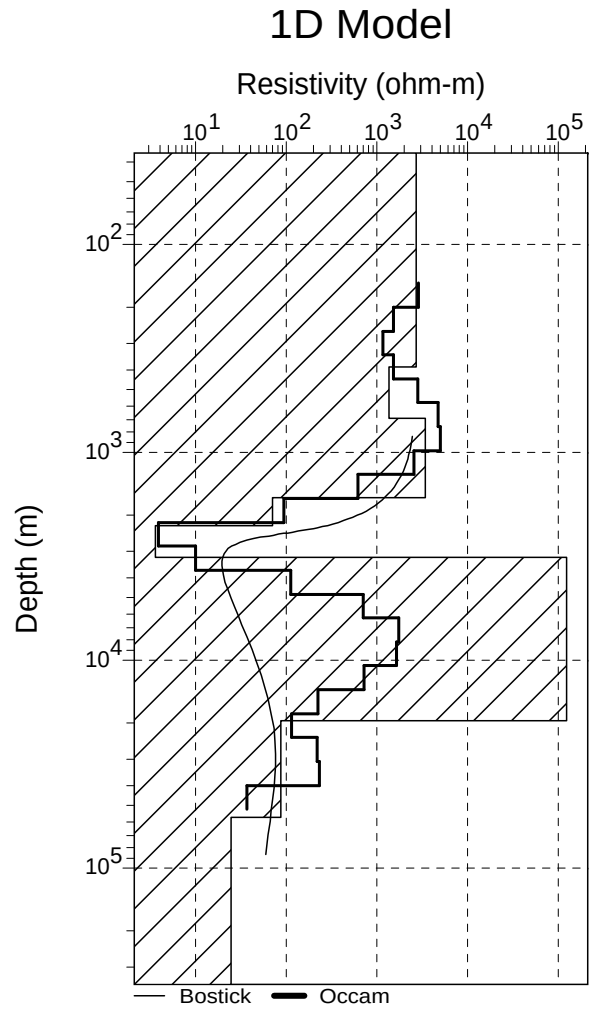

Sounding: MR009
Area: Mauna Kea
26/Dec/2016

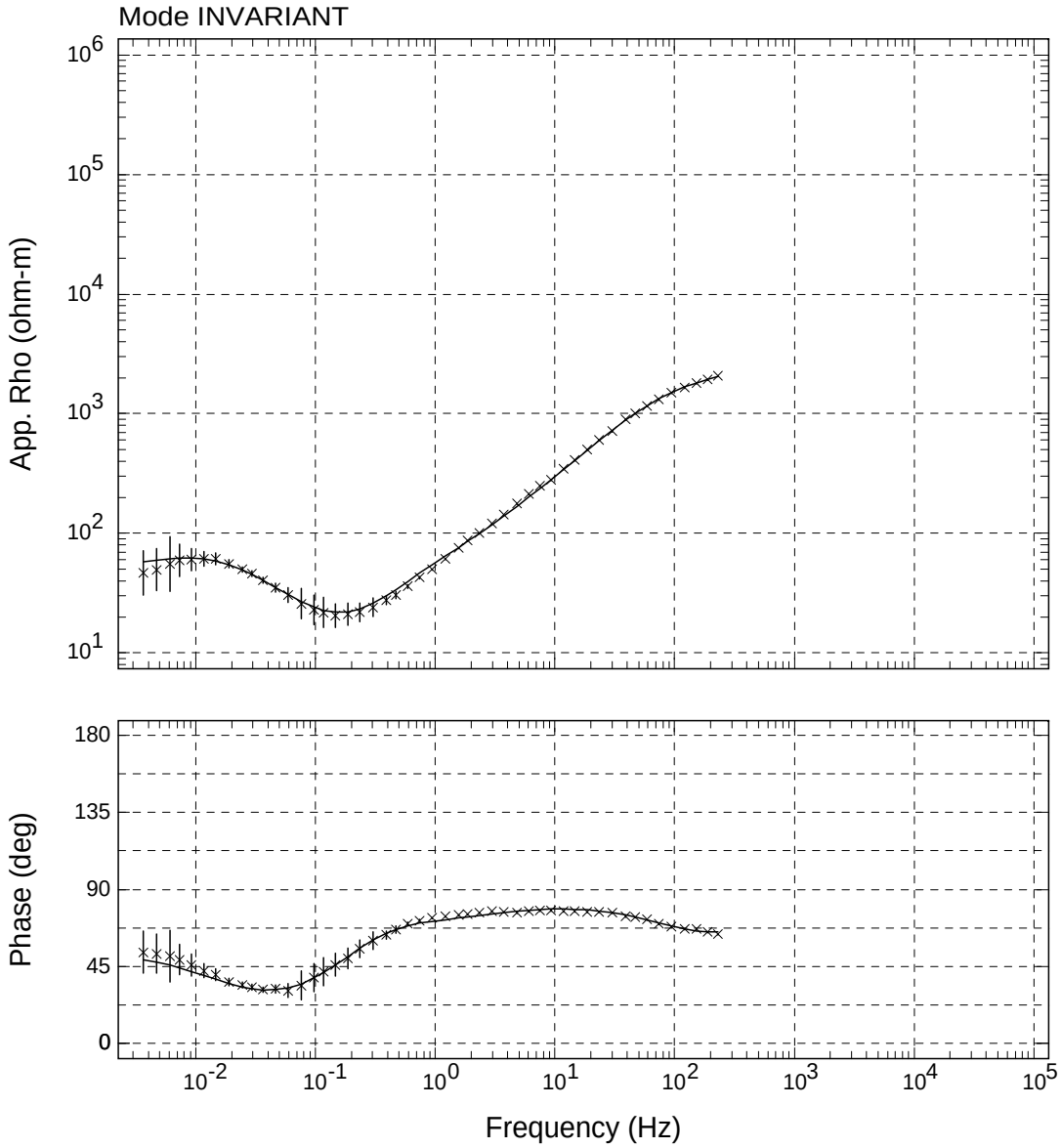

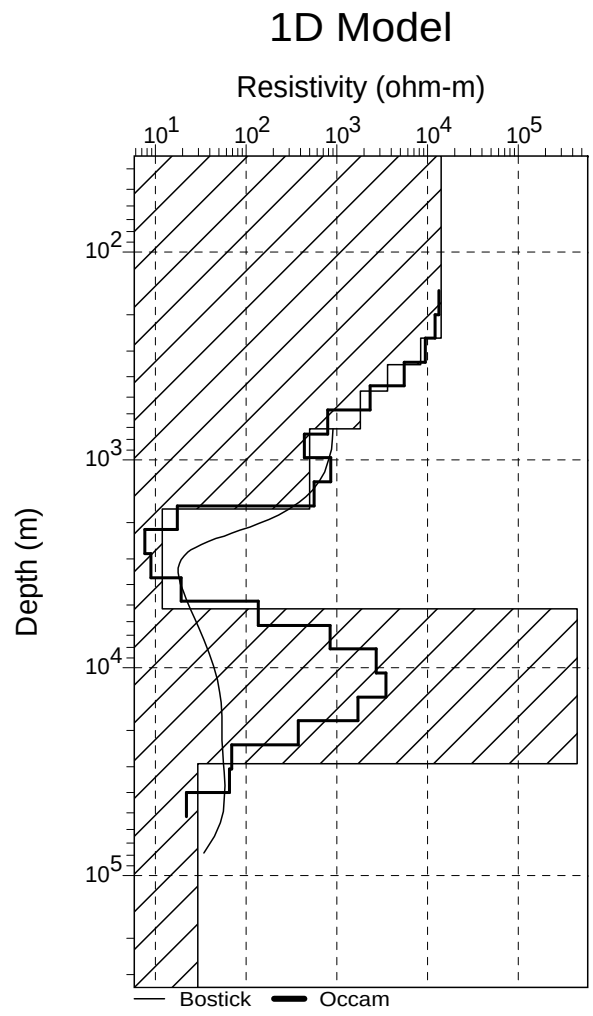

Sounding: MR010
Area: Mauna Kea
26/Dec/2016

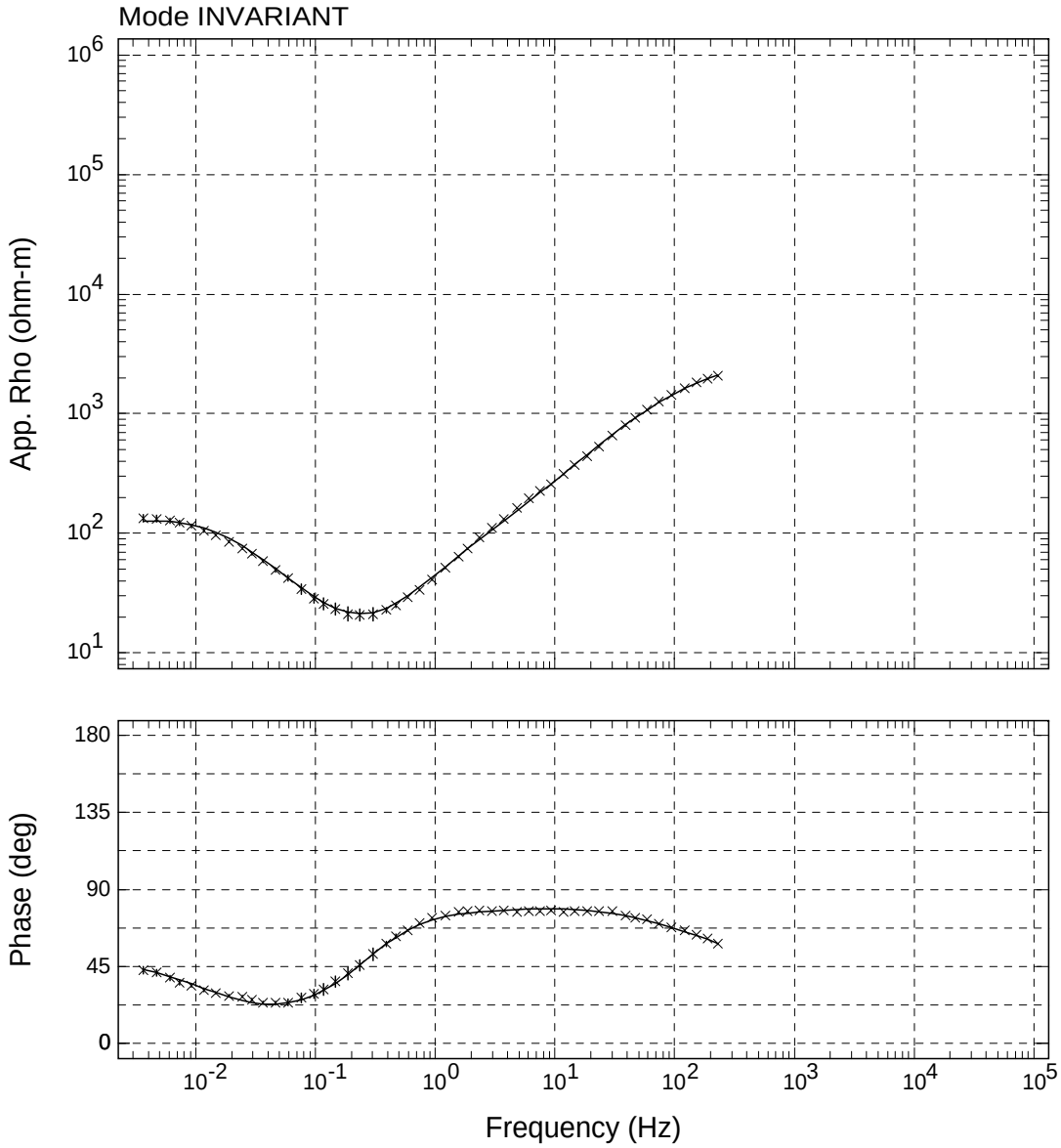

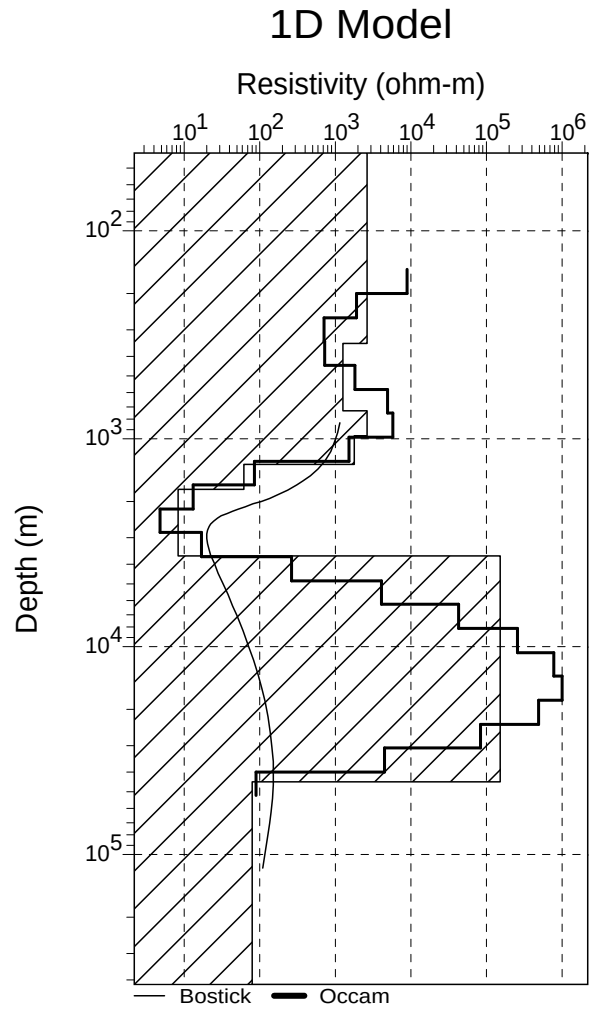

Sounding: MR011
Area: Mauna Kea
26/Dec/2016

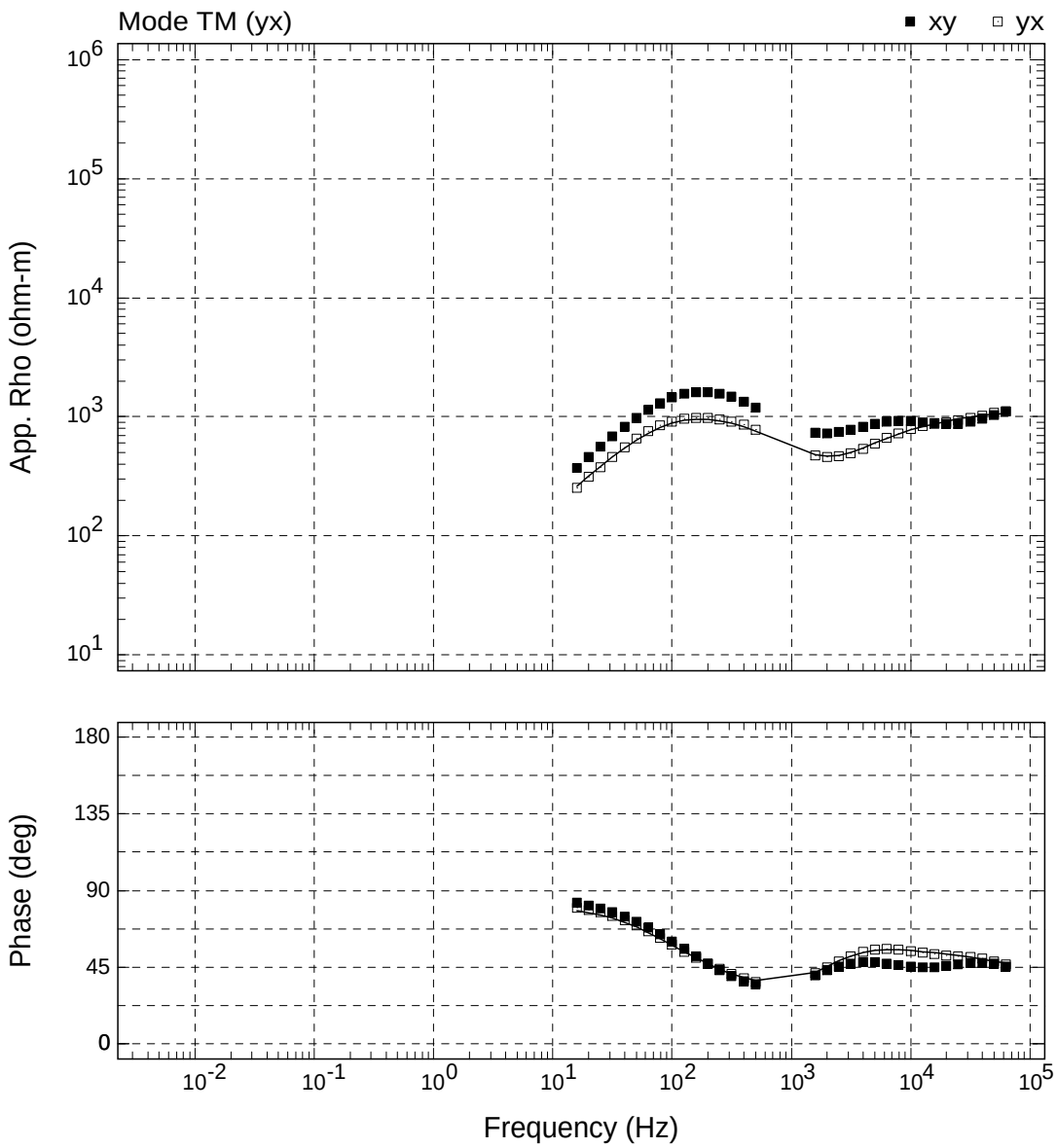

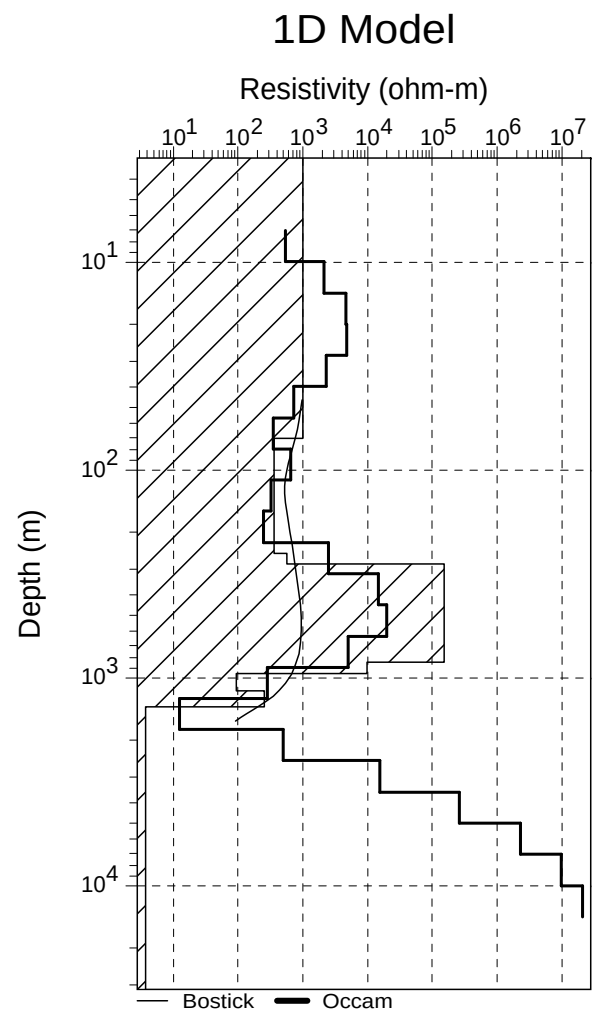

Sounding: ZMR004

Area: Mauna Kea

26/Dec/2016

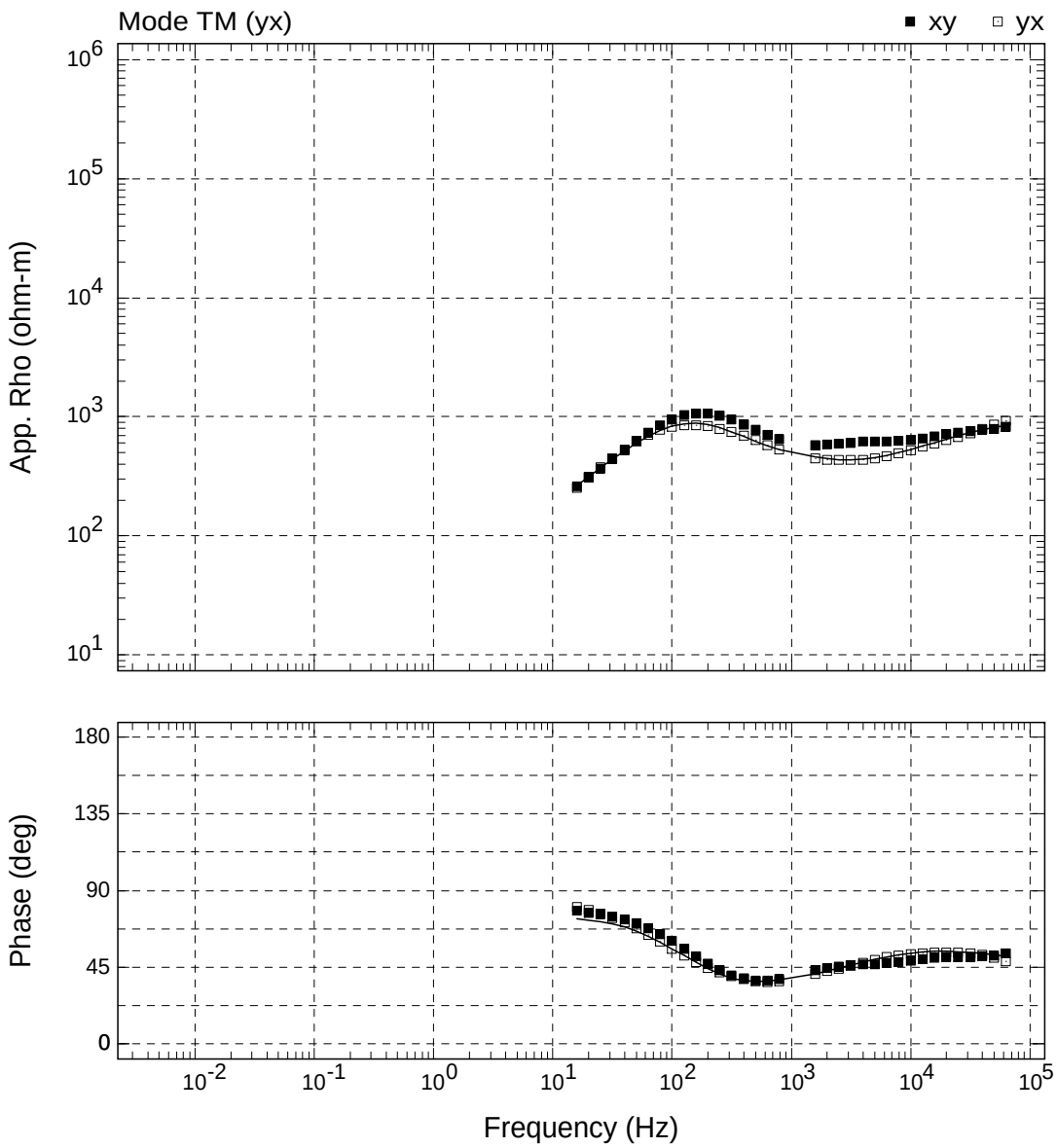

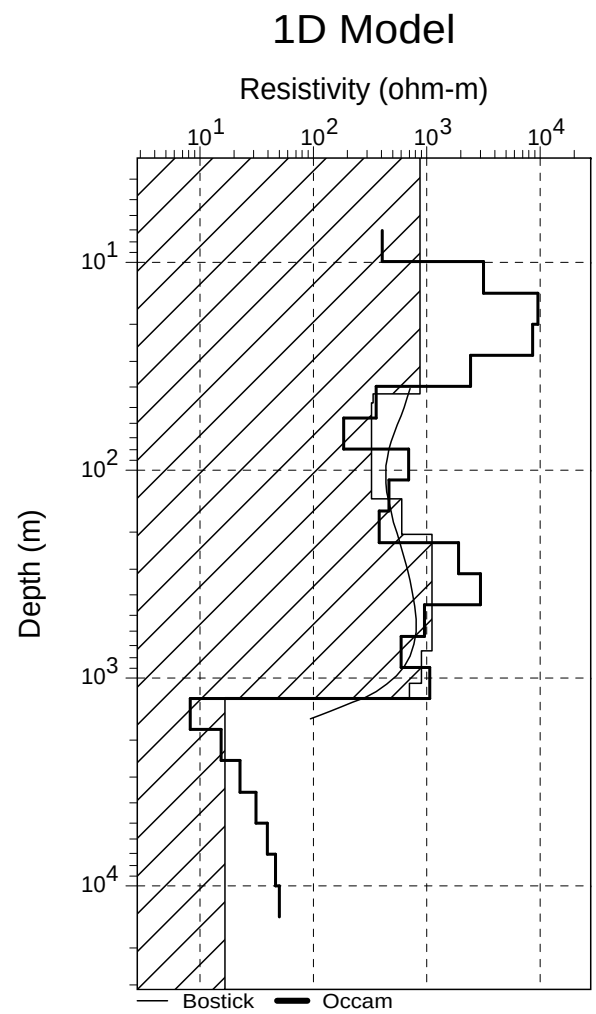

Sounding: ZMR005

Area: Mauna Kea

26/Dec/2016

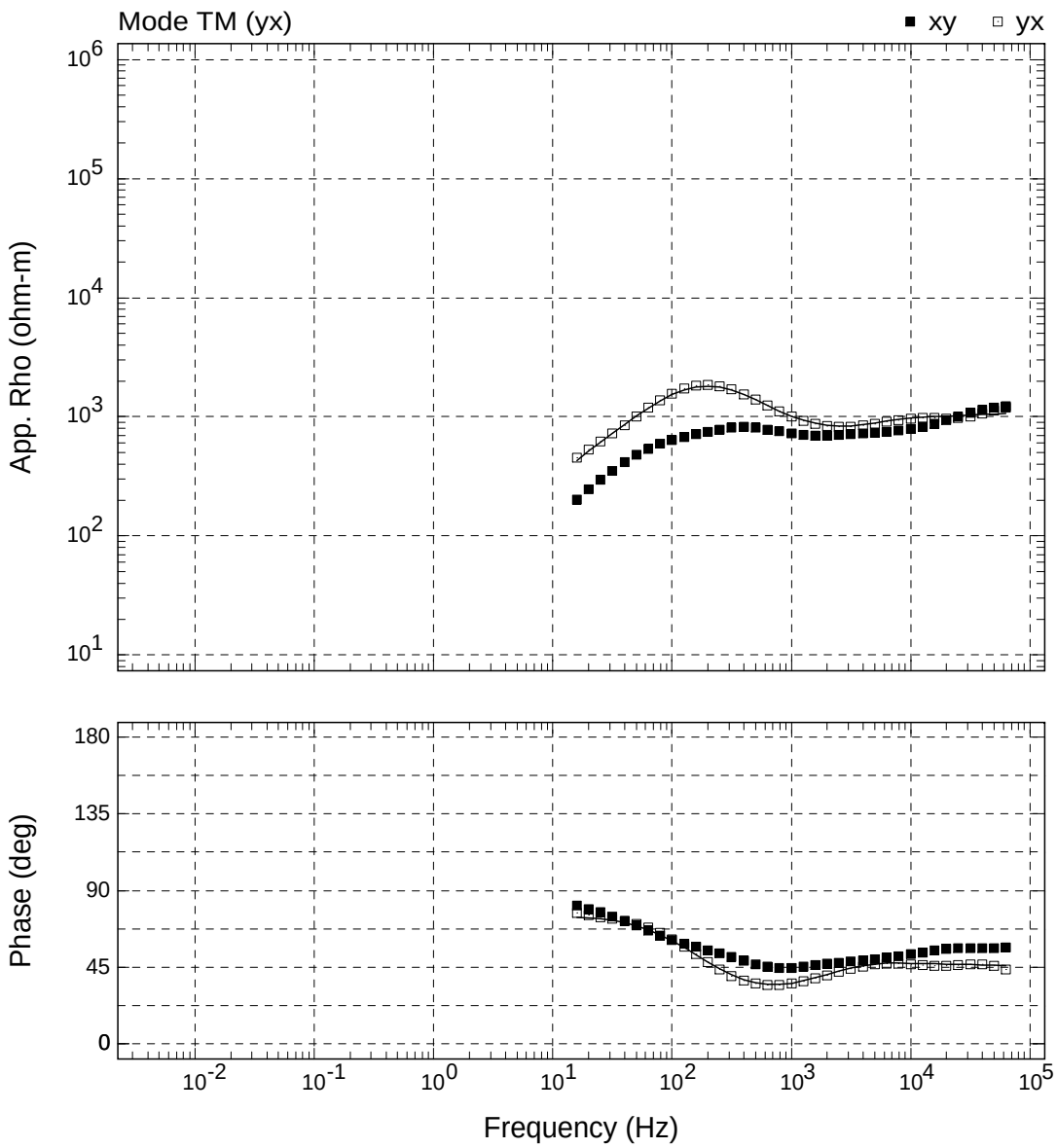

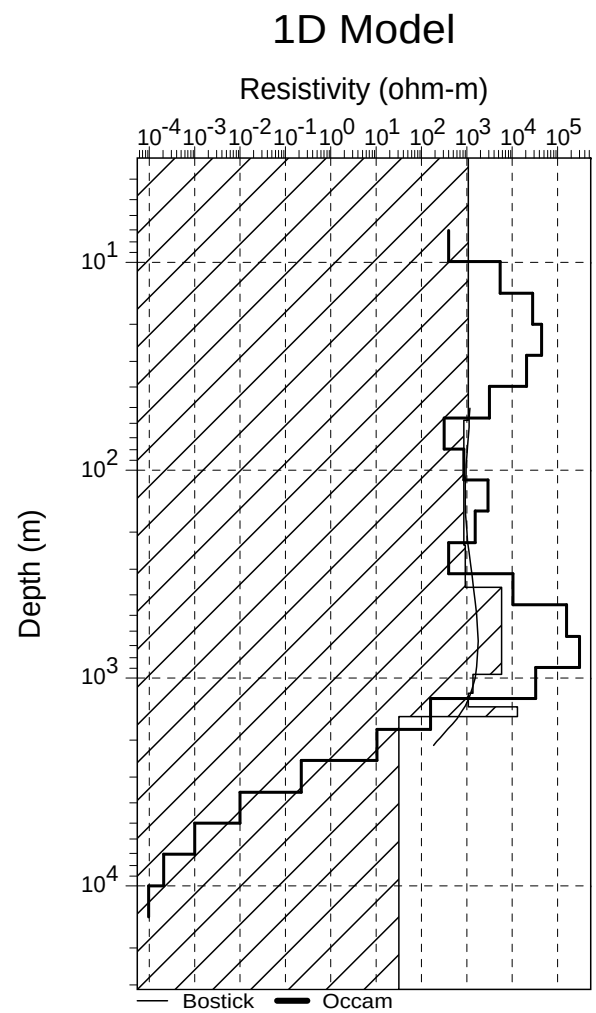

Sounding: ZMR006

Area: Mauna Kea

26/Dec/2016

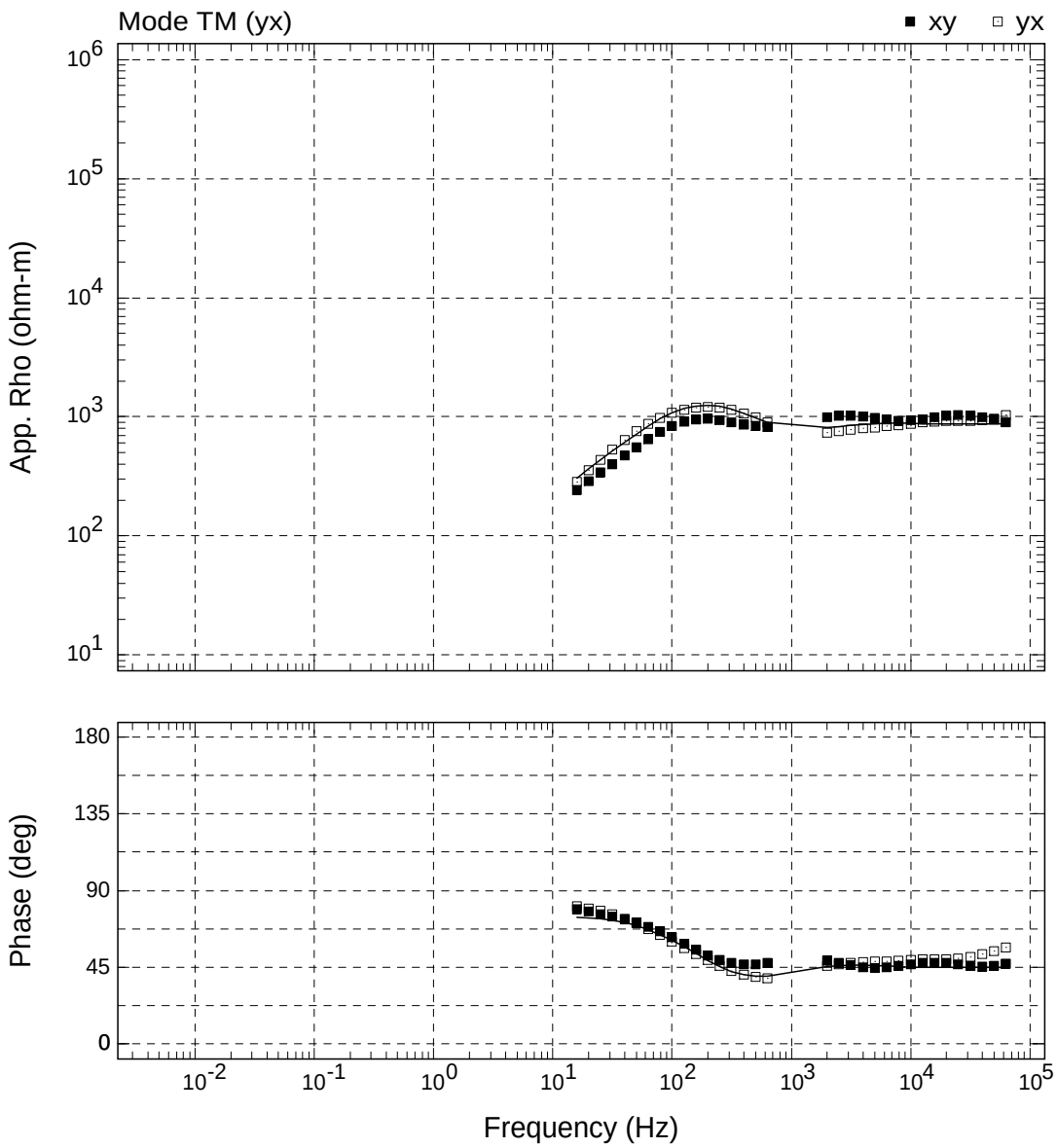

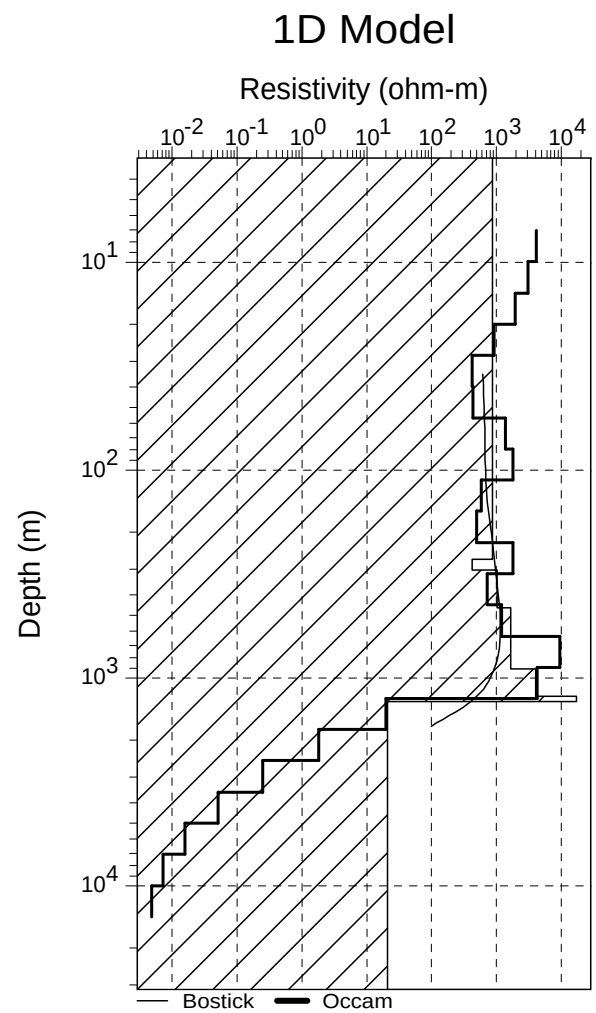

Sounding: ZMR007

Area: Mauna Kea

26/Dec/2016

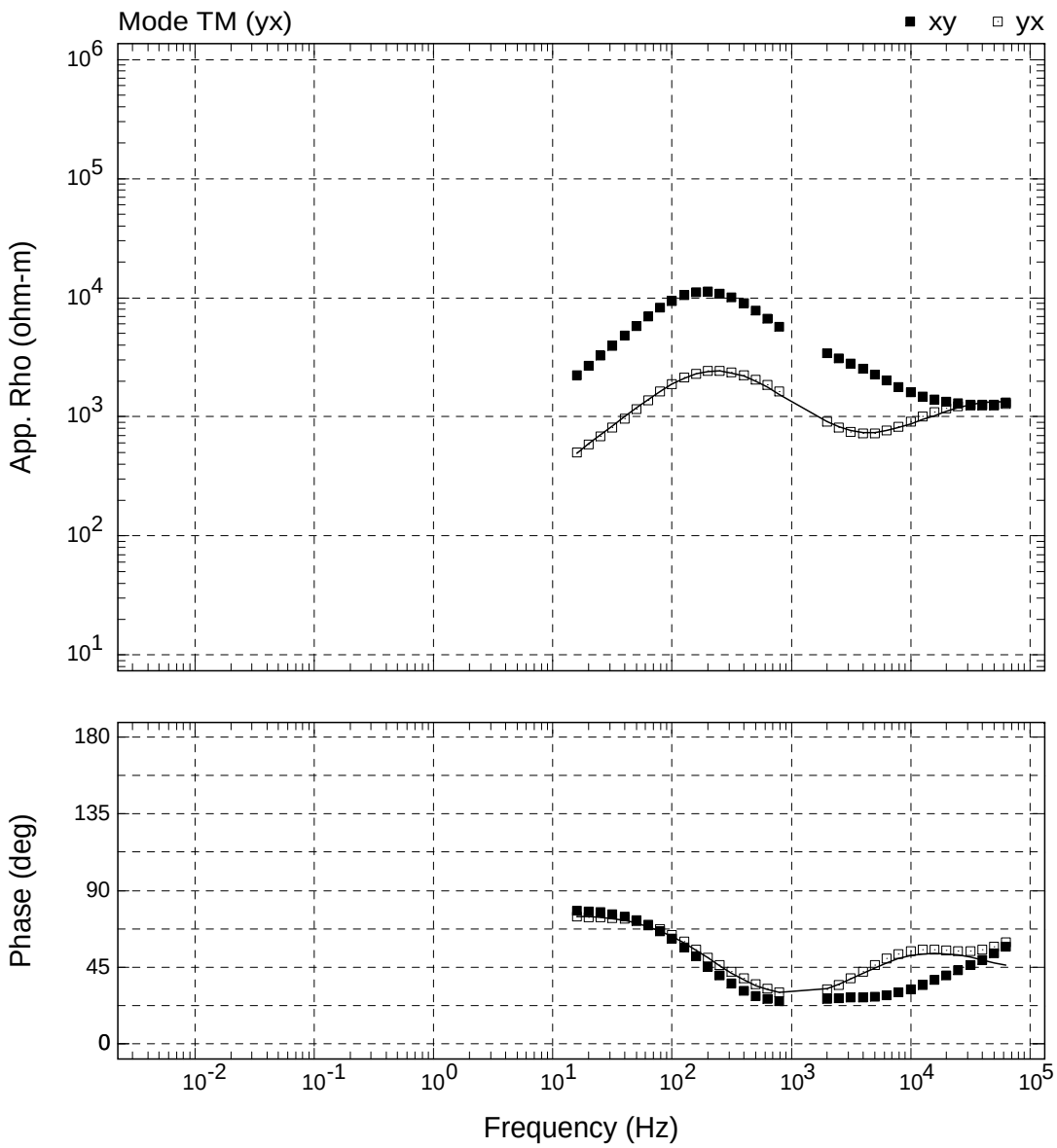

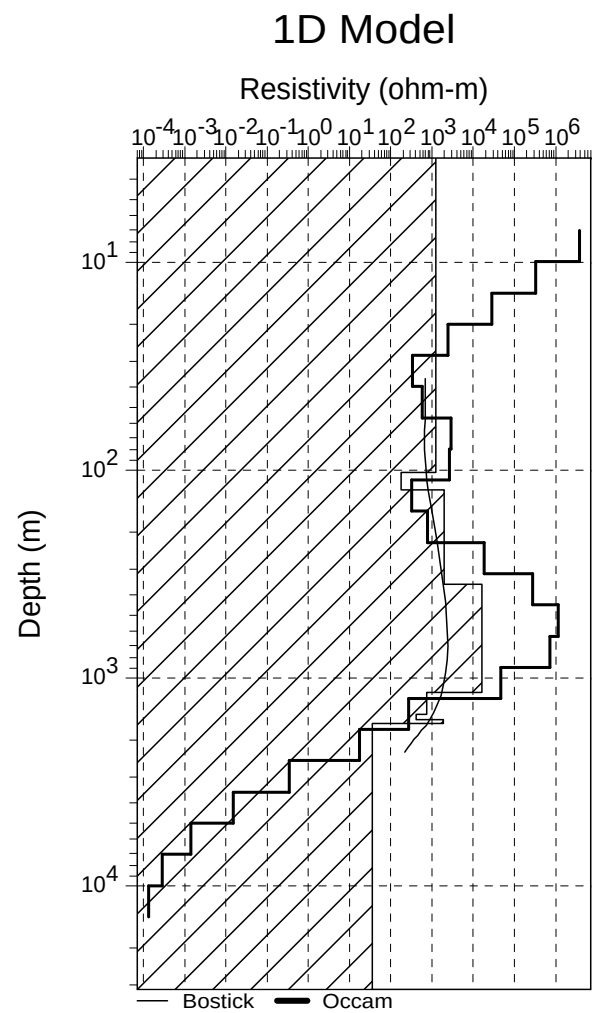

Sounding: ZMR008
Area: Mauna Kea
26/Dec/2016

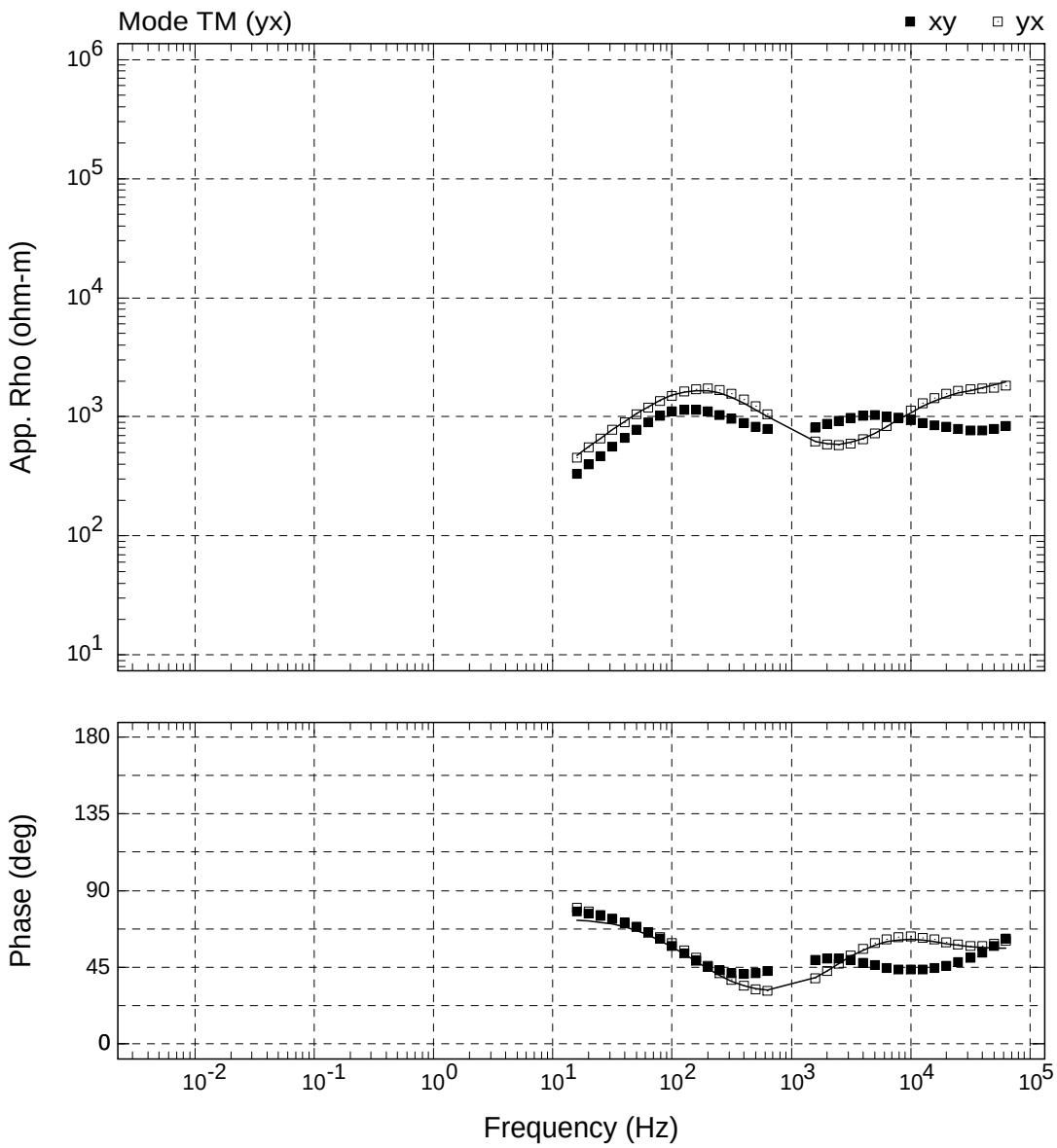

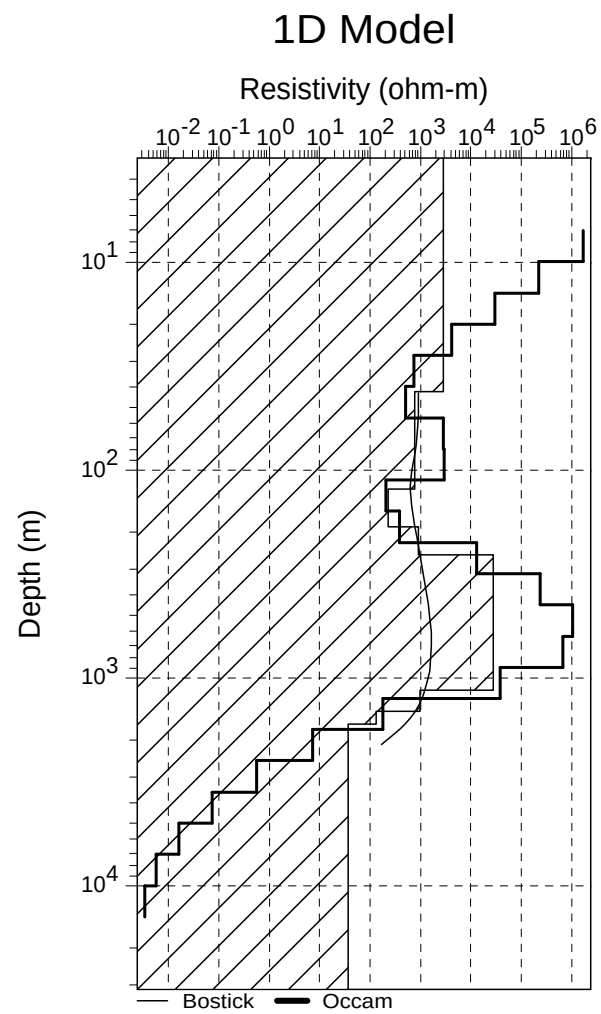

Sounding: ZMR009

Area: Mauna Kea

26/Dec/2016

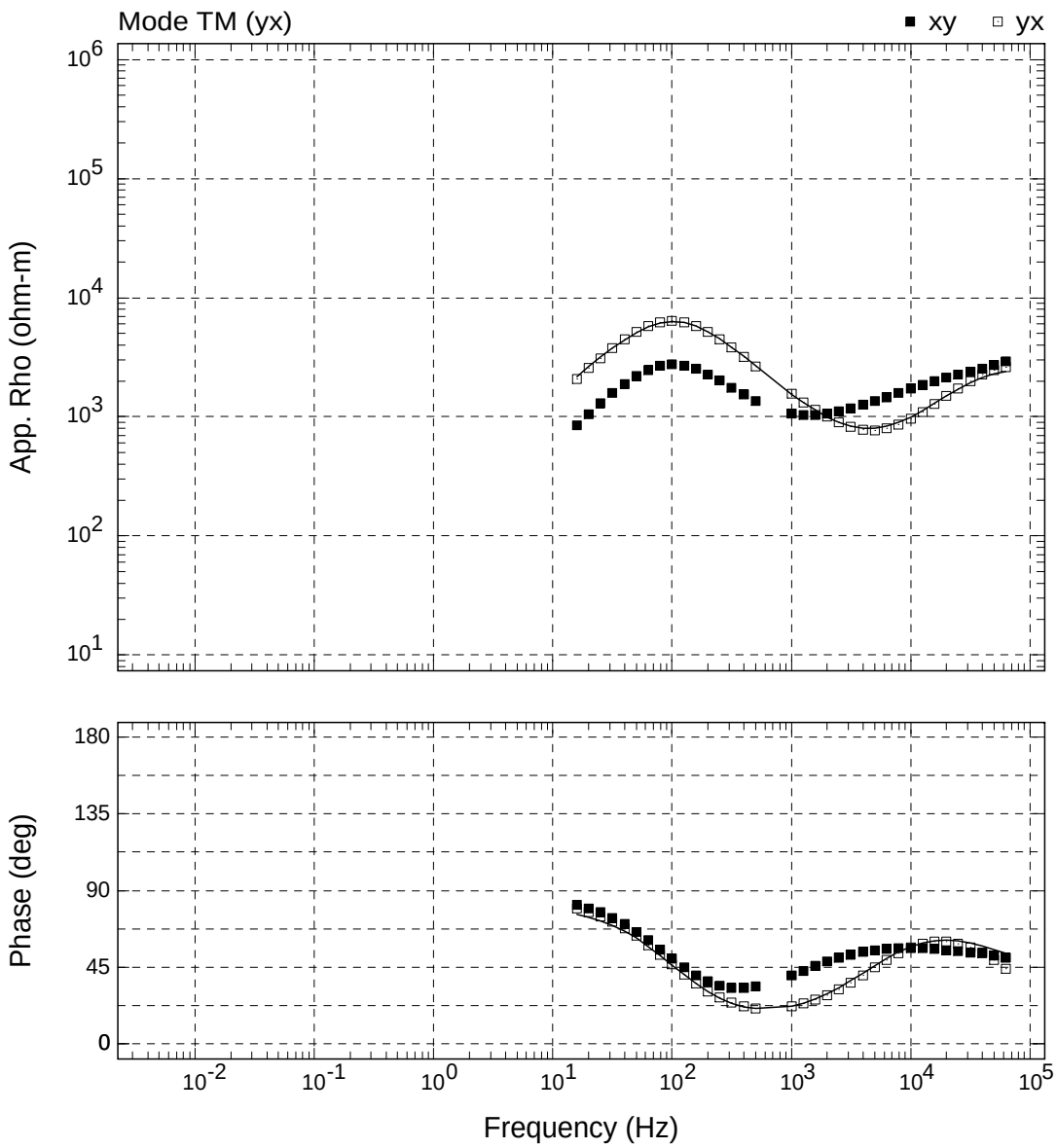

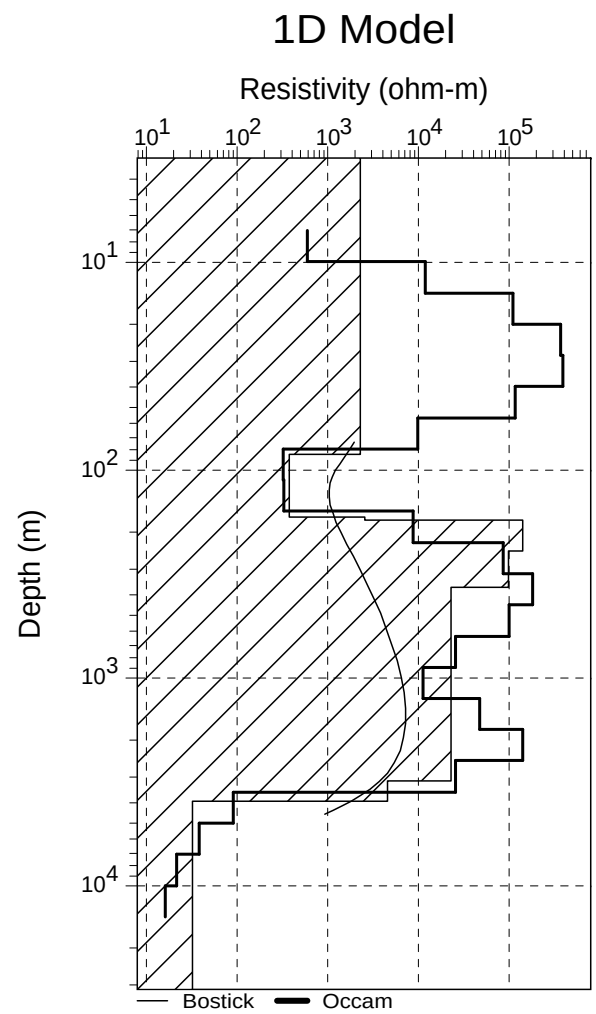

Sounding: ZMR010

Area: Mauna Kea

26/Dec/2016

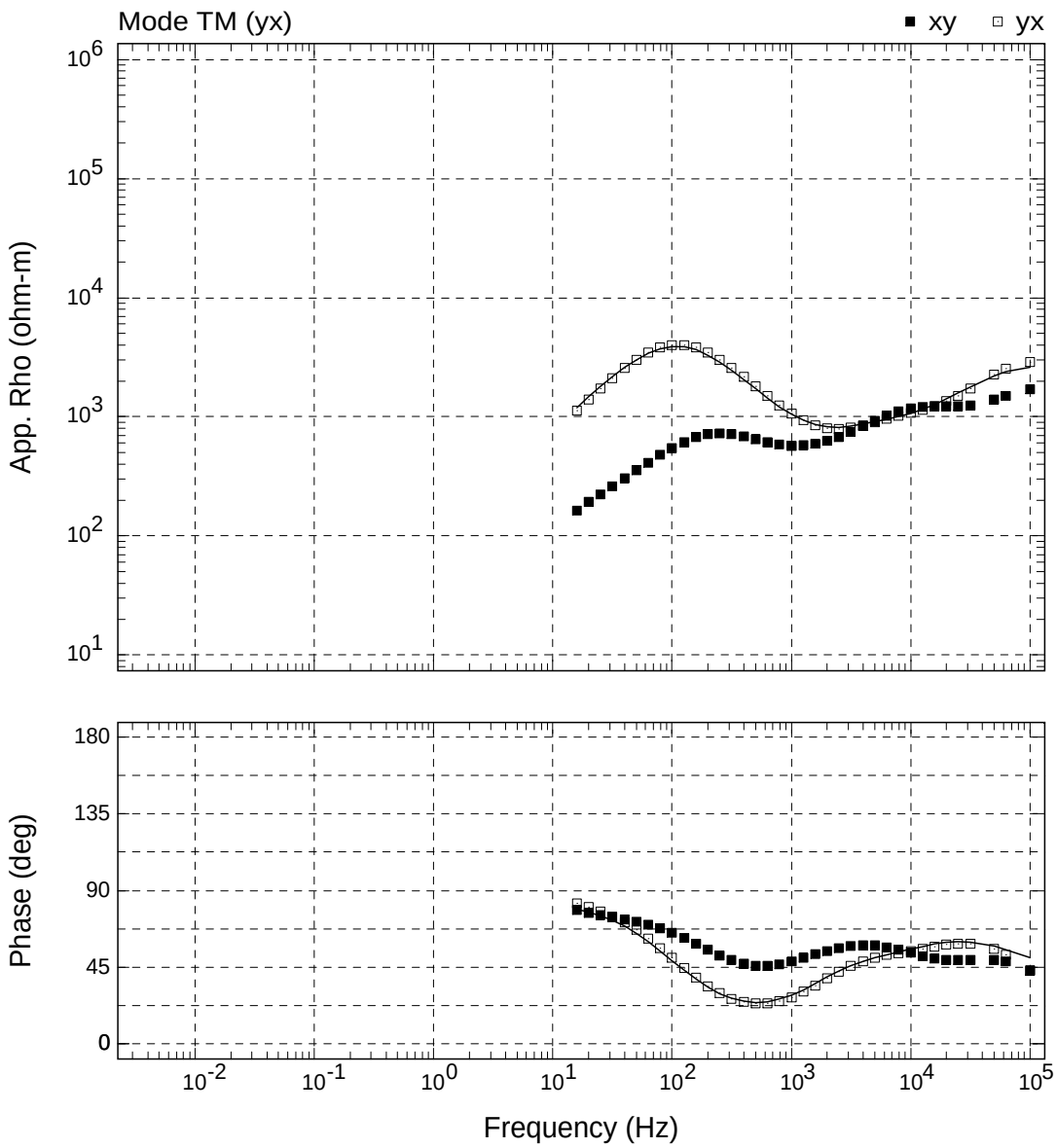

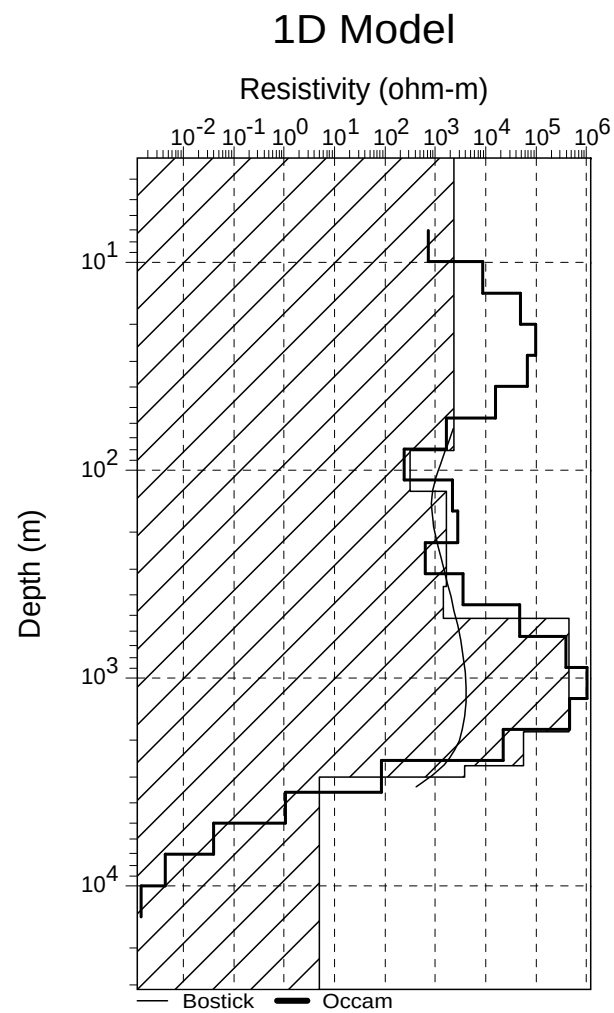

Sounding: ZMR011

Area: Mauna Kea

26/Dec/2016

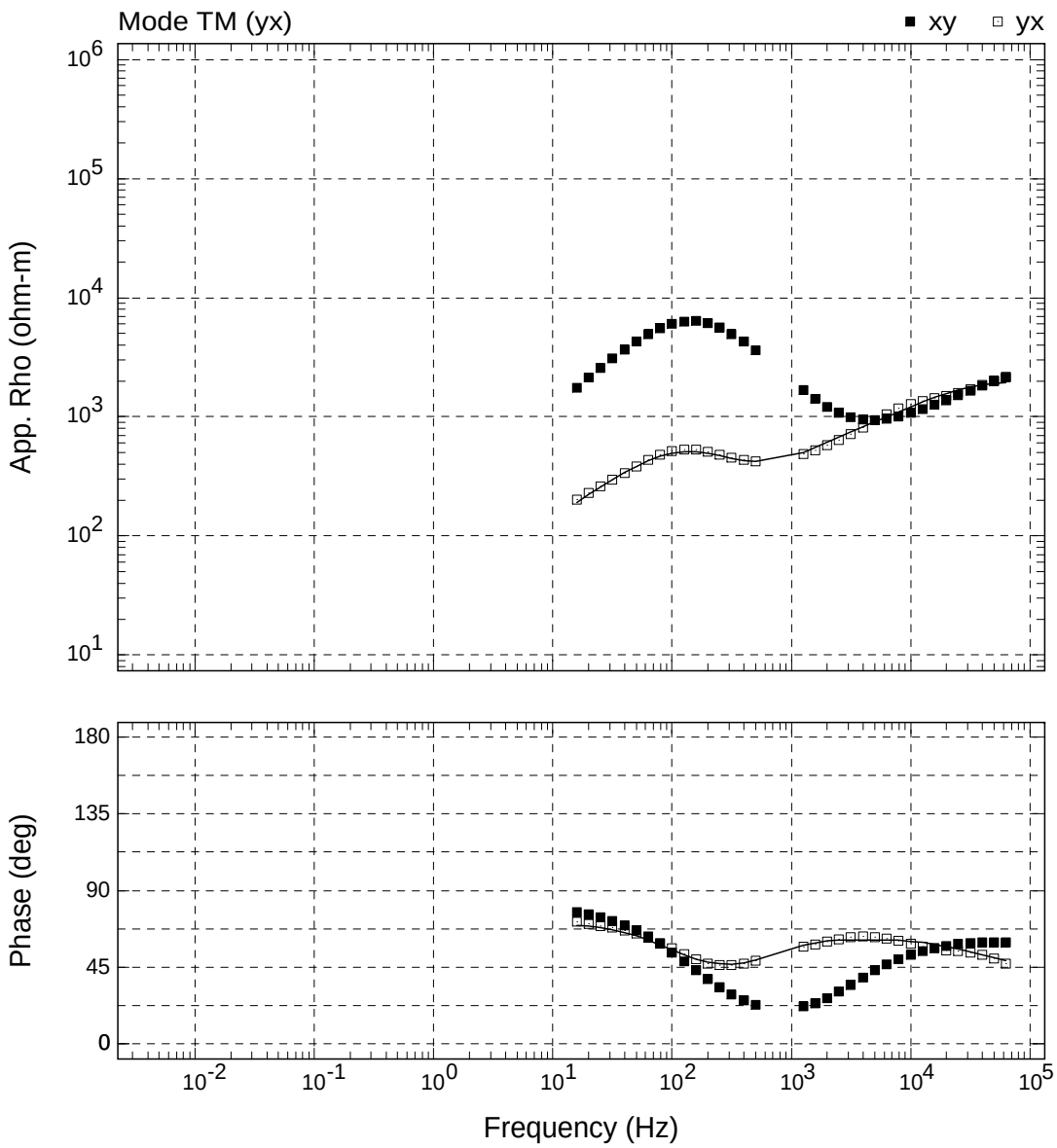

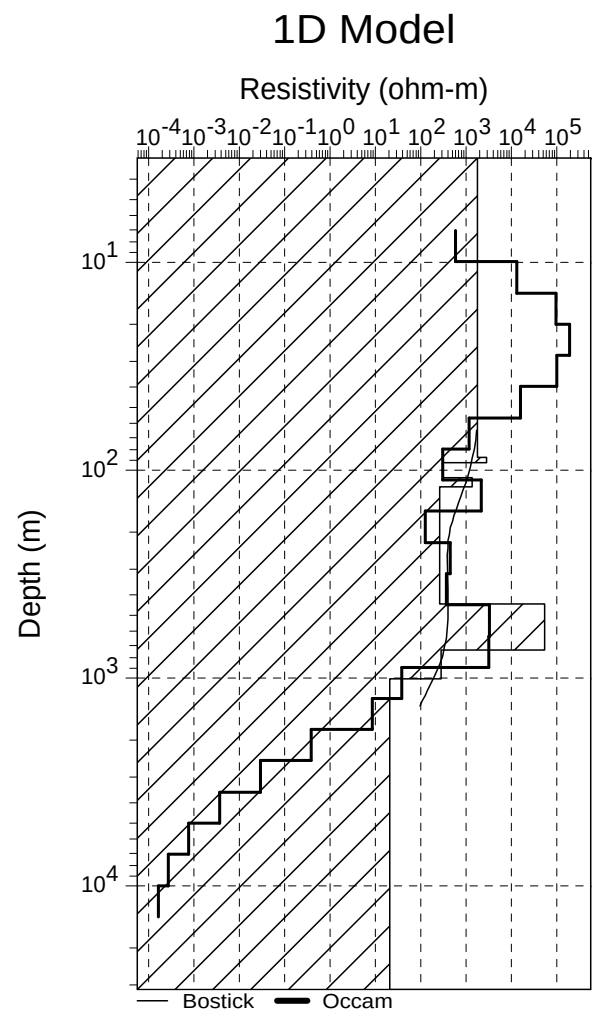

Sounding: ZMR012

Area: Mauna Kea

26/Dec/2016

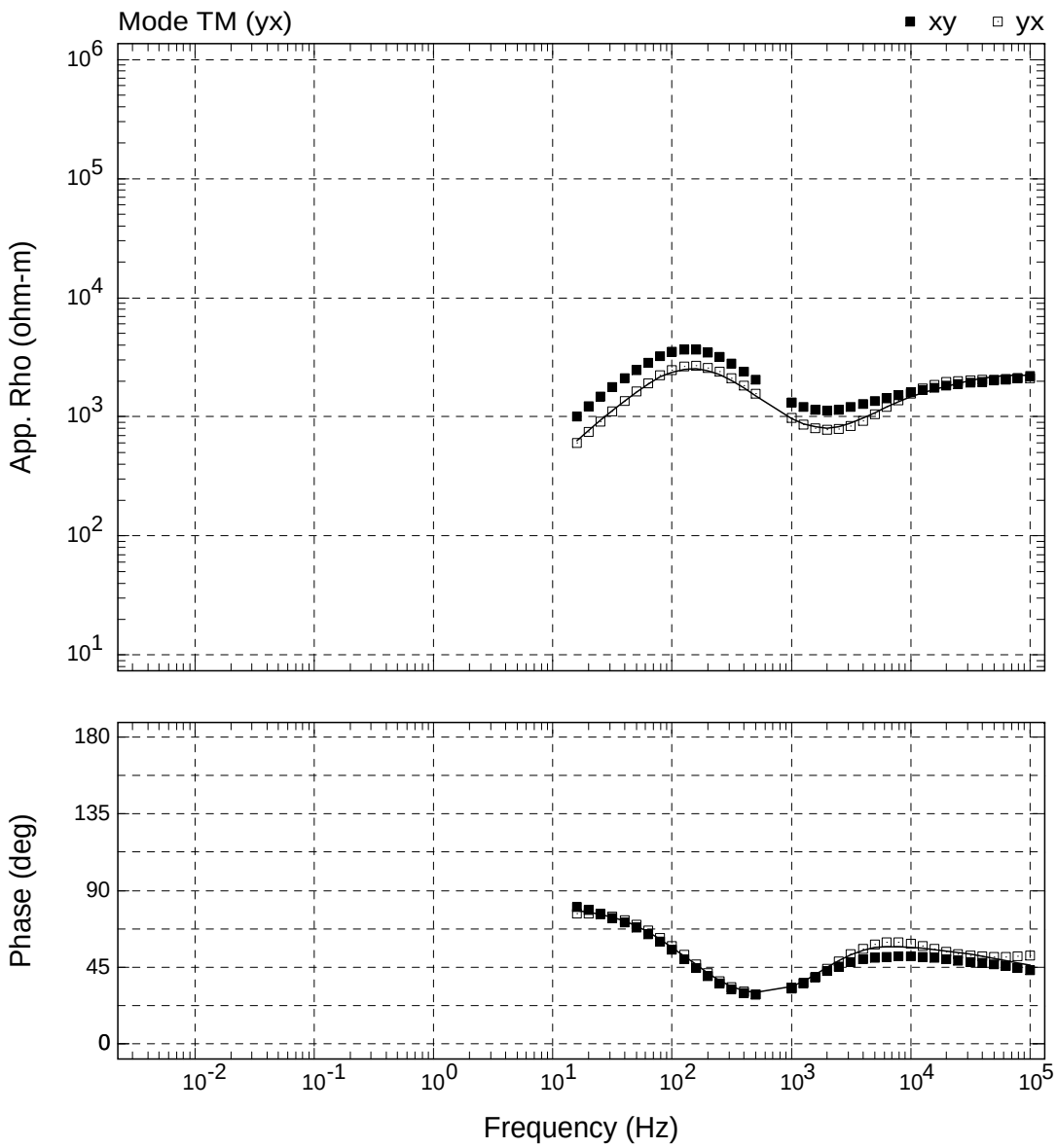

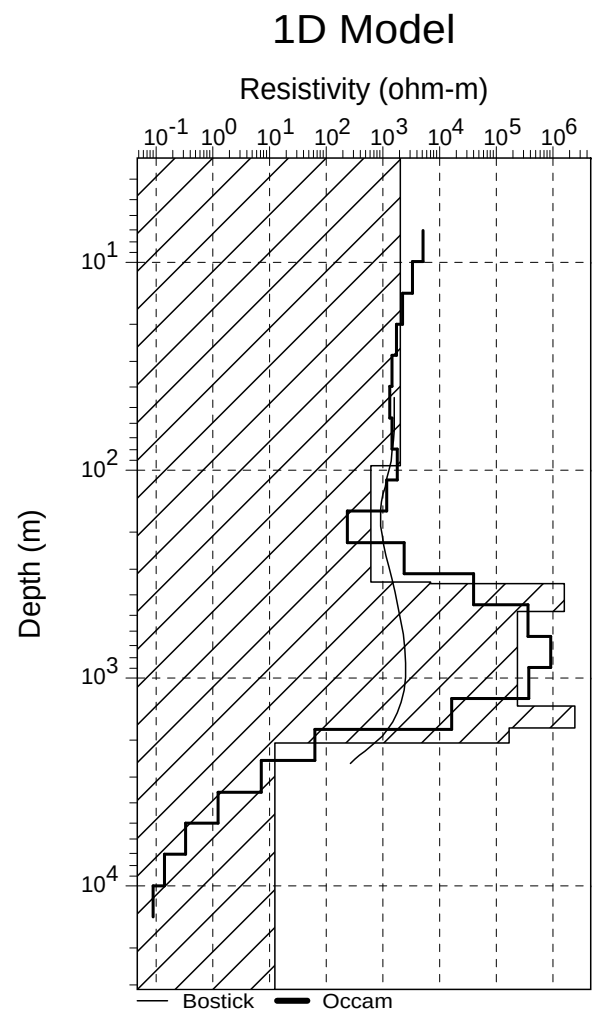

Sounding: ZMR013

Area: Mauna Kea

26/Dec/2016

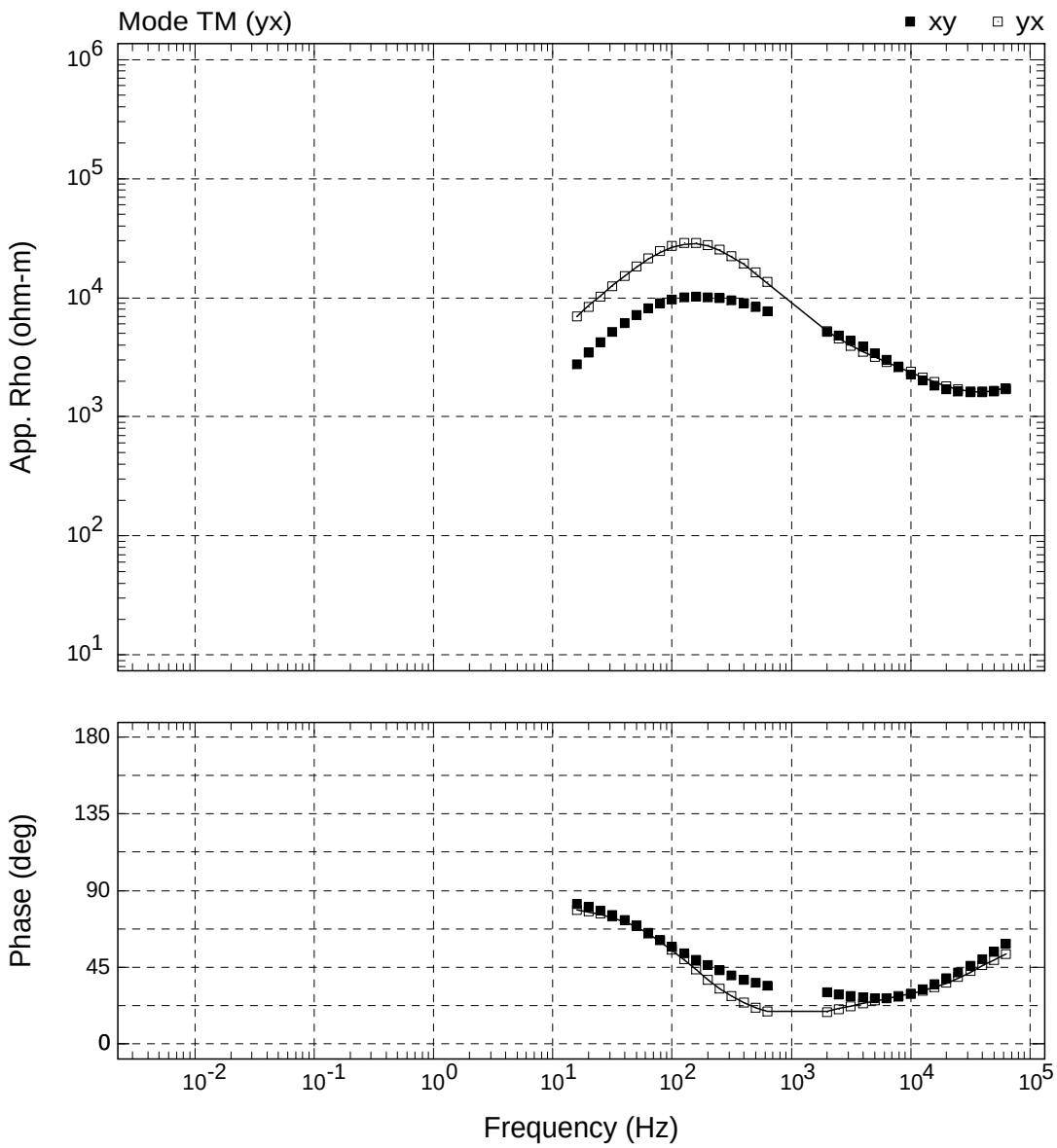

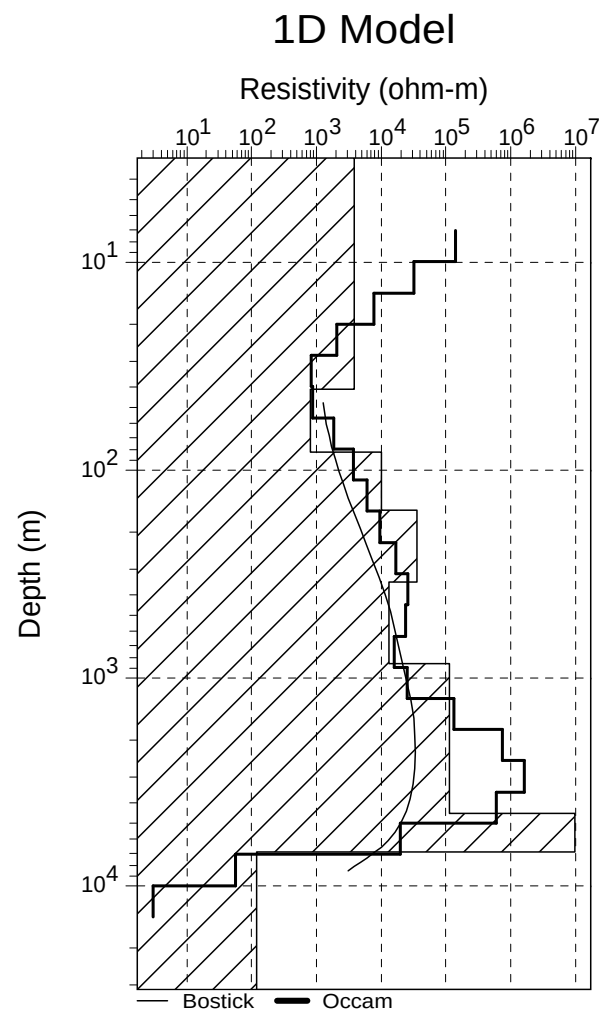

Sounding: ZMR014

Area: Mauna Kea

26/Dec/2016

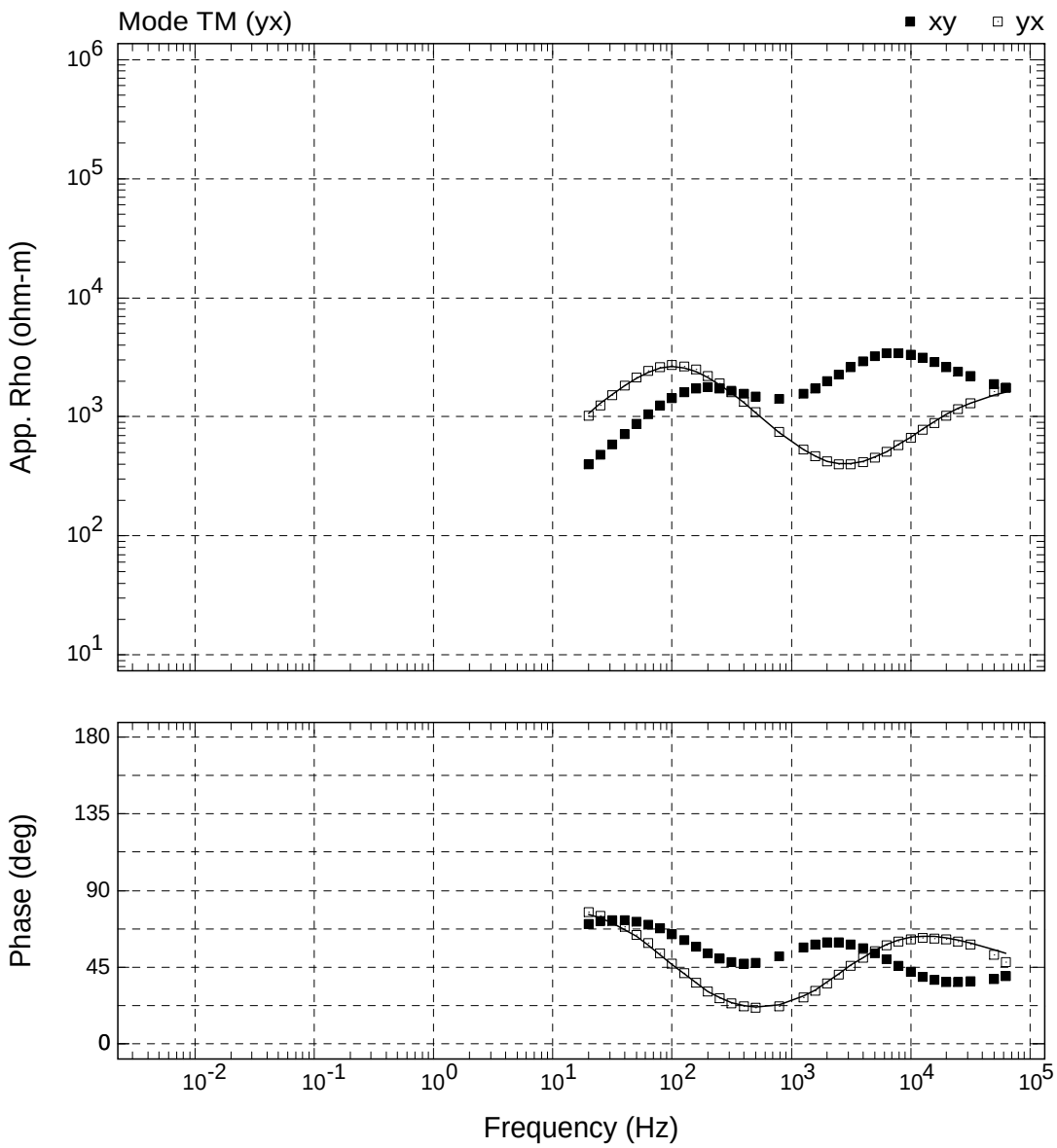

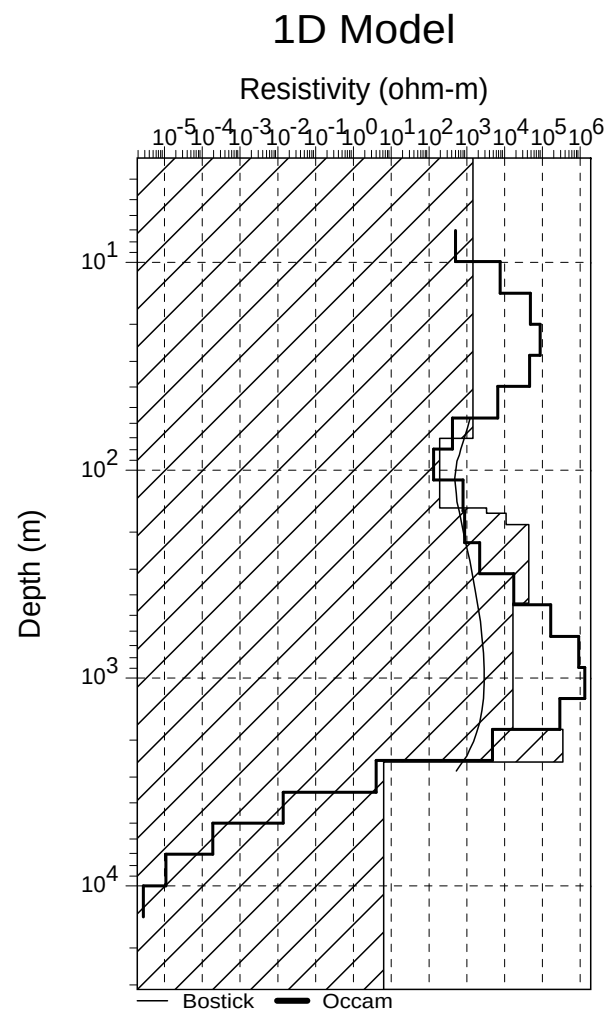

Sounding: ZMR015

Area: Mauna Kea

26/Dec/2016

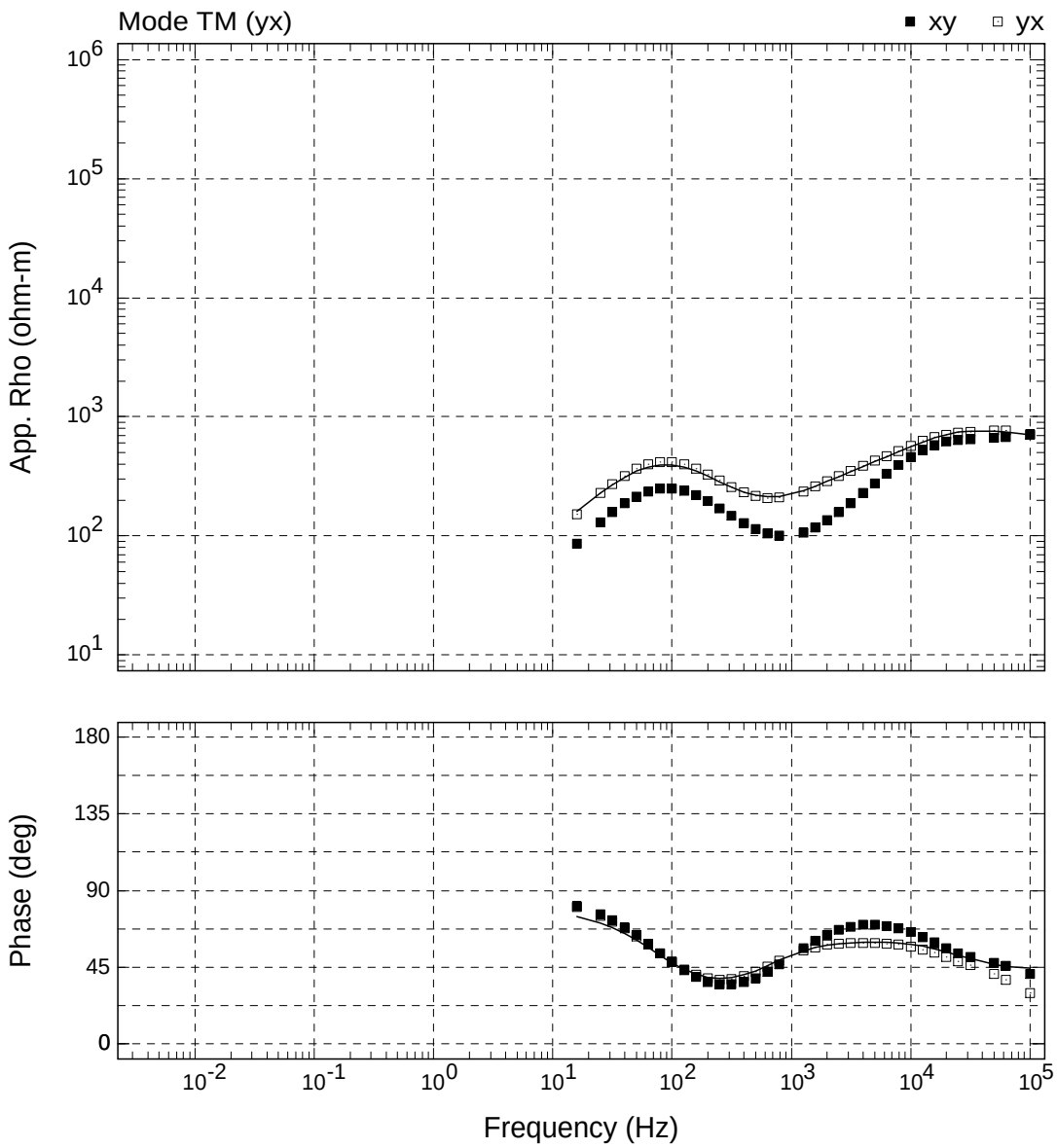

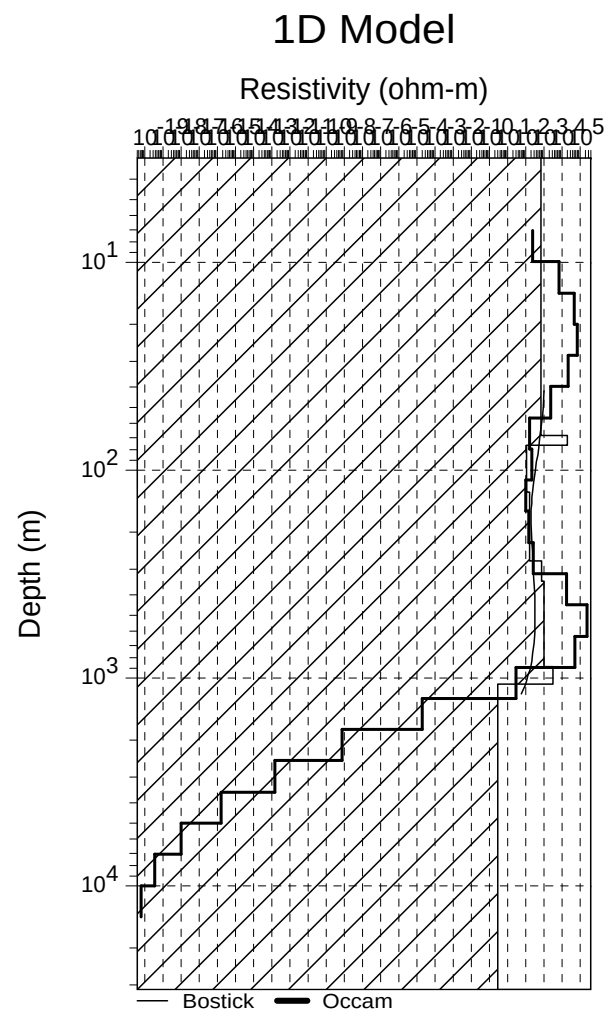

Sounding: ZMR016
Area: Mauna Kea
26/Dec/2016

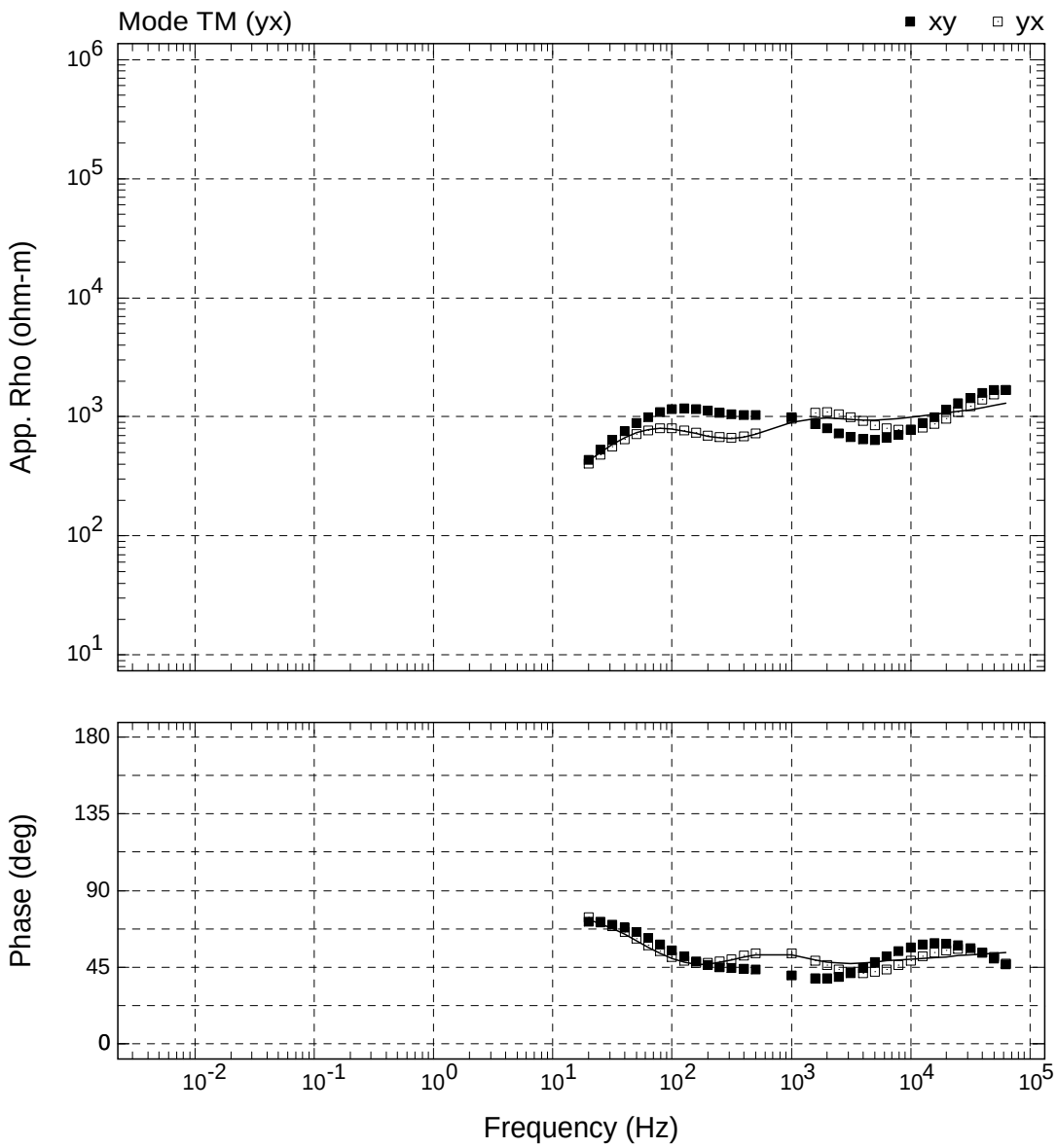

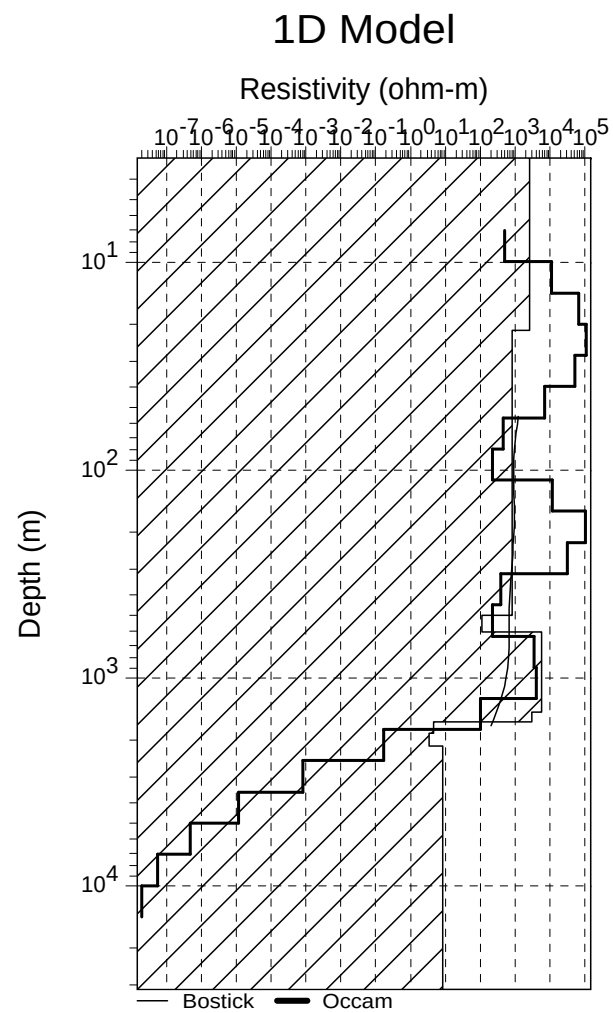

Sounding: ZMR017

Area: Mauna Kea

26/Dec/2016

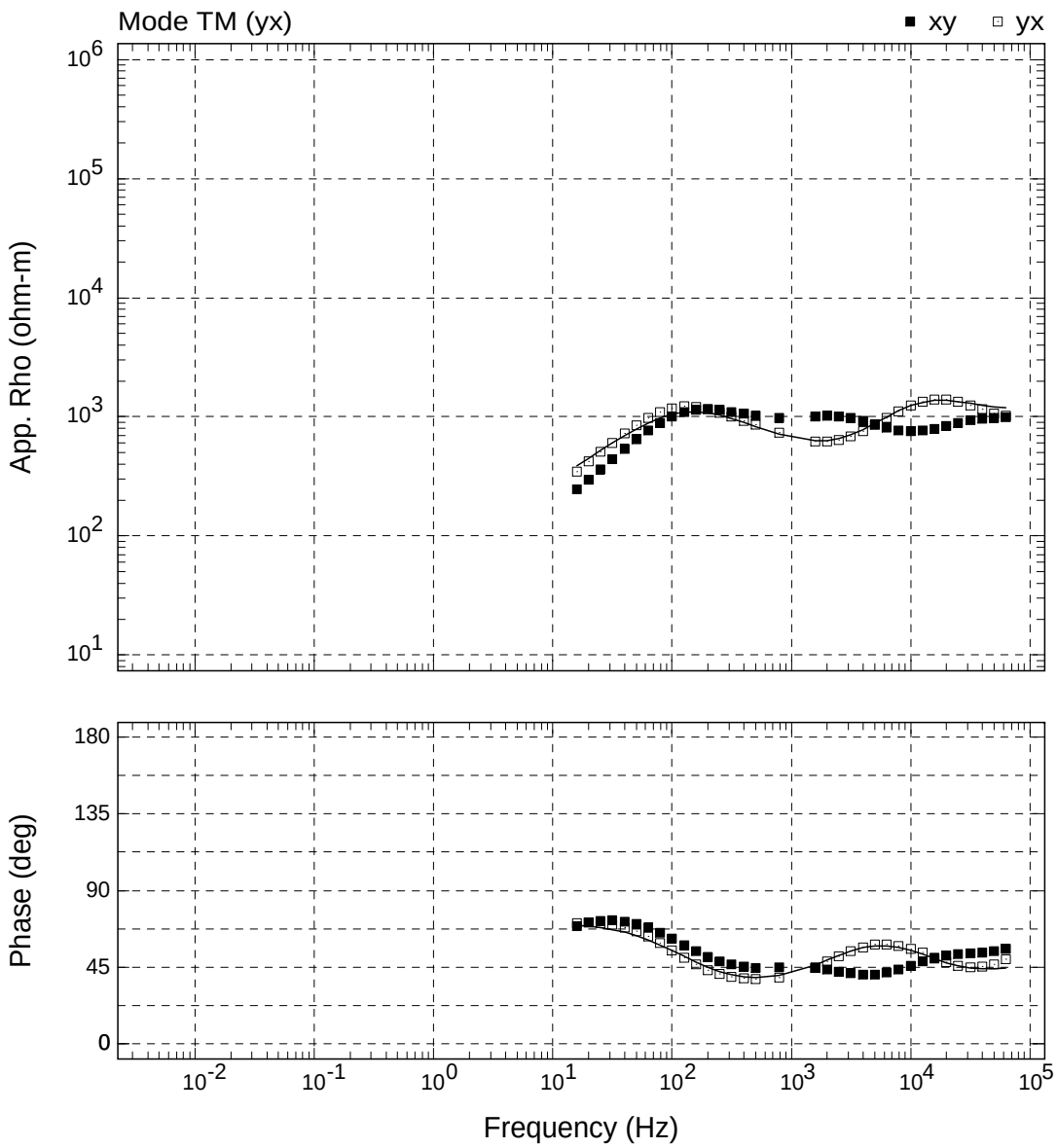

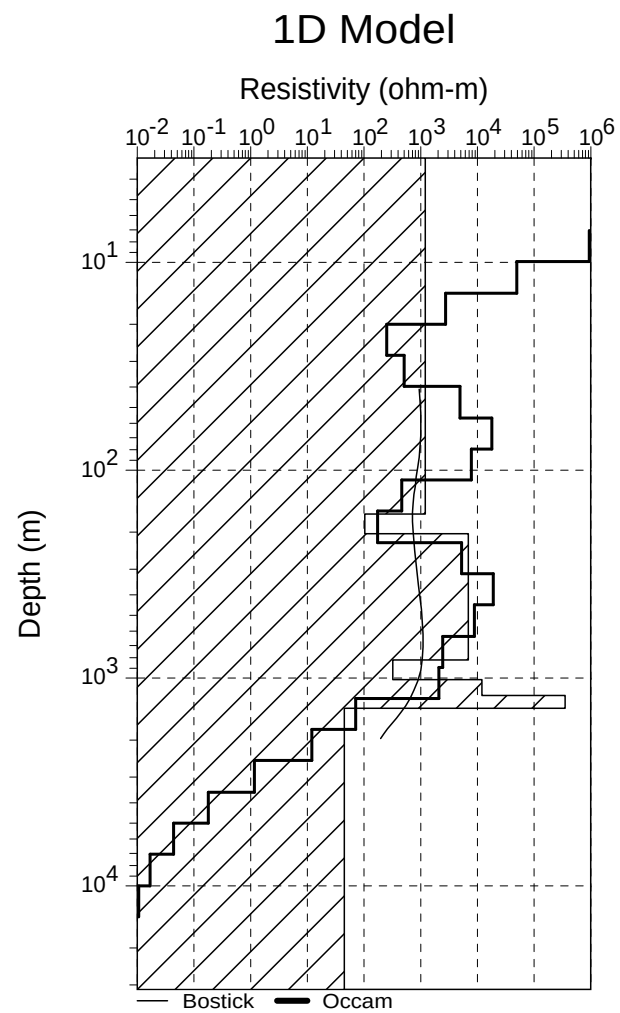

Sounding: ZMR018

Area: Mauna Kea

26/Dec/2016

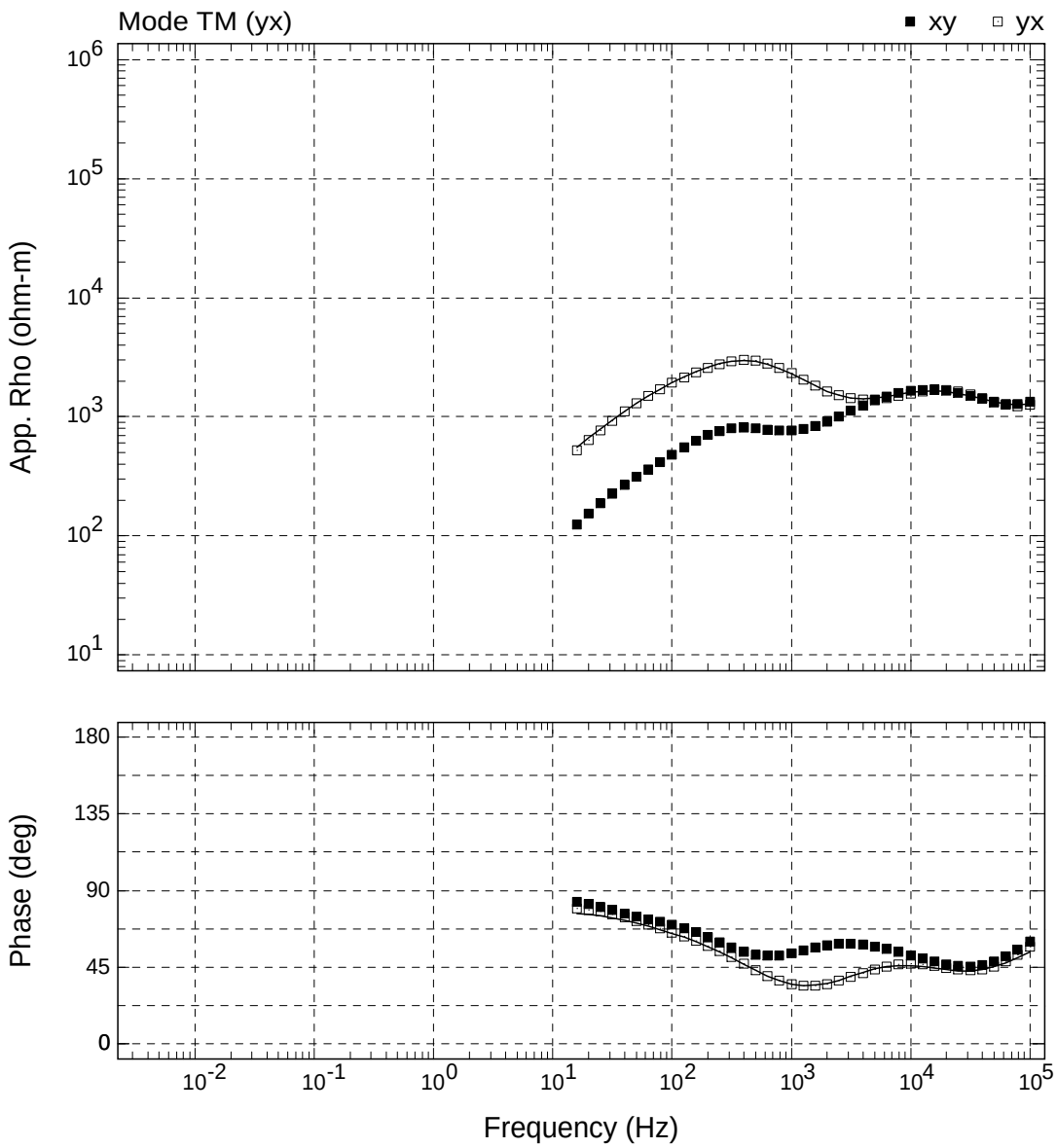

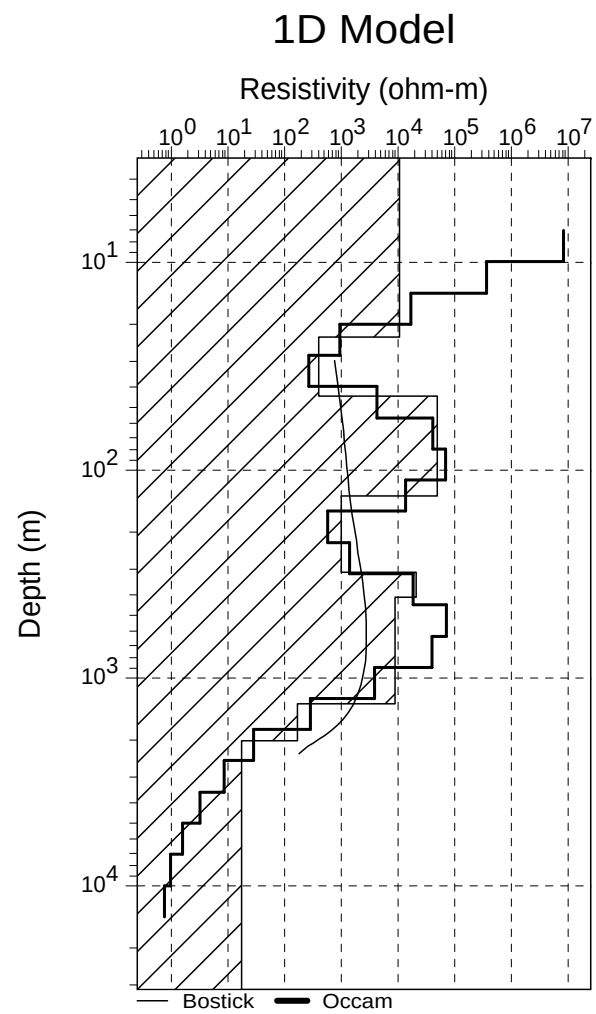

Sounding: ZMR019

Area: Mauna Kea

26/Dec/2016

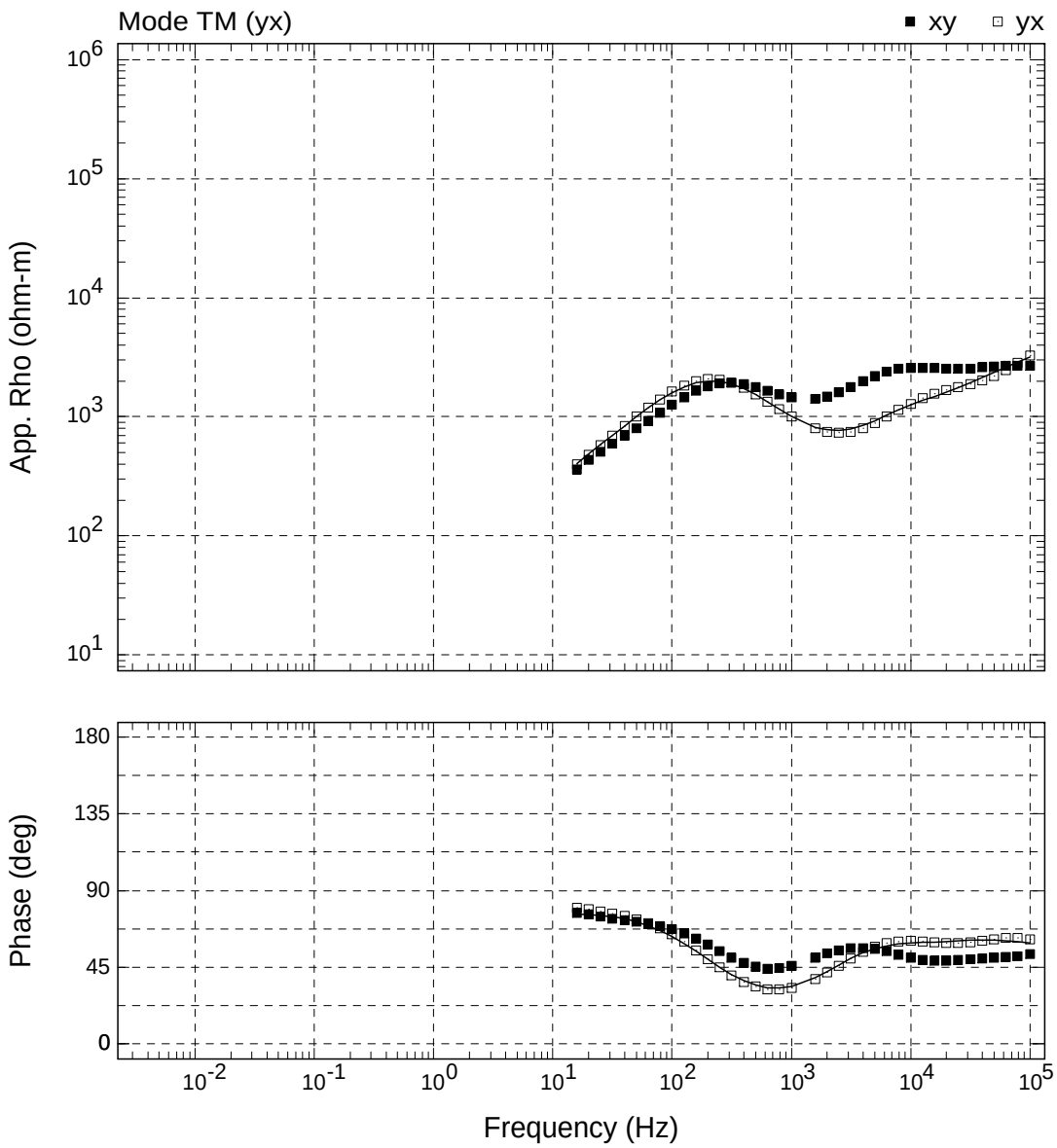

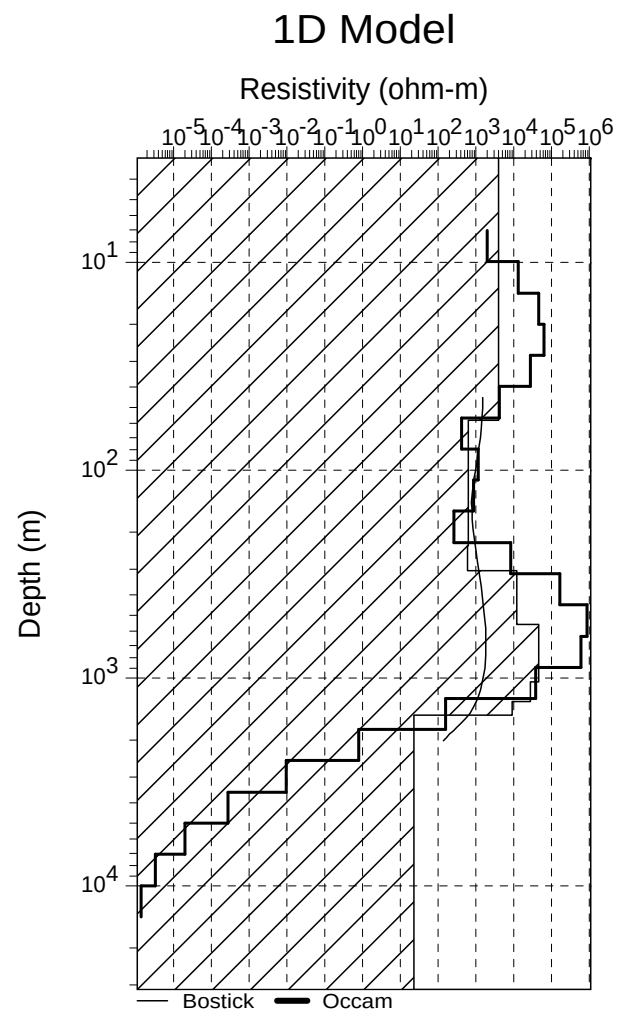

Sounding: ZMR020

Area: Mauna Kea

26/Dec/2016

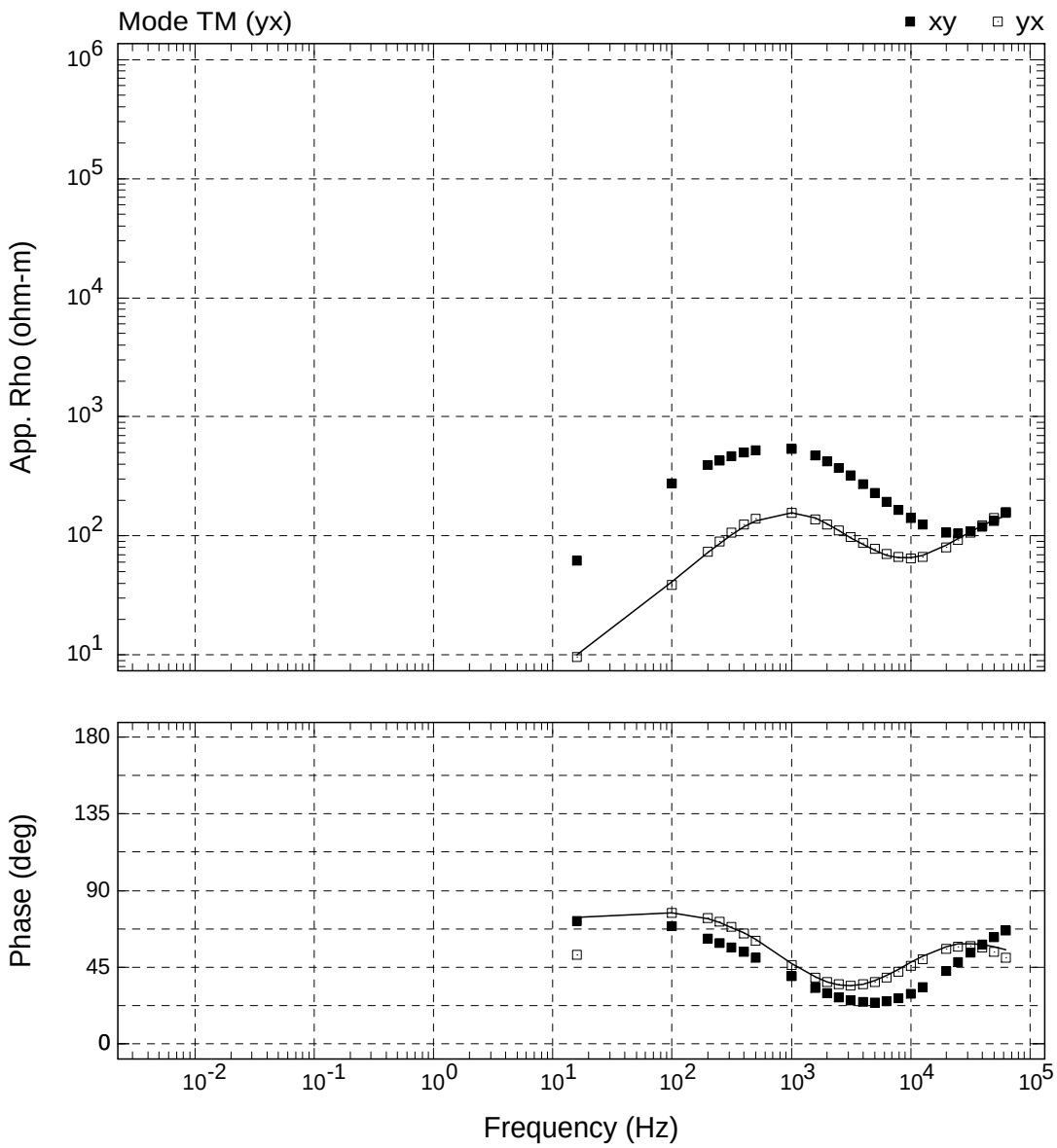

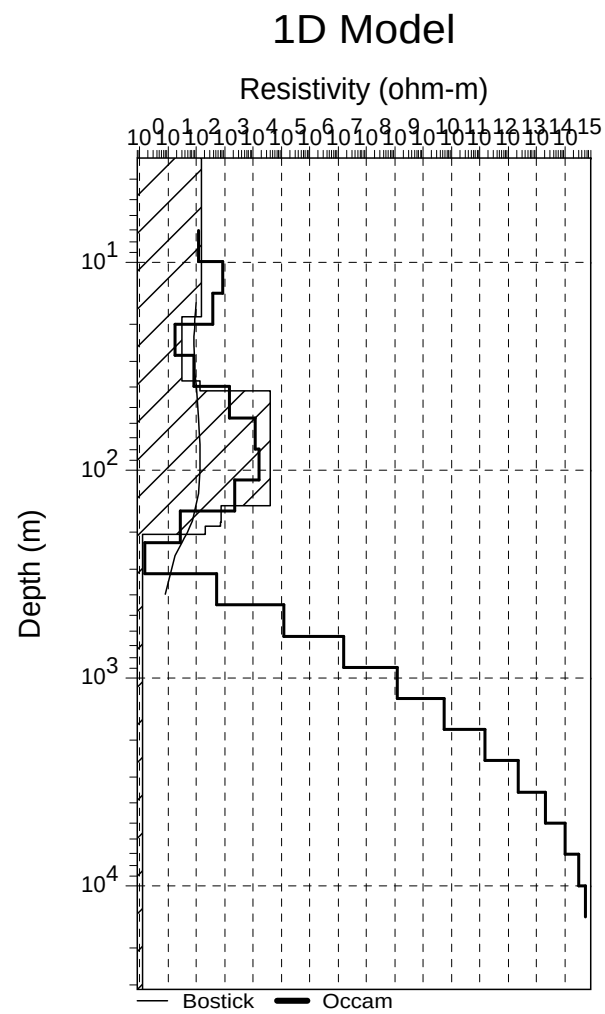

Sounding: ZMR021

Area: Mauna Kea

26/Dec/2016

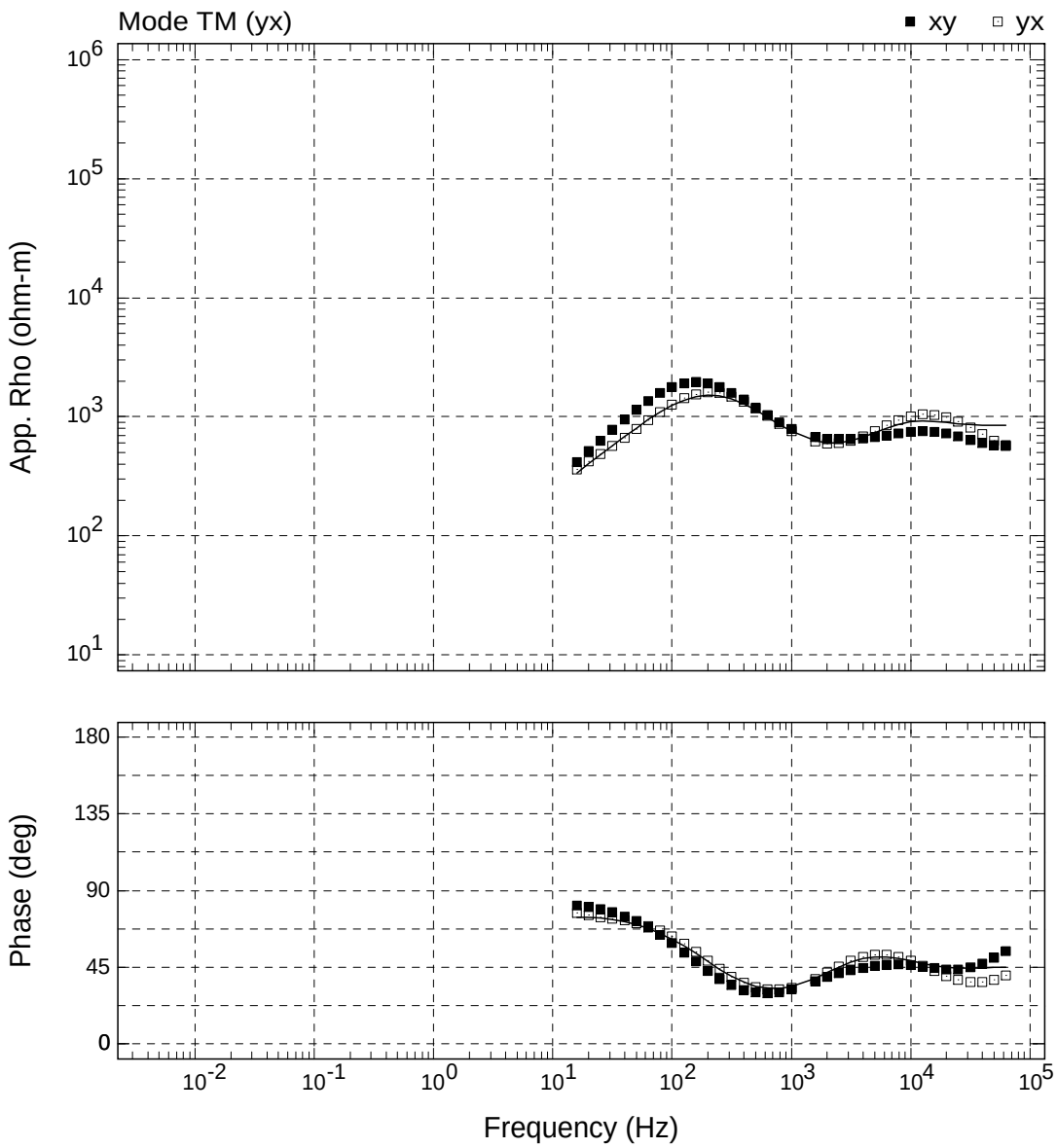

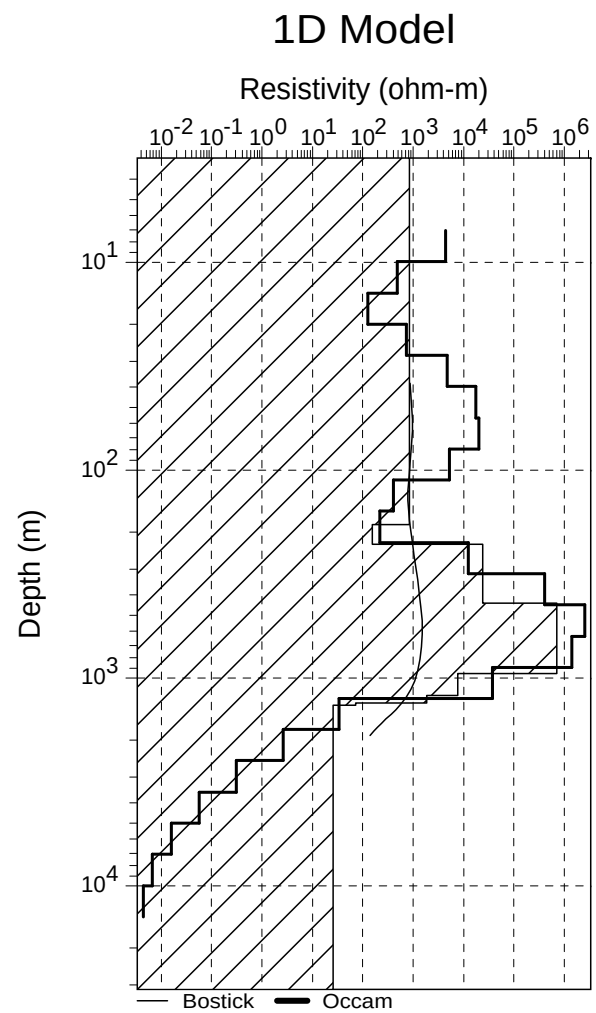

Sounding: ZMR022

Area: Mauna Kea

26/Dec/2016

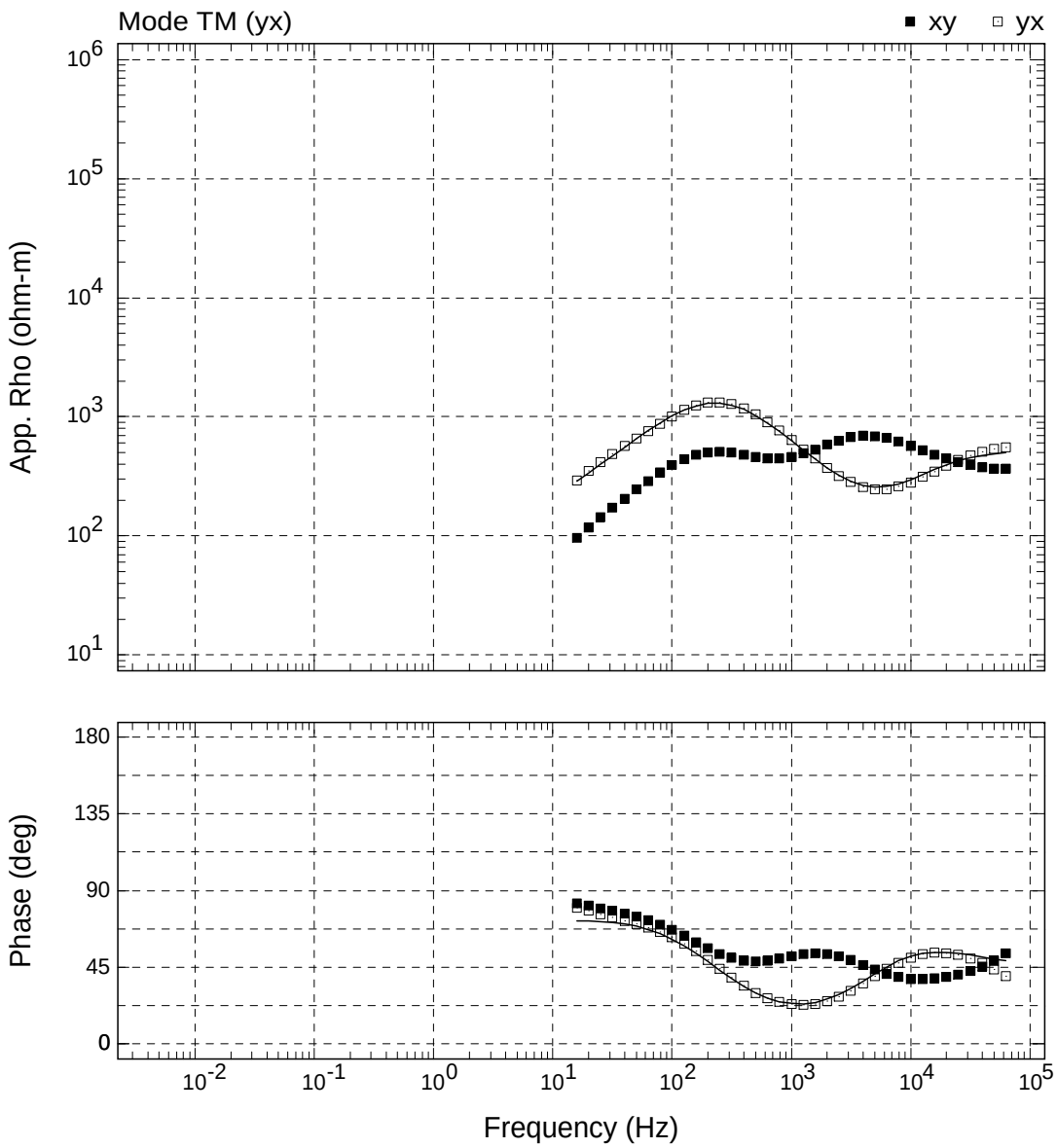

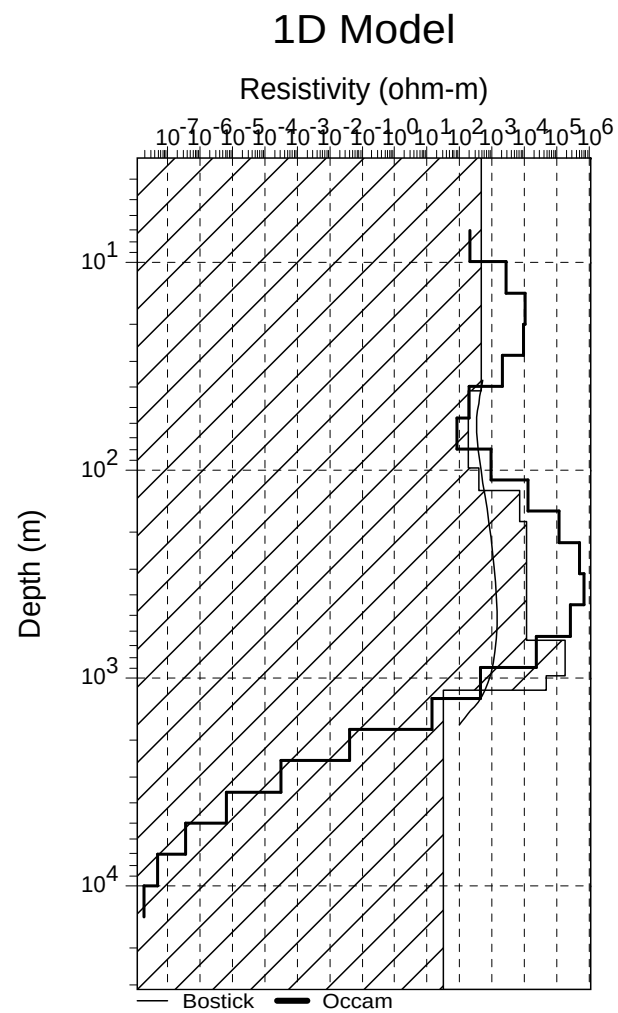

Sounding: ZMR023

Area: Mauna Kea

26/Dec/2016

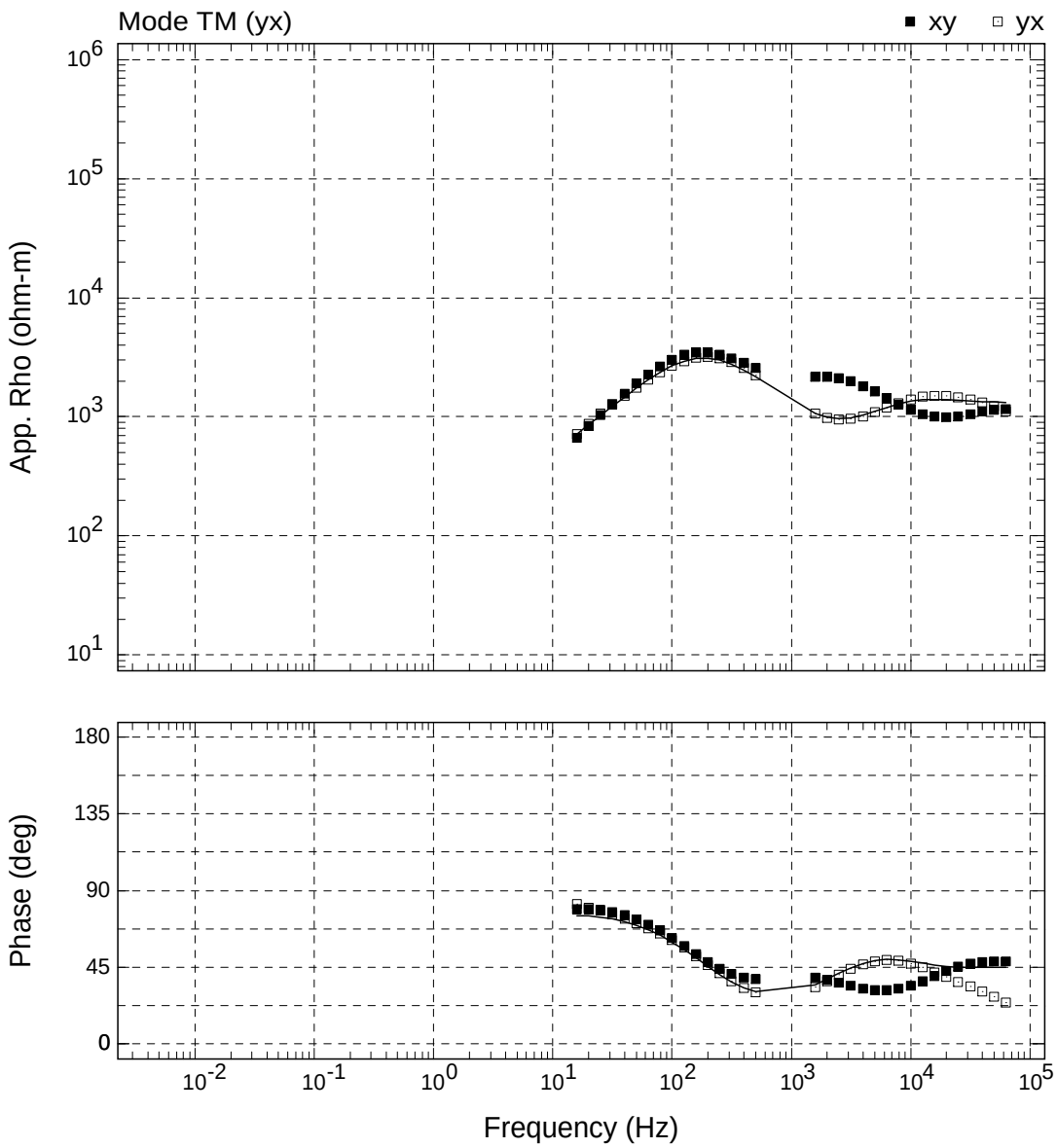

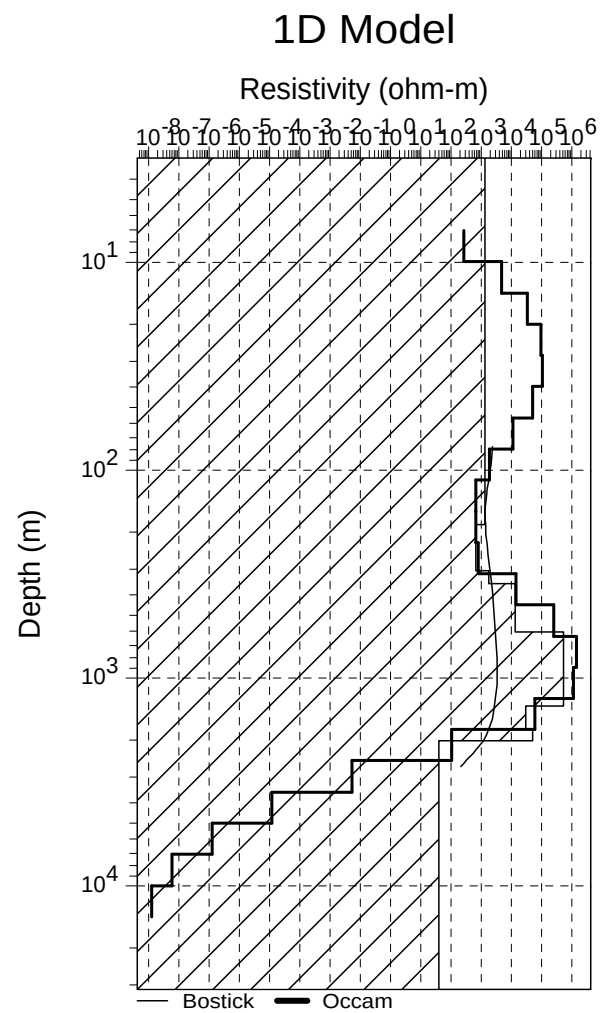

Sounding: ZMR024
Area: Mauna Kea
26/Dec/2016

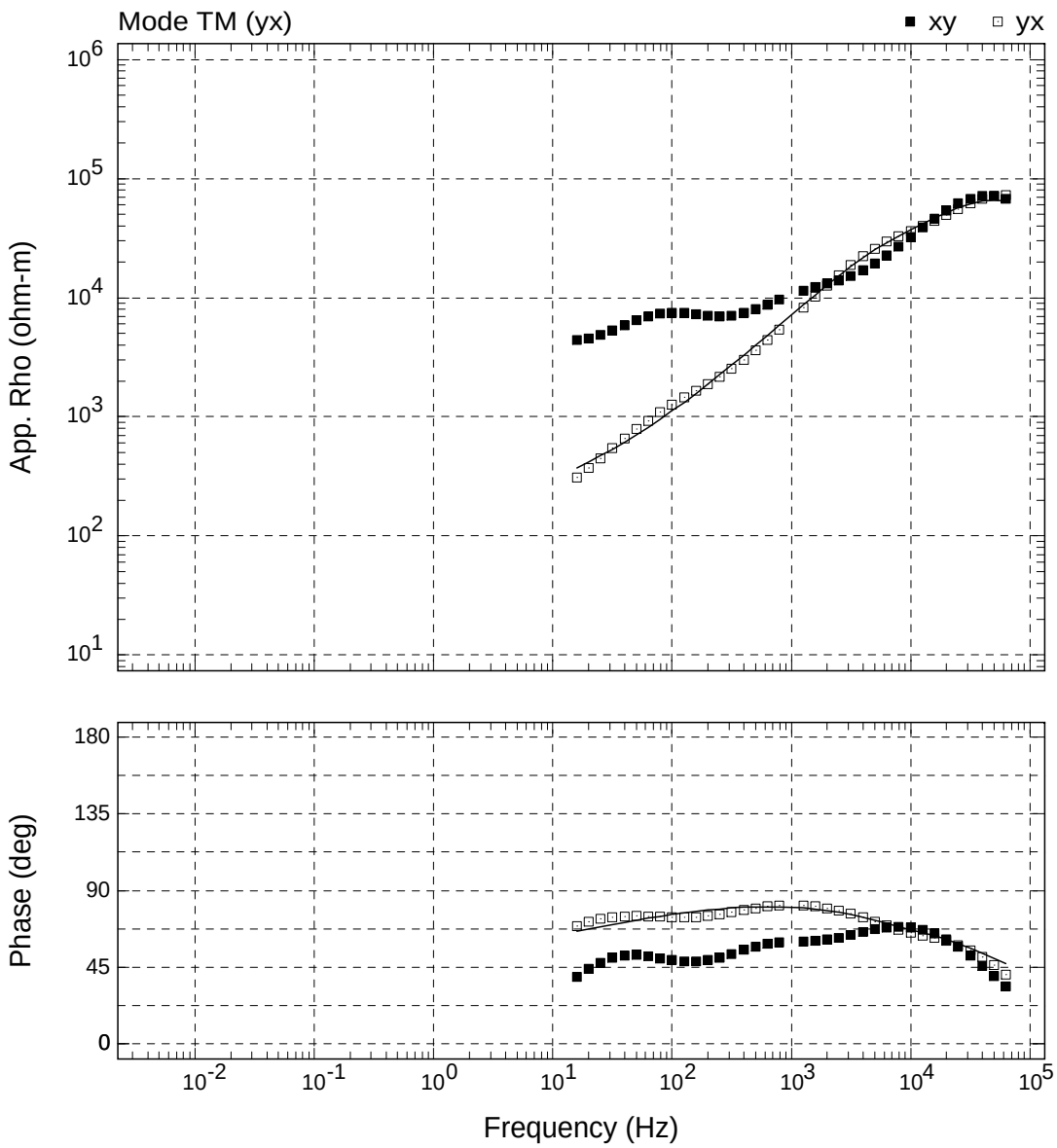

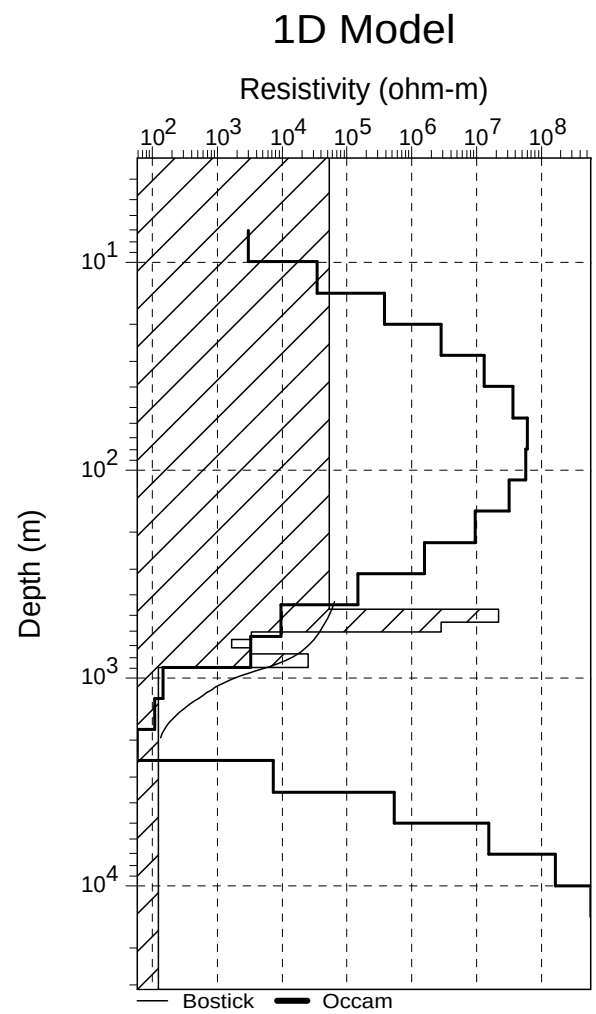

Sounding: ZMR025

Area: Mauna Kea

26/Dec/2016

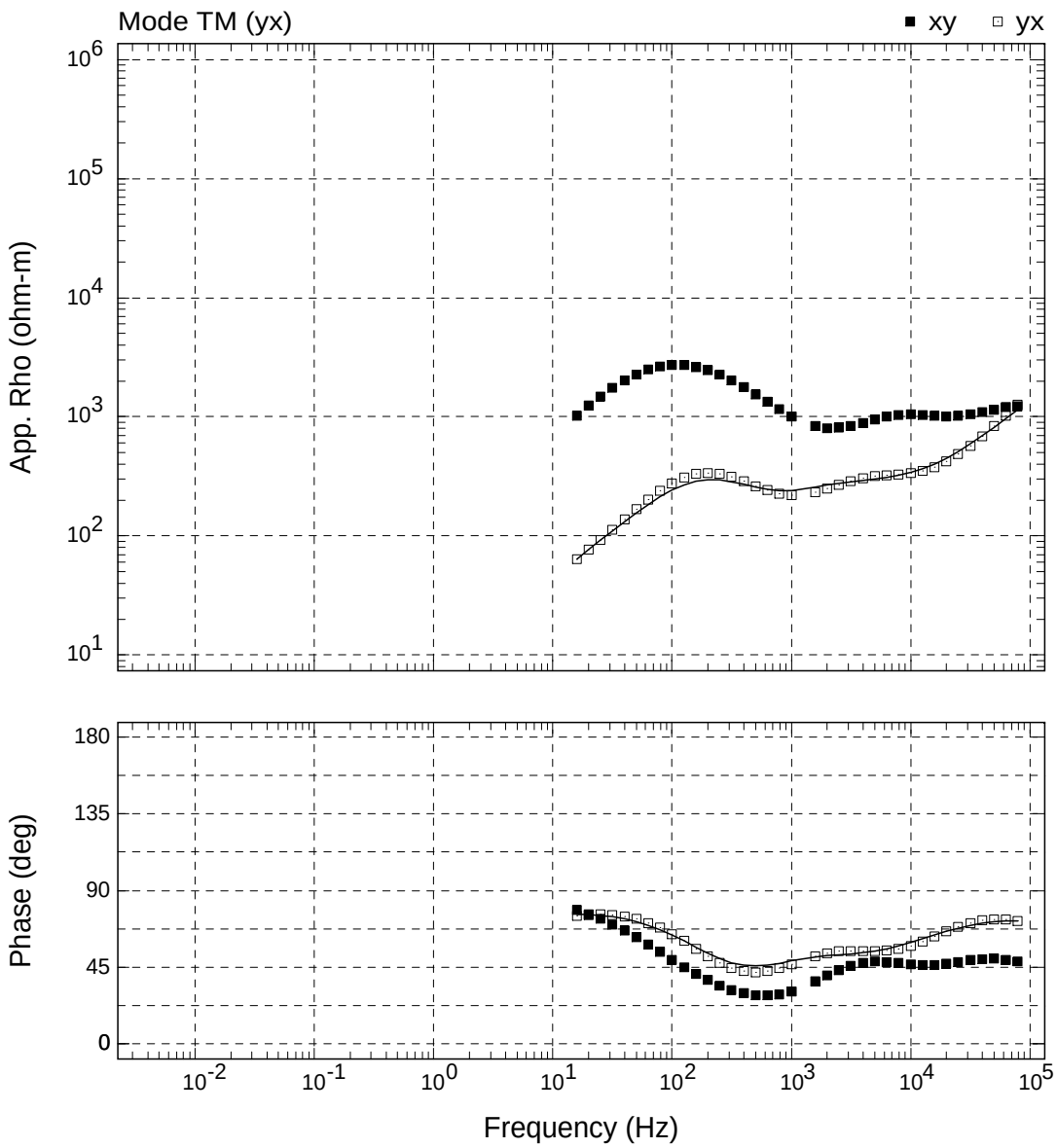

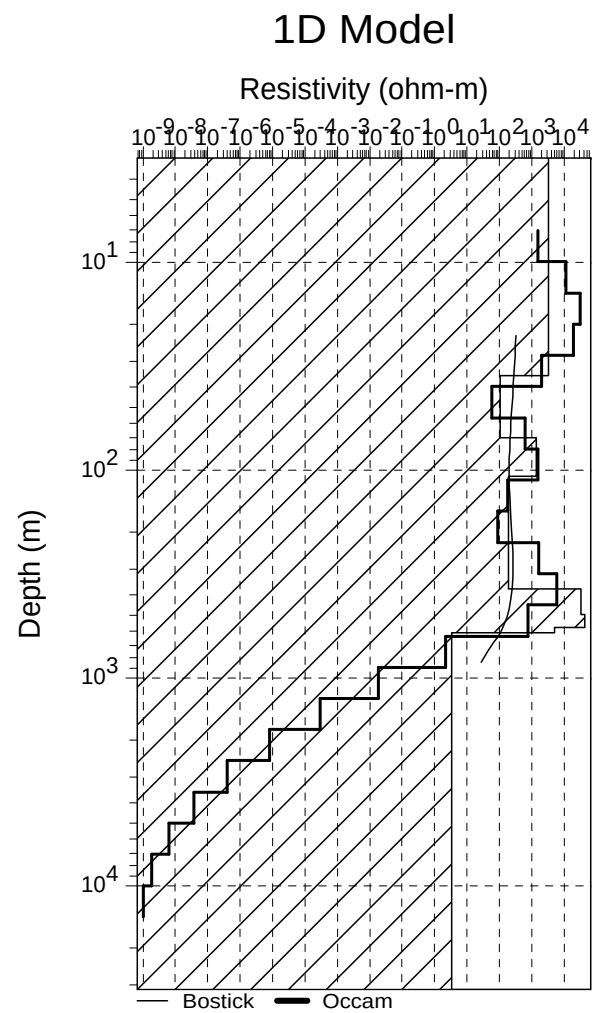

Sounding: ZMR026

Area: Mauna Kea

26/Dec/2016

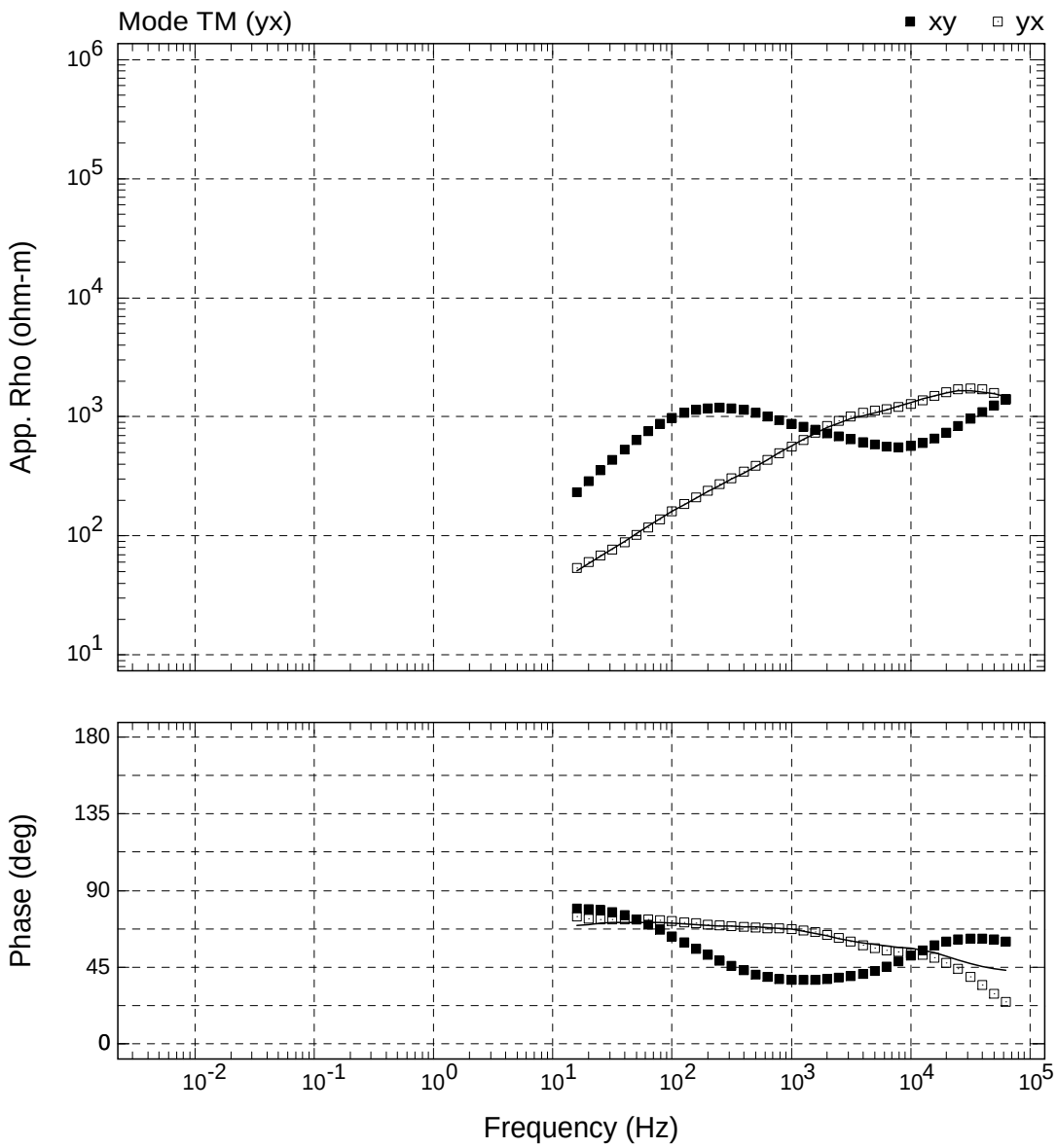

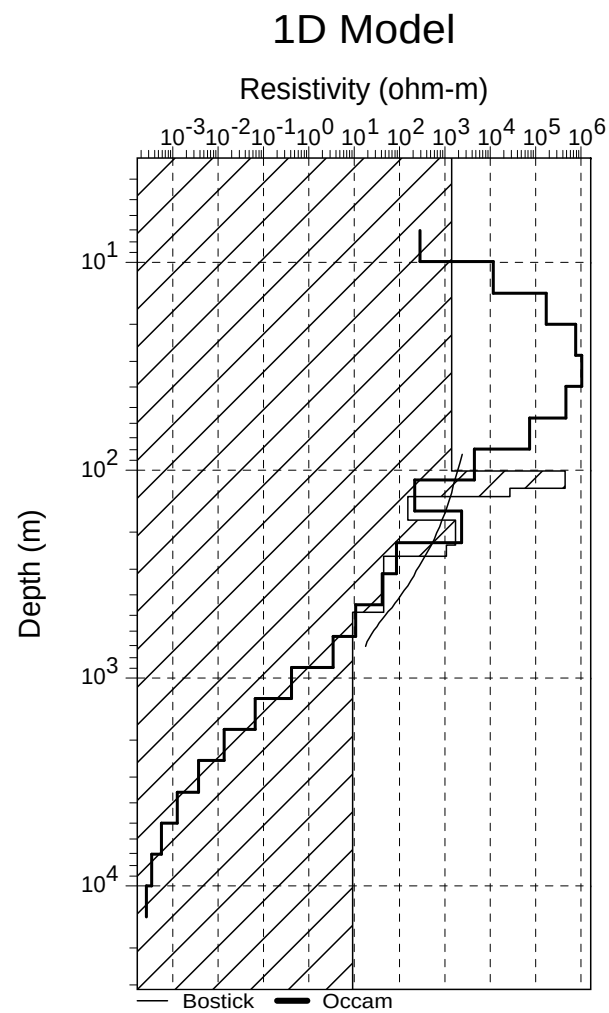

Sounding: ZMR027

Area: Mauna Kea

26/Dec/2016

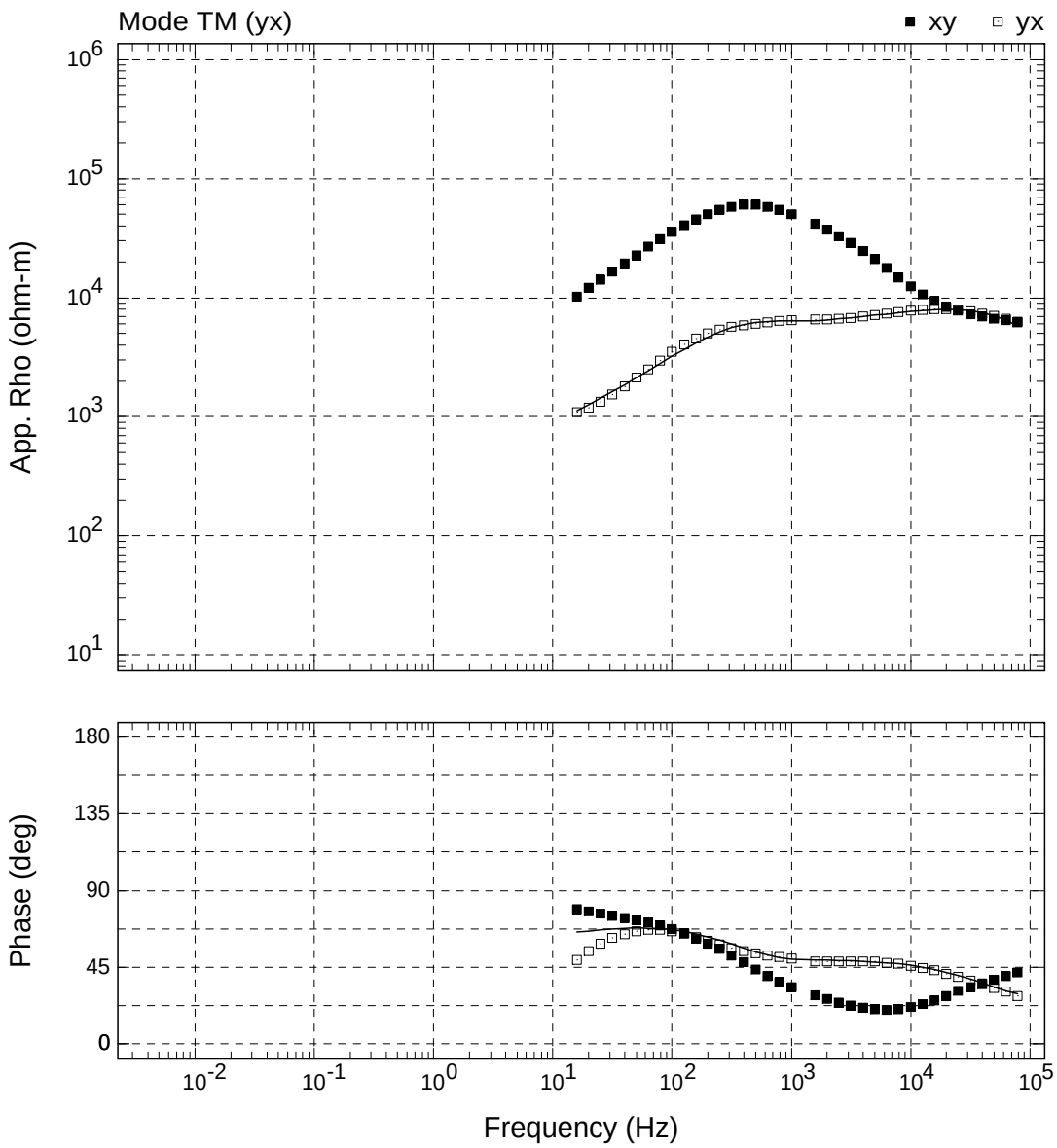

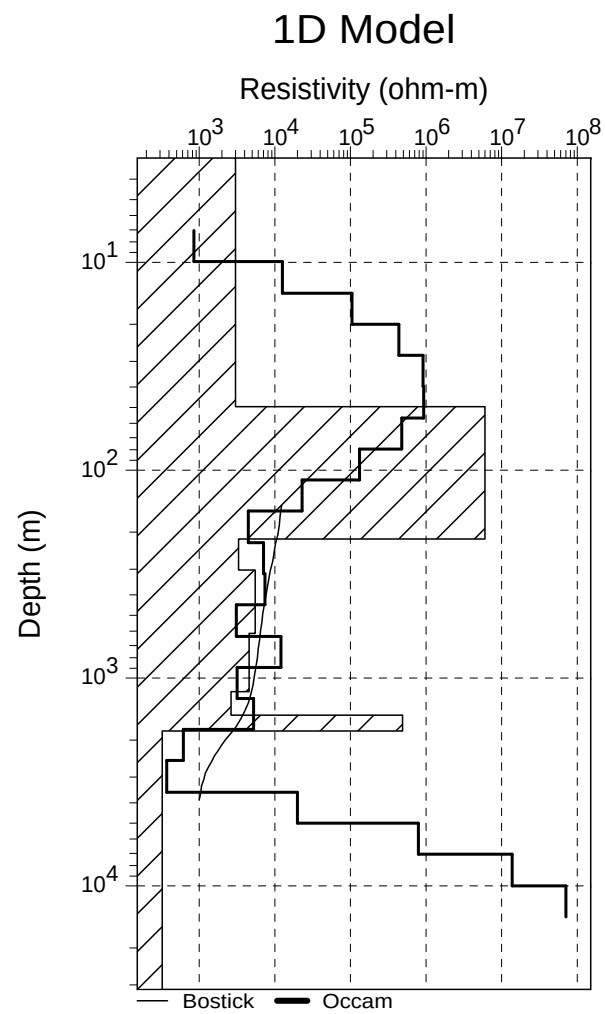

Sounding: ZMR028

Area: Mauna Kea

26/Dec/2016

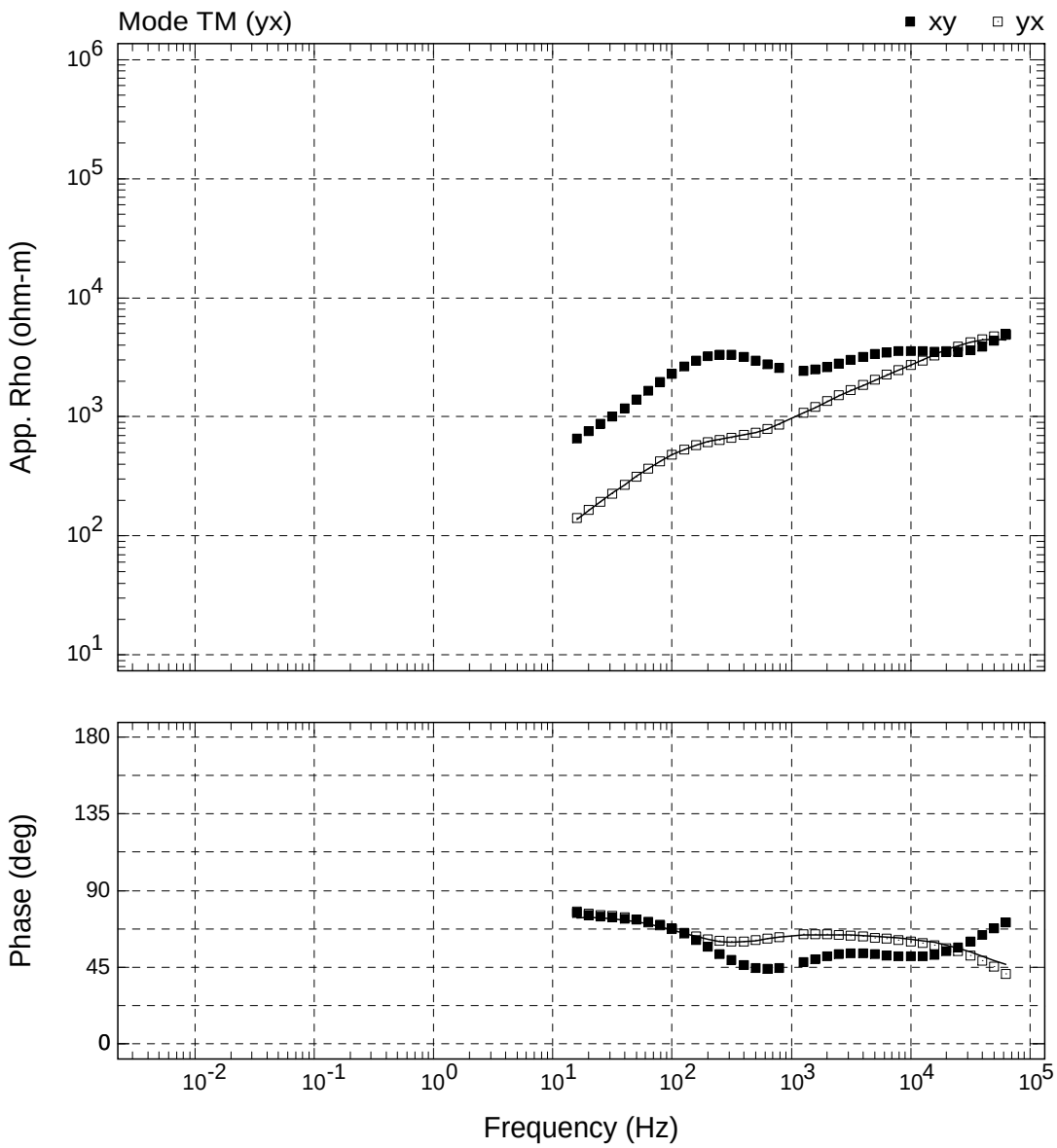

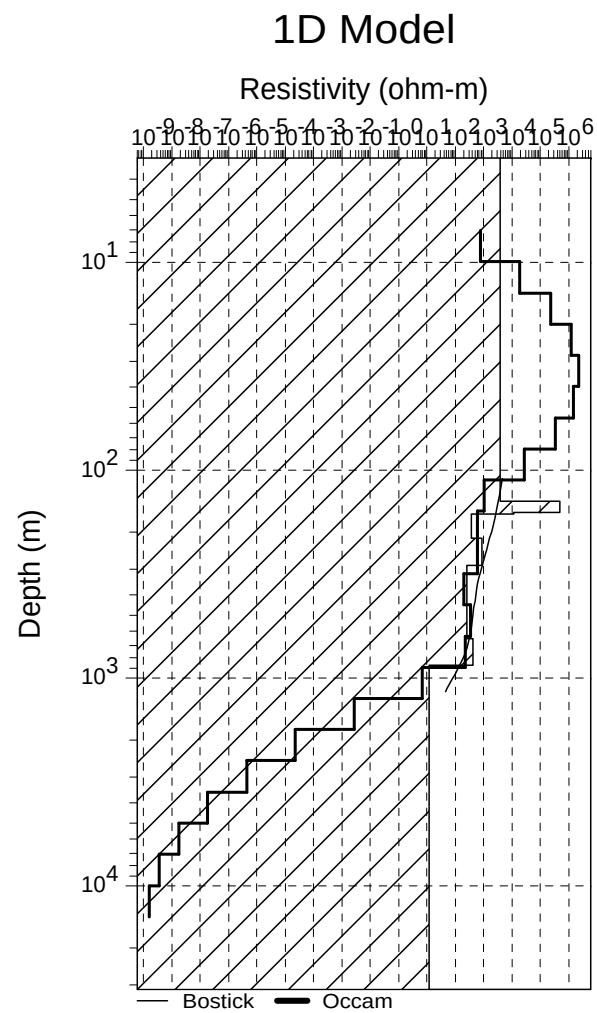

Sounding: ZMR029

Area: Mauna Kea

26/Dec/2016

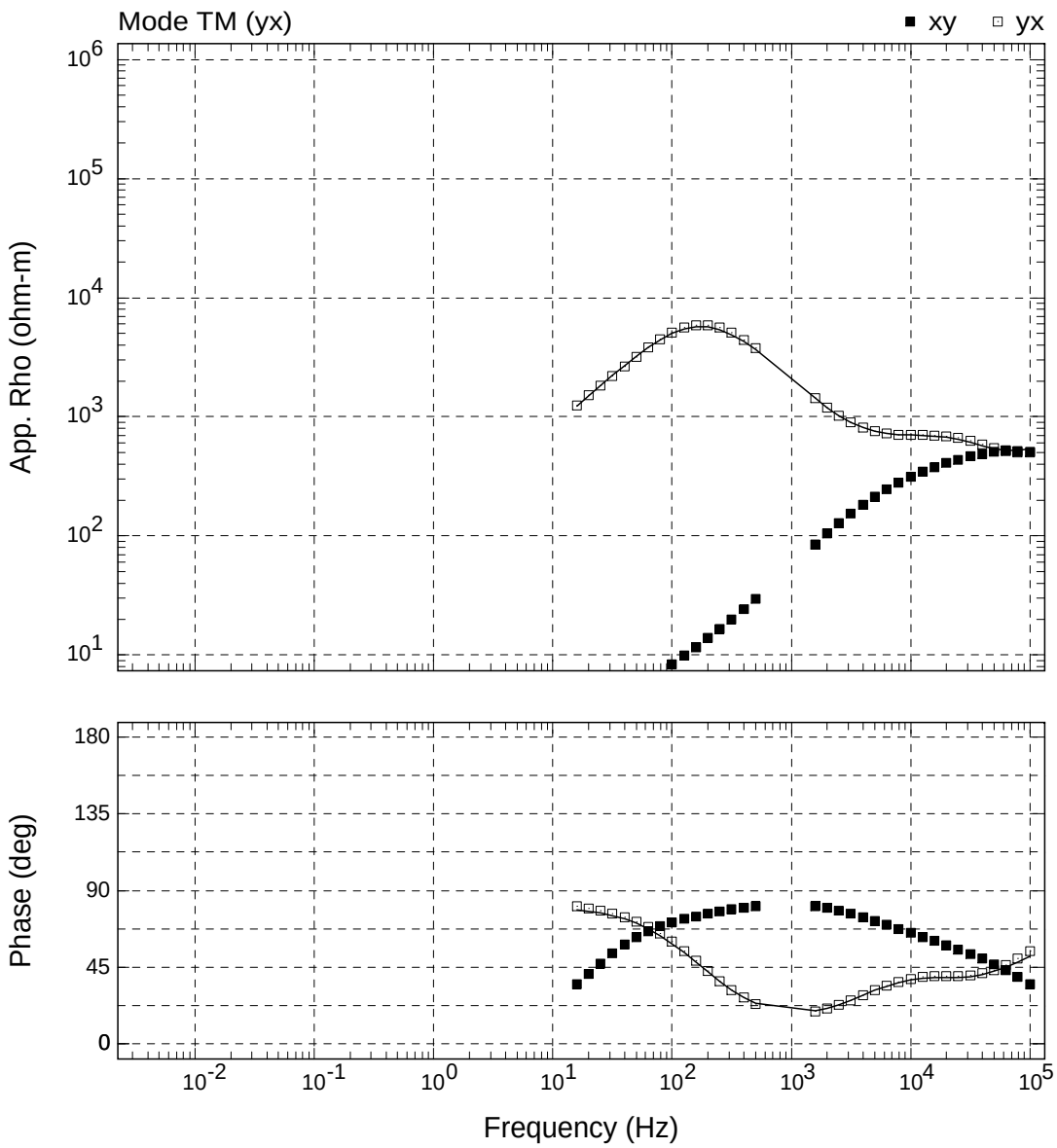

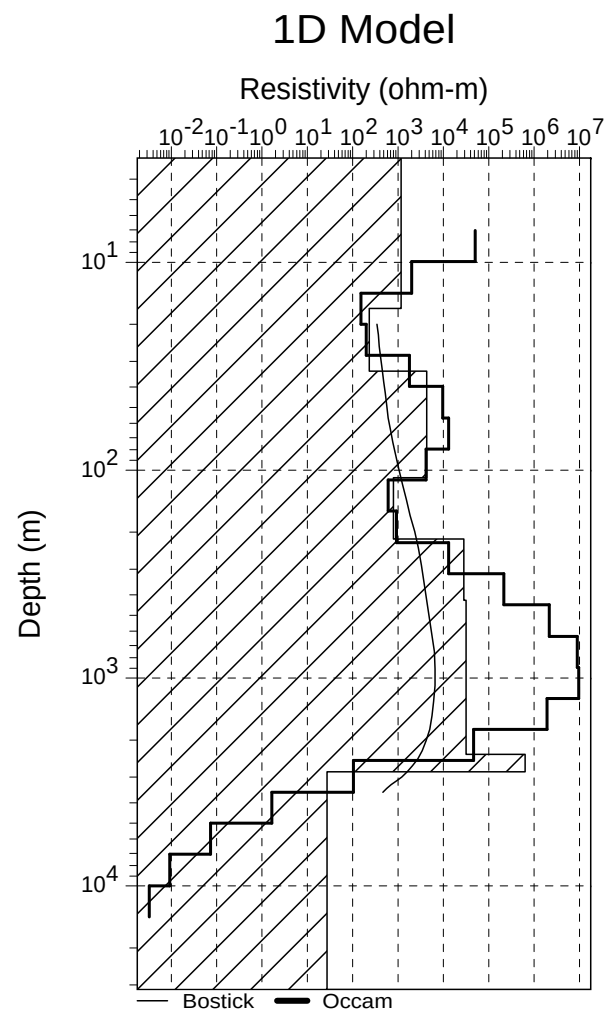

Sounding: ZMR030

Area: Mauna Kea

26/Dec/2016

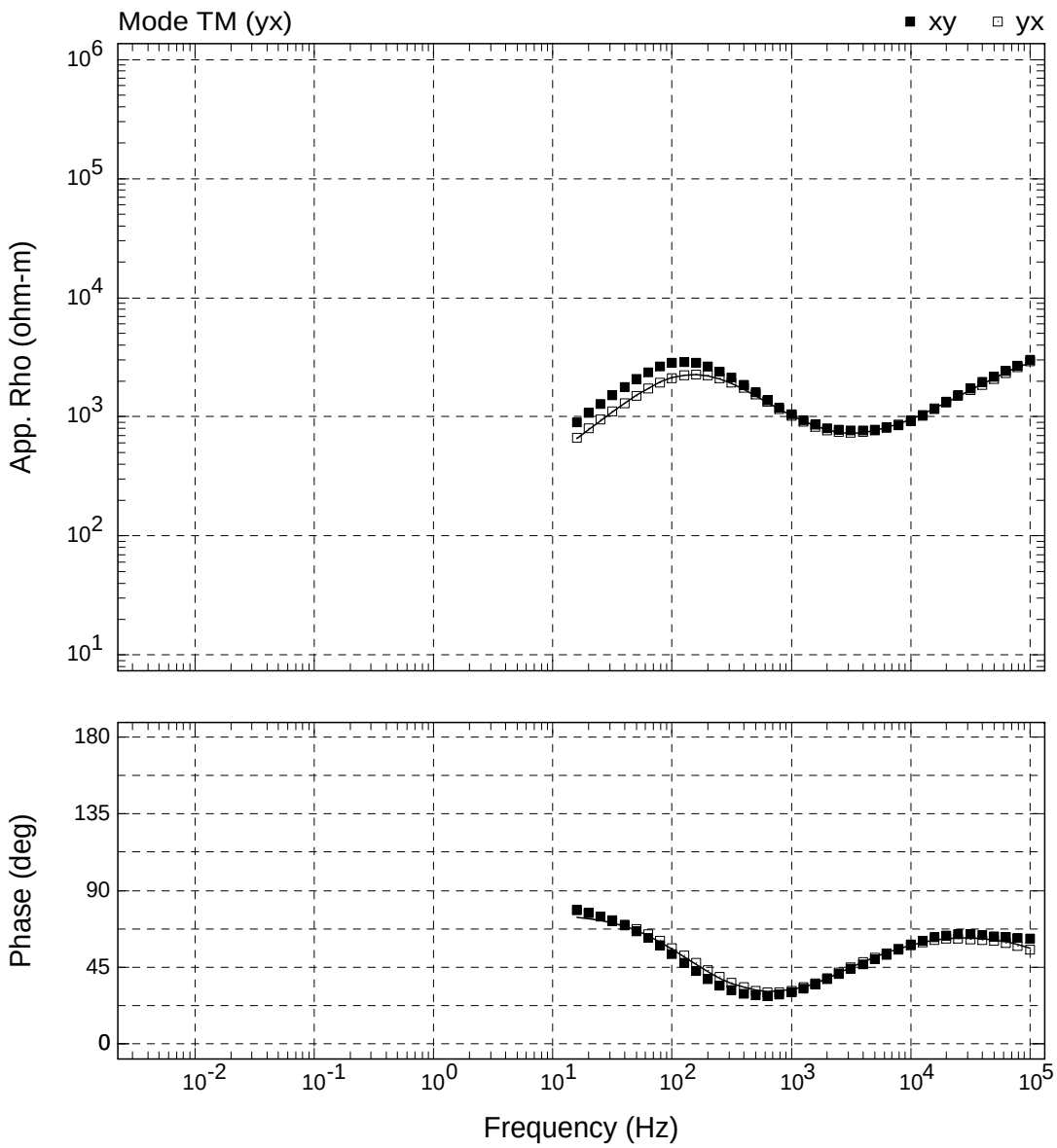

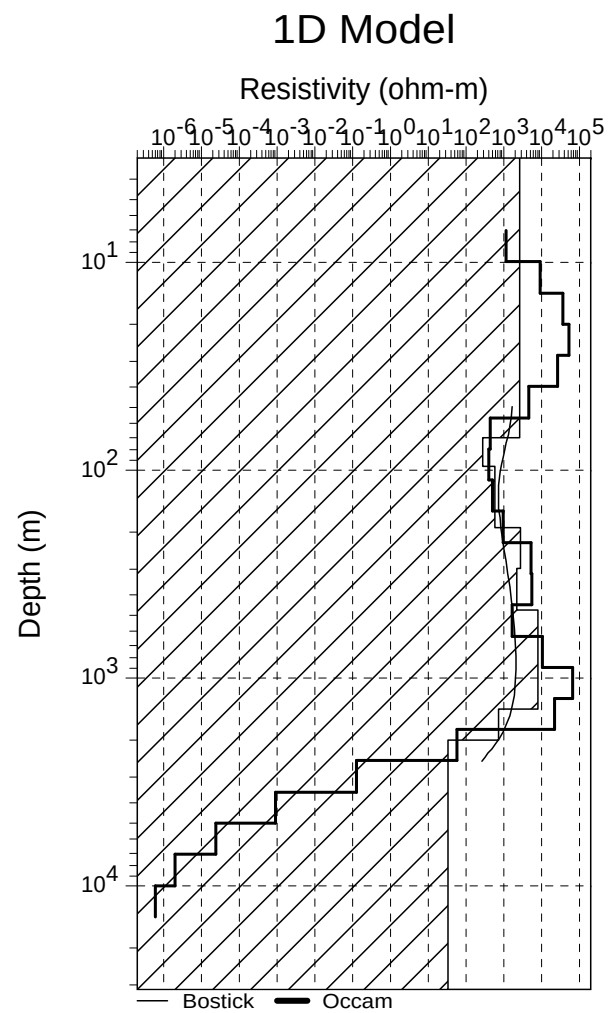

Sounding: ZMR031

Area: Mauna Kea

26/Dec/2016

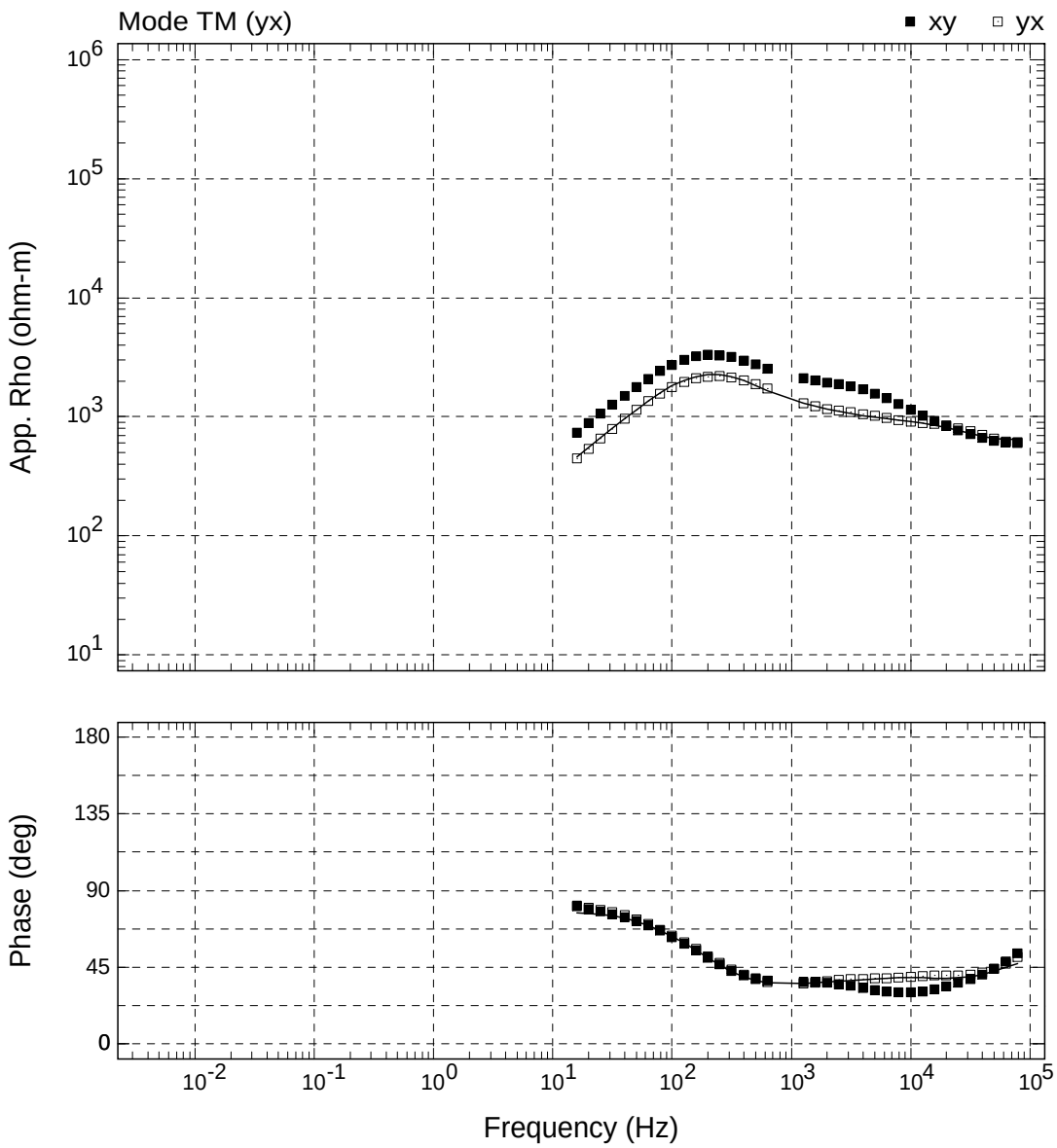

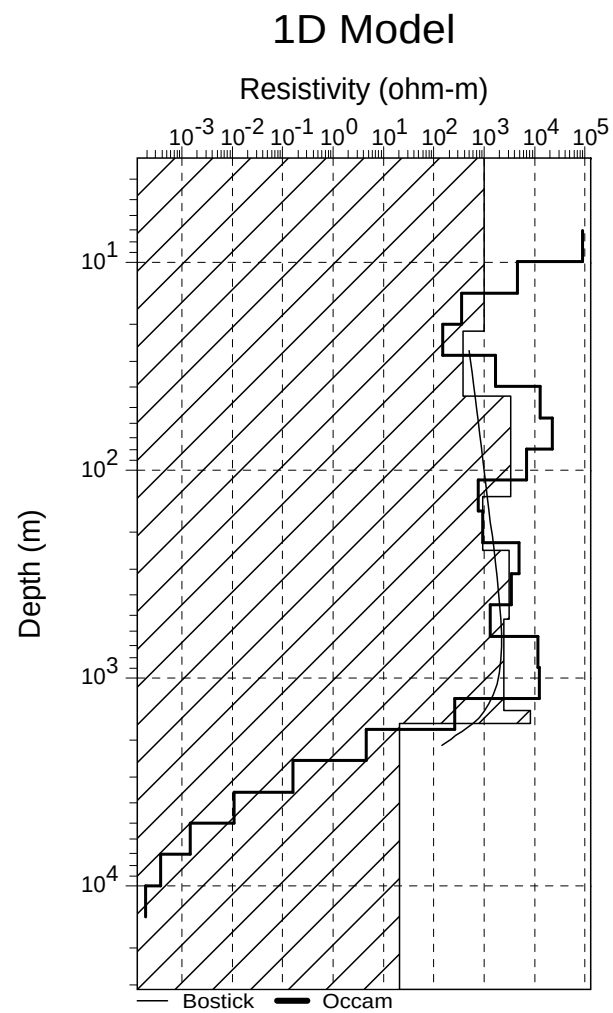

Sounding: ZMR032

Area: Mauna Kea

26/Dec/2016

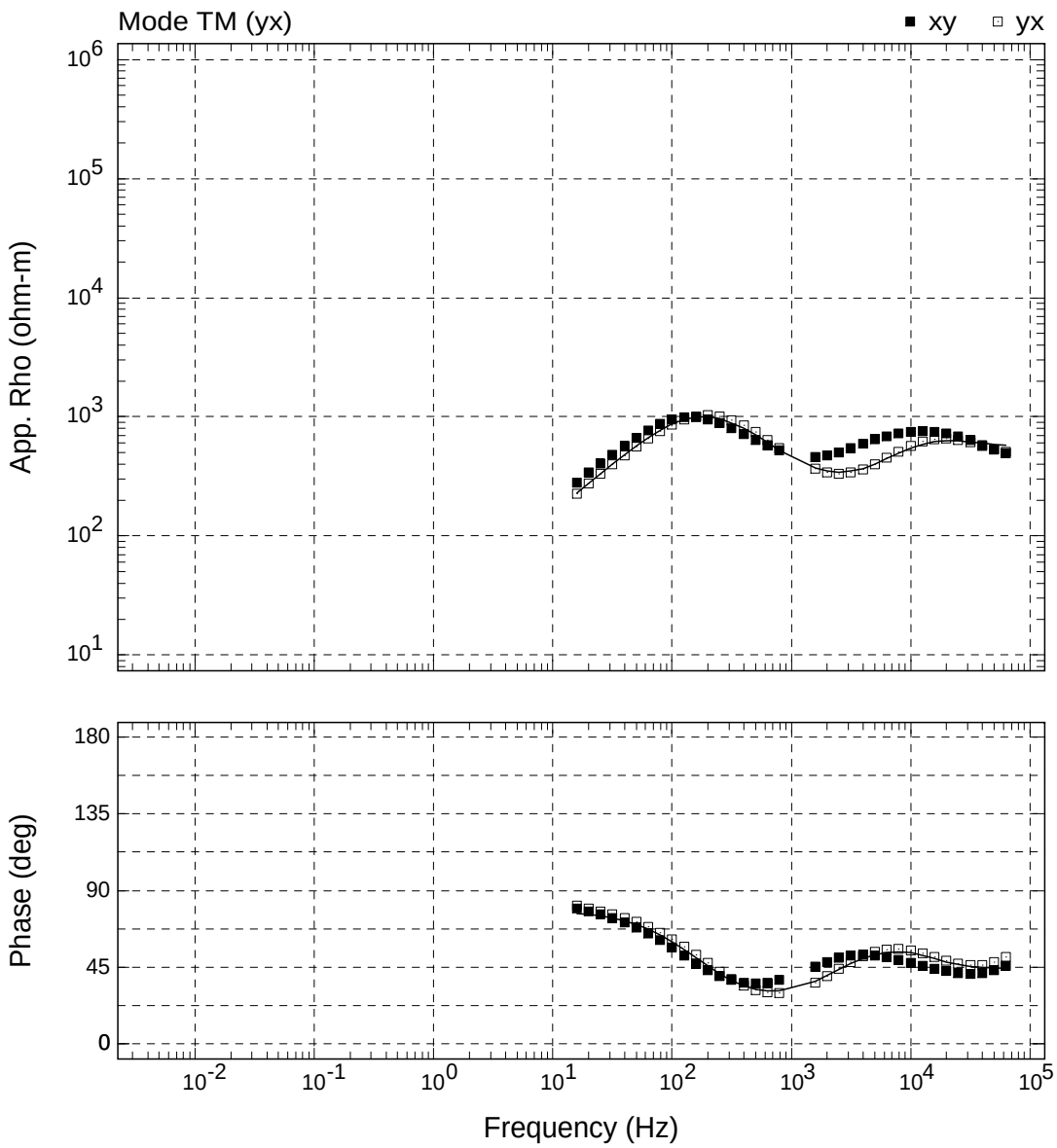

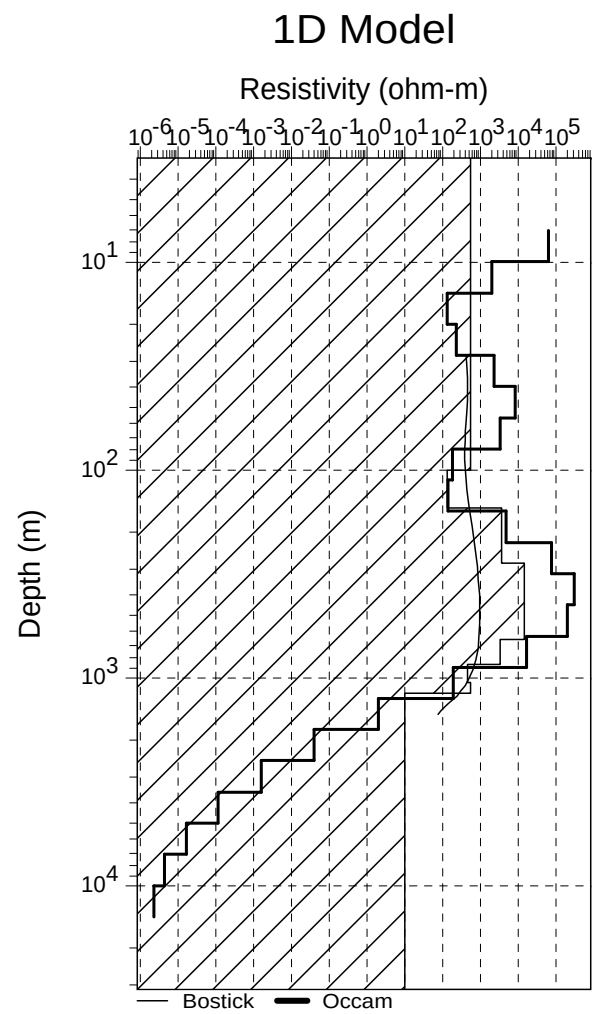

Sounding: ZMR033

Area: Mauna Kea

26/Dec/2016

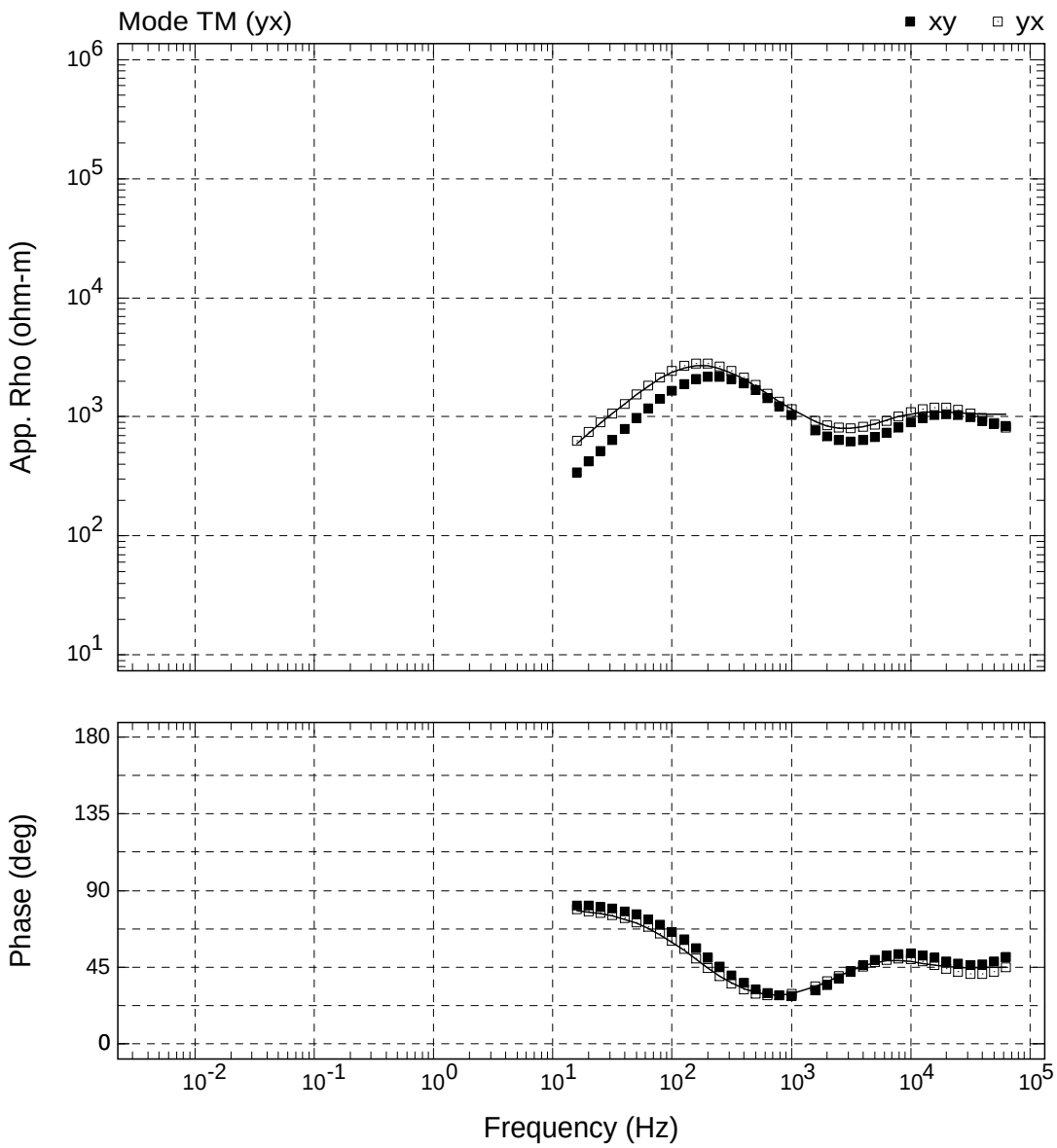

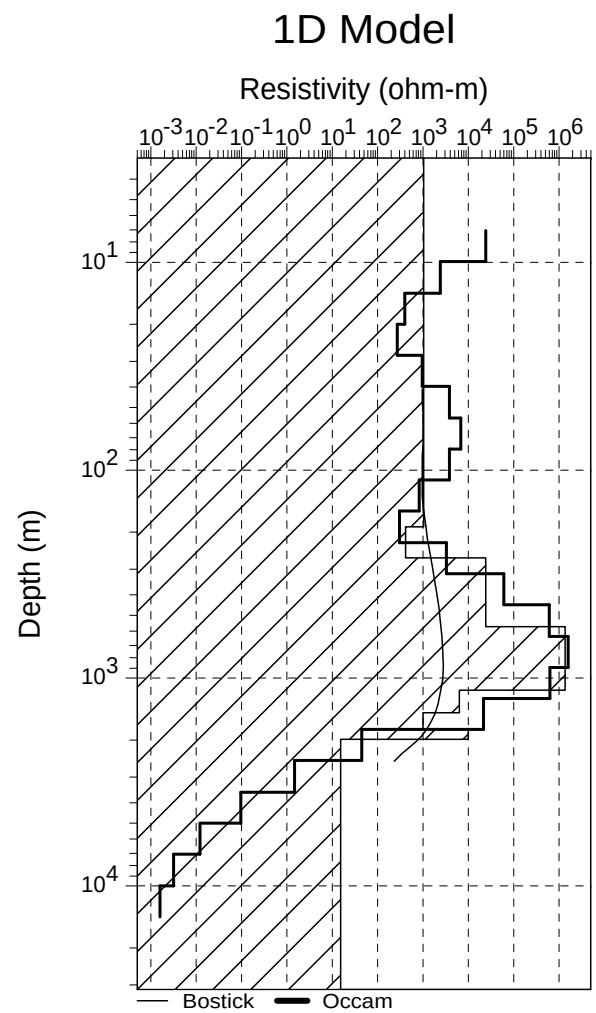

Sounding: ZMR034

Area: Mauna Kea

26/Dec/2016

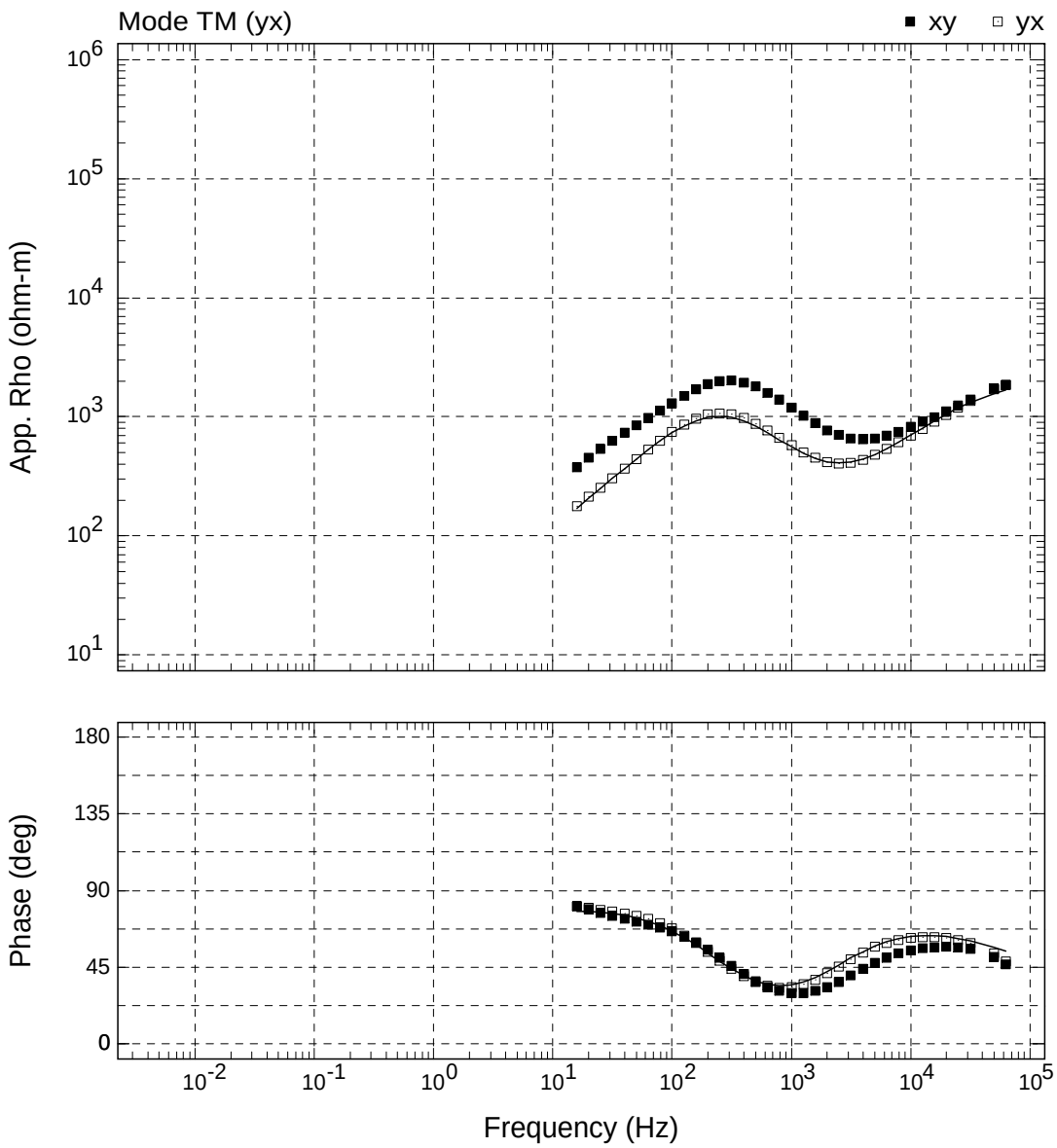

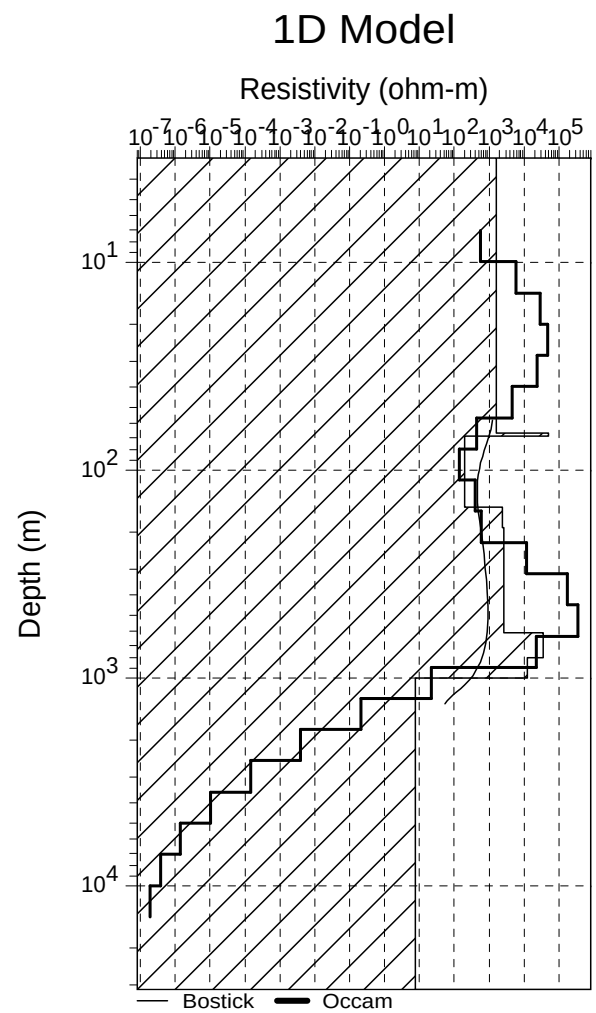

Sounding: ZMR035
Area: Mauna Kea
26/Dec/2016

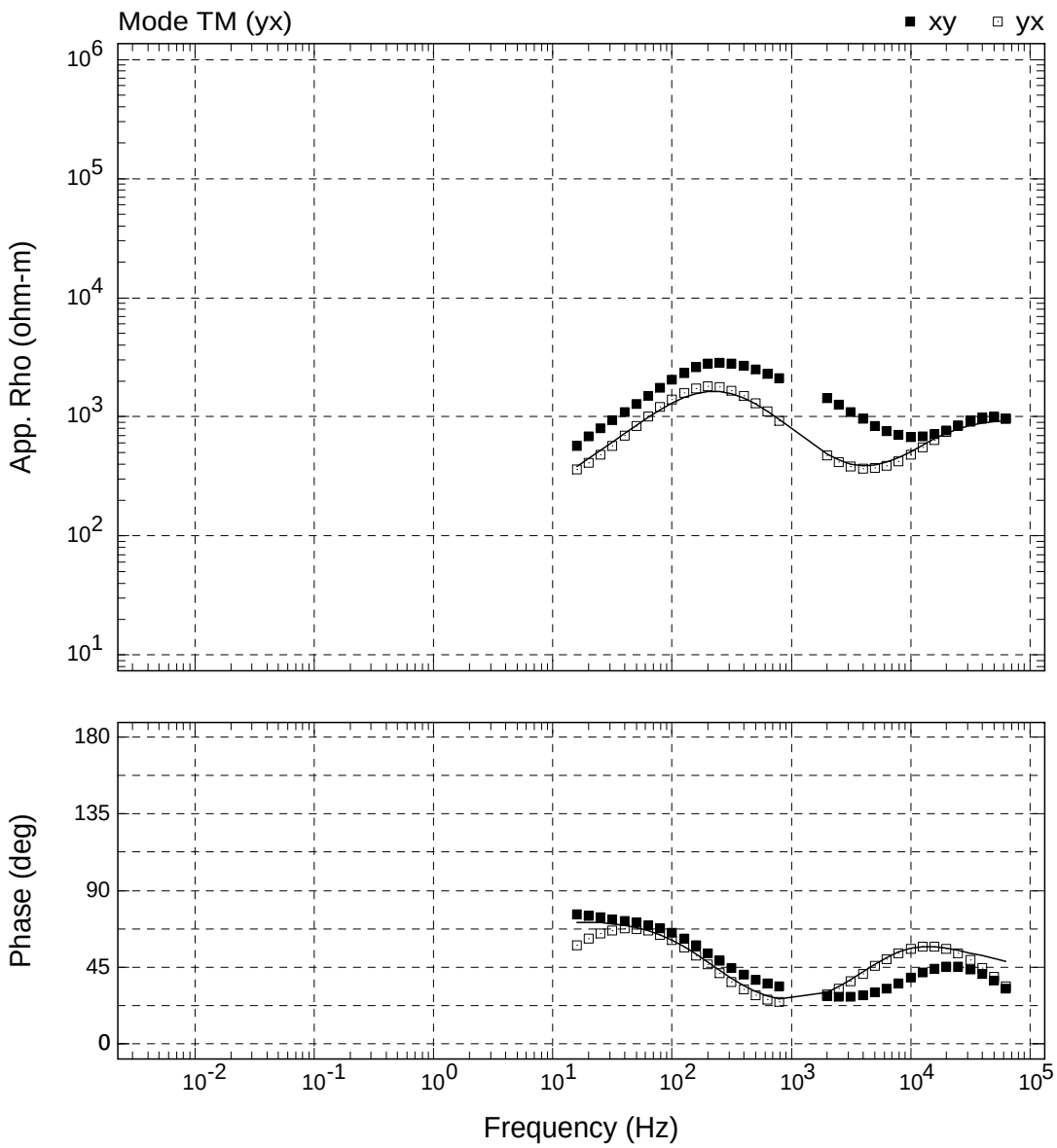

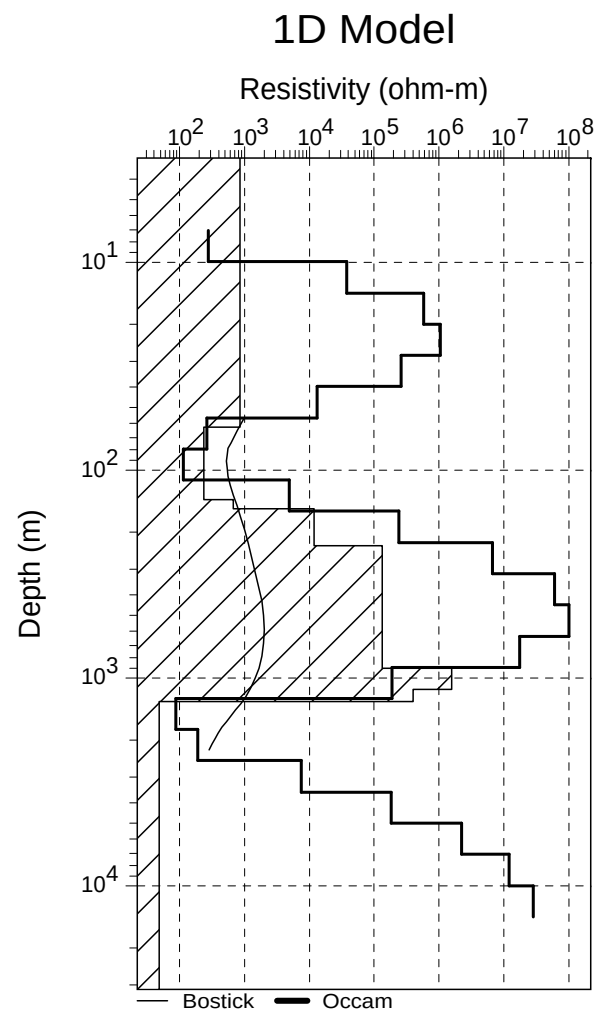

Sounding: ZMR036

Area: Mauna Kea

26/Dec/2016

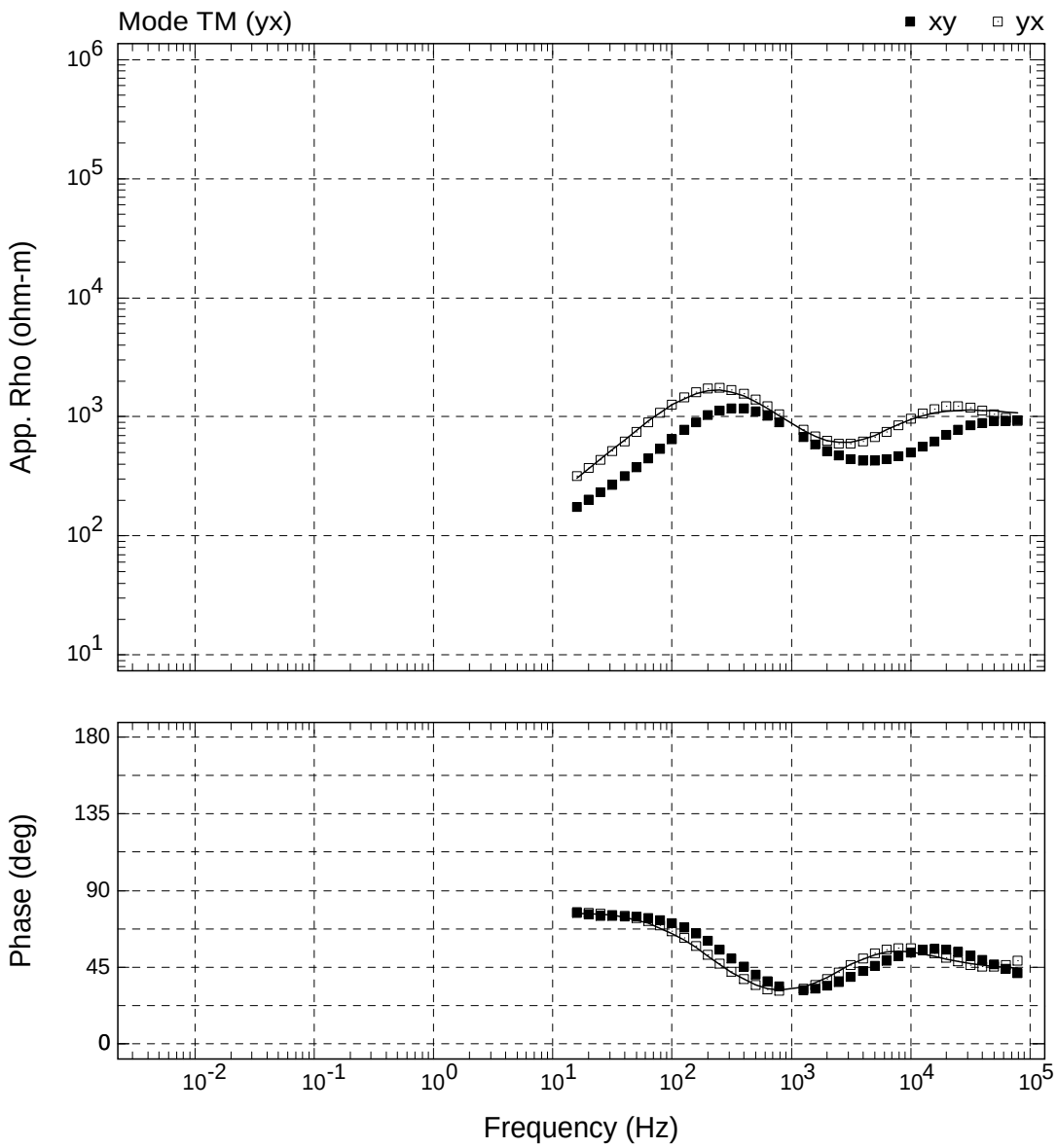

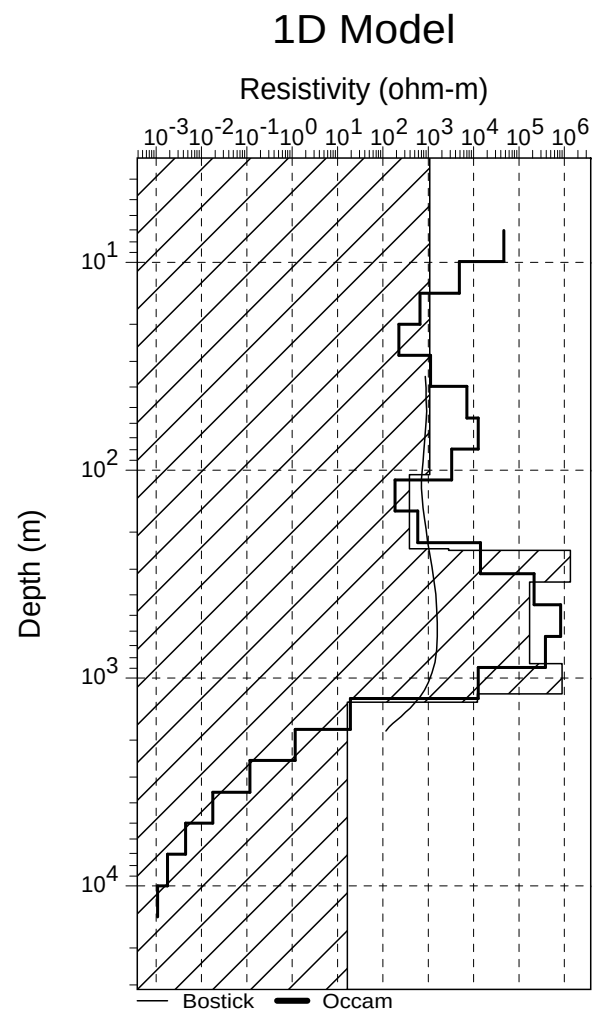

Sounding: ZMR037

Area: Mauna Kea

26/Dec/2016

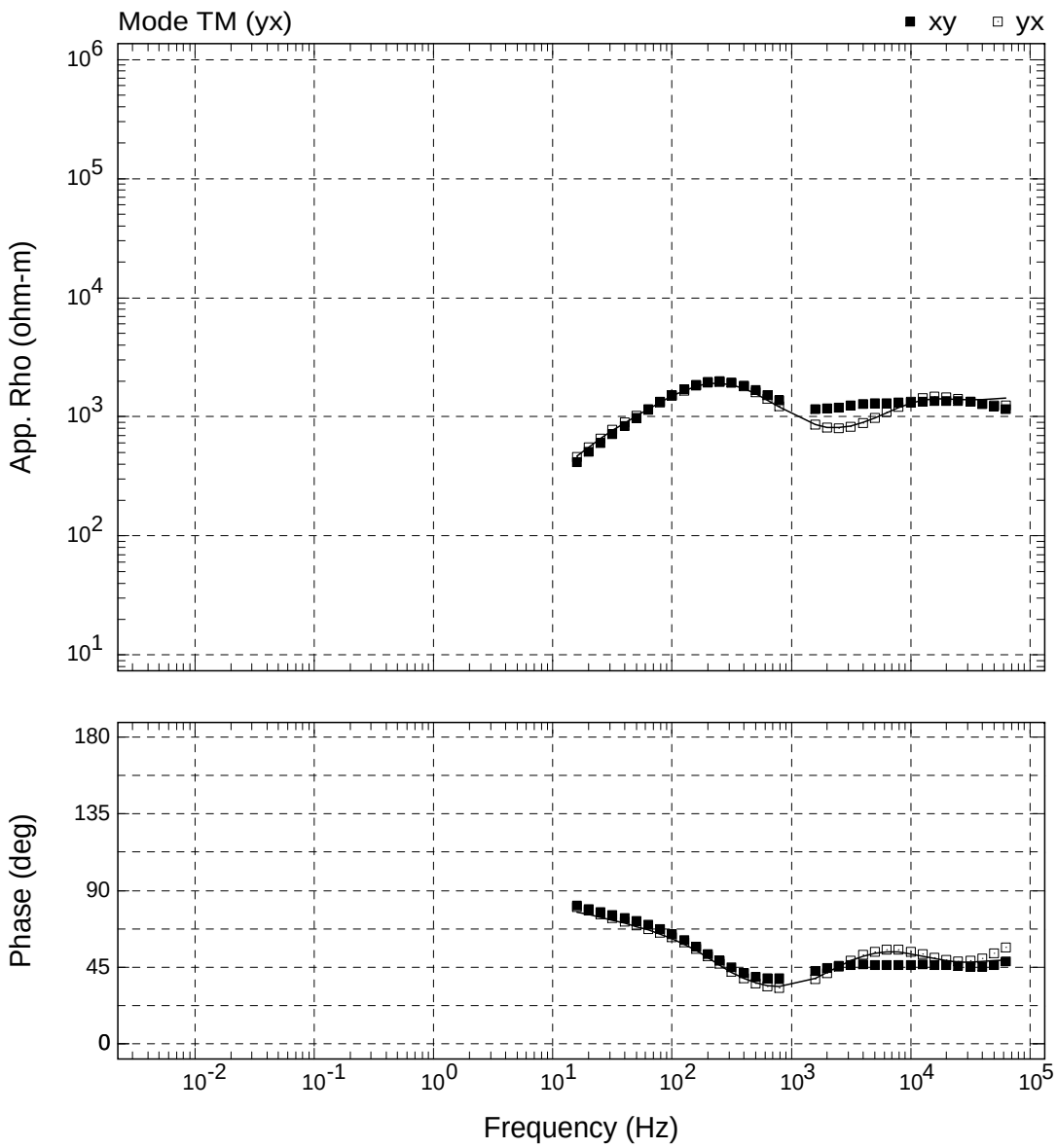

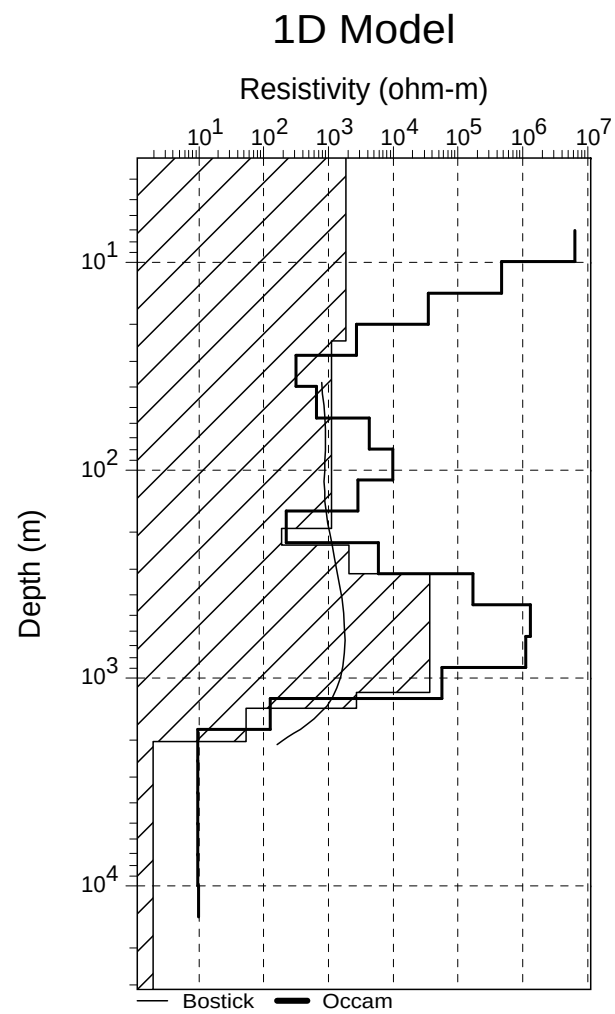

Sounding: ZMR038

Area: Mauna Kea

26/Dec/2016

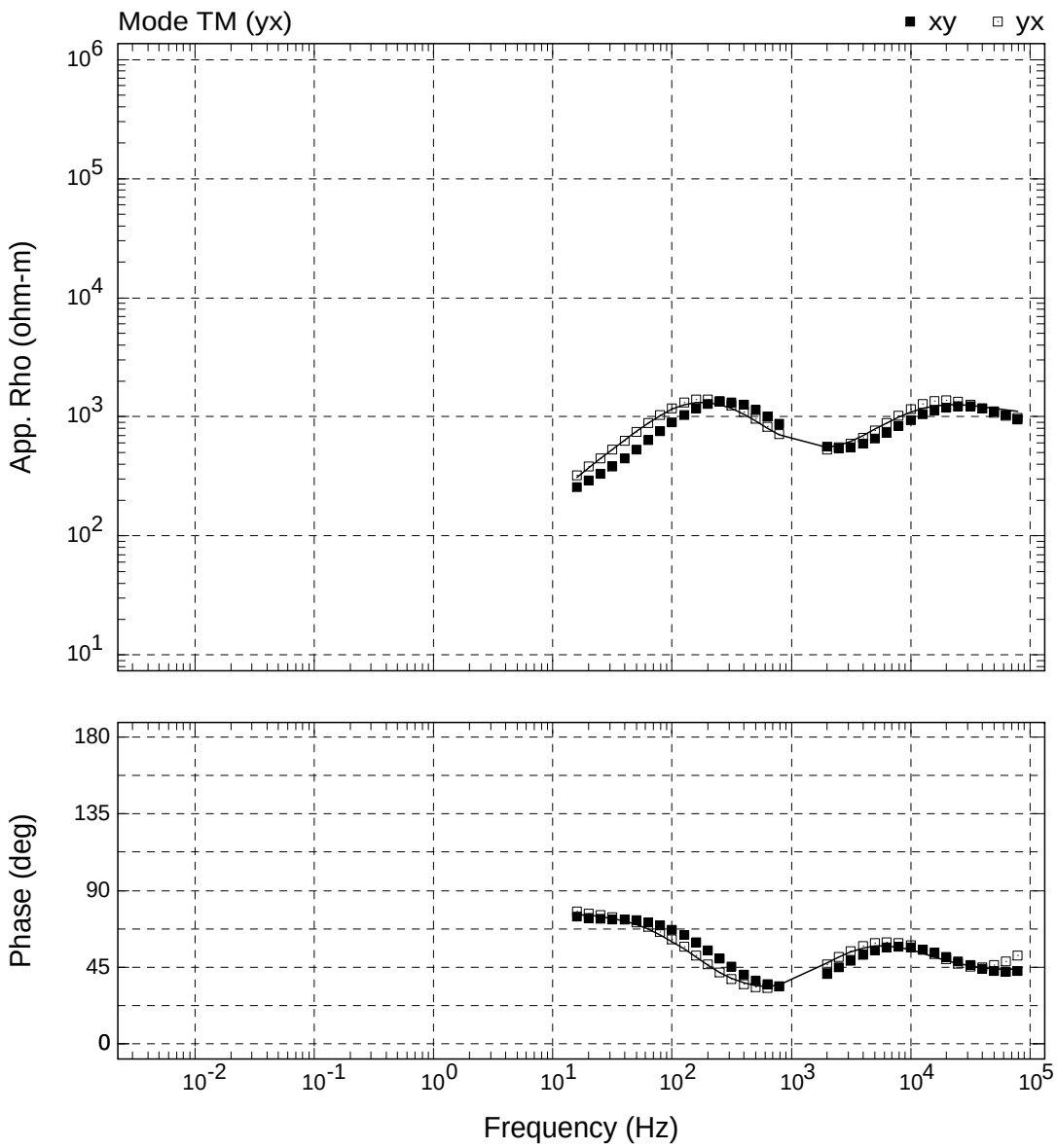

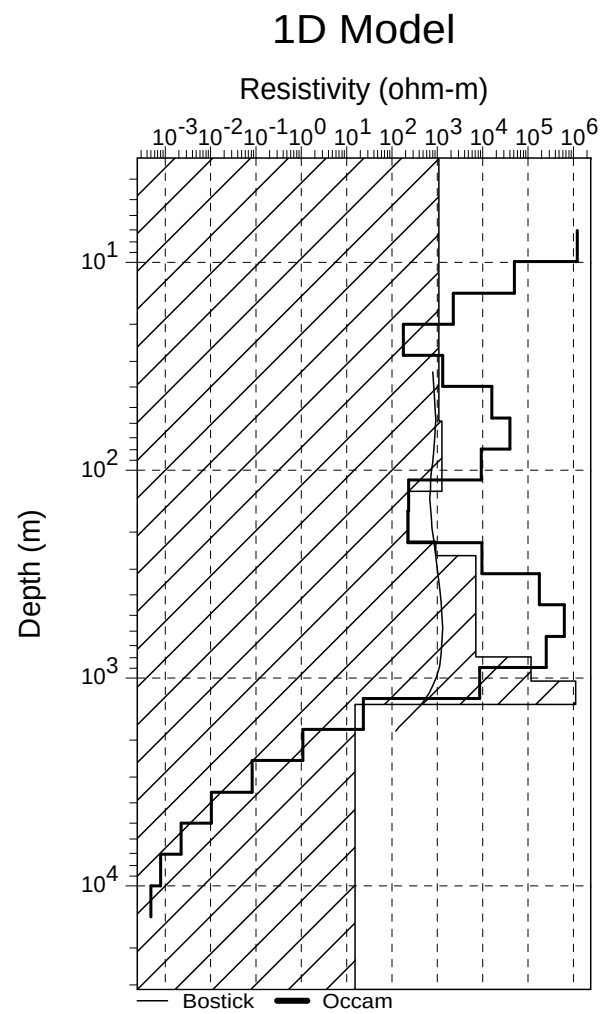

Sounding: ZMR039

Area: Mauna Kea

26/Dec/2016

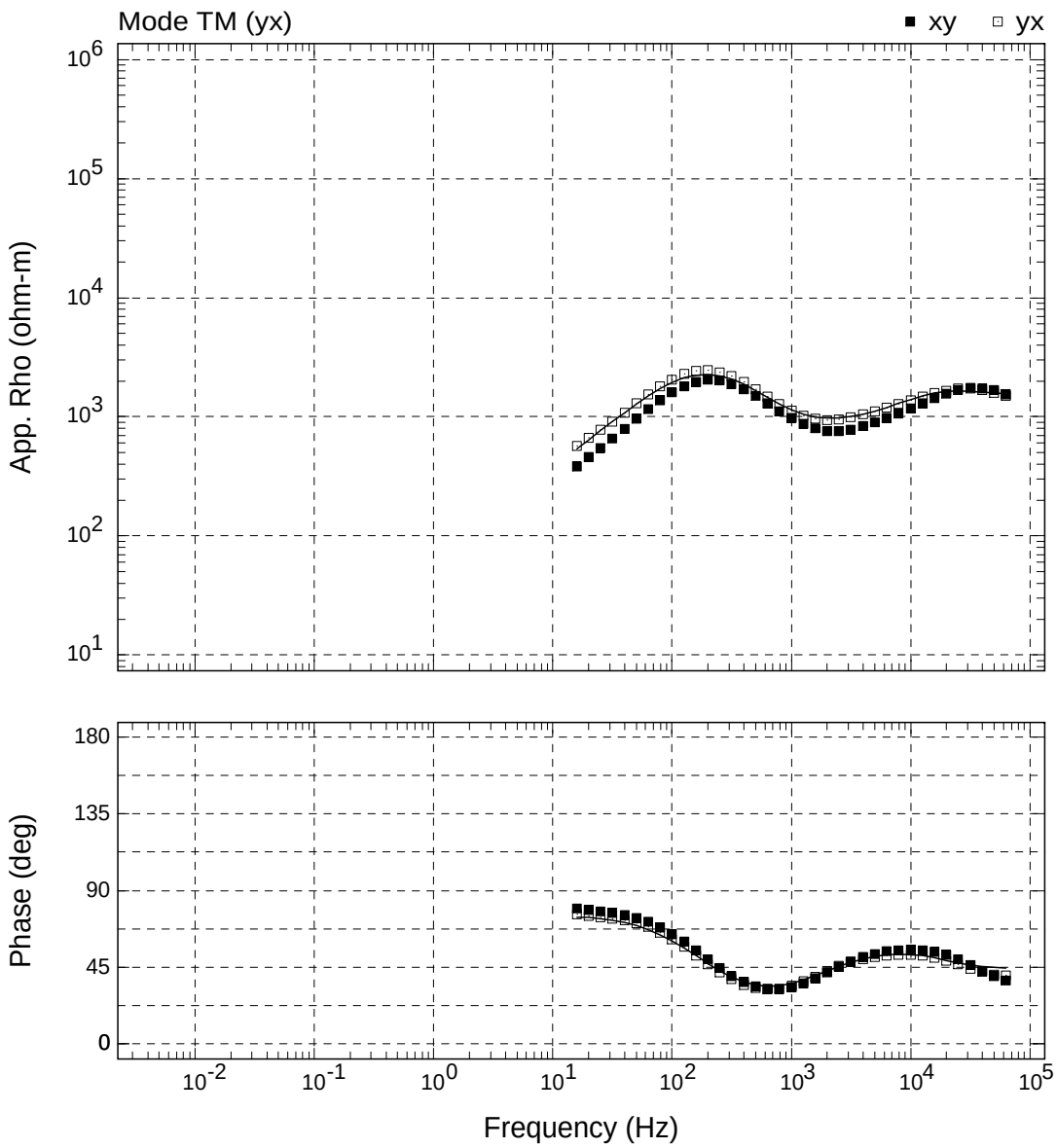

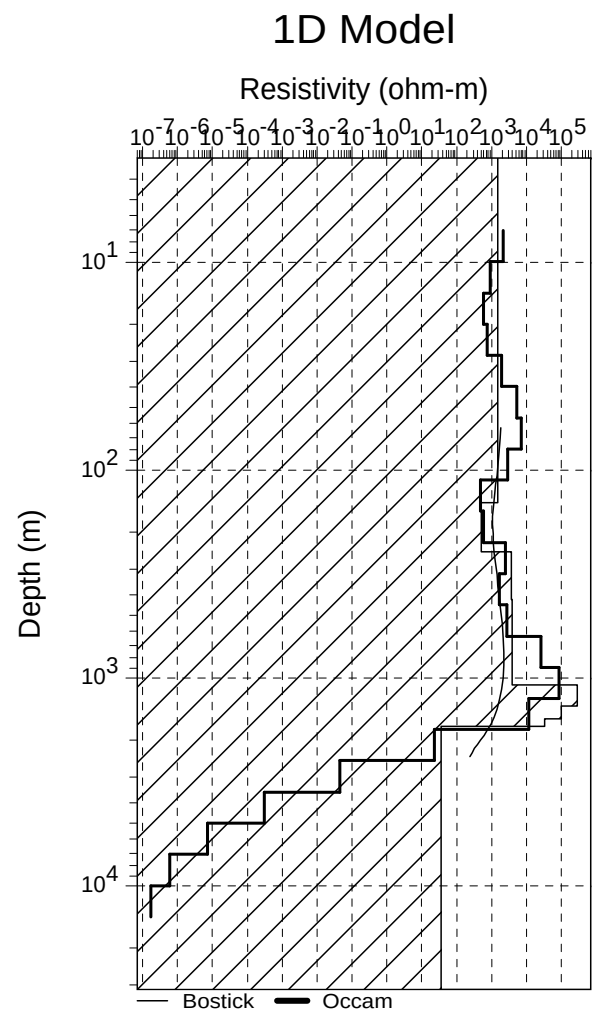

Sounding: ZMR040

Area: Mauna Kea

26/Dec/2016

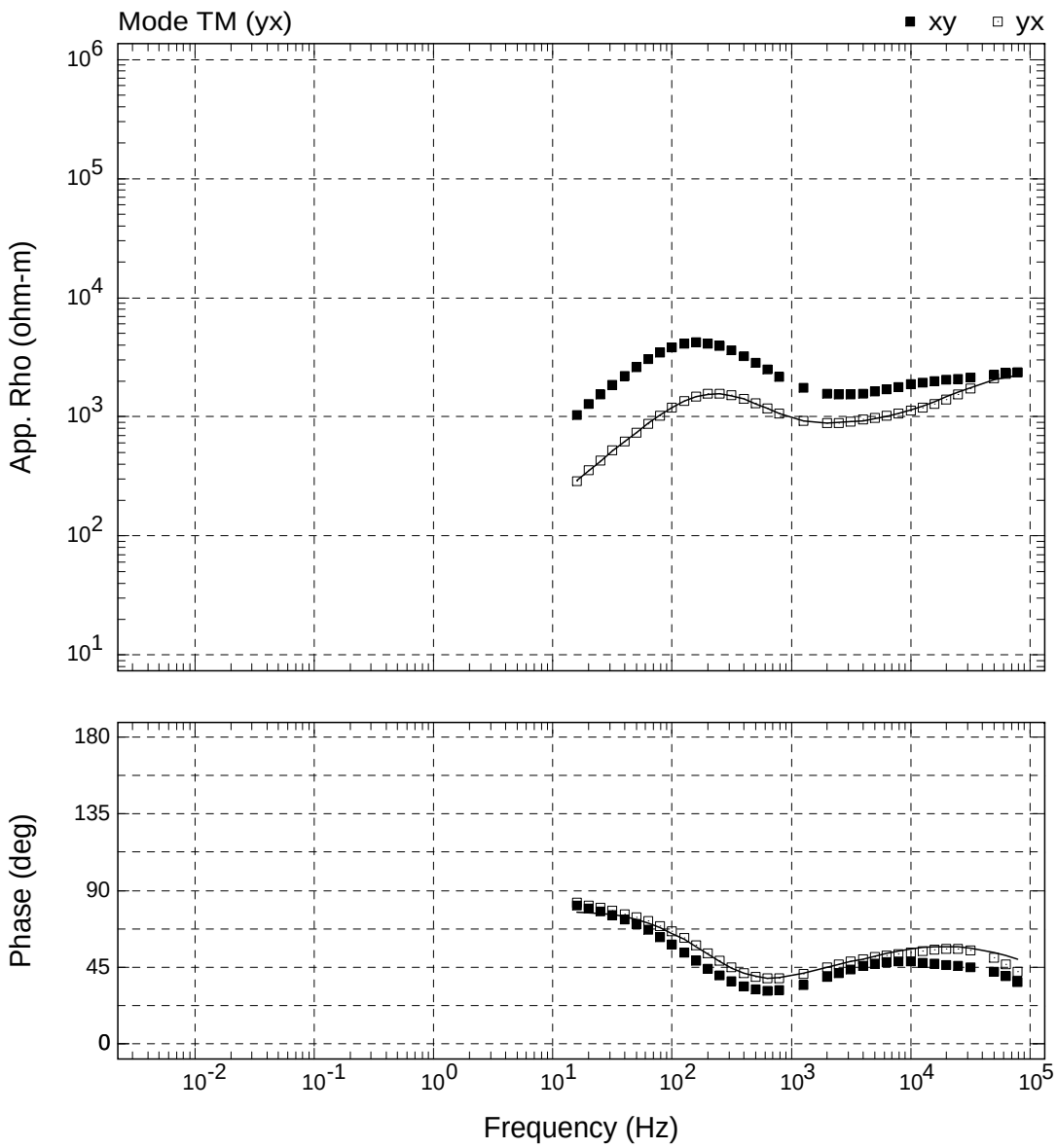

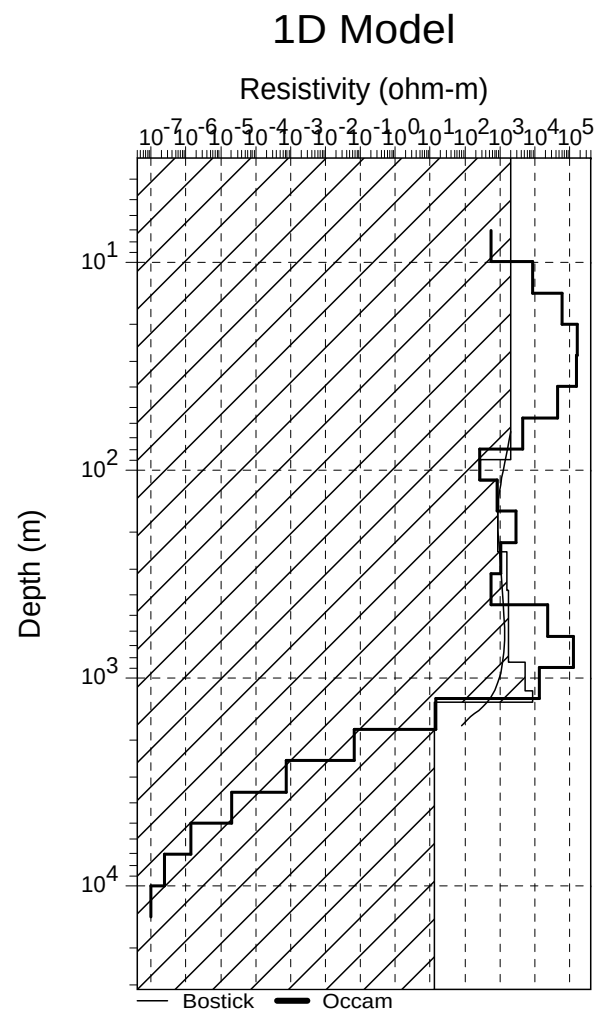

Sounding: ZMR041
Area: Mauna Kea
26/Dec/2016

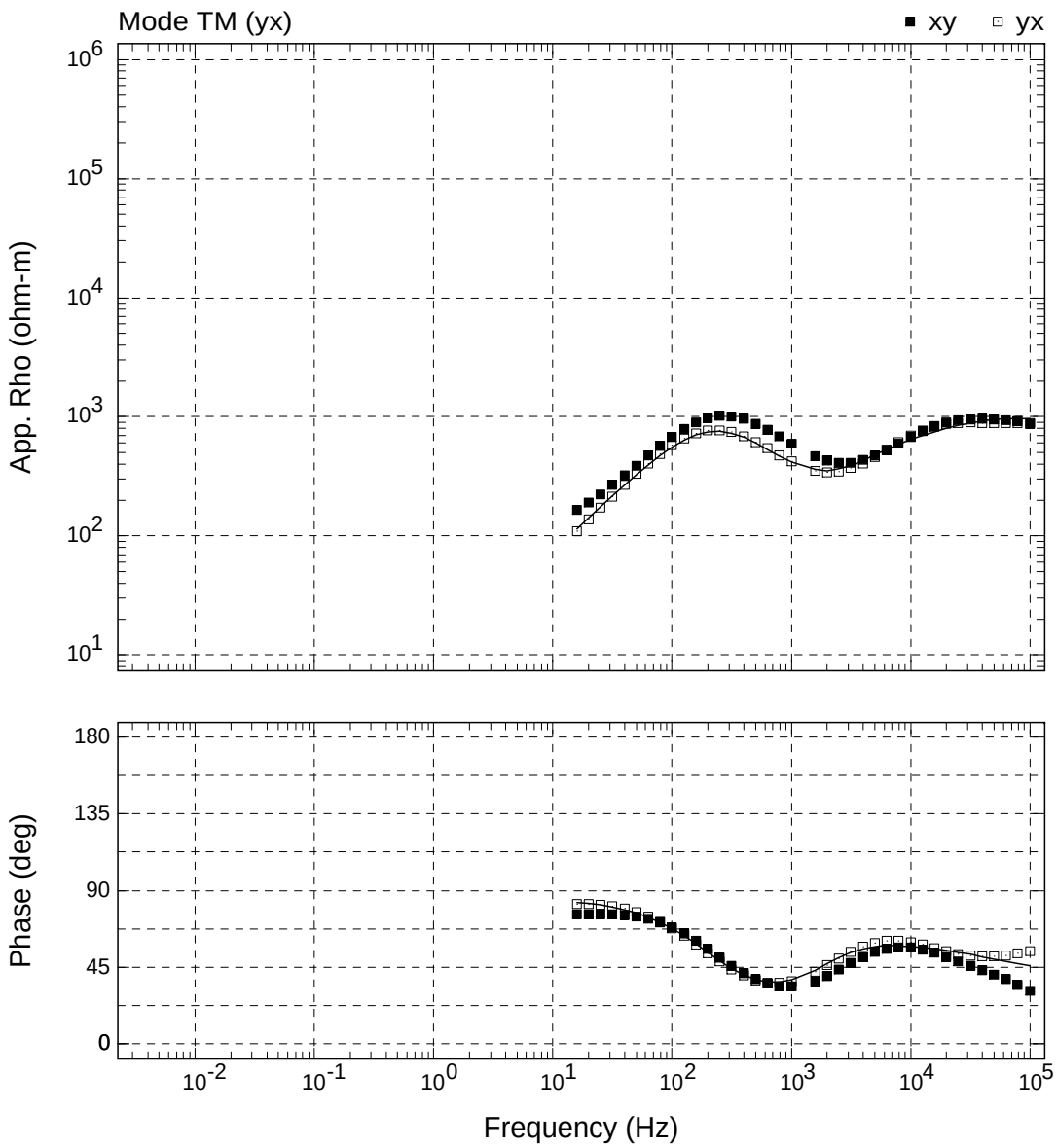

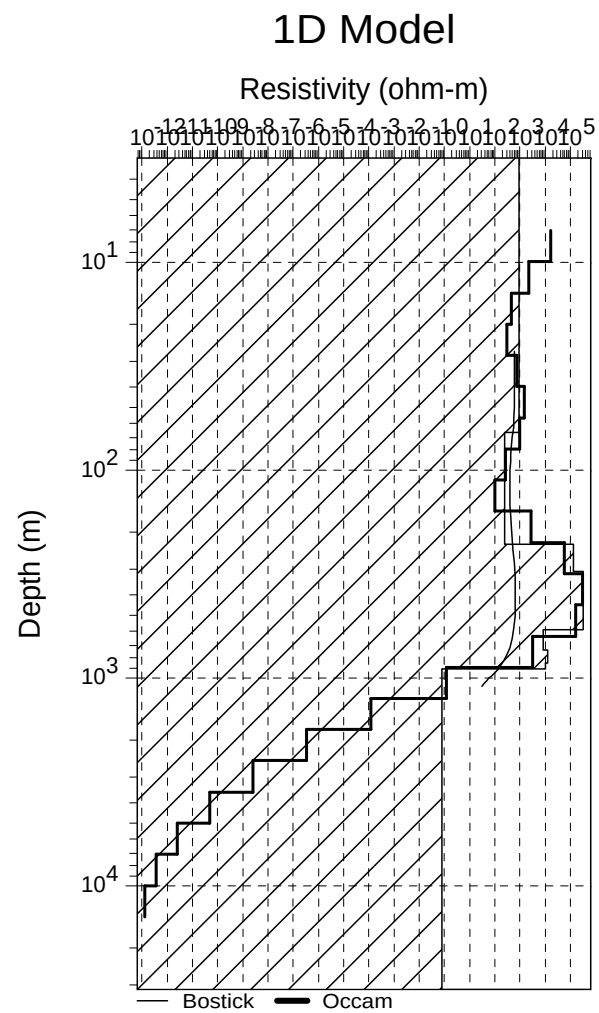

Sounding: ZMR042
Area: Mauna Kea
26/Dec/2016

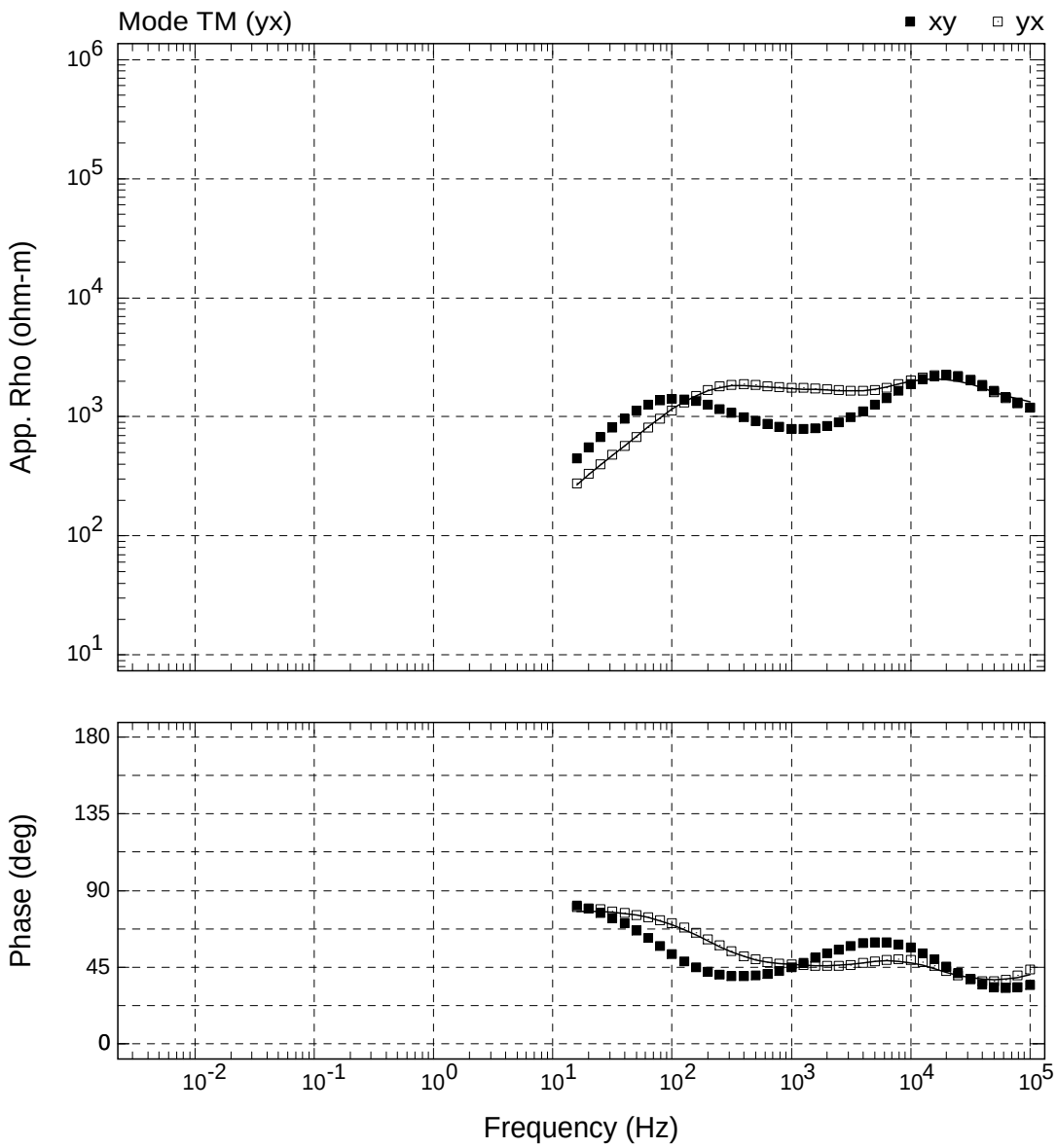

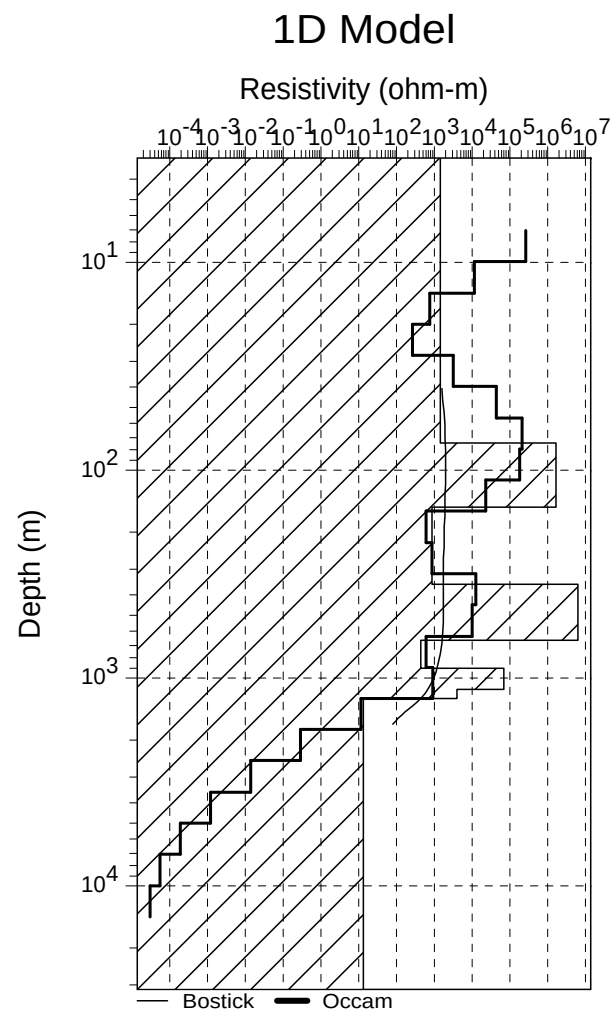

Sounding: ZMR043
Area: Mauna Kea
26/Dec/2016

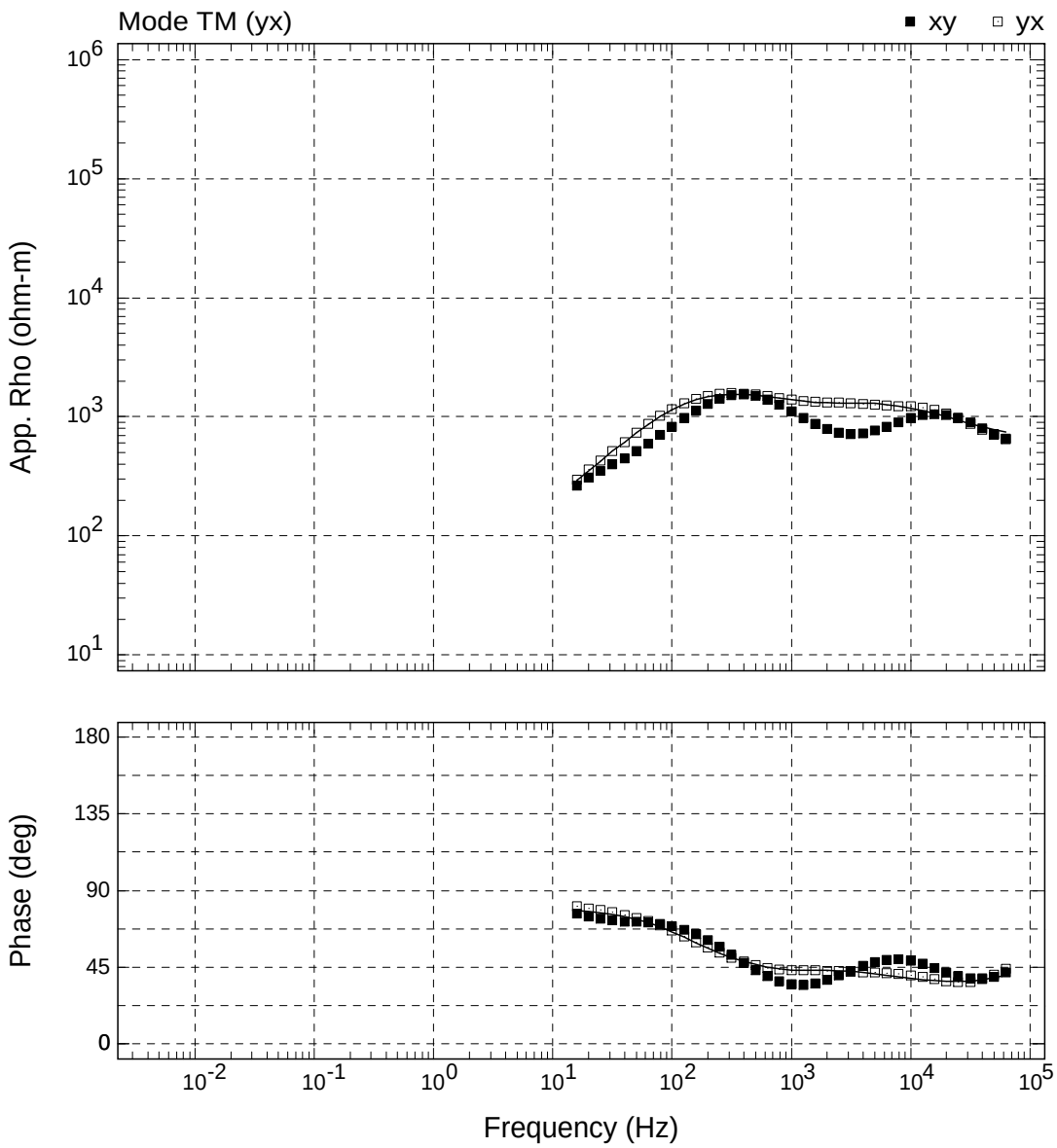

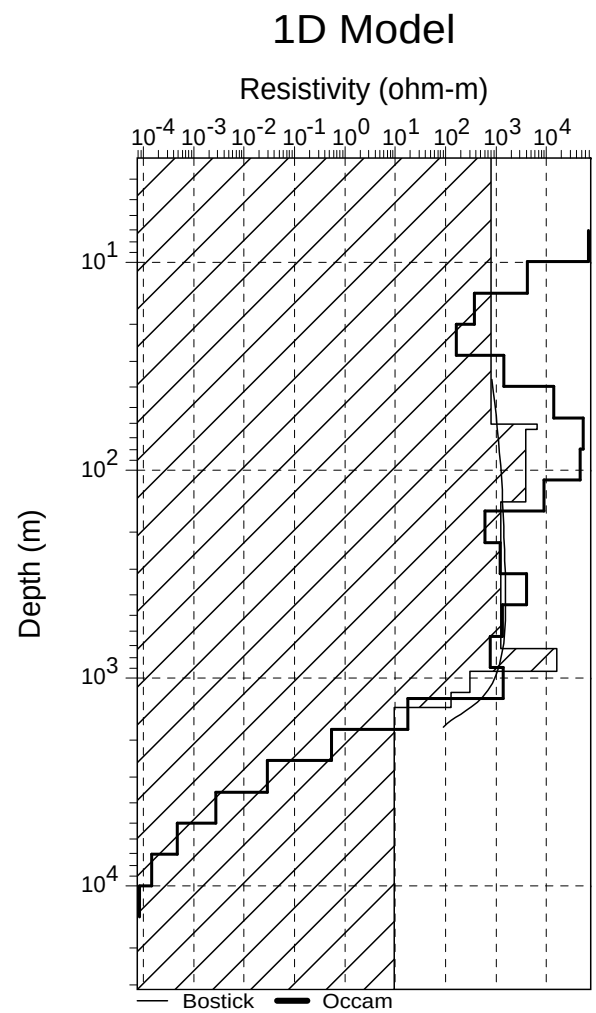

Sounding: ZMR044

Area: Mauna Kea

26/Dec/2016

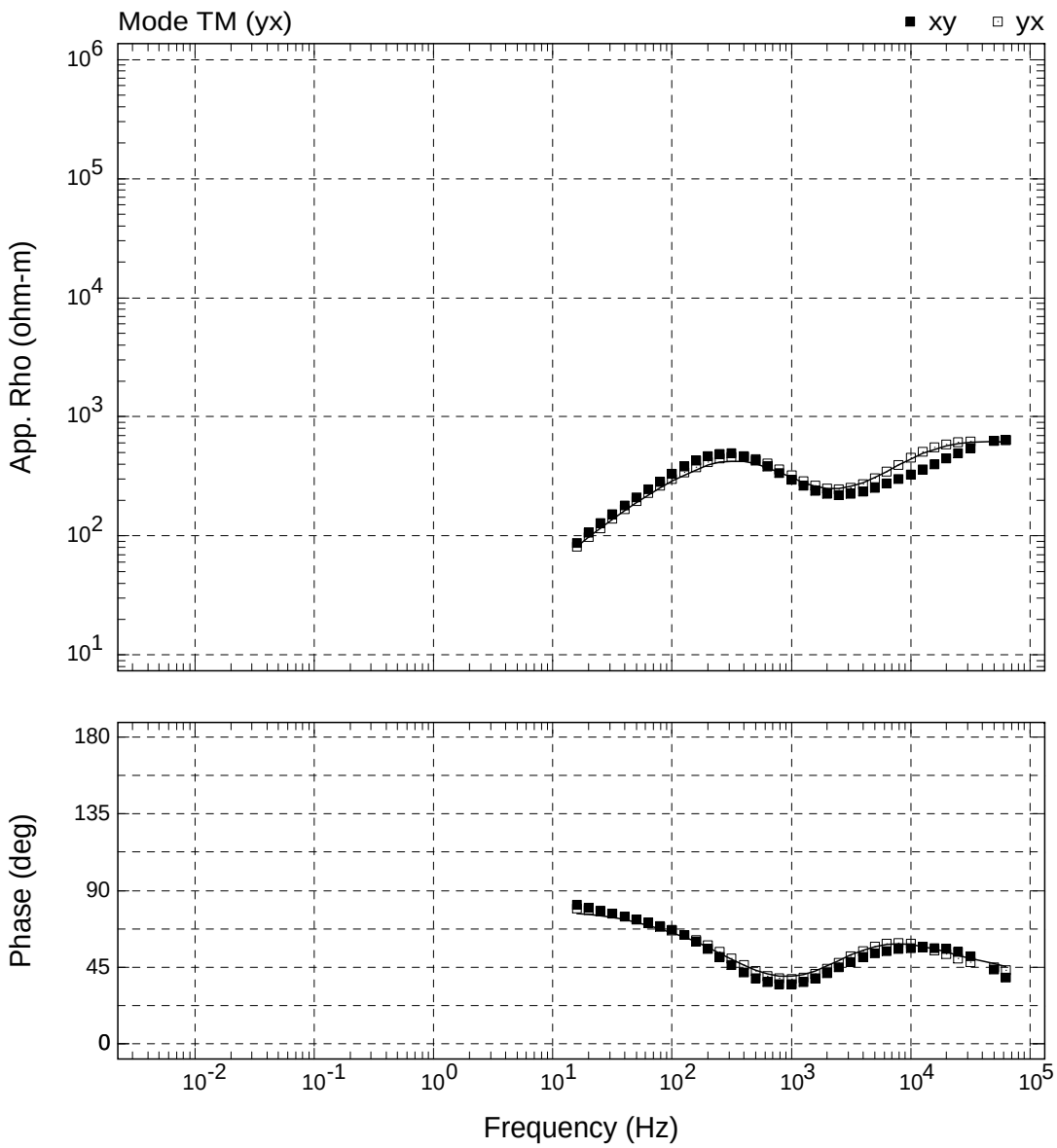

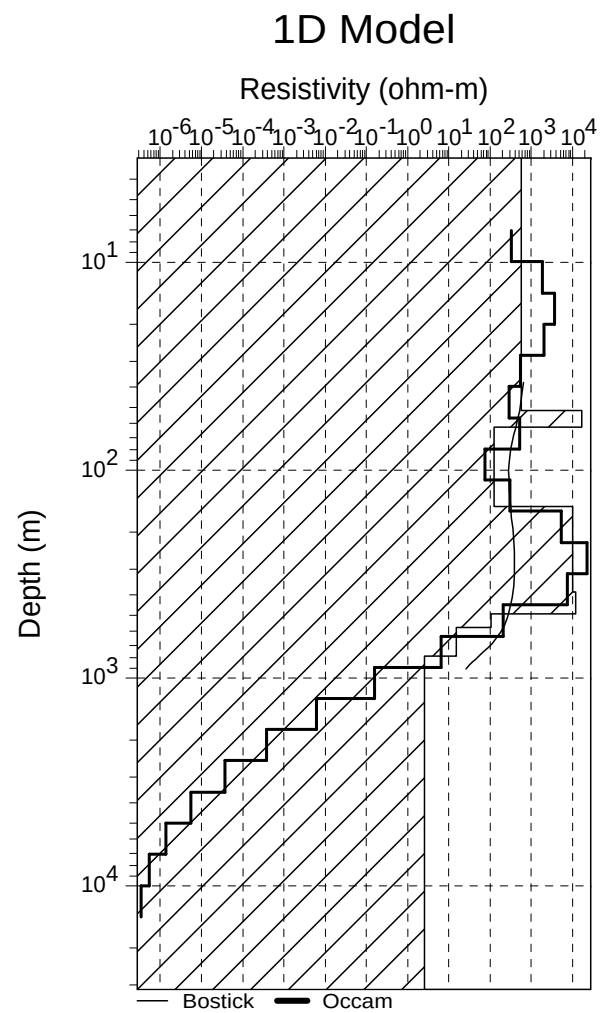

Sounding: ZMR045

Area: Mauna Kea

26/Dec/2016

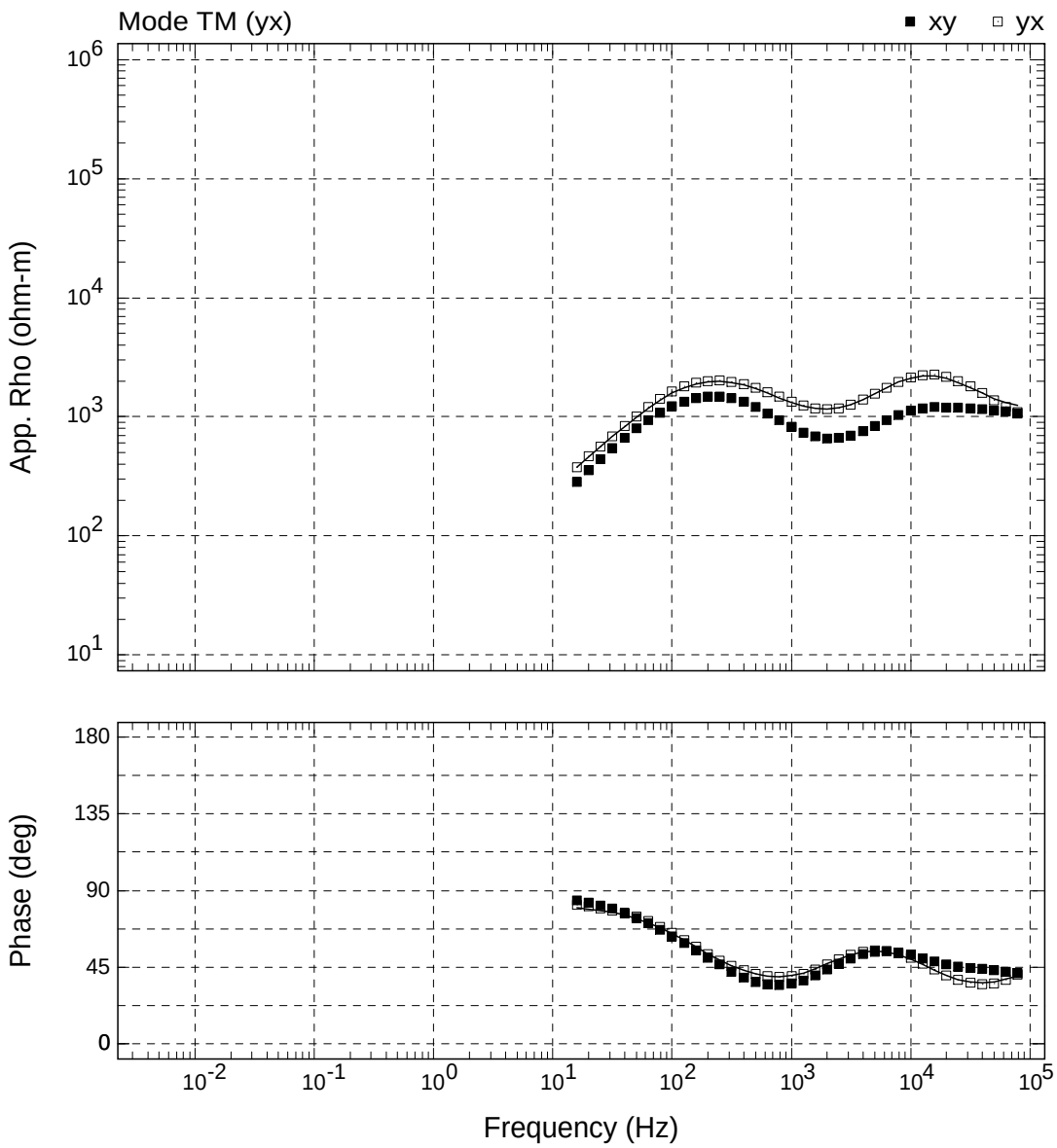

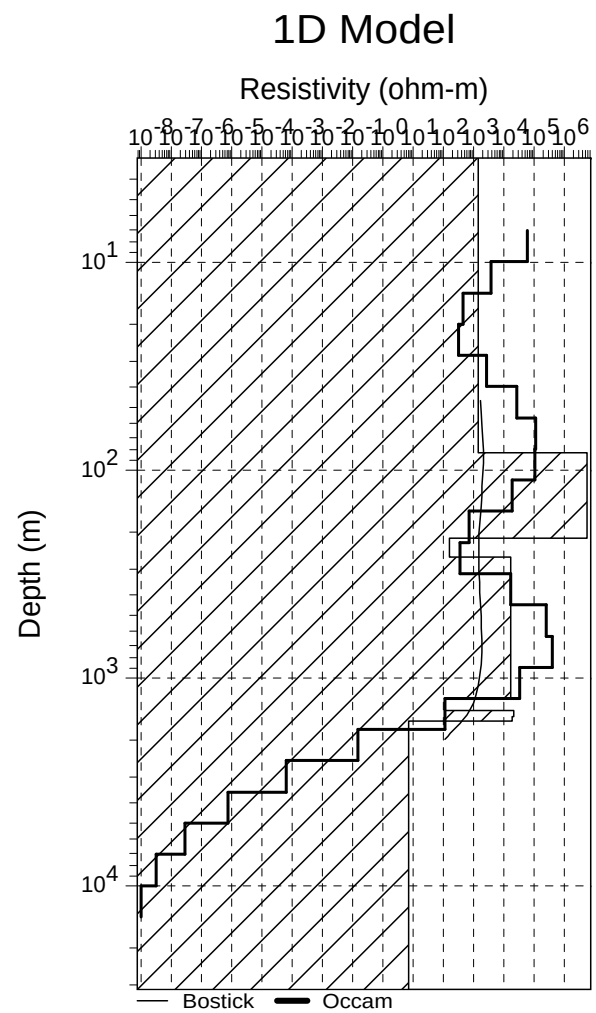

Sounding: ZMR046
Area: Mauna Kea
26/Dec/2016

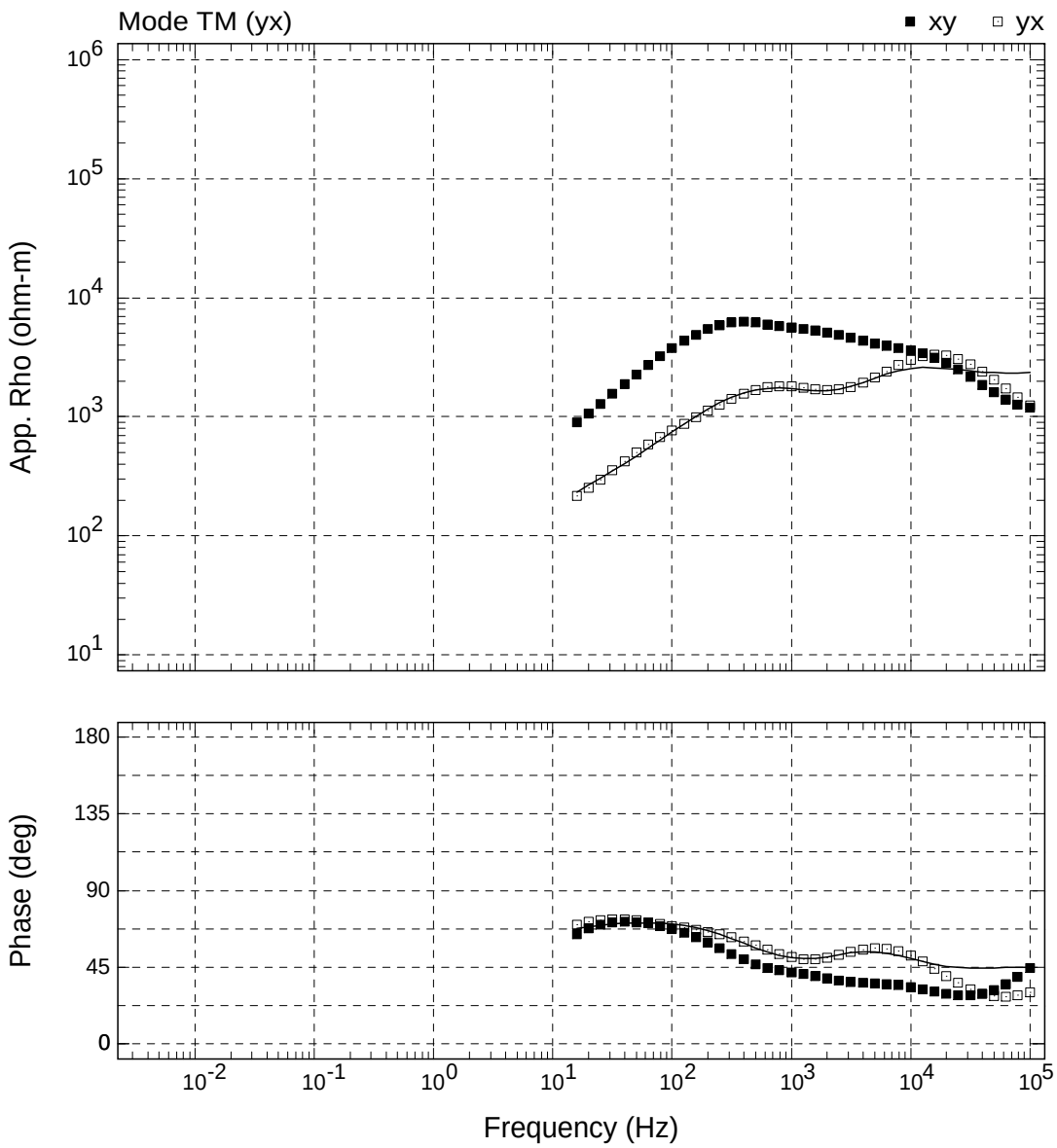

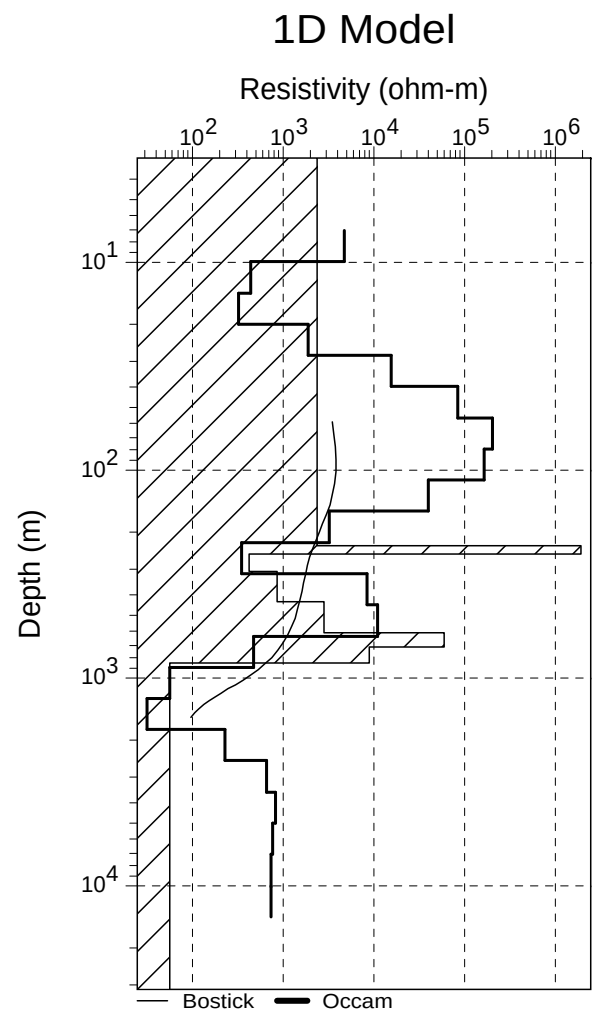

Sounding: ZMR047

Area: Mauna Kea

26/Dec/2016

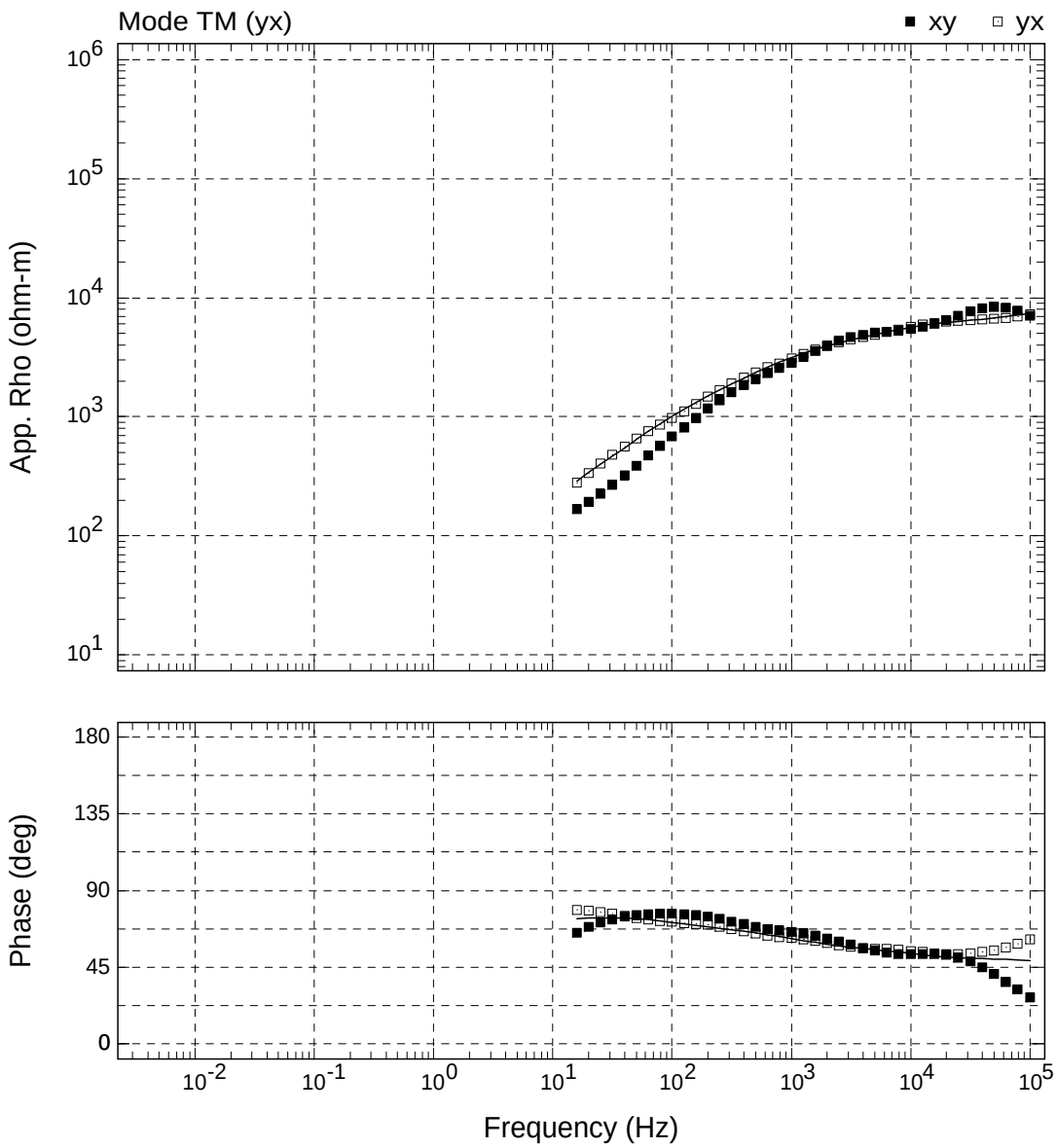

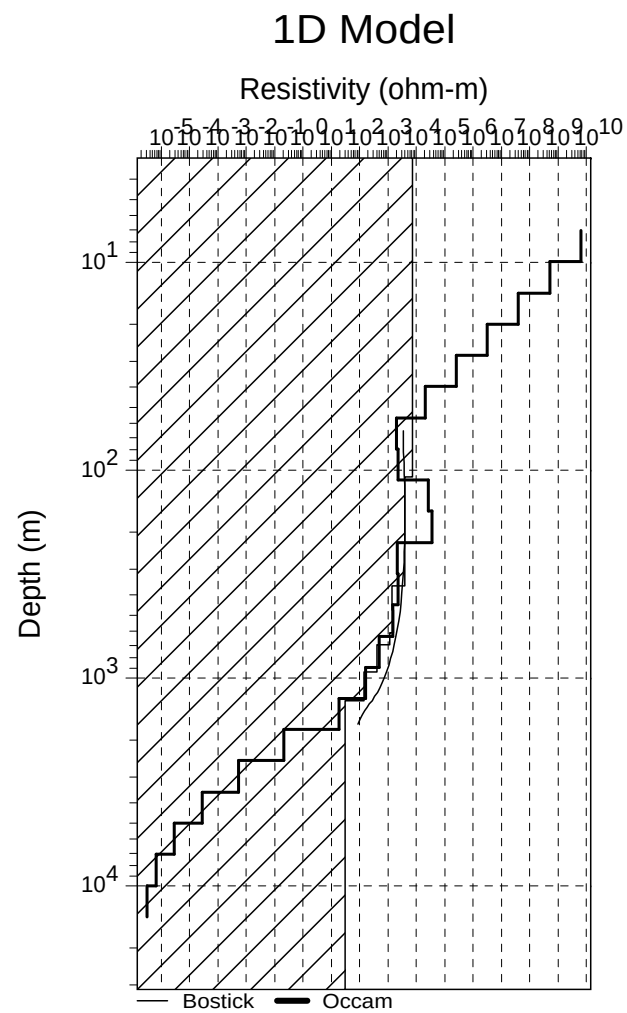

Sounding: ZMR048
Area: Mauna Kea
26/Dec/2016

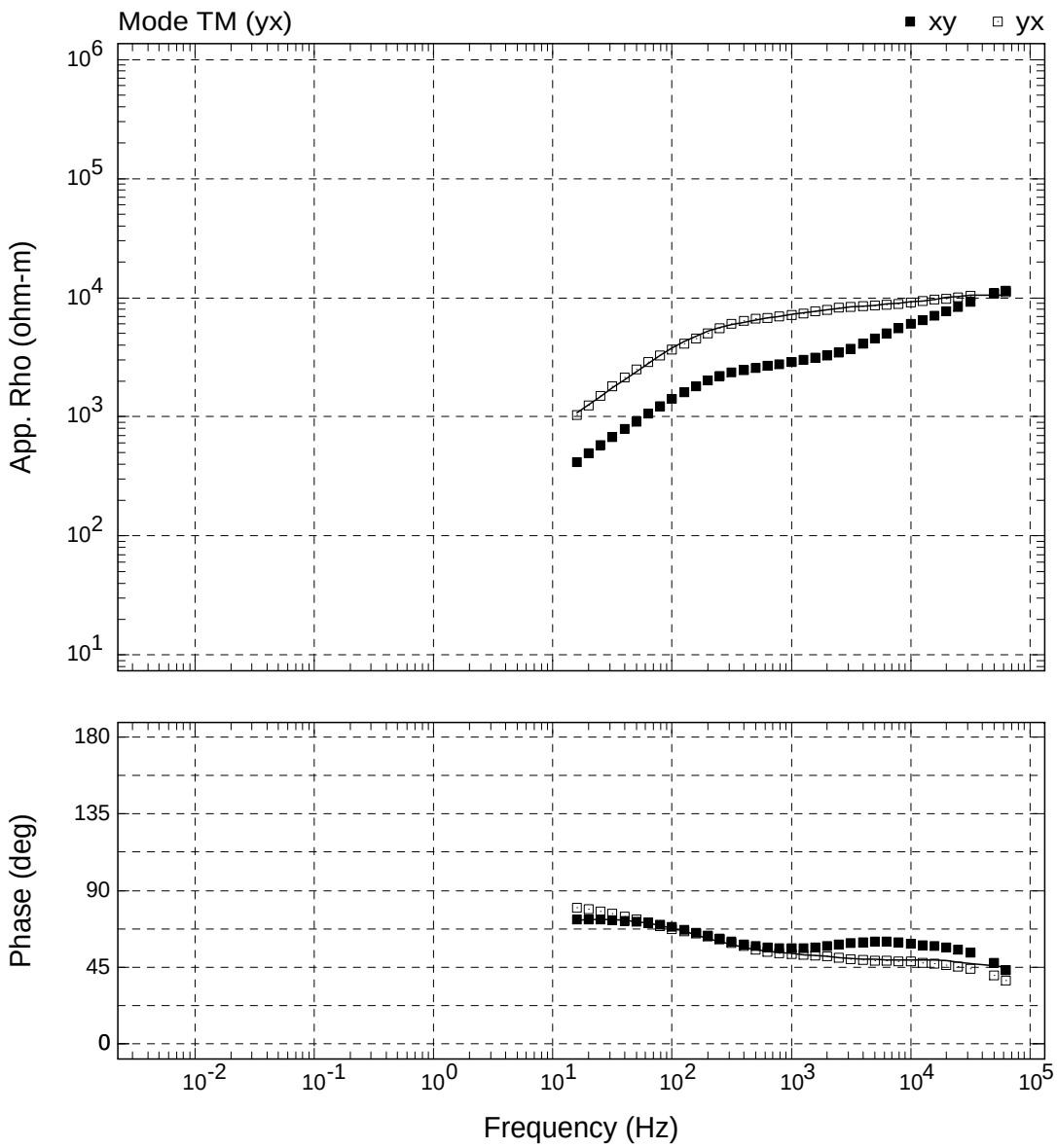

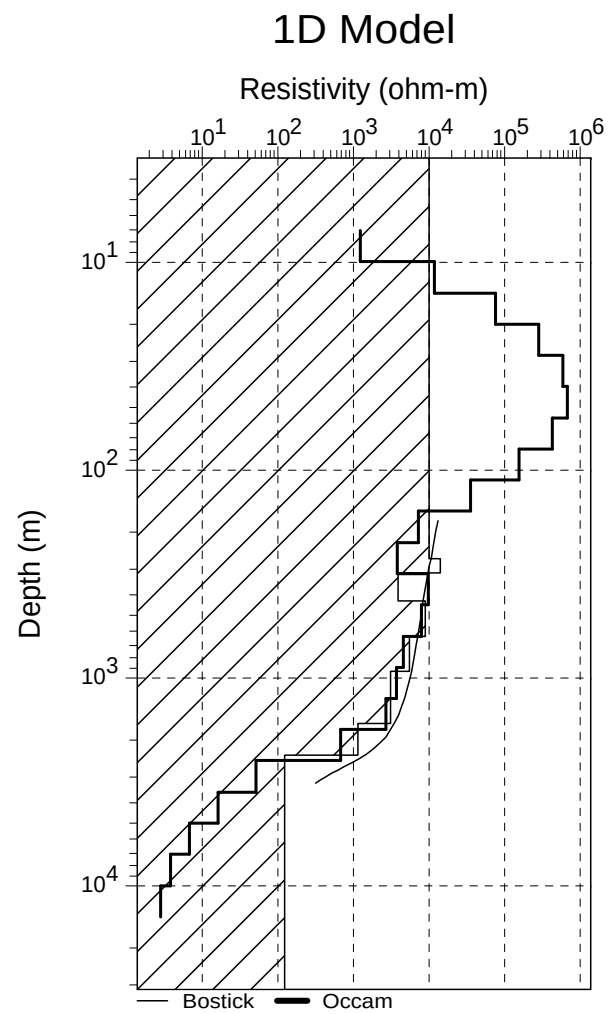

Sounding: ZMR049

Area: Mauna Kea

26/Dec/2016

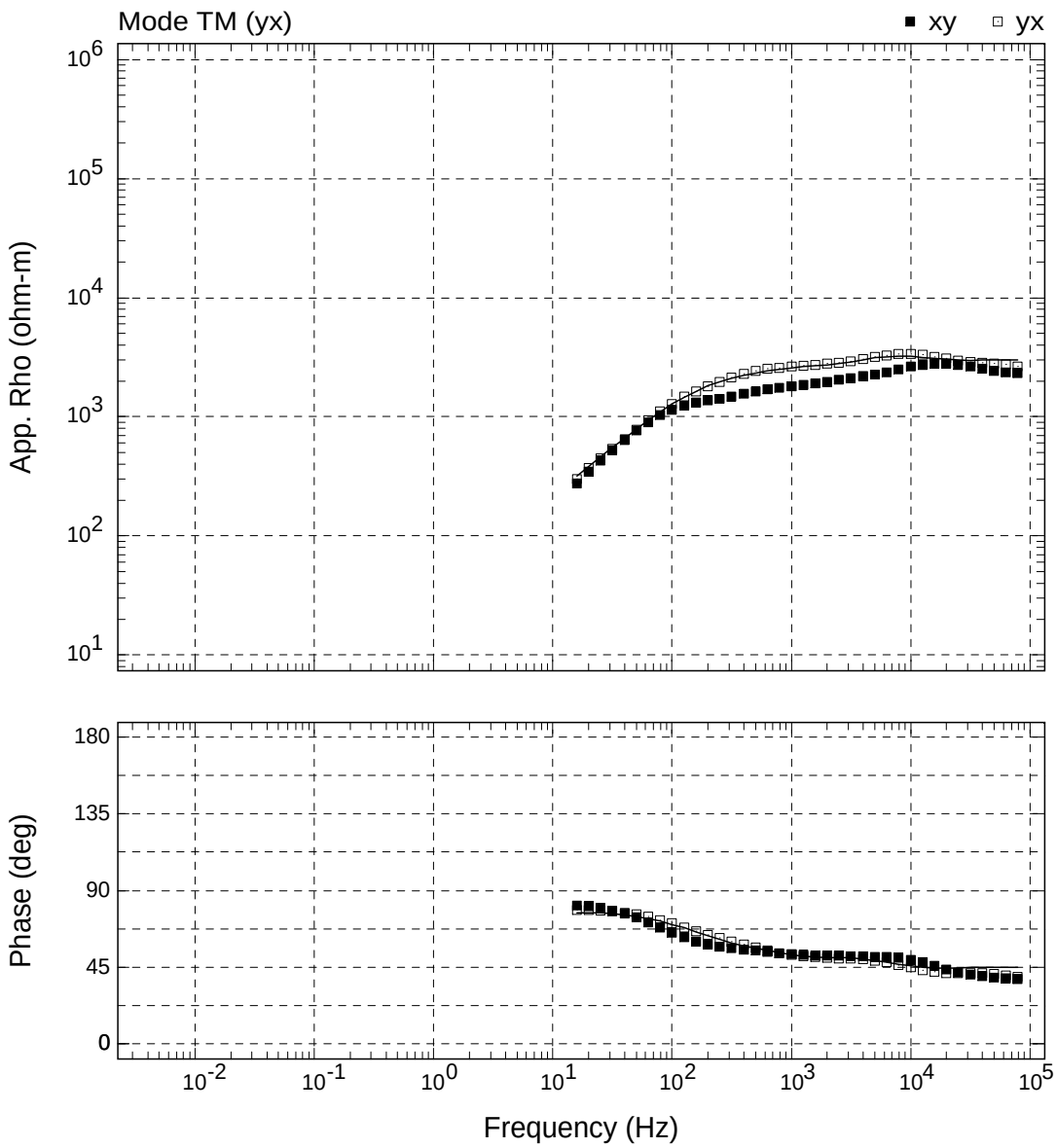

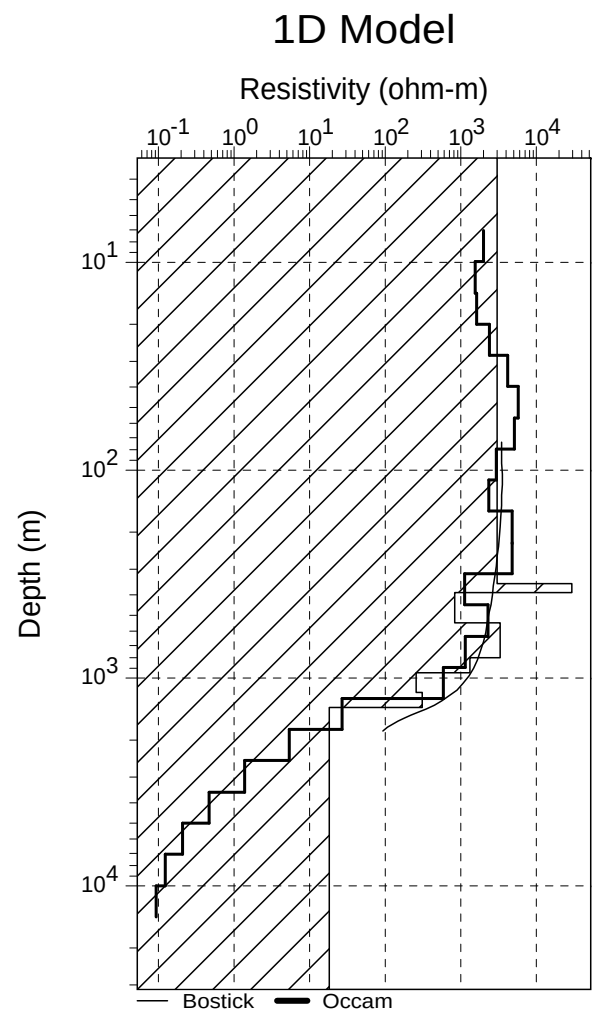

Sounding: ZMR051

Area: Mauna Kea

26/Dec/2016

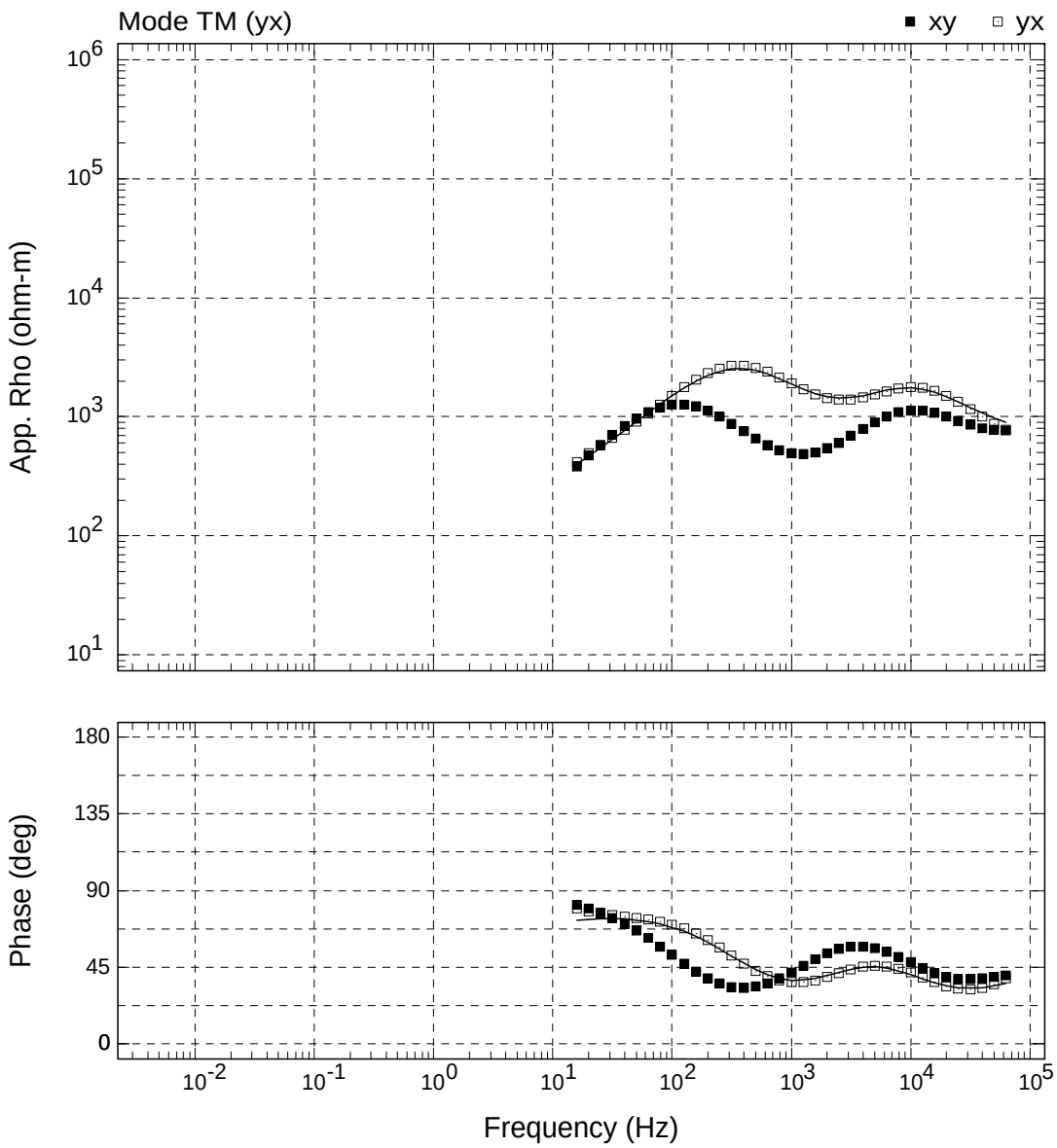

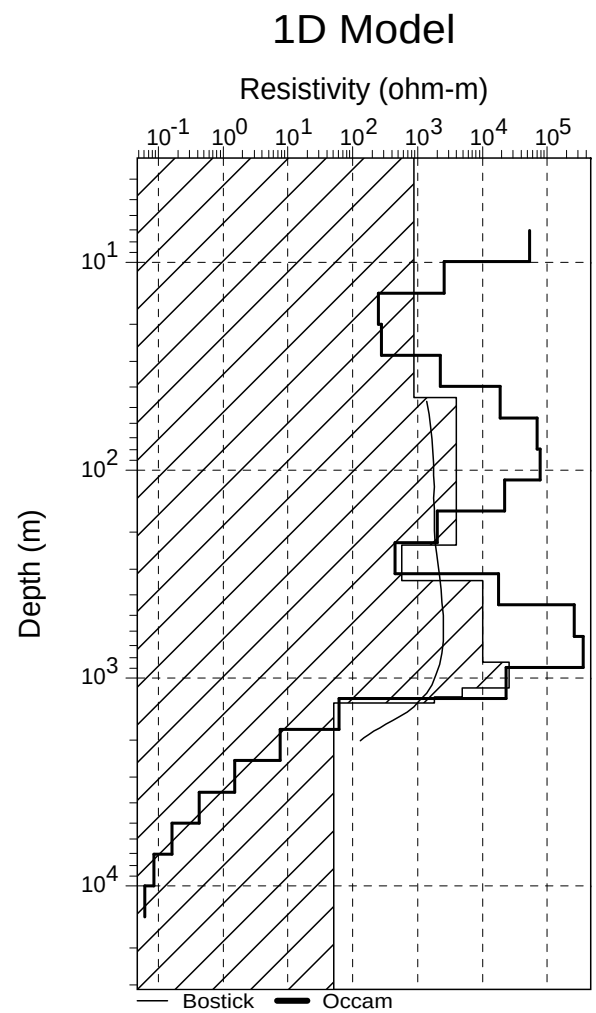

Sounding: ZMR052

Area: Mauna Kea

26/Dec/2016

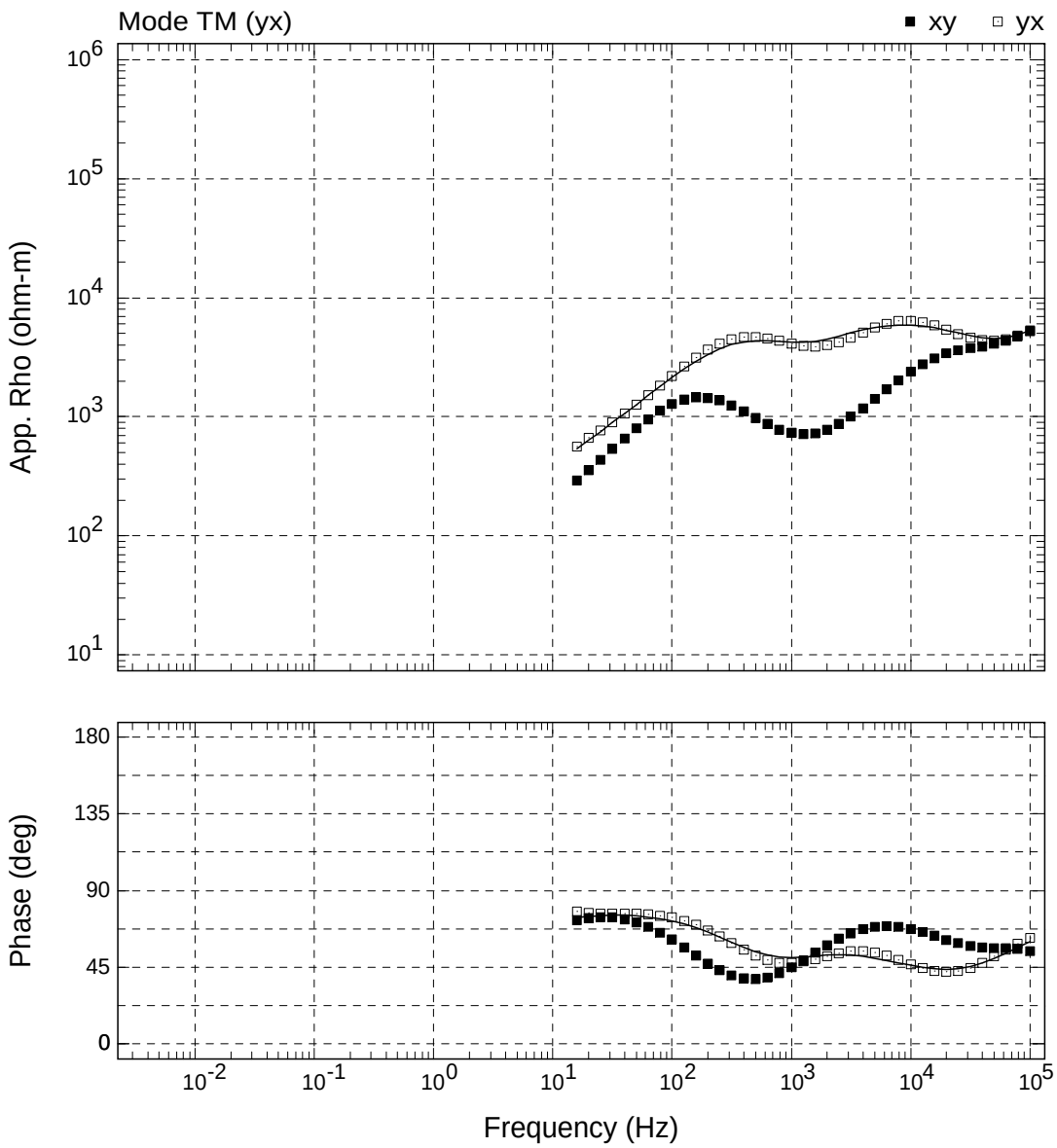

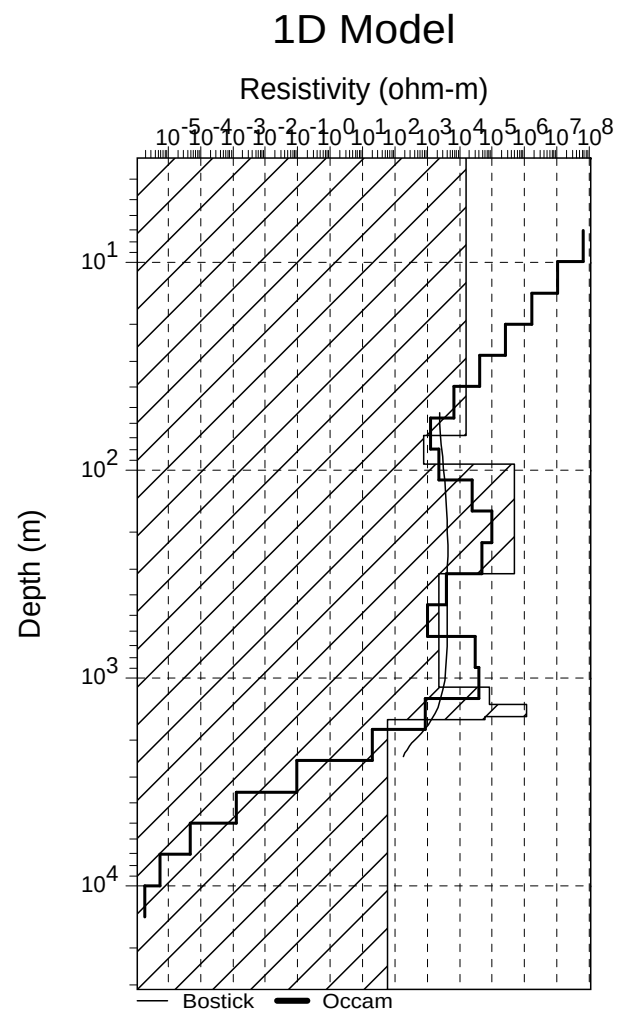

Sounding: ZMR053

Area: Mauna Kea

26/Dec/2016

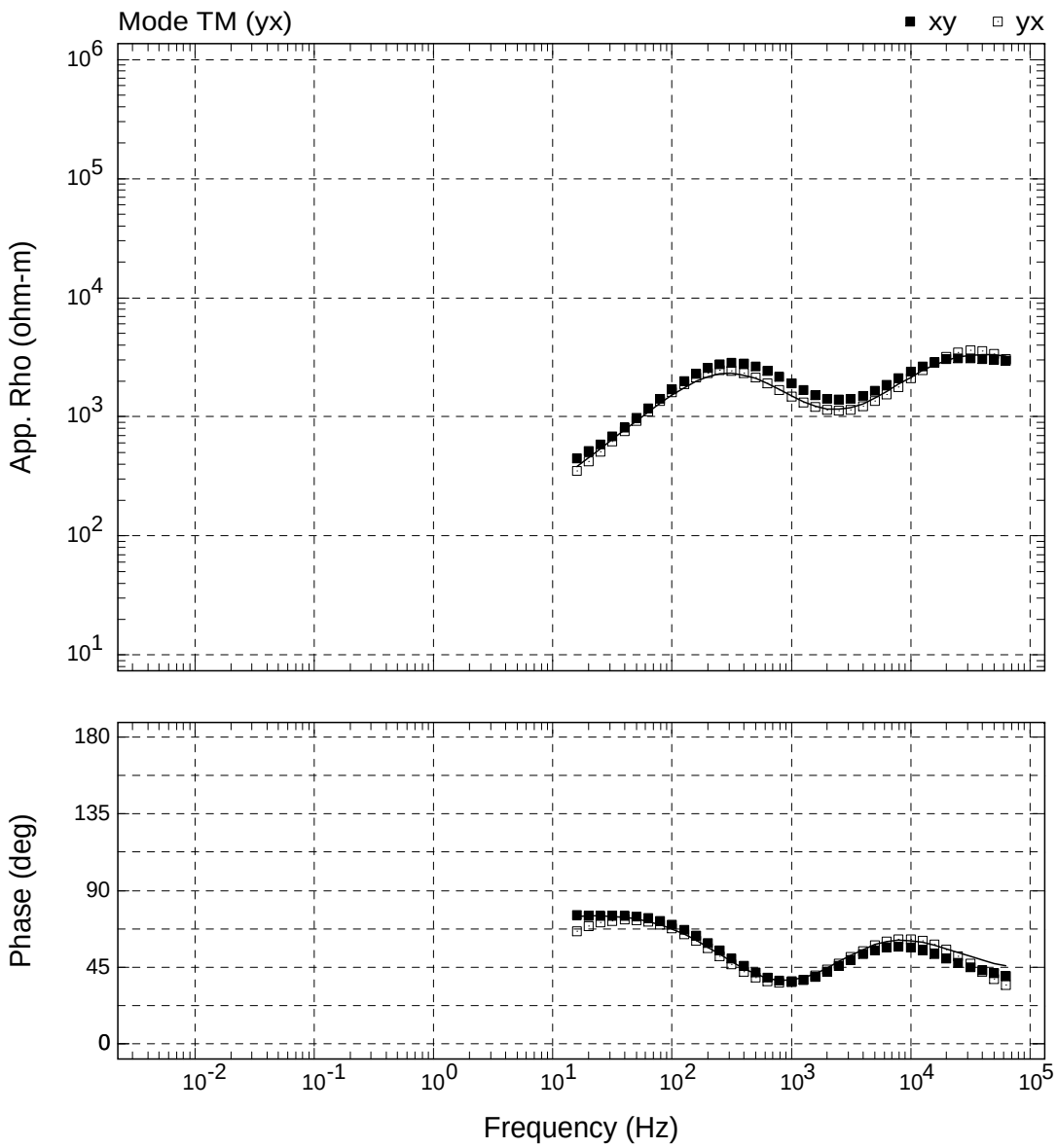

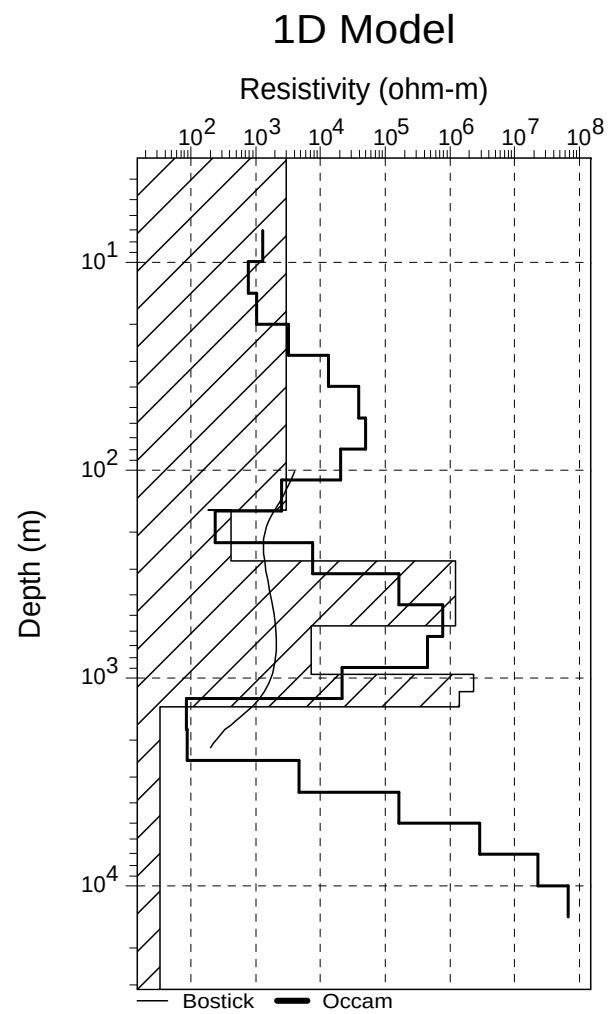

Sounding: ZMR054

Area: Mauna Kea

26/Dec/2016

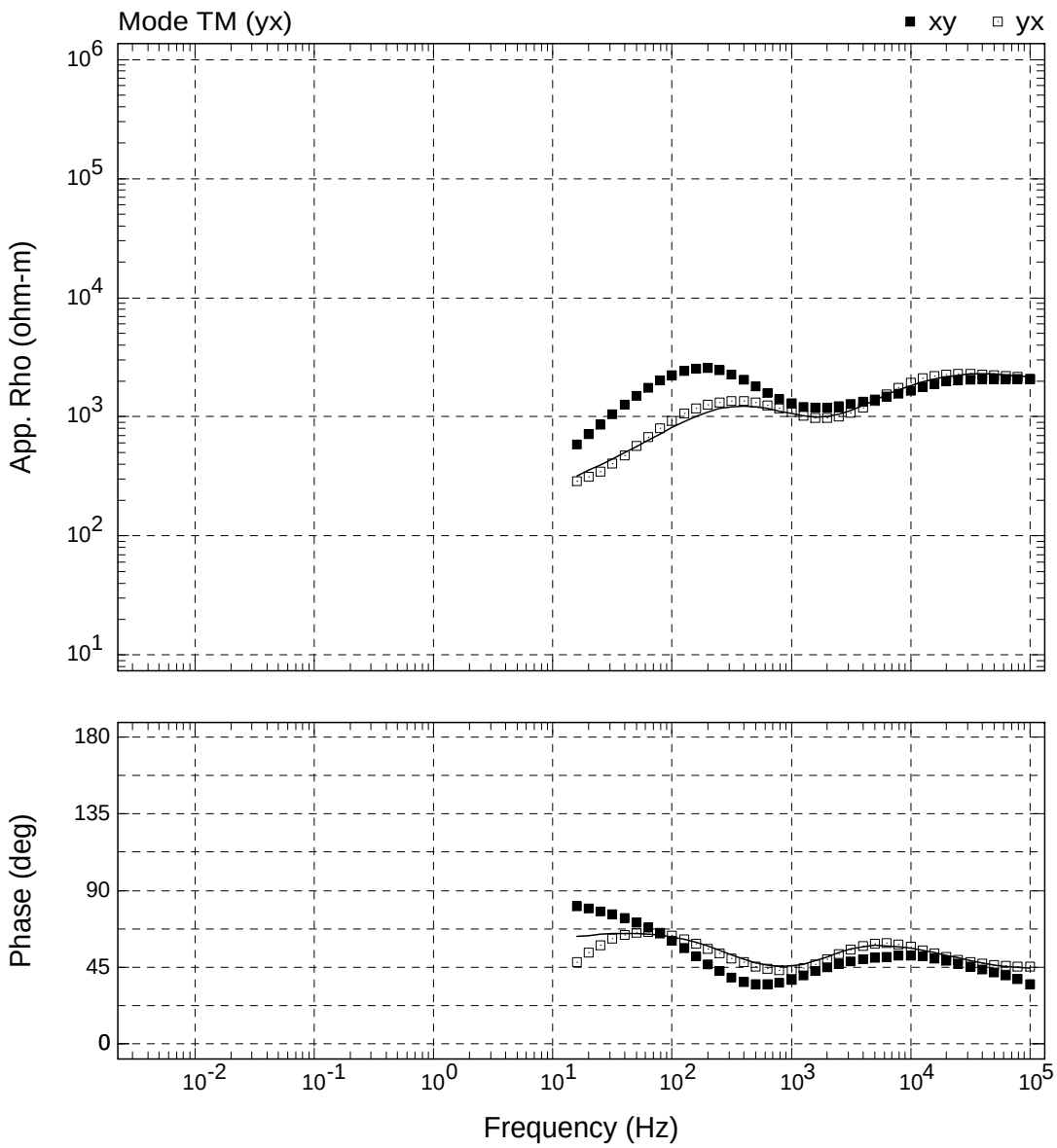

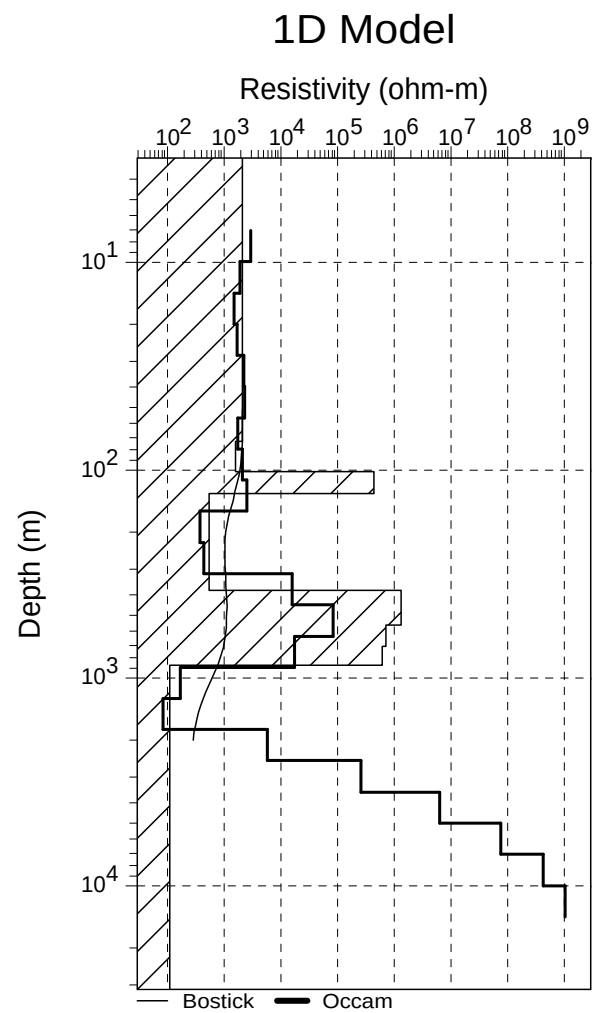

Sounding: ZMR055

Area: Mauna Kea

26/Dec/2016

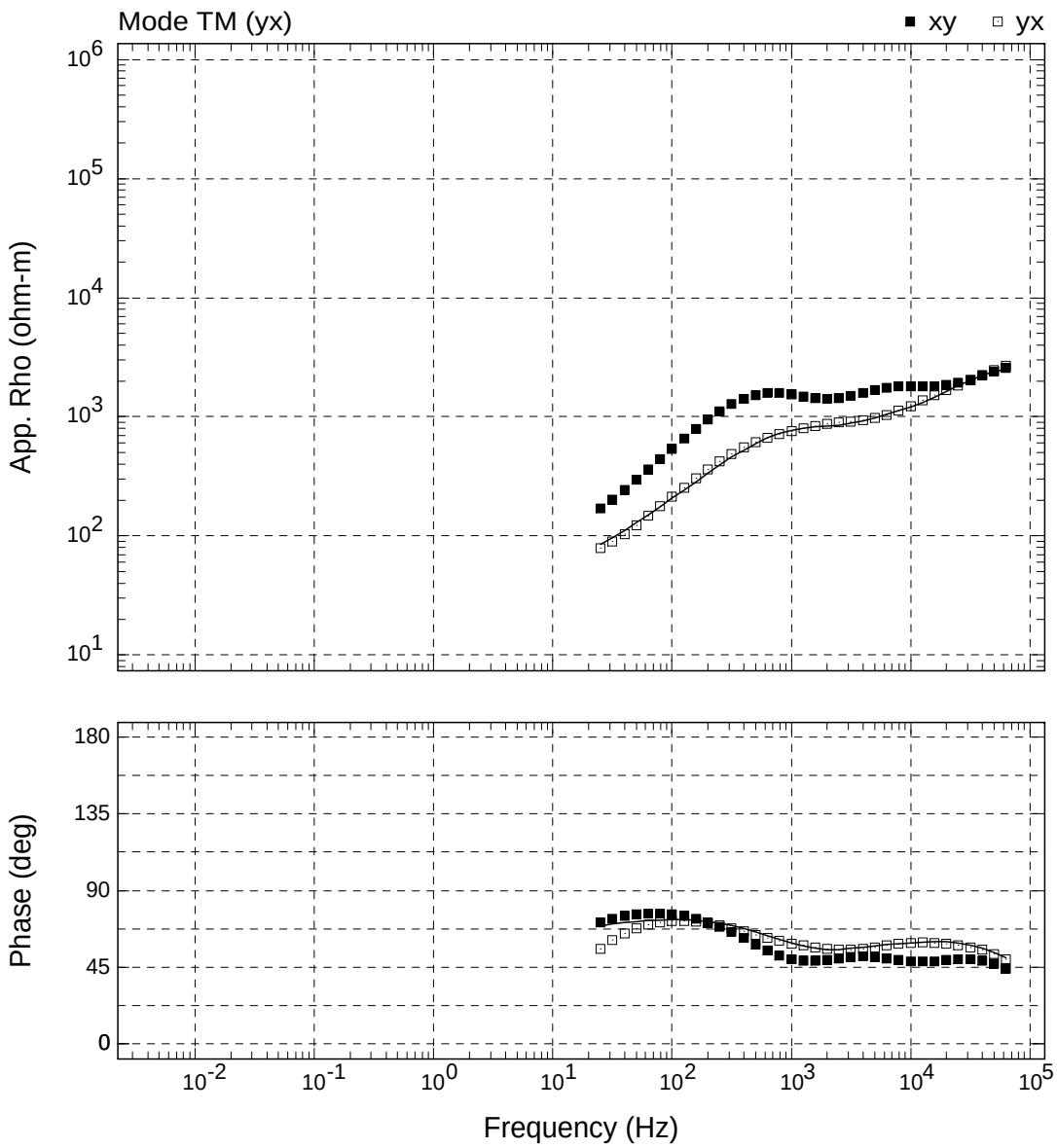

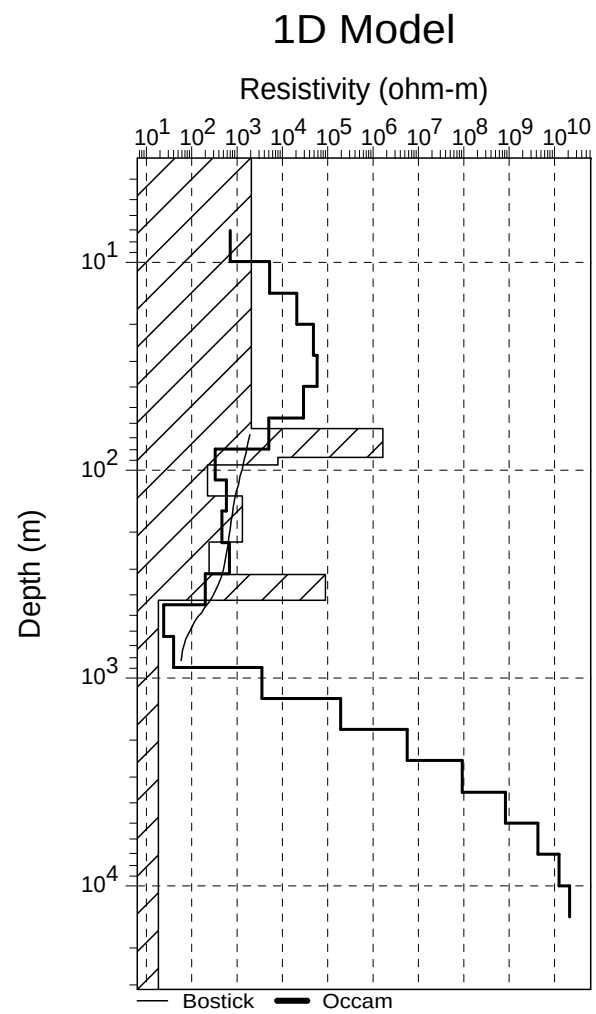

Sounding: ZMR056

Area: Mauna Kea

26/Dec/2016

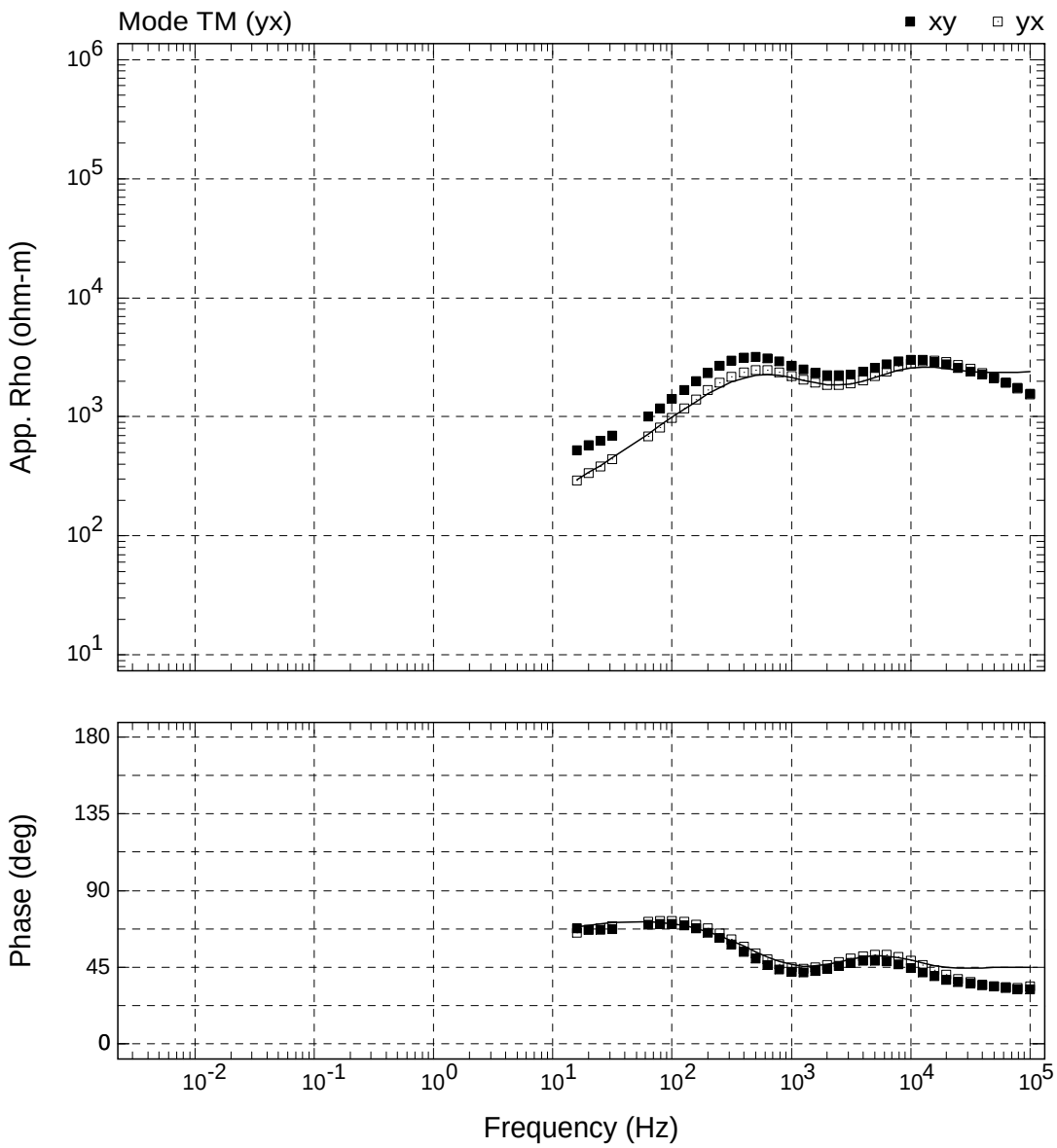

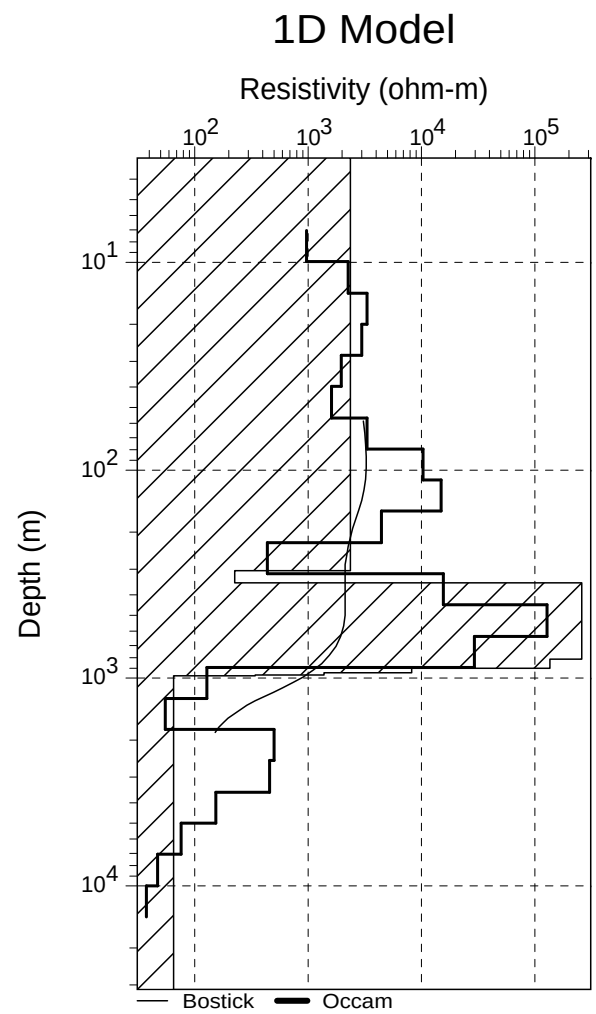

Sounding: ZMR057

Area: Mauna Kea

26/Dec/2016